Research Topics

Synergistic effects of climate change and air pollution on health

Edited by
Zhaobin Sun, Shupeng Zhu and Xingqin An

Published in
Frontiers in Public Health

ISSN 1664-8714
ISBN 978-2-8325-6345-8
DOI 10.3389/978-2-8325-6345-8

About Frontiers

Frontiers is more than just an open access publisher of scholarly articles: it is a pioneering approach to the world of academia, radically improving the way scholarly research is managed. The grand vision of Frontiers is a world where all people have an equal opportunity to seek, share and generate knowledge. Frontiers provides immediate and permanent online open access to all its publications, but this alone is not enough to realize our grand goals.

Frontiers journal series

The Frontiers journal series is a multi-tier and interdisciplinary set of open-access, online journals, promising a paradigm shift from the current review, selection and dissemination processes in academic publishing. All Frontiers journals are driven by researchers for researchers; therefore, they constitute a service to the scholarly community. At the same time, the *Frontiers journal series* operates on a revolutionary invention, the tiered publishing system, initially addressing specific communities of scholars, and gradually climbing up to broader public understanding, thus serving the interests of the lay society, too.

Dedication to quality

Each Frontiers article is a landmark of the highest quality, thanks to genuinely collaborative interactions between authors and review editors, who include some of the world's best academicians. Research must be certified by peers before entering a stream of knowledge that may eventually reach the public - and shape society; therefore, Frontiers only applies the most rigorous and unbiased reviews. Frontiers revolutionizes research publishing by freely delivering the most outstanding research, evaluated with no bias from both the academic and social point of view. By applying the most advanced information technologies, Frontiers is catapulting scholarly publishing into a new generation.

What are Frontiers Research Topics?

Frontiers Research Topics are very popular trademarks of the *Frontiers journals series*: they are collections of at least ten articles, all centered on a particular subject. With their unique mix of varied contributions from Original Research to Review Articles, Frontiers Research Topics unify the most influential researchers, the latest key findings and historical advances in a hot research area.

Find out more on how to host your own Frontiers Research Topic or contribute to one as an author by contacting the Frontiers editorial office: frontiersin.org/about/contact

Synergistic effects of climate change and air pollution on health

Topic editors

Zhaobin Sun — Chinese Academy of Meteorological Sciences, China
Shupeng Zhu — Zhejiang University, China
Xingqin An — China Meteorological Administration, China

Citation

Sun, Z., Zhu, S., An, X., eds. (2025). *Synergistic effects of climate change and air pollution on health*. Lausanne: Frontiers Media SA. doi: 10.3389/978-2-8325-6345-8

Table of contents

frontiers | Frontiers in Public Health

TYPE Original Research
PUBLISHED 07 August 2023
DOI 10.3389/fpubh.2023.1232715

Check for updates

OPEN ACCESS

EDITED BY
Zhaobin Sun,
Chinese Academy of Meteorological Sciences, China

REVIEWED BY
Jianxiong Hu,
Guangdong Provincial Center for Disease Control and Prevention, China
Zhang Shuwen,
Beijing University of Chinese Medicine, China

*CORRESPONDENCE
Jinyuan Xin
✉ xjy@mail.iap.ac.cn
Shihong Li
✉ lshltz1@163.com

RECEIVED 01 June 2023
ACCEPTED 03 July 2023
PUBLISHED 07 August 2023

CITATION
Zhang Y, Zhang S, Xin J, Wang S, He X, Zheng C and Li S (2023) Short-term joint effects of ambient $PM_{2.5}$ and O_3 on mortality in Beijing, China.
Front. Public Health 11:1232715.
doi: 10.3389/fpubh.2023.1232715

Short-term joint effects of ambient $PM_{2.5}$ and O_3 on mortality in Beijing, China

Ying Zhang[1,2], Shaobo Zhang[1], Jinyuan Xin[2]*, Shigong Wang[1], Xiaonan He[3], Canjun Zheng[4] and Shihong Li[5]*

[1]Plateau Atmosphere and Environment Key Laboratory of Sichuan Province, School of Atmospheric Sciences, Chengdu University of Information Technology, Chengdu, China, [2]State Key Laboratory of Atmospheric Boundary Layer Physics and Atmospheric Chemistry, Institute of Atmospheric Physics, Chinese Academy of Sciences, Beijing, China, [3]Beijing Anzhen Hospital, Capital Medical University, Beijing, China, [4]Chinese Center for Disease Control and Prevention, National Institute for Communicable Disease Control and Prevention, Beijing, China, [5]Department of Respiratory and Critical Care Medicine, Beijing Institute of Respiratory Medicine and Beijing Chao-Yang Hospital, Capital Medical University, Beijing, China

Introduction: In recent years, air pollution caused by co-occurring $PM_{2.5}$ and O_3, named combined air pollution (CAP), has been observed in Beijing, China, although the health effects of CAP on population mortality are unclear.

Methods: We employed Poisson generalized additive models (GAMs) to evaluate the individual and joint effects of $PM_{2.5}$ and O_3 on mortality (nonaccidental, respiratory, and cardiovascular mortality) in Beijing, China, during the whole period (2014–2016) and the CAP period. Adverse health effects were assessed for percentage increases (%) in the three mortality categories with each 10-$\mu g/m^3$ increase in $PM_{2.5}$ and O_3. The cumulative risk index (*CRI*) was adopted as a novel approach to quantify the joint effects.

Results: The results suggested that both $PM_{2.5}$ and O_3 exhibited the greatest individual effects on the three mortality categories with cumulative lag day 01. Increases in the nonaccidental, cardiovascular, and respiratory mortality categories were 0.32%, 0.36%, and 0.43% for $PM_{2.5}$ (lag day 01) and 0.22%, 0.37%, and 0.25% for O_3 (lag day 01), respectively. There were remarkably synergistic interactions between $PM_{2.5}$ and O_3 on the three mortality categories. The study showed that the combined effects of $PM_{2.5}$ and O_3 on nonaccidental, cardiovascular, and respiratory mortality were 0.34%, 0.43%, and 0.46%, respectively, during the whole period and 0.58%, 0.79%, and 0.75%, respectively, during the CAP period. Our findings suggest that combined exposure to $PM_{2.5}$ and O_3, particularly during CAP periods, could further exacerbate their single-pollutant health risks.

Conclusion: These findings provide essential scientific evidence for the possible creation and implementation of environmental protection strategies by policymakers.

KEYWORDS

$PM_{2.5}$, O_3, combined air pollution, joint effects, mortality, Beijing

1. Introduction

Significant epidemiological research has shown that short-term exposure to ambient air pollution is substantially related to numerous detrimental health consequences (Fan et al., 2020; Stafoggia et al., 2022) (1). Among the various ambient air pollutants, particles with diameters ≤2.5 μm ($PM_{2.5}$) and ozone (O_3) are considered have serious dangerous to human health (2).

At one time, China, the world's largest developing country, had the worst air pollution issue than other countries, which led to almost 2 million premature deaths annually (3). The Chinese government has implemented a variety of pollution prevention and control measures since 2013 to protect public health, including policy changes in energy, industrial, and transportation infrastructure (4). According to (5), there was a significant reduction of 30–50% in $PM_{2.5}$ concentrations from 2013 to 2017. Despite this reduction, PM2.5 pollution episodes persist in China, especially in megacities (6, 7). Furthermore, the decreased $PM_{2.5}$ also slow down the sink of hydroperoxy radicals and thus speeding up O_3 production, resulting in the ground-level O_3 levels in China have grown annually (8). Consequently, there was a cooccurrence of $PM_{2.5}$ and O_3 pollution (9–11). This cooccurrence is known as combined air pollution (CAP). CAP has received much interest in atmospheric environmental research (12, 13). However, the health risks caused by CAP are still unclear.

Given that humans are exposed to more than one air pollutant in real life, biological responses to inhaled pollutants likely depend on the interaction between individual pollutants (14). Ground-level O_3 and $PM_{2.5}$ are closely related and interact with each other, and thus they may have a combined negative impact on human body (15). Traditional time-series studies have focused on assessing health effects using single-pollutant models. Research on the combined health effects of multiple pollutants has been inadequate. In recent years, some new models and methods have been developed to simultaneously quantify the combined health effects of multiple pollutants. One such technique is the use of the cumulative risk index (*CRI*), which involves the linear combination of individual coefficients. This approach enables accurate estimation of cumulative effects, even in cases where there is a high correlation among variables (14), and has been recommended for joint estimates of multipollutant exposure effects on health outcomes (16). However, *CRI*-related studies are quite limited; most of these studies have been conducted in developed countries, and studies in developing countries are lacking (17, 18).

Beijing, as the capital of China, has a serious air pollution issue. CAP appears in Beijing from time to time, and the frequency continues to increase (19). It is still unknown how the CAP affects the health outcomes of a local population. Therefore, the goal of this manuscript was to evaluate the individual and combined effects of $PM_{2.5}$ and O_3 on nonaccidental and cause-specific mortality in Beijing, China, across the entire time period and during the CAP period, respectively. The joint health effects of $PM_{2.5}$ and O_3 were estimated by using the *CRI* index.

2. Data and methods

2.1. Health data

In this study, we collected data on the daily death counts in Beijing from January 1, 2014, to December 31, 2016, from the Chinese Center for Disease Control and Prevention (CDC). To classify the causes of death, we used the International Classification of Diseases, Tenth Revision (ICD-10). Nonaccidental causes, cardiovascular diseases, and respiratory diseases were categorized as A00-R99, I00-I99, and J00-J99, respectively.

2.2. Environmental data

$PM_{2.5}$ and O_3 data were retrieved from the China National Environmental Monitoring Center. The maximal 8-h average ozone concentration was selected as the O_3 concentration metric according to World Health Organization (WHO) recommendations (20). $PM_{2.5}$ and O_3 concentrations were recorded hourly at 12 stationary monitoring sites (Olympic Sports Center, Dongsi, Changping, Tiantan, Guanyuan, Shunyi, Huairou, Dingling, Agriculture Exhibition Hall, Haidian, Wanshou Temple, and Gucheng) in Beijing. We first calculated the mean of the hourly $PM_{2.5}$ and O_3 concentrations from all 12 monitoring sites and then calculated the 24-h mean $PM_{2.5}$ and daily maximal 8-h average ozone concentrations. Details of the $PM_{2.5}$ and O_3 concentration data collection methods can be found in our published articles (21). According to the Ministry of Ecology and Environment of China's national Ambient Air Quality Standards released in 2012 (22), $PM_{2.5}$ pollution levels are defined as daily average $PM_{2.5}$ concentrations $>75\,\mu g{\cdot}m^{-3}$, and O_3 pollution levels are defined as daily average O_3 concentrations $>160\,\mu g{\cdot}m^{-3}$. As a result, CAP days were designated as days when both O_3 and $PM_{2.5}$ values were above the criterion for co-occurring air pollution, with O_3 concentrations $>160\,\mu g{\cdot}m^{-3}$ and $PM_{2.5}$ concentrations $>75\,\mu g{\cdot}m^{-3}$. In addition, we collected data on some meteorological factors, including the daily average surface temperature (°C) and relative humidity (*RH*) (%), which were retrieved from the China Meteorological Data Sharing Service System.[1]

2.3. Statistical methods

We employed four parallel time-series Poisson generalized additive models (GAMs) to evaluate the individual and joint effects of O_3 and $PM_{2.5}$ on nonaccidental, cardiovascular, and respiratory mortality during the whole period and the CAP period. These models include a single-pollutant model, multipollutant model, nonparametric bivariate response surface model, and stratification model.

First, we utilized the single-pollutant model as the basis to assess the individual effects of a single pollutant on health outcomes at different lag days, including single (lag days 0 and 1) and cumulative (lag days 01 and 04) effects. The following is an expression for Model 1:

$$\begin{aligned}\log\left[E\left(Y_t\right)\right] = \alpha + NS\left(Time{,}3*6/\text{year}\right) + NS\left(Temp{,}3\right) + \\ NS\left(RH{,}3\right) + \text{as.factor}\left(DOW\right) + \\ \text{as.factor}\left(Holiday\right) + \beta_{kt}x_{kt} = \beta_{kt}x_{kt} + COVs \quad (1)\end{aligned}$$

where Y_t and $E(Y_t)$ signify the daily death counts and predicted death counts on day t, respectively. α refers to the intercept. $NS(\ )$ is the natural cubic spline function. According to the minimum Akaike information criterion (AIC), *Time* with the degrees of freedom (*df*) 6/year was selected to control for secular trends, and the *df* of the daily mean temperature (Temp) and *RH* are both 3. *DOW* and *Holiday* are two dummy variables that indicate weekday and public holidays,

1 http://data.cma.cn/

respectively (23). x_{kt} and β_{kt} denote the specific air pollutant concentrations and the corresponding coefficient on day *t*, respectively. Additionally, *COVs* represent all covariates including time, mean temperature, relative humidity, weekday, public holidays, and the intercept, respectively.

On this basis, we utilized a multipollutant model to evaluate the joint effects of $PM_{2.5}$ and O_3 on health outcomes at different lag days. The *CRI*, which was developed using estimates from multipollutant models, was used to assess the joint effects of multipollutant exposures (24). The multipollutant model and the formula for the *CRI* can be expressed as follows:

$$\log\left[E\left(Y_t\right)\right] = \sum_{k=1}^{p} \beta_{kt} x_{kt} + COVs \tag{2}$$

$$CRI_t = \exp\left(\sum_{k=1}^{p} \beta_{kt} * 10\right) \tag{3}$$

where x_{kt} and β_{kt} denote the specific air pollutant concentrations and the corresponding coefficient on day *t*, respectively. The *COVs* are identical to those in Model (1). *p* indicates the type of air pollutant. CRI_t denotes the joint effects of *p* air pollutant mixtures on day *t*.

The *CRIs* obtained from the multipollutant models were compared with the effect estimates of the single-pollutant models. If the effect estimate from the single-pollutant model was as high as the *CRI* from the multipollutant model, it indicated that the influence of only one pollutant was adequate to reflect the total pollutant mixture and that there were no synergistic effects.

Third, we also used a nonparametric bivariate response surface model to intuitively analyze the combined effects of $PM_{2.5}$ and O_3 on health outcomes. The model can be expressed as follows:

$$\log\left[E\left(Y_t \middle| X\right)\right] = ST\left(PM_{2.5}, O_3\right) + COVs \tag{4}$$

ST () denotes the cubic regression splines. The *COVs* are identical to those in Model (1).

Fourth, the pollutant stratification model was employed to quantitatively assess the joint effects of $PM_{2.5}$ and O_3 on health outcomes during the CAP period. The model can be expressed as follows:

$$\log\left[E\left(Y_t \middle| X\right)\right] = m\beta_{it} O_3 + m\beta_{jt} PM_{2.5} + COVs \tag{5}$$

where *m* is an indicator variable that is used to represent the CAP days. $m = 1$ represents co-occurring air pollution of $PM_{2.5}$ and O_3; otherwise, $m = 0$. β_{it} and β_{jt} represent the coefficients of O_3 and $PM_{2.5}$ on day t, respectively. The *COVs* are the same as those in Model (1).

To evaluate the models' robustness, several sensitivity studies were carried out. We changed the *df* of *Time* from 7 to 10 per year and the *df* of mean temperature and *RH* from 3 to 5 for the single-pollutant model.

R 4.2.3 software with the "mgcv" package was used for all analyzes. For each 10-μg/m^3 increase in $PM_{2.5}$ and O_3, the estimated individual and joint effects are shown as percentage changes (%) along with 95% confidence intervals (95% CIs).

3. Results

Table 1 summarizes the environmental and mortality data in Beijing, China, from 2014 to 2016. On average, there were 146 nonaccidental deaths per day, of which 64 were due to cardiovascular diseases and 17 were due to respiratory diseases. The annual mean temperature and *RH* were 15.65°C and 53%, respectively. Additionally, the annual average concentrations of $PM_{2.5}$ and O_3 were 78.97 and 118.10 μg/m^3, respectively. Based on the statistical analysis, the daily average $PM_{2.5}$ and O_3 concentrations exceeded the threshold set by the Air Quality II Guidelines (75 μg·m^{-3} for $PM_{2.5}$ and 160 μg·m^{-3} for O_3, respectively) on 322 and 280 days, respectively (22). There were 59 CAP days during the study period, indicating serious air pollution in Beijing, China.

The Spearman correlation coefficients of the three mortality categories and different environmental factors are shown in Figure 1. The three mortality categories were all significantly negatively correlated with the mean temperature, *RH*, and O_3 concentration and significantly positively correlated with the $PM_{2.5}$ concentration. The Spearman correlation between $PM_{2.5}$ and O_3 was low even though it was statistically significant ($r = -0.07$, $p < 0.001$),

TABLE 1 Daily summary statistics of the air pollution levels, meteorological variables and number of deaths in Beijing, China, from 2014 to 2016.

Variables	Daily measures						No. of days
	Mean	Minimum	1st Q	Median	3rd Q	Maximum	
Deaths (*n*)							
Nonaccidental	146 ± 22	95	130	142	158	242	1,096
Cardiovascular	64 ± 14	33	55	62	72	125	1,096
Respiratory	17 ± 6	4	13	16	20	38	1,096
Environment variables							
Mean temperature (°C)	15.65 ± 10.97	−14.30	3.00	15.65	24.10	32.60	1,096
Relative humidity (%)	53.00 ± 20.03	8.00	37.00	53.00	69.00	99.00	1,096
$PM_{2.5}$ (μg/m^3)	78.97 ± 70.41	7.68	30.00	59.73	104.44	477.43	1,096
O_3 (μg/m^3)	118.10 ± 72.17	2.00	60.70	100.10	170.20	348.10	1,096

1st Q, first quartile; 3rd Q, third quartile.

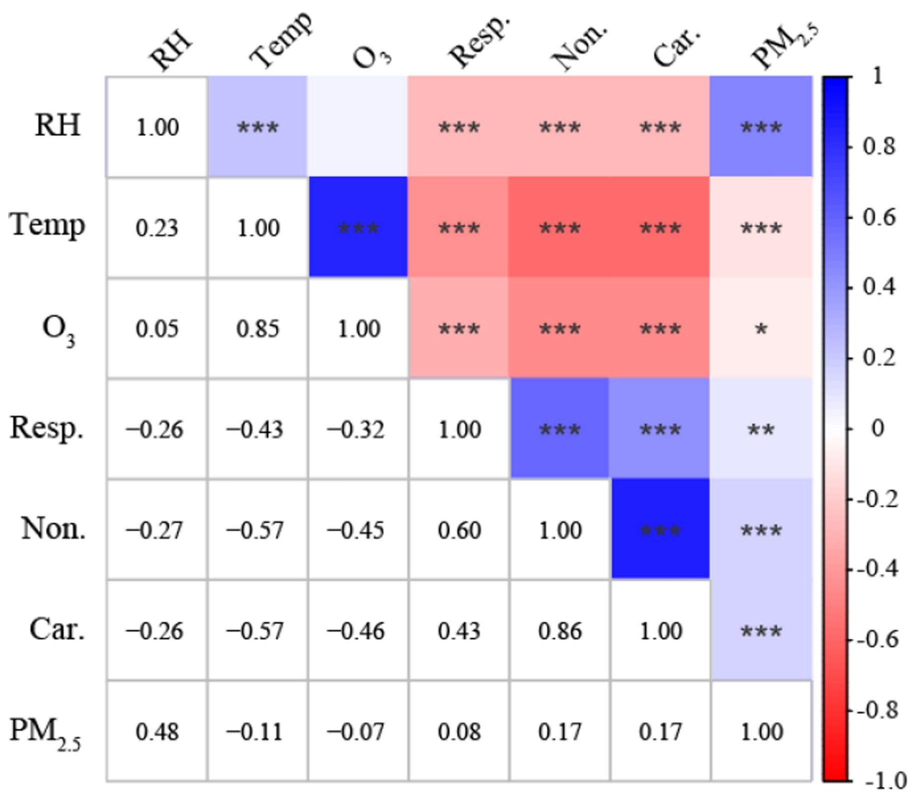

FIGURE 1
Spearman correlation matrix between the three mortality categories and different environmental factors in Beijing, China. *$p < 0.05$, **$p < 0.01$, ***$p < 0.001$. Non, Nonaccidental mortality; Car, Cardiovascular mortality; Resp, Respiratory mortality; Temp, mean temperature; RH, relative humidity.

indicating the possibility of interaction effects on three mortality categories.

Figure 2 illustrates the individual effects of $PM_{2.5}$ and O_3 on health outcomes at different lags. The individual effects of $PM_{2.5}$ and O_3 on the three mortality categories all peaked at lag day 01. Specifically, the increase in the nonaccidental, cardiovascular, and respiratory mortality categories was 0.32% (95% CI: 0.21, 0.43%), 0.36% (95% CI: 0.21, 0.50%), and 0.43% (95% CI: 0.28, 0.58%) for each 10-μm^{-3} increase in the $PM_{2.5}$ concentration (lag day 01), and 0.22% (95% CI: 0.08, 0.36%), 0.37% (95% CI: 0.21, 0.53%), and 0.25% (95% CI: 0.12, 0.37%) for each 10-μg/m^3 increase in the O_3 concentration (lag day 01), respectively.

Figure 3 depicts the joint effects of $PM_{2.5}$ and O_3 on health outcomes at different lags. As with the individual effects of $PM_{2.5}$ and O_3, the joint effects of $PM_{2.5}$ and O_3 on the three mortality categories all peaked at lag day 01. The corresponding *CRIs* for nonaccidental, respiratory and cardiovascular mortality were 0.34% (95% CI: 0.16, 0.52%), 0.43% (95% CI: 0.21, 0.65%), and 0.46% (95% CI: 0.23, 0.70%), respectively. Importantly, for the same category of diseases, the joint effect represented by *CRI* was higher than for any single pollutant effect estimate at lag day 01. Overall, the *CRIs* implied that a single-pollutant effect did not accurately represent the whole health effects of the mixture. In the subsequent analysis, both $PM_{2.5}$ and O_3 at lag day 01 were used as the research objects.

Figure 4 illustrates the combined effects of $PM_{2.5}$ and O_3 on the three mortality categories using three-dimensional visualization graphs. The response surfaces show that the combined effects of $PM_{2.5}$ (lag day 01) and O_3 (lag day 01) on nonaccidental, cardiovascular, and respiratory deaths were complicated. Notably, when high concentrations of $PM_{2.5}$ and O_3 coexisted, all three categories (nonaccidental, cardiovascular, and respiratory fatalities) reached their maximums, showing that the interaction effects could be synergistic.

Table 2 depicts the individual and joint effects of $PM_{2.5}$ (lag day 01) and O_3 (lag day 01) on health outcomes during the whole period and the CAP period. For the same kind of illness, the *CRIs* of the joint effects during both the whole period and the CAP period were higher than any single-pollutant effect estimates. In addition, the joint effects during the CAP period were remarkably larger than those during the whole period, indicating that the CAP period further exacerbated the combined effects of $PM_{2.5}$ and O_3 on the three mortality categories.

According to the results of the sensitivity analyzes, the effects of O_3 (or $PM_{2.5}$) remained robust regardless of the change in the *df* of the time (see Supplementary Figure S1), the *df* of the mean temperature, and the *df* of the *RH* (see Supplementary Table S1).

4. Discussion

The CAP of $PM_{2.5}$ and O_3 has become a major environmental and health concern worldwide (7). Evaluating the short-term individual and joint effects of $PM_{2.5}$ and O_3 on health outcomes

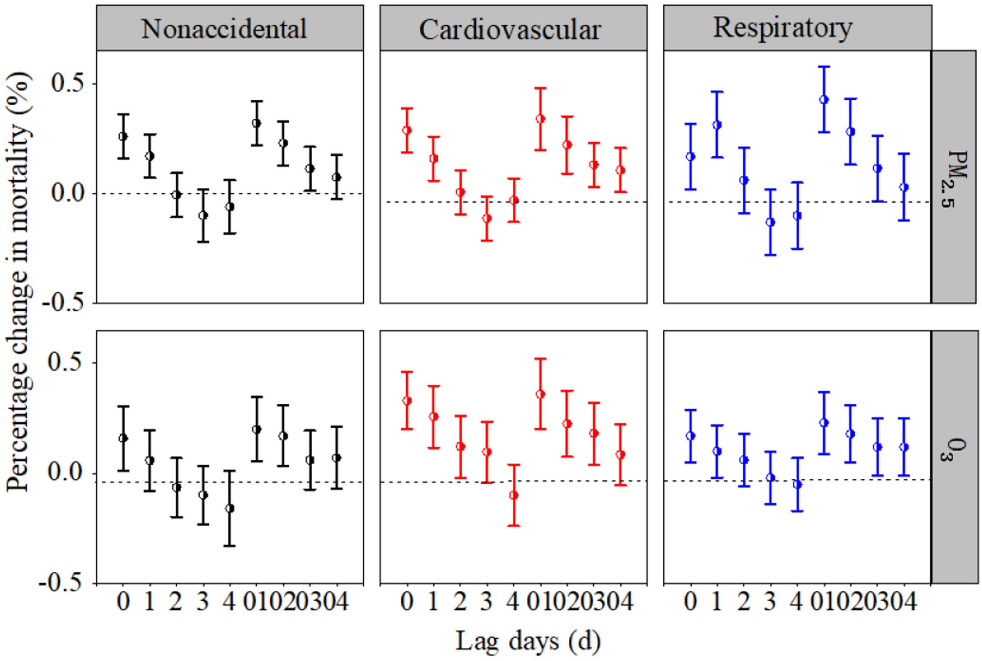

FIGURE 2
Percentage changes (%) in the three mortality categories associated with each 10-μg/m^3 increase in $PM_{2.5}$ and O_3 concentrations at different lag days in the single-pollutant models.

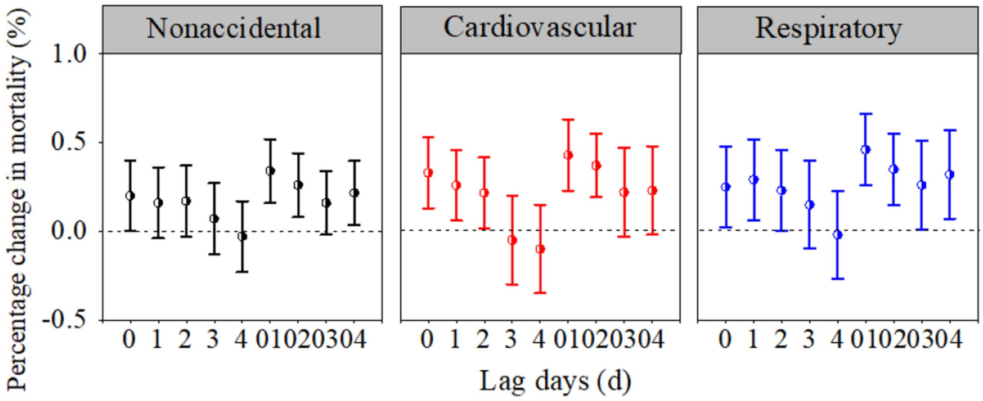

FIGURE 3
Percentage changes (%) in the three mortality categories associated with each 10-μg/m^3 increase in the $PM_{2.5}$ and O_3 concentrations at different lag days in the multipollutant models.

could provide valuable evidence for policymakers to regulate and prevent the accumulation of $PM_{2.5}$ and O_3. Our findings demonstrated that $PM_{2.5}/O_3$ was significantly associated with nonaccidental and cause-specific (cardiovascular and respiratory) mortality in Beijing, China. Additionally, the joint effects of the dual pollutants could further exacerbate their individual effects, especially during the CAP period.

Numerous studies of the individual effects of air pollutants, particularly $PM_{2.5}$ and O_3, on public health have been conducted (1, 25). For example, a meta-analysis conducted in 272 Chinese cities by Chen et al. (26) showed that a 10-μg/m^3 increase in the $PM_{2.5}$ concentration was associated with an increase in nonaccidental, cardiovascular, and respiratory mortality of 0.27, 0.39, and 0.29%, respectively. Another meta-analysis in China (27) revealed that an increase of 10-μg/m^3 in the O_3 concentration caused increases of 0.24 and 0.27% in nonaccidental and cardiovascular mortality, respectively. In this study, the results from the single-pollutant models revealed that each 10-μg/m^3 increase in the $PM_{2.5}$ concentration caused increases of 0.32, 0.36, and 0.43% in nonaccidental, cardiovascular, and respiratory mortality, respectively, and each 10-μg/m^3 increase in the O_3 concentration caused increases of 0.22, 0.37, and 0.25% in nonaccidental, cardiovascular, and respiratory mortality, respectively, in Beijing, China. Our estimates of the $PM_{2.5}$–mortality and O_3–mortality relationships were generally consistent with those of previous studies.

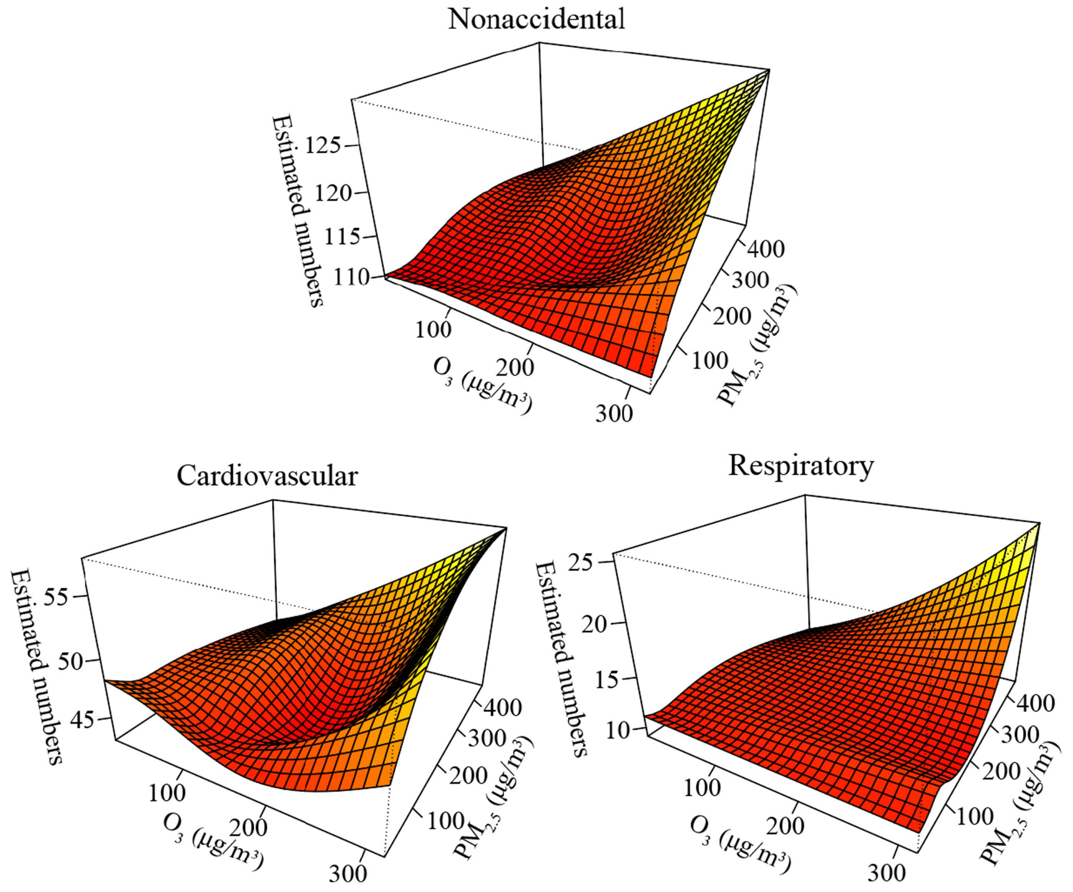

FIGURE 4
Bivariate response surfaces of $PM_{2.5}$ and O_3 for nonaccidental, cardiovascular, and respiratory deaths in Beijing, China.

TABLE 2 Percentage changes (%) in nonaccidental, respiratory, and cardiovascular mortality associated with each 10-μg/m³ increase in the $PM_{2.5}$ and O_3 concentrations during the whole period and the CAP period.

Air pollutants	Percentage change% (95% CI)		
	Nonaccidental	Cardiovascular	Respiratory
Single-pollutant models			
$PM_{2.5}$[a]	0.32 (0.21, 0.43)*	0.36 (0.21, 0.52)*	0.43 (0.28, 0.58)*
O_3[a]	0.22 (0.08, 0.36)*	0.37 (0.21, 0.53)*	0.25 (0.12, 0.37)*
$PM_{2.5}$[b]	0.29 (0.17, 0.41)*	0.41 (0.12, 0.70)*	0.42 (0.18, 0.66)*
O_3[b]	0.28 (0.08, 0.49)*	0.42 (0.23, 0.62)*	0.31 (0.15, 0.47)*
Multipollutant models			
$O_3 + PM_{2.5}$[a]	0.34 (0.16, 0.52)*	0.43 (0.21, 0.65)*	0.46 (0.23, 0.70)*
$O_3 + PM_{2.5}$[b]	0.58 (0.20, 0.96)*	0.79 (0.46, 1.12)*	0.75 (0.42, 1.08)*

[a]During the whole period.
[b]During the CAP period of co-occurring air pollution of $PM_{2.5}$ and O_3.
*indicates $p < 0.05$.

In the multipollutant models, our findings suggested that the estimates of the joint effects of the two air pollutants on mortality were higher than those for any individual effect for the same kind of illness. Consistent with our findings, a study conducted by Lei et al. (28) in Hefei, China, indicated that the effects of the health risks caused by $PM_{2.5}$ on nonaccidental mortality increased when O_3 was included, and vice versa, indicating that O_3 and $PM_{2.5}$ could aggravate each other's unfavorable health effects. A cross-sectional study conducted in six countries revealed a synergistic interaction effect of $PM_{2.5}$ and O_3 on disease deterioration (29). However, in contrast to our findings, Qu et al. (30) observed that when O_3 was included, the effect of $PM_{2.5}$ on nonaccidental mortality was reduced. Moreover, several earlier studies showed no interaction effects of $PM_{2.5}$ and O_3 (31, 32). This inconsistency could be attributed to differences in the chemical composition, source, and toxicity of $PM_{2.5}$ and O_3 in different regions. Furthermore, the differences in study methods and individual sensitivity to pollutants can also lead to different results (33).

Notably, the patterns of the combined effects of $PM_{2.5}$ and O_3 on mortality demonstrated that coexisting high concentrations of $PM_{2.5}$ and O_3 could have synergistic effects on three mortality categories (34). Biological mechanisms have been somewhat postulated to explain the potential interaction effect of $PM_{2.5}$ and O_3 pollution on respiratory and cardiovascular mortality, despite the lack of clear evidence for a direct synergistic effect of the two pollutants on illnesses. For example, a few toxicology experiments on rats validated that the particulate matter served as a carrier for O_3, delivering O_3 into the body (35). Inhaling particles and O_3 together had a synergistic impact on airway responsiveness and allergic inflammation in mice (36), suggesting that combined exposure to O_3 and $PM_{2.5}$ markedly increased health risks (37). Therefore, people, especially those with chronic respiratory and cardiovascular diseases, should strengthen protection measures and reduce outdoor activities, especially on CAP of $PM_{2.5}$ and O_3 days.

The key advantage of this study is as follows: Current research on CAP primarily focuses on the characteristics of changes in $PM_{2.5}$ and O_3 concentrations, meteorological causes, and their mutual influences. However, there is less emphasis on the joint health effects of $PM_{2.5}$ and O_3 during CAP periods (7, 38). Furthermore, traditional multipollutant models mainly focus on describing the difference in the health effects of a single pollutant before and after the addition of other pollutants without quantifying the combined effects of multiple pollutants (6). Our study differs from traditional studies, as we utilized multiple methods to examine the harmful health effects associated with exposure to one and two pollutants. We also conducted stratification studies on pollution, with a specific focus on the combined health effects of $PM_{2.5}$ and O_3 during the CAP period. Furthermore, we used the *CRI* to accurately quantify the joint effects of $PM_{2.5}$ and O_3 during both the whole and CAP periods. This approach addresses the limitations of previous research to a significant extent (16).

There are several limitations of our study that should be acknowledged. First and foremost, due to the difficulty in obtaining disease data in China, the study only included a 3-year disease death time series, and the time coverage was relatively limited. The latest year's death data could not be obtained, which could reduce the statistical power. Second, in keeping with many previous studies (4, 39), we did not collect data on the real-time pollution exposure levels of individuals and only used the outdoor air pollutant concentration to represent individual $PM_{2.5}$ and O_3 exposure levels, which inevitably led to some deviation in the results (33). Third, the two most dangerous pollutants in China at this time are $PM_{2.5}$ and O_3. This study only tentatively carried out research on the interaction effect between $PM_{2.5}$ and O_3 on public health and did not carry out in-depth research on interaction effects with other air pollutants (such as O_3 and nitrogen dioxide, sulfur dioxide and $PM_{2.5}$). Therefore, with the improvement of research methods at a later stage, further in-depth study of the health effects of interactions between different air pollutants on human health should be carried out.

5. Conclusion

Our findings showed that exposure to $PM_{2.5}$ and O_3 may be significant risk factors for nonaccidental, cardiovascular, and respiratory mortality in Beijing, China. Moreover, we found that combined exposure to $PM_{2.5}$ and O_3 could amplify their individual effects on three mortality categories, particularly during CAP of $PM_{2.5}$ and O_3 periods. Therefore, during the CAP periods, the public should take timely preventive measures and reduce outdoor activities to some extent to reduce air pollution hazards.

Data availability statement

The data analyzed in this study is subject to the following licenses/restrictions: Authors are not allowed to disclose data. Requests to access these datasets should be directed to YZ, zhangy881208@126.com.

Author contributions

YZ: writing—review and editing, methodology, designed the research, and wrote the manuscript. SZ and XH: methodology and designed the research. JX: methodology, designed and reviewed the research, and reviewed the research. SW: formal analysis and reviewed the research. CZ: collected and analyzed the data. SL: writing—review and editing, formal analysis, and collected and analyzed the data. All authors contributed to the article and approved the submitted version.

Funding

This study was supported by the National Nature Science Foundation of China (42005136), Innovation Team Fund of Southwest Regional Meteorological Center, China Meteorological Administration (XNQYCXTD-202203), China Postdoctoral Science Foundation (2020M670419), and National Key Research and Development Project Program of China (2016YFA0602004). This work was supported in part by Chengdu Plain Urban Meteorology and Environment Sichuan Provincial Field Scientific Observation and Research Station, Chengdu, China.

Conflict of interest

The authors declare that the research was conducted in the absence of any commercial or financial relationships that could be construed as a potential conflict of interest.

Publisher's note

Supplementary material

The Supplementary material for this article can be found online at: https://www.frontiersin.org/articles/10.3389/fpubh.2023.1232715/full#supplementary-material

References

1. Bont J, Jaganathan S, Dahlquist M, Persson Å, Stafoggia M, Ljungman P. Ambient air pollution and cardiovascular diseases: an umbrella review of systematic reviews and meta-analyses. *J Intern Med*. (2022) 291:779–800. doi: 10.1111/joim.13467

2. Dimakopoulou K, Grivas G, Samoli E, et al. Determinants of personal exposure to ozone in school children. Results from a panel study in Greece. *Environmental research*. (2017) 154:66–72.

3. Yin P, Brauer M, Cohen AJ, Wang H, Li J, Burnett RT, et al. The effect of air pollution on deaths, disease burden, and life expectancy across China and its province, 1990-2017: an analysis for the global of disease study 2017. *Lancet Planet Health*. (2020) 4:e386–98. doi: 10.1016/S2542-5196(20)30161-3

4. Chen K, Wolf K, Hampel R, Stafoggia M, Breitner S, Cyrys J, et al. Does temperature-confounding control influence the modifying effect of air temperature in ozone–mortality associations? *Environ Epidemiol*. (2018) 2:1. doi: 10.1097/EE9.0000000000000008

5. Fan S J, Heinrich J, Bloom M S, et al. Ambient air pollution and depression: a systematic review with meta-analysis up to 2019. *Sci. Total Environ.*. (2020) 701:134721.

6. Li M, Dong H, Wang B, Zhao W, Zare Sakhvidi MJ, Li L, et al. Association between ambient ozone pollution and mortality from a spectrum of causes in Guangzhou China. *Sci. Total Environ.* (2020) 754:142110. doi: 10.1016/j.scitotenv.2020.142110

7. Wu XY, Xin JY, Zhang WY, Gao W, Ma Y, Ma Y, et al. Variation characteristics of air combined pollution in Beijing City. *Atmos Res*. (2022) 274:106197. doi: 10.1016/j.atmosres.2022.106197

8. Li K, Jacob DJ, Liao H, Shen L, Zhang Q, Bates KH. Anthropogenic drivers of 2013–2017 trends in summer surface ozone in China. *Proc Natl Acad Sci*. (2019) 116:422–7. doi: 10.1073/pnas.1812168116

9. Lu X, Zhang L, Wang X, Gao M, Li K, Zhang Y, et al. Rapid increases in warm-season surface ozone and resulting health impact in China since 2013. *Environ Sci Technol Lett*. (2020) 7:240–7. doi: 10.1021/acs.estlett.0c00171

10. Luo Y, Zhao T, Yang Y, Zong L, Kumar KR, Wang H, et al. Seasonal changes in the recent decline of combined high $PM_{2.5}$ and O_3 pollution and associated chemical and meteorological drivers in the Beijing–Tianjin–Hebei region, China. *Sci Total Environ*. (2022) 838:156312. doi: 10.1016/j.scitotenv.2022.156312

11. Zhai SX, Jacob DJ, Wang X, Shen L, Li K, Zhang Y, et al. Fine particulate matter ($PM_{2.5}$) trends in China, 2013–2018: separating contributions from anthropogenic emissions and meteorology. *Atmos Chem Phys*. (2019) 19:11031–41. doi: 10.5194/acp-19-11031-2019

12. Chen XK, Jiang Z, Shen YN, Li R, Fu Y, Liu J, et al. Chinese regulations are working-why is surface ozone over industrialized areas still high? Applying lessons from northeast US air quality evolution. *Geophys Res Lett*. (2021) 48:e2021GL092816. doi: 10.1029/2021GL092816

13. Zhao SP, Yin DY, Yu Y, Kang S, Qin D, Dong L, et al. $PM_{2.5}$ and O_3 pollution during 2015–2019 over 367 Chinese cities: spatiotemporal variations, meteorological and topographical impacts. *Environ Pollut*. (2020) 264:114694. doi: 10.1016/j.envpol.2020.114694

14. Winquist A, Kirrane E, Klein M, Strickland M, Darrow LA, Sarnat SE, et al. Joint effects of ambient air pollutants on pediatric asthma emergency department visits in Atlanta, 1998-2004. *Epidemiology*. (2014) 25:666–73. doi: 10.1097/EDE.0000000000000146

15. Bae S, Lim Y H, Hong Y C. Causal association between ambient ozone concentration and mortality in Seoul, Korea. *Environ Res*. (2020) 182:109098.3.

16. Huang WZ, He WY, Knibbs LD, Jalaludin B, Guo YM, Morawska L, et al. Improved morbidity-based air quality health index development using Bayesian multi-pollutant weighted model. *Environ Res*. (2022) 204:112397. doi: 10.1016/j.envres.2021.112397

17. Costa AF, Hoek G, Brunekreef B, Ponce de Leon ACM. Air pollution and deaths among elderly residents of São Paulo, Brazil: an analysis of mortality displacement. *Environ Health Perspect*. (2017) 125:349–54. doi: 10.1289/EHP98

18. Samoli E, Atkinson RW, Analitis A, Fuller GW, Green DC, Mudway I, et al. Associations of short-term exposure to traffic-related air pollution with cardiovascular and respiratory hospital admissions in London UK. *Occup Environ Med*. (2016) 73:300–7. doi: 10.1136/oemed-2015-103136

19. Meng X, Long Y. Shrinking cities in China: evidence from the latest two population censuses 2010–2020. *Environ Plan A*. (2022) 54:449–53. doi: 10.1177/0308518X221076499

20. WHO. *Meta-Analysis of Time-Series Studies and Panel Studies of Particulate Matter (PM) and Ozone (O_3). Document EUR/04/5042688*. Copenhagen: WHO Regional Office for Europe (2004).

21. Zhang Y, Wang S, Fan X, Ye X. Temperature modulation of the health effects of particulate matter in Beijing, China. *Environ Sci Pollut Res*. (2018) 25:10857–66. doi: 10.1007/s11356-018-1256-3

22. GB 3095-2012. Ambient air quality standards. Available at: http://www.wxbh.gov.cn/doc/2021/11/04/3479116.shtml

23. Gasparrini A, Guo YM, Hashizume M, Lavigne E, Zanobetti A, Schwartz J, et al. Mortality risk attributable to high and low ambient temperature: a multicountry observational study. *Lancet*. (2015) 386:369–75. doi: 10.1016/S0140-6736(14)62114-0

24. Jerrett M, Burnett RT, Beckerman BS, Turner MC, Krewski D, Thurston G, et al. Spatial analysis of air pollution and mortality in California. *Am J Respir Crit Care Med*. (2013) 188:593–9. doi: 10.1164/rccm.201303-0609OC

25. Stafoggia M, Oftedal B, Chen J, et al. Long-term exposure to low ambient air pollution concentrations and mortality among 28 million people: results from seven large European cohorts within the ELAPSE project. *Lancet Planet. Health*. (2022) 6:e9–e18.

26. Chen R, Yin P, Meng X, Liu C, Wang L, Xu X, et al. Fine particulate air pollution and daily mortality. A nationwide analysis in 272 Chinese cities. *Am J Respir Crit Care Med*. (2017) 196:73–81. doi: 10.1164/rccm.201609-1862OC

27. Yin P, Chen R, Wang L, Meng X, Liu C, Niu Y, et al. Ambient ozone pollution and daily mortality: a nationwide study in 272 Chinese cities. *Environ Health Perspect*. (2017) 125:117006. doi: 10.1289/EHP1849

28. Lei R, Zhu F, Cheng H, Liu J, Shen C, Zhang C, et al. Short-term effect of $PM_{2.5}/O_3$ on non-accidental and respiratory deaths in highly polluted area of China. Atmospheric. *Pollut Res*. (2019) 10:1412–9. doi: 10.1016/j.apr.2019.03.013

29. Lin H, Guo Y, Ruan Z, Yang Y, Chen Y, Zheng Y, et al. Ambient $PM_{2.5}$ and O_3 and their combined effects on prevalence of presbyopia among the elderly: a cross-sectional study in six low-and middle-income countries. *Sci Total Environ*. (2019) 655:168–73. doi: 10.1016/j.scitotenv.2018.11.239

30. Qu Y, Pan Y, Niu H, He Y, Li M, Li L, et al. Short-term effects of fine particulate matter on non-accidental and circulatory diseases mortality: a time series study among the elder in Changchun. *PLoS One*. (2018) 13:e0209793. doi: 10.1371/journal.pone.0209793

31. Guo J, Ma MY, Xiao CL, Zhang C, Chen J, Lin H, et al. Association of air pollution and mortality of acute lower respiratory tract infections in Shenyang, China: a time series analysis study. *Iran J Public Health*. (2018) 47:1261–71.

32. Song J, Lu M, Zheng L, Liu Y, Xu P, Li Y, et al. Acute effects of ambient air pollution on outpatient children with respiratory diseases in Shijiazhuang, China. *BMC Pulm Med*. (2018) 18:1–10. doi: 10.1186/s12890-018-0716-3

33. Zhang Y, Wang S, Zhang X, Ni C, Zhang J, Zheng C. Temperature modulation of the adverse consequences on human mortality due to exposure to fine particulates: a study of multiple cities in China. *Environ Res*. (2020) 185:109353. doi: 10.1016/j.envres.2020.109353

34. Pope CA, Burnett RT, Thurston GD, Thun MJ, Calle EE, Krewski D, et al. Cardiovascular mortality and Long-term exposure to particulate air pollution epidemiological evidence of general pathophysiological pathways of disease. *Circulation*. (2004) 109:71–7. doi: 10.1161/01.CIR.0000108927.80044.7F

35. Warren D L, Last J A. Synergistic interaction of ozone and respirable aerosols on rat lungs: III. Ozone and sulfuric acid aerosol. *Toxicol. Appl. Pharmacol*. (1987) 88:203–216.

36. Kobzik L, Goldsmith CA, Ning YY, Qin G, Morgan B, Imrich A, et al. Effects of combined ozone and air pollution particle exposure in mice. *Res Rep Health Eff Inst*. (2001) 106:5–29.

37. Mølhave L, Kjærgaard SK, Sigsgaard T, Lebowitz M. Interaction between ozone and airborne particulate matter in office air. *Indoor Air*. (2005) 15:383–92. doi: 10.1111/j.1600-0668.2005.00366.x

38. Wang M, Tang G, Liu Y, Ma M, Yu M, Hu B, et al. The difference in the boundary layer height between urban and suburban areas in Beijing and its implications for air pollution. *Atmos Environ*. (2021) 260:118552. doi: 10.1016/j.atmosenv.2021.118552

39. Lu X, Lin C, Li W, Chen Y, Huang Y, Fung JCH, et al. Analysis of the adverse health effects of $PM_{2.5}$ from 2001 to 2017 in China and the role of urbanization in aggravating the health burden. *Sci Total Environ*. (2019) 652:683–95. doi: 10.1016/j.scitotenv.2018.10.140

TYPE Original Research
PUBLISHED 21 August 2023
DOI 10.3389/fpubh.2023.1239378

OPEN ACCESS

EDITED BY
Zhaobin Sun,
Chinese Academy of Meteorological Sciences, China

REVIEWED BY
Ling Han,
National Institute for Communicable Disease Control and Prevention (China CDC), China
Faxue Zhang,
Wuhan University, China

*CORRESPONDENCE
Dongqing Ye
✉ ydq@ahmu.edu.cn
Xinyu Fang
✉ xinyufang@ahmu.edu.cn

[†]These authors have contributed equally to this work and share first authorship

RECEIVED 13 June 2023
ACCEPTED 24 July 2023
PUBLISHED 21 August 2023

CITATION
Chen H, Duan Q, Zhu H, Wan S, Zhao X, Ye D and Fang X (2023) Short-term association of CO and NO_2 with hospital visits for glomerulonephritis in Hefei, China: a time series study.
Front. Public Health 11:1239378.
doi: 10.3389/fpubh.2023.1239378

Short-term association of CO and NO_2 with hospital visits for glomerulonephritis in Hefei, China: a time series study

Haifeng Chen[1,2†], Qiong Duan[3†], Huahui Zhu[1,2], Shuai Wan[1,2], Xinyi Zhao[1,2], Dongqing Ye[1,2]* and Xinyu Fang[1,2]*

[1]Department of Epidemiology and Biostatistics, School of Public Health, Anhui Medical University, Hefei, Anhui, China, [2]Inflammation and Immune Mediated Diseases Laboratory of Anhui Province, Hefei, Anhui, China, [3]Department of Health Management Center, The First Affiliated Hospital of Anhui Medical University, Hefei, Anhui, China

Objective: Recent studies suggest air pollution as an underlying factor to kidney disease. However, there is still limited knowledge about the short-term correlation between glomerulonephritis (GN) and air pollution. Thus, we aim to fill this research gap by investigating the short-term correlation between GN clinical visits and air pollution exposure.

Methods: Between 2015 and 2019, daily GN visit data from two grade A tertiary hospitals in Hefei City were collected, along with corresponding air pollution and meteorological data. A generalized linear model integrated with a distributed lag nonlinear model was employed to analyze the relationship between GN visits and air pollutants. Moreover, we incorporated a dual pollutant model to account for the combined effects of multiple pollutants. Furthermore, subgroup analyses were performed to identify vulnerable populations based on gender, age, and season.

Results: The association between 23,475 GN visits and air pollutants was assessed, and significant positive associations were found between CO and NO_2 exposure and GN visit risk. The single-day lagged effect model for CO showed increased risks for GN visits from lag0 (RR: 1.129, 95% CI: 1.031–1.236) to lag2 (RR: 1.034, 95% CI: 1.011–1.022), with the highest risk at lag0. In contrast, NO_2 displayed a more persistent impact (lag1–lag4) on GN visit risk, peaking at lag2 (RR: 1.017, 95% CI: 1.011–1.022). Within the dual-pollutant model, the significance persisted for both CO and NO_2 after adjusting for each other. Subgroup analyses showed that the cumulative harm of CO was greater in the cold-season and older adult groups. Meanwhile, the female group was more vulnerable to the harmful effects of cumulative exposure to NO_2.

Conclusion: Our study indicated that CO and NO_2 exposure can raise the risk of GN visits, and female and older adult populations exhibited greater susceptibility.

KEYWORDS
air pollution, glomerulonephritis, carbon monoxide, nitrogen dioxide, distributed lag nonlinear model, time-series study air pollution, time-series study

1. Introduction

Glomerulonephritis (GN) is a heterogeneous collection of diseases identified by inflammatory damage within the renal small vessels and glomeruli (1). Ranking as the third and second leading causes of chronic kidney disease (CKD) (2) and end-stage renal disease (ESRD) (3) worldwide, GN has witnessed a considerable escalation in disease burden, with 6.9 million disability-adjusted life years (DALYs) due to CKD brought about GN in 2019, representing a 66% increase compared to 1990 (2). Despite progress in the nosogenesis of GN, the etiology of GN remains elusive. In recent years, environmental factors, notably air pollution, have been increasingly recognized as potential factors to the occurrence and progression of kidney diseases, including GN (4–8).

In a groundbreaking nanomedicine study (9), researchers have shown initial evidence of inhaled aerosol particles' potential to interact with renal tissue. The investigation revealed that gold nanoparticles with a diameter of ≤4 nm, when inhaled, can penetrate alveolar tissue, subsequently entering the bloodstream and being detected in participants' urine within three months. Supporting these findings, *in vivo* experiments (10–12) have demonstrated that sustained exposure to fine particulate matter of 2.5 μm or less in diameter ($PM_{2.5}$) may elicit renal inflammatory responses, structural damage, and oxidative stress in the kidneys of rodent models.

Despite these findings, only a few researchers have explored the correlation between atmospheric contaminant exposure and some clinical subtypes of GN. These studies (5–8) have provided some indications that exposure to elevated concentrations of $PM_{2.5}$ or acidic gases increases the risk of developing IgA nephropathy (only for $PM_{2.5}$) and nephrotic syndrome. However, there is still limited knowledge regarding the short-term link between GN and air pollution. Moreover, the combined effects of multiple pollutants and the differences in risk among populations with different demographic characteristics are still unclear.

To fill this research gap and elucidate the potential correlation between exposure to atmospheric contaminants and GN, we inquired into the short-term relationship between GN visits and air pollution exposure based on data from nephrology clinics at two grade a class 3 hospitals in Hefei, China, from 2015 to 2019. In addition, we further identified risk patterns across age and gender to explain the latent impact of discrepancies in susceptibility between subpopulations.

2. Materials and methods

2.1. Study area

The study was conducted in Hefei City, encompassing four Districts. As the capital of Anhui Province, Hefei spans 11,445 km^2 and houses approximately 8.19 million inhabitants (13). Situated within the mid-latitude zone (31°N, 117°E), Hefei experiences a humid subtropical monsoon climate typical of the region. As part of the "Yangtze River Delta" city cluster, Hefei is located in the coastal hinterland and serves as a vital industrial economic center. Consequently, the city grapples with significant air pollution issues, resulting in substantial public health concerns (14).

2.2. Study population

We amassed daily visit data for GN patients between 2015 and 2019 from the electronic medical record information systems of the First Affiliated Hospital of Anhui Medical University and the First Affiliated USTC. The variables compiled for the GN data encompassed age, gender, outpatient date, and residential address. The diagnostic criteria for GN are as follows: (1) Persistent proteinuria and/or hematuria over an extended period; (2) A history of prolonged hypertension, mild renal impairment, or/and edema; (3) Gradual, relentless progression of renal impairment, culminating in end-stage renal failure in later stages; (4) Symmetrical reduction in kidney size; and (5) Exclusion of secondary chronic nephritis syndrome, which would point toward a primary diagnosis (3, 15). The inclusion criteria for GN patients in this investigation were: (1) adherence to the diagnostic criteria for GN; (2) current address in Hefei; and (3) possession of hospital records. Furthermore, we applied exclusion criteria: (1) concurrent visits or a second visit to both hospitals within a brief period; (2) unclear diagnosis; (3) non-local residents; and (4) patients devoid of demographic information (e.g., age and gender). The data variables utilized in this study were anonymized, negating the need for ethical restrictions due to the absence of risk research requirements.

2.3. Air pollution and meteorological data

Air pollution data were procured from the average values of 10 ambient air pollution monitoring stations at the Hefei Environmental Monitoring Center, which included 24-h average levels of particulate matter of 10 μm or less in diameter (PM_{10}), $PM_{2.5}$, carbon monoxide (CO), nitrogen dioxide (NO_2), sulfur dioxide (SO_2), and daily maximum 8-h average ozone (O_3-8h) concentration. Concurrently, meteorological data were acquired from the China meteorological data network,[1] comprising daily average temperature (Temp), air humidity (RH), sunshine duration (SSD), and rainfall (RF).

2.4. Statistical analysis

By aggregating daily data, we employed a time-series study to calculate the risk of GN visits associated with short-term exposure to atmospheric contaminants from 2015 to 2019. As GN visits represent a low probability event within the population and exhibit overdispersion (Supplementary Table S1), a typical time series generalized linear model (GLM) with a quasi-Poisson connection was integrated with the distributed lag nonlinear model (DLNM) to determine the relationship between atmospheric contaminants and GN visits (16). The maximum delay on day 7 was utilized to capture the lagged impact of atmospheric contaminants (16).

To circumvent multicollinearity issues and account for the non-normal distribution (Supplementary Table S2) of variables, we performed Spearman correlation analysis on all variables,

1 http://data.cma.cn/

excluding those with correlation coefficients greater than 0.7 (17). The final model is presented below:

$$\log\left(E\left[Y_t\right]\right) = \alpha + \beta cb\left(X_0\right) + ns\left(time,dfs\right) + ns\left(meteorological\ factors,dfs\right) + ns\left(air\ pollutions,dfs\right) + as.factor\left(DOW\right) + as.factor\left(holiday\right) \quad (1)$$

Here, $E[Y_t]$ represents the anticipated count of patients with GN on day t; $cb(X_0)$ denotes the cross-basis function of the explanatory variable, which employs the "lin" function and "poly" function (degree = 3) to define the matrices of exposure and lag (0–7), respectively; α signifies the intercept; β stands for the cross-basis function's coefficient; ns represents the natural cubic spline (ns) function; time refers to the long-term time trend effect; dfs is the degrees of freedom, which is chosen based on the minimum value of the Akaike information criterion (AIC) applicable to the quasi-Poisson model (16). To control potential confounders, we introduced meteorological factors (Temp, RH, SSD, and RF) and other atmospheric contaminants (when X_0 is CO: NO_2, SO_2, O_3-8h, and PM_{10}) with ns function. Furthermore, we incorporated holiday parameters and DOW into the model as categorical variables to control the holiday and day-of-the-week effects.

We incorporated air pollutants individually upon constructing a working model (the core model) containing all control variables and verifying their suitability. Subsequently, we calculated the lag effect of atmospheric contaminants on GN visits from the current day (lag0) to 7 days prior (lag7). Previous research (18) has indicated that single-day lag models may neglect the cumulative effect. Consequently, we integrated the cumulative lag effect analysis into the model. Relative risk (RR) values and 95% confidence interval (CI) of air pollutant concentration per 10 μg/m^3 increment (1 mg/m^3 CO) were employed to calculate the short-term correlation between atmospheric contaminants and GN visits. Lastly, we used P50 as the reference base to calculate the association between the single-day effect and the cumulative lag effect of increasing air pollutant concentration on GN visits.

While the single pollutant model can predict the association between one atmospheric contaminant and GN visits, air pollutants often coexist and interact, resulting in a comprehensive impact on human health (19). To assess this potential combined effect and the robustness of the impact caused by pollutants, we established a dual pollutant model to study the intermingling effects of pollutants. The formulation of the dual pollutant model is as under:

$$\log\left(E\left[Y_t\right]\right) = \alpha + \beta_1 cb\left(X_a\right) + \beta_2 cb\left(X_b\right) + ns\left(time,dfs\right) + ns\left(air\ pollutions,dfs\right) + ns\left(meteorological\ factors,dfs\right) + as.factor\left(DOW\right) + as.factor\left(holiday\right) \quad (2)$$

Here, $cb(X_a)$ and $cb(X_b)$ are the cross-basis functions of the included dual pollutants, and β is the coefficient. All other parameters remain the same as in Model (1).

Additionally, to identify vulnerable populations and seasons, we further stratified the population by gender (male and female), season (cold season: November–April in the next year; warm season: May–October), and age (<65 and ≥ 65 years) to conduct subgroup analyses (20). Subsequently, the Wilcoxon signed-rank test was employed to confirm dissimilarities among the aforementioned subgroups.

2.5. Sensitivity analyses

To evaluate the reliability of the results, we carried out sensitivity assessments. First, we varied the dfs (3–8 dfs) (21) for the *time*, *air pollutions*, and *meteorological factors*. Second, we adjusted the maximum delay of air pollutants to intervals of 14 and 21 days to examine the harvesting effect (22, 23). Lastly, we set the reference values of all pollutants to 0, plotted the overall exposure-response curves, and calculated the relative risk (RR) values for the corresponding pollutants.

All statistical computations were performed with the aid of R software (version 4.2.3). Statistical significance of the effect was acknowledged when $p < 0.05$ (two-sided).

3. Results

3.1. Descriptive analysis

Between 2015 and 2019, the electronic medical record information system registered 23,475 GN visits at the two hospitals, comprising 47.23% males (11,088), 10.02% older adults aged ≥65 (2,352), and 49.37% occurring during the cold season (11,589). Throughout the research duration, the daily mean levels (with standard deviation) of CO, NO_2, PM_{10}, $PM_{2.5}$, SO_2, and O_3-8h were 0.84 (0.28) mg/m^3, 40.31 (17.76) μg/m^3, 76.17 (38.90) μg/m^3, 52.29 (33.41) μg/m^3, 10.55 (6.08) μg/m^3, and 86.32 (44.01) μg/m^3, respectively. Additionally, Temp, RH, SSD, and RF (with standard deviation) were found to be 16.85 (9.21)°C, 76.51 (11.99)%, 4.92 (4.02) h, and 3.18 (8.88) mm, respectively (Table 1). To better illustrate the geographical context of our study, we have included a map showcasing the locations of these two hospitals and 10 ambient air pollution monitoring stations within the city (Figure 1). Besides, the time series distribution of the data over 5 years is illustrated in Supplementary Figure S1. The Spearman correlation analysis revealed a strong correlation between $PM_{2.5}$ with PM_{10} ($r_s = 0.806$, $p < 0.001$) and CO ($r_s = 0.812$, $p < 0.001$), prompting its exclusion from the model (Supplementary Figure S2).

3.2. Overall effects

The overall exposure-response relationship between atmospheric contaminants (CO, NO_2, PM_{10}, SO_2, and O_3-8h) and GN visits is predicted by the DLNM model (Supplementary Figure S3). The curves demonstrated a positive correlation between CO and NO_2 exposure and an escalated risk of GN visits when the maximum lag was 7 days (Supplementary Figures S3A,B). No significant overall exposure-response associations were observed between SO_2, PM_{10}, and O_3-8h and GN visits, as their 95% CIs included the null value (RR = 1.000) throughout the entire range (Supplementary Figures S3C–E). Consequently, the model included PM_{10}, SO_2, and O_3-8h as covariates for subsequent analyses to account for potential confounding effects.

TABLE 1 Descriptive statistics of the daily outpatient visits for GN, air pollutant concentrations, and meteorological parameters in Hefei City, 2015–2019.

Variables	*n* (%)	Mean ± *sd*	Min	P_{25}	P_{50}	P_{75}	Max
Visits							
Total	23,475 (100.00)	12.86 ± 9.45	0.00	5.00	12.00	19.00	57.00
Gender							
Male	11,088 (47.23)	6.07 ± 4.86	0.00	2.00	5.00	9.00	31.00
Female	12,387 (52.77)	6.78 ± 5.35	0.00	2.00	6.00	10.00	30.00
Age (years)							
<65	21,123 (89.98)	11.57 ± 8.44	0.00	4.00	11.00	17.00	47.00
≥65	2,352 (10.02)	1.29 ± 1.66	0.00	0.00	1.00	2.00	12.00
Season							
Cold	11,589 (49.37)	12.79 ± 9.56	0.00	4.00	12.00	19.00	50.00
Warm	11,886 (50.63)	12.92 ± 9.33	0.00	5.00	12.00	18.00	57.00
Air pollutant concentration							
CO (mg/m^3)		0.84 ± 0.28	0.30	0.60	0.80	1.00	2.60
NO_2 (μg/m^3)		40.31 ± 17.76	9.00	27.00	36.00	51.00	125.00
SO_2 (μg/m^3)		10.55 ± 6.08	2.00	6.00	9.00	13.00	51.00
PM_{10} (μg/m^3)		76.17 ± 38.90	8.00	48.00	71.00	97.00	308.00
$PM_{2.5}$ (μg/m^3)		52.29 ± 33.41	6.00	29.00	44.00	66.00	237.00
O_3-8h (μg/m^3)		86.32 ± 44.01	4.00	52.00	79.00	115.00	241.00
Meteorological conditions							
Temp (°C)		16.85 ± 9.21	−6.20	8.60	17.60	24.50	34.80
RH (%)		76.51 ± 11.99	39.20	68.70	77.00	85.70	98.30
SSD (h)		4.92 ± 4.02	0.00	0.40	5.10	8.50	12.90
RH (mm)		3.18 ± 8.88	0.00	0.00	0.00	1.60	134.00

The exposure-response correlation between GN visits and two atmospheric contaminants, CO and NO_2, reveals a significant positive association at low lag days when concentrations of CO and NO_2 are high (with reference concentrations of 0.8 mg/m^3 and 36 μg/m^3, respectively). However, as the lag time increases, exposure to elevated levels of CO and NO_2 appeared to diminish the risk of GN visits (Figures 2, 3).

3.3. Association between air pollutants and GN visits in a single pollutant model

Our analysis revealed variations in the RR values corresponding to 1 mg/m^3 per CO concentration increment and 10 μg/m^3 per NO_2 concentration increment across different lag days for GN visitations (Figure 4; Supplementary Table S3). In the single-day lag effect model for CO, the risks for GN visits were positively associated with CO from lag0 (RR: 1.129, 95% CI: 1.031–1.236) to lag2 (RR: 1.034, 95% CI: 1.000–1.070), peaking at lag0. Conversely, the risks decreased at lag4 (RR: 0.968, 95% CI: 0.943–0.993) and lag5 (RR: 0.961, 95% CI: 0.930–0.993). Cumulative lagged effects analysis of CO revealed increased risks of GN visits for all lag days except lag06, and the risk reached its maximum value at lag02 (RR: 1.263, 95% CI: 1.132–1.410).

In contrast to CO, the harm of NO_2 came more slowly. When considering a single-day lag, increased NO_2 exposure elevated GN visit risk during the preceding 4 days (lag1–lag4), peaking at lag2 (RR: 1.017, 95% CI: 1.011–1.022). However, the risk decreased at lag6 (RR: 0.994, 95% CI: 0.989–0.998). Furthermore, cumulative lag models showed harmful NO_2 effects persisting from lag02 to lag07, with the highest risk observed on lag04 (RR: 1.041, 95% CI: 1.021–1.060).

3.4. Association between air pollutants and GN visits in a dual-pollutant model

In the dual-pollutant model, the significance of NO_2 and CO persisted when controlling for each other. With NO_2 adjustment, the single-day lagged effect curve of CO exposure on GN risk exhibited a U-shaped pattern, peaking on exposure day (RR: 1.193, 95% CI: 1.086–1.310) and at the lowest point on the lag3 (RR: 0.936, 95% CI: 0.905–0.968; Figure 5A; Supplementary Table S4). In the cumulative lag model, CO exposure only increased GN visits during the first 3 days (lag01–lag03; Figure 5B; Supplementary Table S4).

After adjusting for CO, the single-day lagged effect trend of NO_2 followed an inverted U-shape with the prolongation of lag days, peaking at lag3 (RR: 1.017, 95% CI: 1.011–1.023; Figure 5C; Supplementary Table S4). In the cumulative lagged effect model of NO_2, lag03–lag07 were positively associated with GN visit risk, and the RR value peaked at lag05 (RR: 1.051, 95% CI: 1.029–1.074; Figure 5D; Supplementary Table S4).

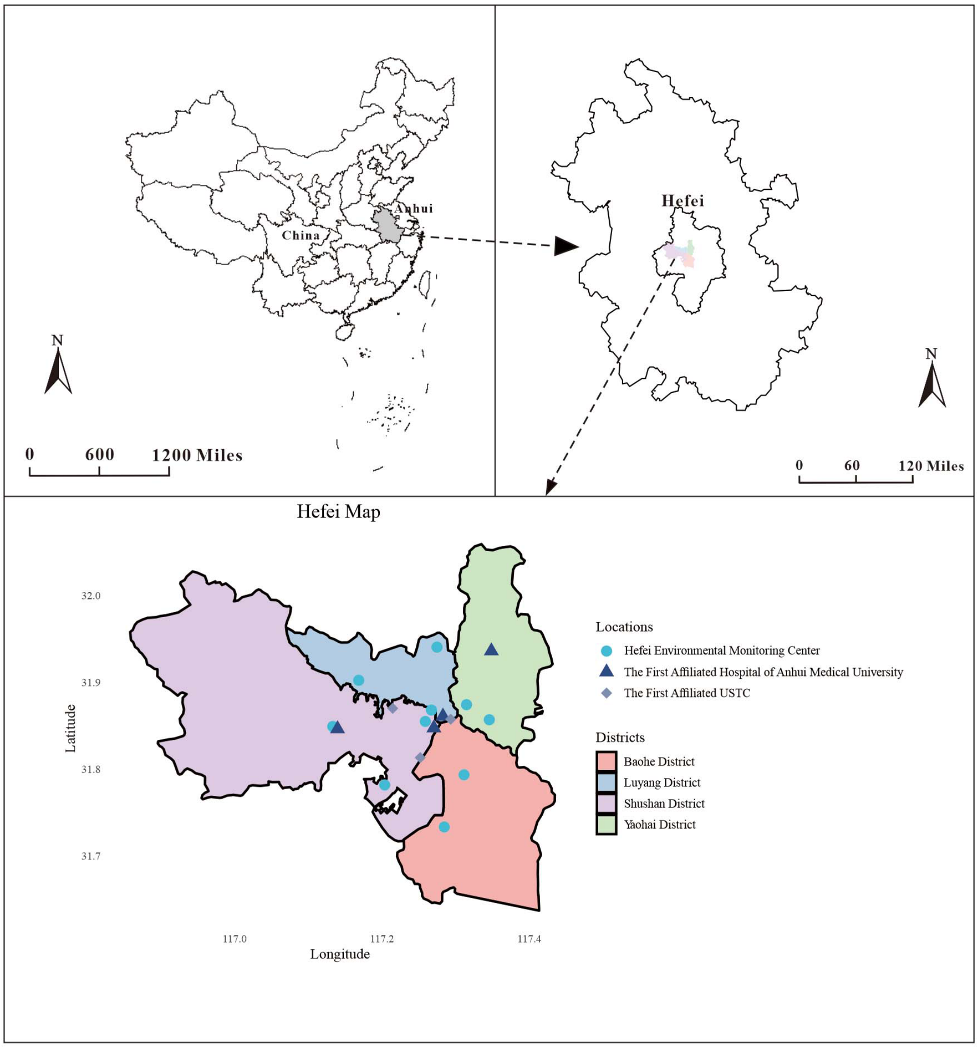

FIGURE 1
Geographical distribution of environmental monitoring stations and the two hospitals in Hefei.

3.5. Subgroup analysis

Upon conducting stratified analyses based on sex, age, and season, we found that contact with CO and NO_2 was linked to an increased risk of GN visits across all subgroups (all $p < 0.05$) except for the cumulative lagged effect of the seasonal grouping of NO_2 (Supplementary Tables S4–S6; Figures 6–9). However, our results from the Wilcoxon signed-rank test showed that only the differences in cumulative lag effect for the age group, season group of CO, and gender group of NO_2 had statistically significant (Supplementary Table S7). Notably, the older adult and cold-season groups exhibited a heightened susceptibility to the cumulative lagged effect of CO exposure compared to age < 65 years and warm-season groups. The female group was more vulnerable to the harmful effects of cumulative exposure to NO_2.

3.6. Sensitivity analyses

The AIC values of the model when choosing different *dfs* (3–8) for *time*, *air pollutions*, and *meteorological factors* are presented in Supplementary Table S8. In the CO and NO_2 models, the AIC value is both the smallest (CO: 11250.67; NO_2:11246.88) when the *dfs* for *time*, *air pollutions*, and *meteorological factors* are 7, 5, and 7, respectively.

Sensitivity analysis results indicated that the consequences of CO and NO_2 contact on the risk of GN visits remain generally robust after varying the *dfs* of the *time*, *air pollutions*, and *meteorological factors* (Supplementary Figures S4–S9) and regulating the maximum lag periods for CO and NO_2 (Supplementary Figures S10, S11). After setting the reference values of each pollutant model to 0, our overall exposure effect results remained unchanged (Supplementary Figures S3, S12). Furthermore, the subsequent analyses of single-day and cumulative lag effects for CO and NO_2 were highly consistent with our previous findings (Figure 4; Supplementary Figure S13; Supplementary Tables S3, S9).

4. Discussion

In this investigation, we analyzed nephritis outpatient records from the two prominent grade A tertiary hospitals from 2015 to 2019 to quantitatively assess the correlation between atmospheric

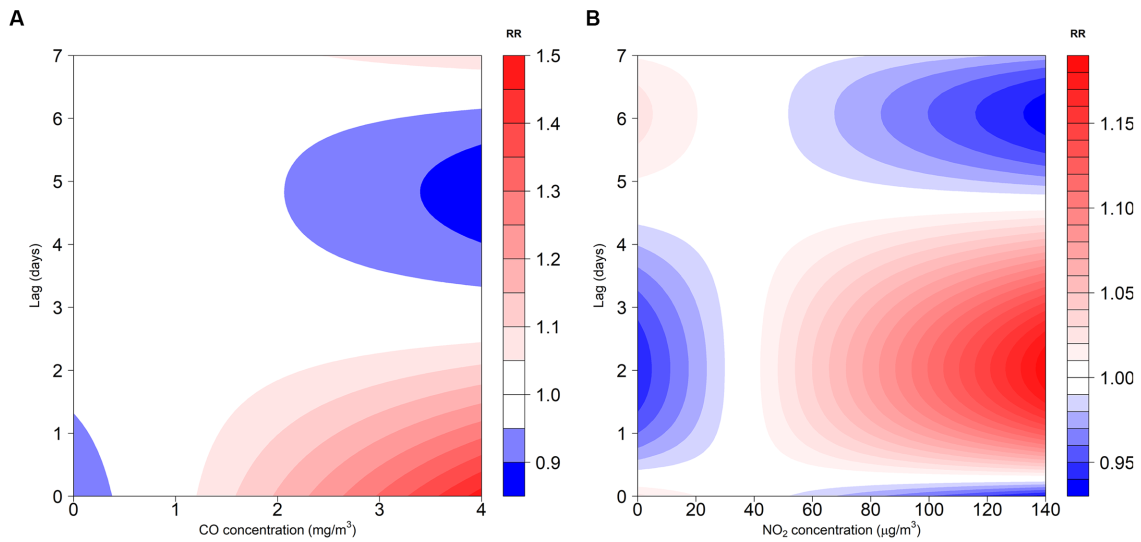

FIGURE 2
Contour plot for the association between air pollutants (CO and NO_2) and GN visits in Hefei, China, 2015–2019. **(A)** Contour plot of CO; **(B)** Contour plot of NO_2. CO, carbon monoxide; NO_2, nitrogen dioxide; and RR, relative risk. The P_{50} was used as the reference concentration. The P_{50} concentration of CO is 0.8 mg/m^3 and the P_{50} concentration of NO_2 is 36 μg/m^3.

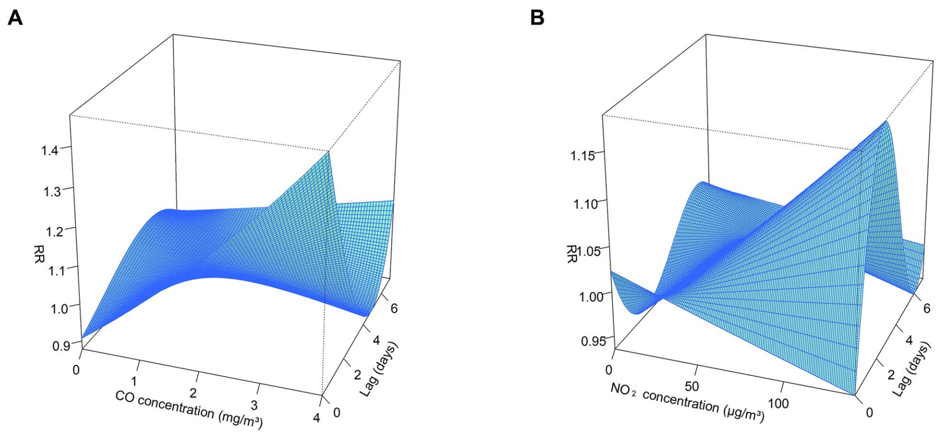

FIGURE 3
3D plot for the association between air pollutants (CO and NO_2) and GN visits in Hefei, China, 2015–2019. **(A)** 3D plot of CO; **(B)** 3D plot of NO_2. CO, carbon monoxide; NO_2, nitrogen dioxide; and RR, relative risk. The P_{50} was used as the reference concentration. The P_{50} concentration of CO is 0.8 mg/m^3 and the P_{50} concentration of NO_2 is 36 μg/m^3.

contaminants and GN visits. Our findings indicated that contact with CO and NO_2 were significantly associated with an elevated risk of GN-related hospital visits, suggesting that these pollutants might be a potential risk factor for GN. For each 1 mg/m^3 elevation in CO level, the GN visit risk escalated by 12.9% in the single-day lag model (lag0, 95% CI: 3.1–23.6%) and by up to 26.3% in the cumulative lag model (lag02, 95% CI: 13.2–41.0%). Meanwhile, every 10 μg/m^3 elevation in NO_2 concentration resulted in a 1.7% increase in GN visit risk (lag2, 95% CI: 1.1–2.2%) in the single-day lag model and a 4.1% increase in the cumulative lag model (lag04, 95% CI: 2.1–6.0%).

Previous epidemiological studies examining the correlation between atmospheric contaminants and GN incidence are scarce, focusing more on CKD or ESRD. Our results are supported by a study (24) conducted on a national cohort of US veterans, which observed a positive correlation between increased interquartile ranges (IQR) of CO and NO_2 concentrations and the decline of glomerular filtration rate, as well as the incidence and progression of CKD and ESRD. However, some studies (25, 26) reported damages of CO exposure on kidney function without identifying an association between kidney disease and NO_2 exposure. A retrospective cohort research (25) of CKD patients in Seoul, South Korea, confirmed the significant correlation between CO and $PM_{2.5}$ and the long-term mortality risks in CKD patients, but no effects of other pollutants (e.g., NO_2) on CKD patient mortality were observed. Another study (26) from Korea found that exposure to CO and SO_2 had the most severe perniciousness on CKD clinic visits. In contrast, studies by Łukasz Kuźma et al. (27) and Szu-Ying Chen et al. (28) identified increased mean levers of NO_2 and $PM_{2.5}$ as relevant factors for the prevalence and progression of CKD in Bialystok, Poland, and Chinese Taipei, respectively. Interestingly, a national study (29) based on the Chinese CKD survey only demonstrated that long-term

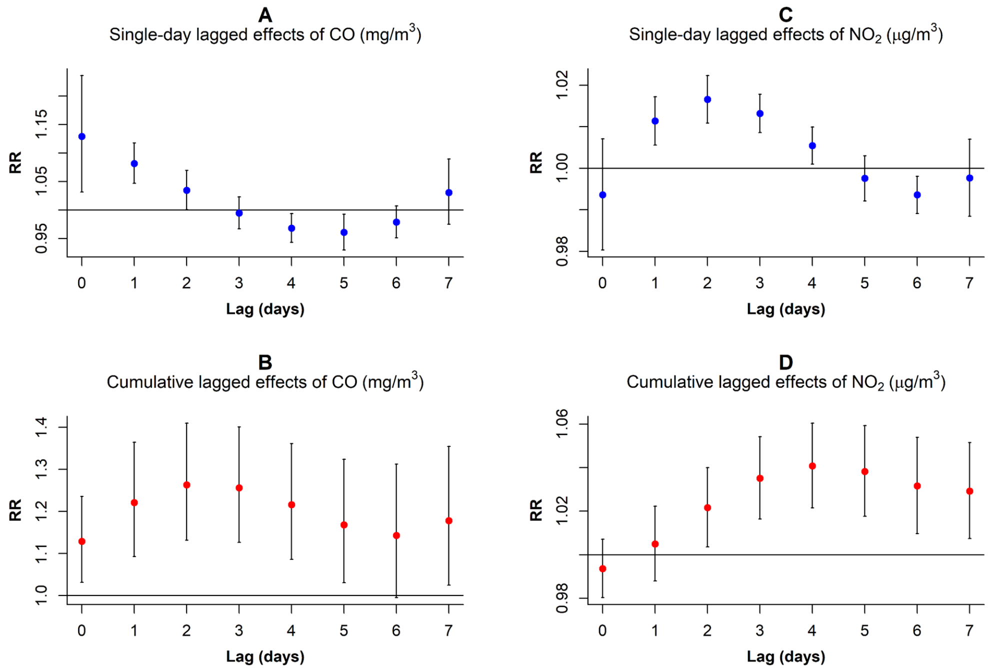

FIGURE 4
RR values and 95% *CI* in the number of daily outpatient visits for GN associated with increases of 1 mg/m^3 in CO and 10 μg/m^3 in NO_2 concentrations at different lag days. **(A)** Single-day lagged effects of CO; **(B)**Cumulative lagged effects of CO; **(C)** Single-day lagged effects of NO_2; **(D)** Cumulative lagged effects of NO_2. CO, carbon monoxide; NO_2, nitrogen dioxide; and RR, relative risk.

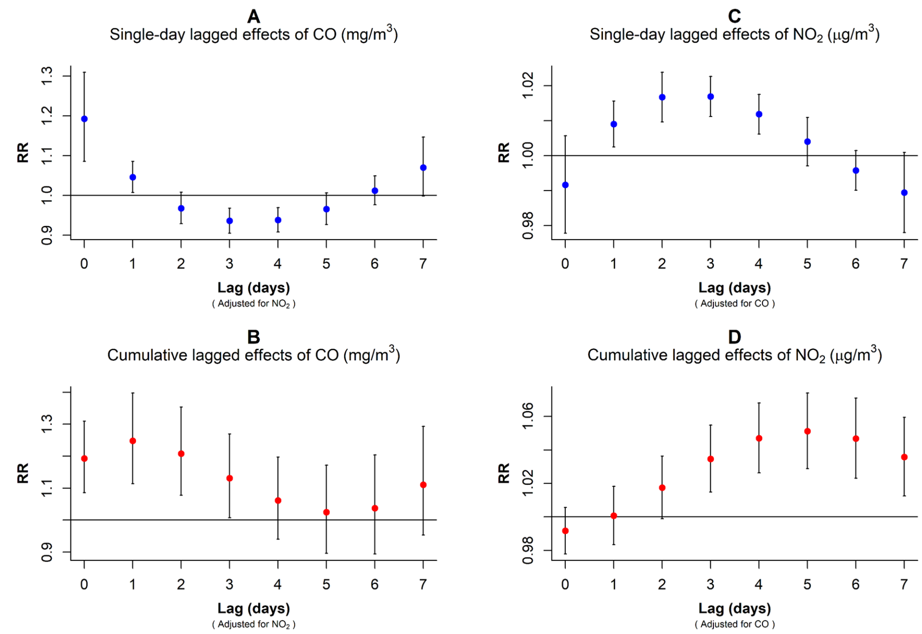

FIGURE 5
RR values and 95% *CI* in the number of daily outpatient visits for GN associated with increases of 1 mg/m^3 in CO and 10 μg/m^3 in NO_2 concentrations in the dual-pollutant model. **(A,B)** Harmful effects of CO exposure after correcting for NO_2 interference. **(C,D)** Harmful effects of NO_2 exposure after correcting for CO interference. CO, carbon monoxide; NO_2, nitrogen dioxide; and RR, relative risk.

exposure to O_3 elevated the risk of CKD in the general Chinese population. The discrepancies and heterogeneity between these studies may arise from geographical variations, participant sizes, data sources, exposure assessment methods, and distinct air pollution conditions across countries. There are several plausible explanations for the discrepancies between our findings and those of other studies: (1)

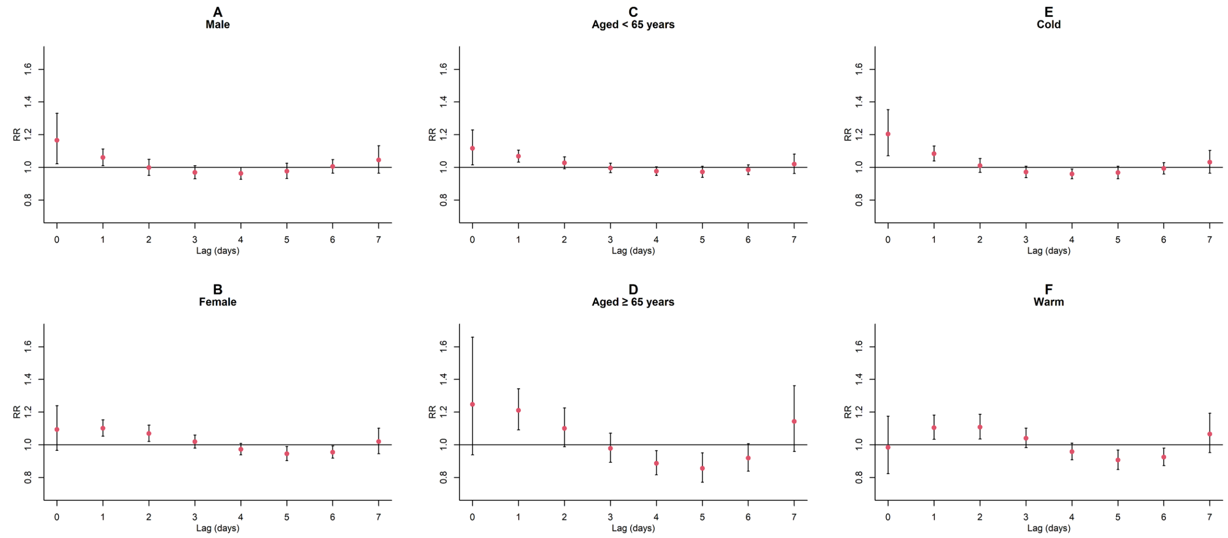

FIGURE 6
Single-day lagged *RR* values and 95% *CI* of GN visits per 1 mg/m^3 increase in CO concentration in a model stratified by gender, age, and season. **(A,B)** Single-day lagged effects of CO grouped by gender; **(C,D)** Single-day lagged effects of CO grouped by age; **(E,F)** Single-day lagged effects of CO grouped by season. Harmful effects of CO stratified by sex, age, and season.

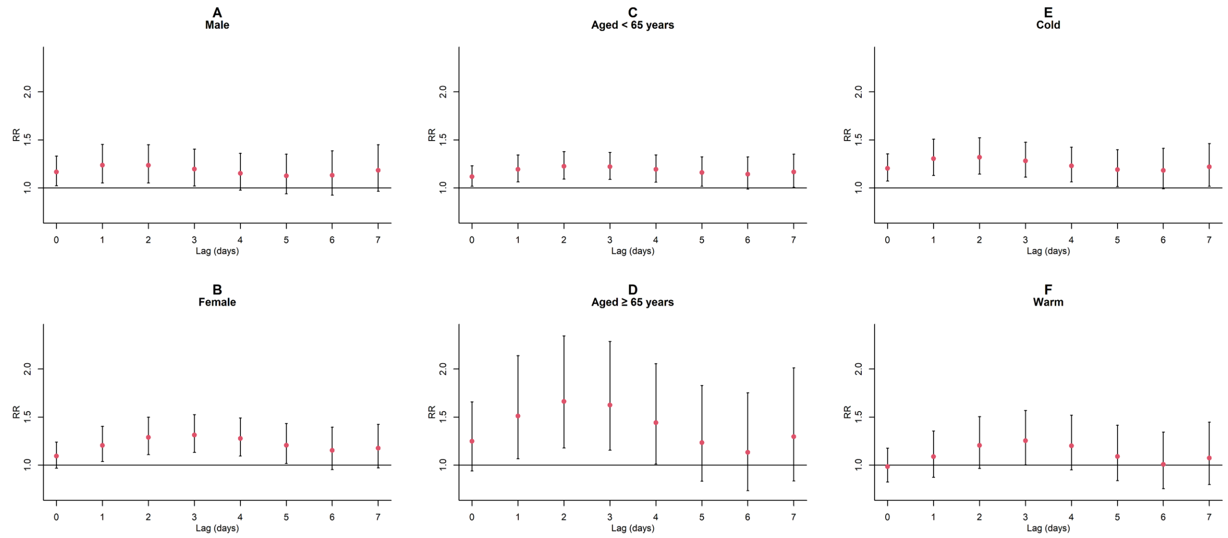

FIGURE 7
Cumulative lagged *RR* values and 95% *CI* of GN visits per 1 mg/m^3 increase in CO concentration in a model stratified by gender, age, and season. **(A,B)** Cumulative lagged effects of CO grouped by gender; **(C,D)** Cumulative lagged effects of CO grouped by age; **(E,F)** Cumulative lagged effects of CO grouped by season. Harmful effects of CO stratified by sex, age, and season.

Substantial differences in air pollution levels between studies could result in the absence of correlation, complicating the comparison of results. For instance, the median annual mean levers of NO_2 and $PM_{2.5}$ in Bialystok, Poland, were 13.1 and 10.9 μg/m^3, respectively (27), while in Taipei, China, the annual average concentrations were 24.3 and 23.5 μg/m^3, respectively (28). Throughout the study period in Hefei City, the levels of NO_2, CO, PM_{10}, $PM_{2.5}$, SO_2, and O_3-8h were 40.31 μg/m^3, 0.84 mg/m^3, 76.17 μg/m^3, 52.29 μg/m^3, 10.55 μg/m^3, and 86.32 μg/m^3, respectively. These considerable differences can partially account for the lack of a significant correlation between $PM_{2.5}$ exposure and our study's increased risk of GN visits. (2) The effects of participants' social and economic status and risky behaviors may also influence the results. Individuals in countries or regions with higher *per capita* income typically have better education and higher income, potentially providing protective effects against the development of kidney disease (30–32). (3) Variations in disease definitions and diagnostic criteria used across studies may lead to inconsistent results. Although GN ranks as the third and second primary cause of CKD (2) and ESRD (3), the biochemical markers and clinical manifestations used for diagnosis are not identical. Furthermore, the data types and study designs employed in different studies could also affect the results. For example, some studies utilized cross-sectional designs and generalized additive models, while our study adopted time series analysis and DLNM, which might have contributed to differences in the results between studies.

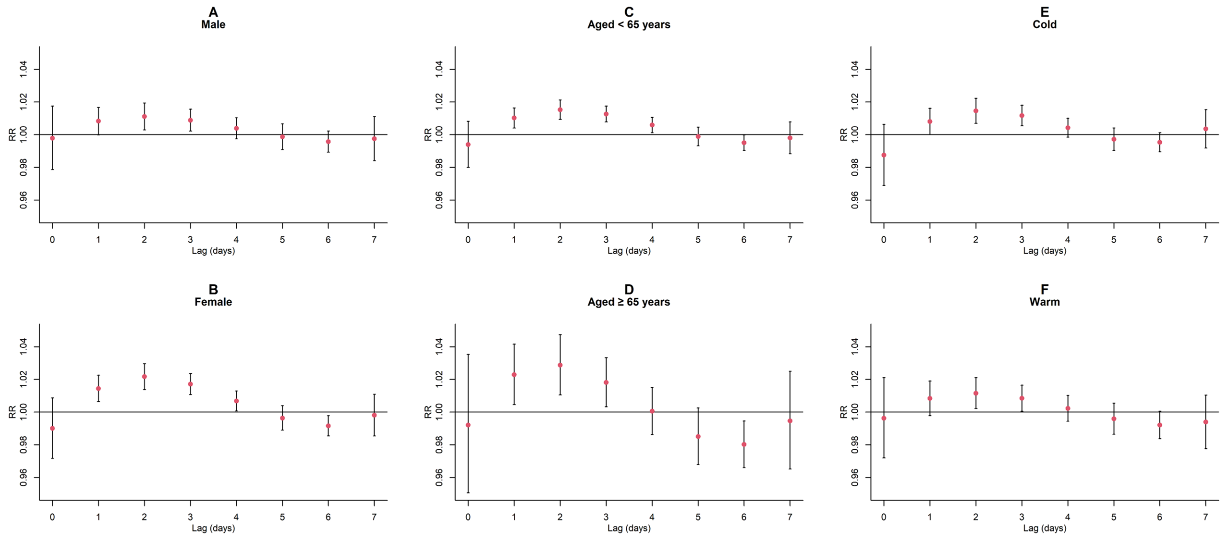

FIGURE 8
Single-day lagged *RR* values and 95% *CI* of GN visits per 10 μg/m^3 increase in NO_2 concentration in a model stratified by gender, age, and season. **(A,B)** Single-day lagged effects of NO_2 grouped by gender; **(C,D)** Single-day lagged effects of NO_2 grouped by age; **(E,F)** Single-day lagged effects of NO_2 grouped by season. Harmful effects of NO_2 stratified by sex, age, and season.

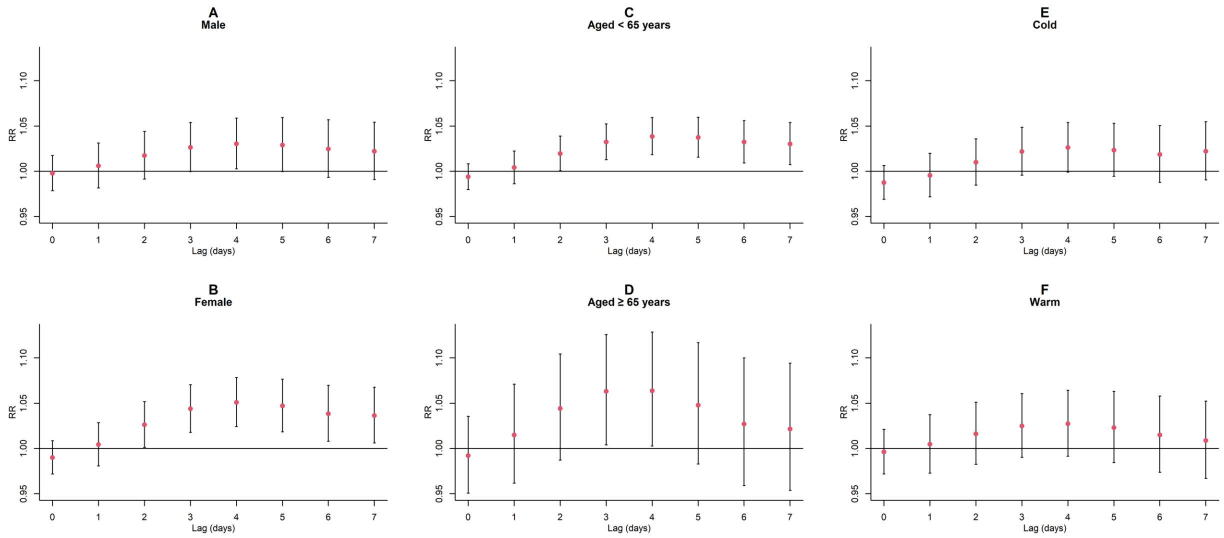

FIGURE 9
Cumulative lagged *RR* values and 95% *CI* of GN visits per 10 μg/m^3 increase in NO_2 concentration in a model stratified by gender, age, and season. **(A,B)** Cumulative lagged effects of NO_2 grouped by gender; **(C,D)** Cumulative lagged effects of NO_2 grouped by age; **(E,F)** Cumulative lagged effects of NO_2 grouped by season. Harmful effects of NO_2 stratified by sex, age, and season.

Previous research on air pollution and public health had commonly employed single-pollutant models, neglecting the complex interplay among various pollutants and their collective impact on environmental and human health. In this study, we incorporated both CO and NO_2 into our model framework. After adjusting for NO_2 interference, we observed a reduction in the lagged impacts of CO exposure on the risk of GN visits. The RR values diminished more swiftly with increasing lag time but still peaked on the day of exposure (lag0) in the single-day lag model. This phenomenon aligns with previous research (26) examining emergency room visits due to kidney disease concerning ambient air pollution in Korea. In order to examine whether this phenomenon is due to the harvesting effect (22, 23), we reevaluated the risk correlation between CO exposure and GN visits for extended maximum lag days (14 and 21), as depicted in Supplementary Figure S10. The absence of a cosine-like plotting pattern was observed, indicating that it is unlikely that the harvesting effect would have a substantial impact on our estimates. Correspondingly, after controlling for CO interference, the detrimental effects of NO_2 exposure manifested later, and the decline in RR values decelerated compared to the single-pollutant model. This phenomenon may be attributed to the differential absorption and metabolism rates of various air pollutants in the human body. For instance, a CO inhalation experiment (33) indicated rapid blood

CO saturation within 4–5 h, while a NO_2 inhalation study (34) demonstrated a more gradual response to exposure. Therefore, it is essential to recognize that high CO concentrations may significantly elevate the risk of GN visits and various comorbidities on the day of exposure, while increased attention should be given to the harmful effects of NO_2 in the days following exposure.

Gender, age, and season are considered influential factors in health assessments and are often standardized as appropriate stratification methods within populations. In this study, we identified compelling results among various subpopulations: females were found to be more susceptible to the effects of NO_2 than males. This observation may be attributed to the fact that non-smokers are more sensitive to air pollution than smokers (35, 36), and that smoking rates among females are much lower than among males in China (37). Furthermore, regarding the association between age and GN visit risk, CO exhibited more excellent detrimental effects on older than younger individuals. This finding aligns with previous researches (38, 39) examining the link between atmospheric contaminants and disease. The underlying cause may be the higher prevalence of chronic diseases such as diabetes (40), and heart disease (41) among older adults, which are linked to the nosogenesis of kidney diseases (42). Concurrently, CO exposure increases the risk of developing diabetes (43, 44), and heart disease (45, 46). These discoveries emphasize the importance of controlling health indicators such as blood glucose and blood pressure levels to maintain kidney function in older adults. In addition, CO exposure was more strongly associated with GN visits during the cold season. This observation could be explained by the physiological adaptations under colder conditions, where the human body's blood vessels constriction, intensifying renal ischemia and decreasing renal resistance to both hypoxia and harmful substances (47). Consequently, susceptible populations in highly polluted environments during the cold season, such as females and older individuals, should adopt additional safeguard procedures to alleviate the deleterious influences of atmospheric contaminants on their health.

Various potential biological mechanisms may help elucidate the connection between NO_2 and CO exposure and the elevated risk of GN visits. CO readily binds to hemoglobin, increasing its affinity for oxygen and subsequently leading to tissue hypoxia (48). Insufficient renal oxygen supply may cause glomerular capillary constriction, impacting filtration function and decreasing glomerular filtration rate (47). Furthermore, tissue hypoxia may result in tubular dysfunction. Animal studies (49) have demonstrated that energy metabolism in renal tubular epithelial cells is impaired under oxygen-deprived conditions, weakening the reabsorption and secretion of filtrate. Additionally, renal hypoxia can stimulate excessive matrix protein production, leading to tissue hardening, functional impairment, and interstitial fibrosis (50). Compared to CO, the biological mechanisms underlying renal injury caused by NO_2 exposure are more complex. Firstly, NO_2 may induce renal damage by increasing oxidative stress responses. Toxicological evidence (51) from an animal model suggests that NO_2 exposure elevates oxidative stress reactions. Moreover, Mirowsky et al. (52) found that genes associated with oxidative stress were highly expressed in primary human bronchial epithelial cells under NO_2 induction, while substantial evidence (53–55) indicates that oxidative stress has detrimental effects on the kidneys. Secondly, toxicological evidence (56, 57) from animal experiments implies that NO_2 might straight damage renal function by augmenting the risk of glomerular damage, expansion, hyperfiltration, and heightening susceptibility to infection. Lastly, NO_2 can activate immune cells, inducing the production of pro-inflammatory cytokines (e.g., TNF-α, IL-1β) (58–60), leading to renal inflammatory responses (61–63).

As an observational investigation, our research presents several limitations that should be considered. Firstly, it is unable to establish causality between atmospheric contaminants and the GN visit risk, and the findings may be subject to residual confounding. Moreover, our study is concentrated solely on Hefei and due to its unique geographical and environmental attributes, the findings might not be universally applicable to other areas. Lastly, we used fixed-site monitoring data to assess air pollution exposure, which does not provide information about individual or indoor exposure levels. Future research should prioritize comprehensive, multi-city analyses and the collection of personal exposure data to assess better potential health risks associated with air pollution exposure.

Notwithstanding its limitations, the present investigation holds considerable merit for multiple reasons. To begin with, it represents the first study that quantifies short-term correlations between CO and NO_2 exposure and the occurrence of GN clinic visits, employing time-series analysis techniques. This exploratory study contributes to the existing body of research in this domain, providing preliminary insights into the potential implications of air pollutants on GN. Furthermore, this study's outpatient and meteorological datasets are complete. This comprehensive data allowed for the robust examination of the correlations between atmospheric contaminants and the risk of GN visits and the identification of susceptible subpopulations. Consequently, our findings have the potential to inform the optimization of health policies and regulations aimed at mitigating the impact of GN.

5. Conclusion

In summary, the present investigation revealed a significant correlation between contact with CO and NO_2 and the rising risk of GN visits. Notably, the detrimental impact of CO was discernible on the day of exposure, whereas NO_2's adverse consequences emerged in subsequent days. Further stratified analysis unveiled that the cumulative harm of CO was greater in cold seasons and older adult groups. Simultaneously, the female population was more susceptible to the harmful effects of cumulative NO2 exposure. Collectively, the findings of this study offer valuable proof that could bolster public health endeavors to mitigate the impacts of GN via synergistic efforts encompassing efficient environmental regulations and preventive approaches.

Data availability statement

The data analyzed in this study are subject to the following licenses/restrictions: the dataset is not publicly available in the article and can be requested from the authors upon request. However, only the basic data of deidentified individuals in the article are provided, and proposals for data acquisition can be submitted within 36 months after the publication of the article. Requests to access these datasets should be directed to XF, xinyufang@ahmu.edu.cn.

Author contributions

HC: conceptualization, data curation, formal analysis, investigation, methodology, validation, visualization, writing—original draft, and writing—review and editing. QD: data curation, writing—original draft, and writing—review and editing. HZ, SW, and XZ: writing—review and editing. DY: data curation, funding acquisition, project administration, resources, supervision, and writing—review and editing. XF: data curation and writing—review and editing. All authors contributed to the article and approved the submitted version.

Funding

This work was funded by Foundation of Anhui Educational Committee (KJ2020A0223); Inflammation and Immune Mediated Diseases Laboratory of Anhui Province Open Project (IMMDL202110); and The Fund of Anhui Provincial Laboratory of Inflammation and Immune Mediated Diseases (Population Epidemiology Study).

Conflict of interest

The authors declare that the research was conducted in the absence of any commercial or financial relationships that could be construed as a potential conflict of interest.

Publisher's note

All claims expressed in this article are solely those of the authors and do not necessarily represent those of their affiliated organizations, or those of the publisher, the editors and the reviewers. Any product that may be evaluated in this article, or claim that may be made by its manufacturer, is not guaranteed or endorsed by the publisher.

Supplementary material

The Supplementary material for this article can be found online at: https://www.frontiersin.org/articles/10.3389/fpubh.2023.1239378/full#supplementary-material

References

1. Nalewajska M, Gurazda K, Styczyńska-Kowalska E, Marchelek-Myśliwiec M, Pawlik A, Dziedziejko V. The role of Micro RNAs in selected forms of glomerulonephritis. *Int J Mol Sci*. (2019) 20:20. doi: 10.3390/ijms20205050

2. Hu J, Ke R, Teixeira W, Dong Y, Ding R, Yang J, et al. Global, regional, and National Burden of CKD due to glomerulonephritis from 1990 to 2019: a systematic analysis from the global burden of disease study 2019. *Clin J Am Soc Nephrol*. (2023) 18:60–71. doi: 10.2215/cjn.0000000000000017

3. Chadban SJ, Atkins RC. Glomerulonephritis. *Lancet*. (2005) 365:1797–806. doi: 10.1016/S0140-6736(05)66583-X

4. Couser WG, Johnson RJ. The etiology of glomerulonephritis: roles of infection and autoimmunity. *Kidney Int*. (2014) 86:905–14. doi: 10.1038/ki.2014.49

5. Luo C, Ouyang Y, Shi S, Li G, Zhao Z, Luo H, et al. Particulate matter of air pollution may increase risk of kidney failure in IgA nephropathy. *Kidney Int*. (2022) 102:1382–91. doi: 10.1016/j.kint.2022.08.020

6. Lin SY, Hsu WH, Lin CL, Lin CC, Lin CH, Wang IK, et al. Association of Exposure to fine-particulate air pollution and acidic gases with incidence of nephrotic syndrome. *Int J Environ Res Public Health*. (2018) 15:15. doi: 10.3390/ijerph15122860

7. Xu X, Wang G, Chen N, Lu T, Nie S, Xu G, et al. Long-term exposure to air pollution and increased risk of membranous nephropathy in China. *J Am Soc Nephrol*. (2016) 27:3739–46. doi: 10.1681/asn.2016010093

8. Wang C, Tsai JD, Wan L, Lin CL, Wei CC. Association between gaseous air pollutants and idiopathic nephrotic syndrome in children: a 12-year population-based cohort study. *Ital J Pediatr*. (2022) 48:70. doi: 10.1186/s13052-022-01269-8

9. Miller MR, Raftis JB, Langrish JP, McLean SG, Samutrtai P, Connell SP, et al. Inhaled nanoparticles accumulate at sites of vascular disease. *ACS Nano*. (2017) 11:4542–52. doi: 10.1021/acsnano.6b08551

10. Nemmar A, Karaca T, Beegam S, Yuvaraju P, Yasin J, Hamadi NK, et al. Prolonged pulmonary exposure to diesel exhaust particles exacerbates renal oxidative stress, inflammation and DNA damage in mice with adenine-induced chronic renal failure. *Cell Physiol Biochem*. (2016) 38:1703–13. doi: 10.1159/000443109

11. Yuan CS, Lai CS, Chang-Chien GP, Tseng YL, Cheng FJ. Kidney damage induced by repeated fine particulate matter exposure: effects of different components. *Sci Total Environ*. (2022) 847:157528. doi: 10.1016/j.scitotenv.2022.157528

12. Tavera Busso I, Mateos AC, Juncos LI, Canals N, Carreras HA. Kidney damage induced by sub-chronic fine particulate matter exposure. *Environ Int*. (2018) 121:635–42. doi: 10.1016/j.envint.2018.10.007

13. Statistics APBo (2022). Anhui statistical yearbook—2019.2019 12-09. Available at: http://tjj.ah.gov.cn/oldfiles/tjj/tjjweb/tjnj/2019/cn.html (Accessed September 12, 2022).

14. Zhang C, Ding R, Xiao C, Xu Y, Cheng H, Zhu F, et al. Association between air pollution and cardiovascular mortality in Hefei, China: a time-series analysis. *Environ Pollut*. (2017) 229:790–7. doi: 10.1016/j.envpol.2017.06.022

15. Sethi S, Haas M, Markowitz GS, D'Agati VD, Rennke HG, Jennette JC, et al. Mayo Clinic/Renal Pathology Society consensus report on pathologic classification, diagnosis, and reporting of GN. *J Am Soc Nephrol*. (2016) 27:1278–87. doi: 10.1681/asn.2015060612

16. Gasparrini A, Armstrong B, Kenward MG. Distributed lag non-linear models. *Stat Med*. (2010) 29:2224–34. doi: 10.1002/sim.3940

17. Wu Q, Xu Z, Dan YL, Cheng J, Zhao CN, Mao YM, et al. Association between traffic-related air pollution and hospital readmissions for rheumatoid arthritis in Hefei, China: a time-series study. *Environ Pollut*. (2021) 268:115628. doi: 10.1016/j.envpol.2020.115628

18. Bell ML, Samet JM, Dominici F. Time-series studies of particulate matter. *Annu Rev Public Health*. (2004) 25:247–80. doi: 10.1146/annurev.publhealth.25.102802.124329

19. Mokoena KK, Ethan CJ, Yu Y, Shale K, Liu F. Ambient air pollution and respiratory mortality in Xi'an, China: a time-series analysis. *Respir Res*. (2019) 20:139. doi: 10.1186/s12931-019-1117-8

20. Gong T, Sun Z, Zhang X, Zhang Y, Wang S, Han L, et al. Associations of black carbon and PM2.5 with daily cardiovascular mortality in Beijing, China. *Atmos Environ*. (2019) 214:116876. doi: 10.1016/j.atmosenv.2019.116876

21. Perperoglou A, Sauerbrei W, Abrahamowicz M, Schmid M. A review of spline function procedures in R. *BMC Med Res Methodol*. (2019) 19:46. doi: 10.1186/s12874-019-0666-3

22. Schwartz J. Is there harvesting in the association of airborne particles with daily deaths and hospital admissions? *Epidemiology*. (2001) 12:55–61. doi: 10.1097/00001648-200101000-00010

23. Zhang F, Zhang H, Wu C, Zhang M, Feng H, Li D, et al. Acute effects of ambient air pollution on clinic visits of college students for upper respiratory tract infection in Wuhan. *China Environ Sci Pollut Res Int*. (2021) 28:29820–30. doi: 10.1007/s11356-021-12828-7

24. Bowe B, Xie Y, Li T, Yan Y, Xian H, Al-Aly Z. Associations of ambient coarse particulate matter, nitrogen dioxide, and carbon monoxide with the risk of kidney disease: a cohort study. *Lancet Planet Health*. (2017) 1:e267–76. doi: 10.1016/s2542-5196(17)30117-1

25. Jung J, Park JY, Kim YC, Lee H, Kim E, Kim YS, et al. Effects of air pollution on mortality of patients with chronic kidney disease: a large observational cohort study. *Sci Total Environ*. (2021) 786:147471. doi: 10.1016/j.scitotenv.2021.147471

26. Lee W, Prifti K, Kim H, Kim E, Yang J, Min J, et al. Short-term exposure to air pollution and attributable risk of kidney diseases: a Nationwide time-series study. *Epidemiology*. (2022) 33:17–24. doi: 10.1097/ede.0000000000001430

27. Kuźma Ł, Małyszko J, Bachórzewska-Gajewska H, Kralisz P, Dobrzycki S. Exposure to air pollution and renal function. *Sci Rep*. (2021) 11:11419. doi: 10.1038/s41598-021-91000-0

28. Chen SY, Chu DC, Lee JH, Yang YR, Chan CC. Traffic-related air pollution associated with chronic kidney disease among elderly residents in Taipei City. *Environ Pollut*. (2018) 234:838–45. doi: 10.1016/j.envpol.2017.11.084

29. Yang C, Wang W, Wang Y, Liang Z, Zhang F, Chen R, et al. Ambient ozone pollution and prevalence of chronic kidney disease: a nationwide study based on the China national survey of chronic kidney disease. *Chemosphere*. (2022) 306:135603. doi: 10.1016/j.chemosphere.2022.135603

30. Venkataramani AS, Brigell R, O'Brien R, Chatterjee P, Kawachi I, Tsai AC. Economic opportunity, health behaviours, and health outcomes in the USA: a population-based cross-sectional study. *Lancet Public Health*. (2016) 1:e18–25. doi: 10.1016/s2468-2667(16)30005-6

31. Olden K. The inaugural Olden distinguished lecture: economic inequality and health disparities. *Environ Health Perspect*. (2021) 129:41001. doi: 10.1289/ehp8631

32. Vega WA, Sribney WM. Growing economic inequality sustains health disparities. *Am J Public Health*. (2017) 107:1606–7. doi: 10.2105/ajph.2017.304024

33. Pedley FG. The effects of small amounts of carbon monoxide on the human organism. *Can Med Assoc J*. (1929) 21:209–10.

34. Brand P, Bertram J, Chaker A, Jörres RA, Kronseder A, Kraus T, et al. Biological effects of inhaled nitrogen dioxide in healthy human subjects. *Int Arch Occup Environ Health*. (2016) 89:1017–24. doi: 10.1007/s00420-016-1139-1

35. Myers R, Brauer M, Dummer T, Atkar-Khattra S, Yee J, Melosky B, et al. High-ambient air pollution exposure among never smokers versus ever smokers with lung Cancer. *J Thorac Oncol*. (2021) 16:1850–8. doi: 10.1016/j.jtho.2021.06.015

36. Fiorito G, Vlaanderen J, Polidoro S, Gulliver J, Galassi C, Ranzi A, et al. Oxidative stress and inflammation mediate the effect of air pollution on cardio-and cerebrovascular disease: a prospective study in nonsmokers. *Environ Mol Mutagen*. (2018) 59:234–46. doi: 10.1002/em.22153

37. Liu S, Zhang M, Yang L, Li Y, Wang L, Huang Z, et al. Prevalence and patterns of tobacco smoking among Chinese adult men and women: findings of the 2010 national smoking survey. *J Epidemiol Community Health*. (2017) 71:154–61. doi: 10.1136/jech-2016-207805

38. Tian Y, Liu H, Zhao Z, Xiang X, Li M, Juan J, et al. Association between ambient air pollution and daily hospital admissions for ischemic stroke: a nationwide time-series analysis. *PLoS Med*. (2018) 15:e1002668. doi: 10.1371/journal.pmed.1002668

39. Wang Z, Zhou Y, Zhang Y, Huang X, Duan X, Ou Y, et al. Association of hospital admission for bronchiectasis with air pollution: a province-wide time-series study in southern China. *Int J Hyg Environ Health*. (2021) 231:113654. doi: 10.1016/j.ijheh.2020.113654

40. Liu M, Liu SW, Wang LJ, Bai YM, Zeng XY, Guo HB, et al. Burden of diabetes, hyperglycaemia in China from to 2016: findings from the 1990 to 2016, global burden of disease study. *Diabetes Metab*. (2019) 45:286–93. doi: 10.1016/j.diabet.2018.08.008

41. Moran AE, Forouzanfar MH, Roth GA, Mensah GA, Ezzati M, Flaxman A, et al. The global burden of ischemic heart disease in 1990 and 2010: the global burden of disease 2010 study. *Circulation*. (2014) 129:1493–501. doi: 10.1161/circulationaha.113.004046

42. Tsioufis C, Tatsis I, Thomopoulos C, Wilcox C, Palm F, Kordalis A, et al. Effects of hypertension, diabetes mellitus, obesity and other factors on kidney haemodynamics. *Curr Vasc Pharmacol*. (2014) 12:537–48. doi: 10.2174/157016111203140518173700

43. Song J, Lu M, Lu J, Chao L, An Z, Liu Y, et al. Acute effect of ambient air pollution on hospitalization in patients with hypertension: a time-series study in Shijiazhuang. *China Ecotoxicol Environ Saf*. (2019) 170:286–92. doi: 10.1016/j.ecoenv.2018.11.125

44. Li Y, Xu L, Shan Z, Teng W, Han C. Association between air pollution and type 2 diabetes: an updated review of the literature. *Ther Adv Endocrinol Metab*. (2019) 10:2042018819897046. doi: 10.1177/2042018819897046

45. Li W, Cao Y, Li R, Ma X, Chen J, Wu Z, et al. The spatial variation in the effects of air pollution on cardiovascular mortality in Beijing, China. *J Expo Sci Environ Epidemiol*. (2018) 28:297–304. doi: 10.1038/jes.2016.21

46. Lim CC, Hayes RB, Ahn J, Shao Y, Silverman DT, Jones RR, et al. Mediterranean diet and the association between air pollution and cardiovascular disease mortality risk. *Circulation*. (2019) 139:1766–75. doi: 10.1161/circulationaha.118.035742

47. Evans RG, Gardiner BS, Smith DW, O'Connor PM. Intrarenal oxygenation: unique challenges and the biophysical basis of homeostasis. *Am J Physiol Ren Physiol*. (2008) 295:F1259–70. doi: 10.1152/ajprenal.90230.2008

48. Chenoweth JA, Albertson TE, Greer MR. Carbon Monoxide Poisoning. *Crit Care Clin*. (2021) 37:657–72. doi: 10.1016/j.ccc.2021.03.010

49. Rosenberger C, Mandriota S, Jürgensen JS, Wiesener MS, Hörstrup JH, Frei U, et al. Expression of hypoxia-inducible factor-1alpha and-2alpha in hypoxic and ischemic rat kidneys. *J Am Soc Nephrol*. (2002) 13:1721–32. doi: 10.1097/01.asn.0000017223.49823.2a

50. Nangaku M, Eckardt KU. Hypoxia and the HIF system in kidney disease. *J Mol Med*. (2007) 85:1325–30. doi: 10.1007/s00109-007-0278-y

51. Lu C, Liu Q, Deng M, Liao H, Yang X, Ma P. Interaction of high temperature and NO (2) exposure on asthma risk: in vivo experimental evidence of inflammation and oxidative stress. *Sci Total Environ*. (2023) 869:161760. doi: 10.1016/j.scitotenv.2023.161760

52. Mirowsky JE, Dailey LA, Devlin RB. Differential expression of pro-inflammatory and oxidative stress mediators induced by nitrogen dioxide and ozone in primary human bronchial epithelial cells. *Inhal Toxicol*. (2016) 28:374–82. doi: 10.1080/08958378.2016.1185199

53. Ogura Y, Kitada M, Koya D. Sirtuins and renal oxidative stress. *Antioxidants*. (2021) 10:10. doi: 10.3390/antiox10081198

54. Coppolino G, Leonardi G, Andreucci M, Bolignano D. Oxidative stress and kidney function: a brief update. *Curr Pharm Des*. (2018) 24:4794–9. doi: 10.2174/1381612825666190112165206

55. Yaribeygi H, Farrokhi FR, Rezaee R, Sahebkar A. Oxidative stress induces renal failure: a review of possible molecular pathways. *J Cell Biochem*. (2018) 119:2990–8. doi: 10.1002/jcb.26450

56. Cattell V, Largen P, de Heer E, Cook T. Glomeruli synthesize nitrite in active Heymann nephritis; the source is infiltrating macrophages. *Kidney Int*. (1991) 40:847–51. doi: 10.1038/ki.1991.284

57. Sugimoto H, Shikata K, Matsuda M, Kushiro M, Hayashi Y, Hiragushi K, et al. Increased expression of endothelial cell nitric oxide synthase (ec NOS) in afferent and glomerular endothelial cells is involved in glomerular hyperfiltration of diabetic nephropathy. *Diabetologia*. (1998) 41:1426–34. doi: 10.1007/s001250051088

58. Devlin RB, McDonnell WF, Mann R, Becker S, House DE, Schreinemachers D, et al. Exposure of humans to ambient levels of ozone for 6.6 hours causes cellular and biochemical changes in the lung. *Am J Respir Cell Mol Biol*. (1991) 4:72–81. doi: 10.1165/ajrcmb/4.1.72

59. Ayyagari VN, Januszkiewicz A, Nath J. Effects of nitrogen dioxide on the expression of intercellular adhesion molecule-1, neutrophil adhesion, and cytotoxicity: studies in human bronchial epithelial cells. *Inhal Toxicol*. (2007) 19:181–94. doi: 10.1080/08958370601052121

60. Amakawa K, Terashima T, Matsuzaki T, Matsumaru A, Sagai M, Yamaguchi K. Suppressive effects of diesel exhaust particles on cytokine release from human and murine alveolar macrophages. *Exp Lung Res*. (2003) 29:149–64. doi: 10.1080/01902140303770

61. Donnahoo KK, Shames BD, Harken AH, Meldrum DR. Review article: the role of tumor necrosis factor in renal ischemia-reperfusion injury. *J Urol*. (1999) 162:196–203. doi: 10.1097/00005392-199907000-00068

62. Mühl H, Pfeilschifter J. Anti-inflammatory properties of pro-inflammatory interferon-gamma. *Int Immunopharmacol*. (2003) 3:1247–55. doi: 10.1016/s1567-5769(03)00131-0

63. Vielhauer V, Anders HJ, Schlöndorff D. Chemokines and chemokine receptors as therapeutic targets in lupus nephritis. *Semin Nephrol*. (2007) 27:81–97. doi: 10.1016/j.semnephrol

frontiers | Frontiers in Public Health

TYPE Original Research
PUBLISHED 03 October 2023
DOI 10.3389/fpubh.2023.1282497

Check for updates

OPEN ACCESS

EDITED BY
Zhaobin Sun,
Chinese Academy of Meteorological Sciences, China

REVIEWED BY
Siguang Zhu,
Nanjing University of Information Science and Technology, China
Zhang Shuwen,
Beijing University of Chinese Medicine, China

*CORRESPONDENCE
Jiaxi Yang
jxyang@ium.cn
Zhiqi Xu
zqxu@ium.cn

RECEIVED 24 August 2023
ACCEPTED 15 September 2023
PUBLISHED 03 October 2023

CITATION
Zhang G, Han L, Yao J, Yang J, Xu Z, Cai X, Huang J and Pei L (2023) Assessing future heat stress across China: combined effects of heat and relative humidity on mortality. *Front. Public Health* 11:1282497. doi: 10.3389/fpubh.2023.1282497

Assessing future heat stress across China: combined effects of heat and relative humidity on mortality

Guwei Zhang[1,2,3], Ling Han[4], Jiajun Yao[5], Jiaxi Yang[1,2,3]*, Zhiqi Xu[1,2,3]*, Xiuhua Cai[6], Jin Huang[7] and Lin Pei[1,2,3]

[1]Institute of Urban Meteorology, China Meteorological Administration, Beijing, China, [2]Key Laboratory of Urban Meteorology, China Meteorological Administration, Beijing, China, [3]Key Laboratory of Transforming Climate Resources to Economy, China Meteorological Administration, Chongqing, China, [4]National Key Laboratory of Intelligent Tracking and Forecasting for Infectious Diseases, National Institute for Communicable Disease Control and Prevention, Chinese Center for Disease Control and Prevention, Beijing, China, [5]Shengzhou Meteorological Bureau, Shaoxing, China, [6]Chinese Academy of Meteorological Sciences, Beijing, China, [7]Chifeng City Center Hospital Ningcheng County, Chifeng, China

This study utilizes China's records of non-accidental mortality along with twenty-five simulations from the NASA Earth Exchange Global Daily Downscaled Projections to evaluate forthcoming heat stress and heat-related mortality across China across four distinct scenarios (SSP1-2.6, SSP2-4.5, SSP3-7.0, and SSP5-8.5). The findings demonstrate a projected escalation in the heat stress index (HSI) throughout China from 2031 to 2100. The most substantial increments compared to the baseline (1995–2014) are observed under SSP5-8.5, indicating a rise of 7.96°C by the year 2100, while under SSP1-2.6, the increase is relatively modest at 1.54°C. Disparities in HSI growth are evident among different subregions, with South China encountering the most significant elevation, whereas Northwest China exhibits the lowest increment. Projected future temperatures align closely with HSI patterns, while relative humidity is anticipated to decrease across the majority of areas. The study's projections indicate that China's heat-related mortality is poised to surpass present levels over the forthcoming decades, spanning a range from 215% to 380% from 2031 to 2100. Notably, higher emission scenarios correspond to heightened heat-related mortality. Additionally, the investigation delves into the respective contributions of humidity and temperature to shifts in heat-related mortality. At present, humidity exerts a greater impact on fluctuations in heat-related mortality within China and its subregions. However, with the projected increase in emissions and global warming, temperature is expected to assume a dominant role in shaping these outcomes. In summary, this study underscores the anticipated escalation of heat stress and heat-related mortality across China in the future. It highlights the imperative of emission reduction as a means to mitigate these risks and underscores the variances in susceptibility to heat stress across different regions.

KEYWORDS
NEX-GDDP-CMIP6, China, heat stress, heat-related mortality, future projections

1. Introduction

In the past decade (2011–2020), carbon emissions have reached unprecedented levels in human history, coinciding with a surge in occurrences of extreme heat events globally (1, 2). The rapid pace of global warming has propelled heat stress to the forefront as a highly perilous climate risk, impacting public health, socioeconomics, and the ecological environment (3).

Elevated ambient temperatures can elevate the body's core temperature and heart rate, leading to conditions like heatstroke, respiratory and circulatory disorders, and even fatalities (4).

Noteworthy past events serve as stark reminders of the dangers associated with extreme heat. For instance, the 1995 heatwave in Chicago, USA claimed the lives of over 700 individuals (5). The record-breaking European heatwaves of 2003 resulted in substantial loss of life and economic devastation (6). Similarly, the 2010 heat event in Russia led to more than 50,000 fatalities (7). More recent occurrences include the North American super-heatwave in 2021, which claimed the lives of over 500 people (8). China has also faced significant negative impacts due to extreme heat events (9–13). According to Cai et al. (9, 10), nearly 15,000 deaths in China during 2020 were attributed to heat events. The escalating impact of climate change underscores the impending severity of heat stress, particularly in densely populated regions around the world (14–16). Given the pressing nature of the current scenario, it is of paramount importance to conduct a thorough assessment of future heat-related risks and undertake comprehensive measures to combat climate change, including emission reduction and strategic planning (1, 2).

Global climate models represent a cutting-edge tool for understanding climate change and projecting future scenarios. The recent Intergovernmental Panel on Climate Change (IPCC) report integrates various factors to quantify development and climate change (17). This integration involves combining shared socioeconomic pathways (SSPs) with representative concentration pathways (18, 19). In line with these novel scenarios, the IPCC introduced the Coupled Model Intercomparison Project Phase 6 (CMIP6), which furnishes the latest projections for future climate change (20).

While extensive efforts have been invested in leveraging the CMIP6 dataset to project future climate (16, 21, 22), the inherent coarse horizontal resolution (ranging from 1° to 3°) of the raw CMIP6 models poses challenges for in-depth regional climate analysis and introduces uncertainties due to model biases. The low resolution of CMIP6 poses a challenge in accurately simulating the impacts of urbanization on local climate. This limitation is particularly problematic for future public health risk assessments, given the substantial urban population (11, 16). Additionally, research has revealed that the original CMIP6 models tend to overestimate future temperatures, with overestimations ranging from 3.4% to 11.6% (23). To address these limitations, NASA has released the NASA Earth Exchange Global Daily Downscaled Projections (NEX-GDDP-CMIP6) dataset (24). These downscaled products are derived from the Bias Correction Spatial Disaggregation (BCSD) method, producing daily variants with an enhanced horizontal resolution of 0.25°. This refinement enhances both simulation accuracy and spatial resolution compared to the original CMIP6 outputs (25, 26). Previous research has demonstrated the alignment of NEX-GDDP-CMIP6 with observational data for modeling daily metrics (27, 28). Wu et al. (28) validated the capability of NEX-GDDP-CMIP6 to replicate China's spatial temperature characteristics. Nonetheless, existing studies employing NEX-GDDP-CMIP6 have predominantly focused on predicting future extreme climate changes, often lacking comprehensive risk assessments (28–30). The NEX-GDDP-CMIP6 dataset provides valuable information for climate change research, impact assessments, and adaptation planning. Understand and respond better to the potential risks as well as impacts of future climate change. To provide better information for governmental strategic planning, it is necessary to employ this dataset to project future heat health risks in China.

Accordingly, this study plans to utilize the newly released and updated high-resolution NEX-GDDP-CMIP6 to project future changes in heat stress across China and its seven sub-regions under various emission scenarios with the heat stress index (HSI) that take into account both air temperature and humidity. Further, we will also employ the HSI-mortality exposure-response relationship and future population datasets to assess future mortality changes and quantify the contributions from temperature and humidity to heat mortality changes. This study aims to project future risks from multiple perspectives to support climate mitigation and strategic planning.

2. Data and methods

2.1. Historical mortality records

The Chinese Centre for Disease Control and Prevention (CDC) furnishes daily records of non-accidental death occurrences. Following the guidelines of the International Classification of Diseases-10th Revision (ICD-10), non-accidental deaths pertain to fatalities resulting from diseases rather than injuries. In the scope of this study, a total of 195 surveillance sites capturing mortality were encompassed (Supplementary Table S1). Recorded fatalities were observed across the majority of districts spanning the years 2010 to 2016. However, in the case of Guangzhou and Xining, recorded deaths were limited to the timeframe of 2012 to 2016.

2.2. Climate data

With a spatial resolution of 0.25° × 0.25°, the NEX-GDDP-CMIP6 dataset (24) offers a collection of scientifically downscaled climatic scenarios spanning from 1950 to 2100. This dataset utilizes the BCSD algorithm in combination with observational data generation to perform bias correction and downscaling of the CMIP6 model outputs. The BCSD method represents a trend-sustaining statistical downscaling technique that has gained widespread use in meteorology (25, 26, 31). The variational approach employed involves comparing the output from global climate models with real-world climate observations from a common reference period. This information is then employed to modify future climate projections to enhance their congruence with historical records and to enhance the accuracy of specific spatial regions. Leveraging the spatial granularity of the observed dataset, the algorithm additionally interpolates the output from global climate models onto a more refined grid, thereby enhancing spatial resolution.

We employed a total of twenty-five models sourced from the NEX-GDDP-CMIP6 dataset (Supplementary Table S2), selected based on their availability of daily mean relative humidity and surface air temperature. This set of models encompasses historical simulations spanning the period from 1995 to 2014, as well as future projections from 2015 to 2100. These projections are offered across four distinct emission scenarios: SSP1-2.6, SSP2-4.5, SSP3-7.0, and SSP5-8.5. These scenarios span a spectrum of carbon emissions, ranging from high to low levels. The four chosen scenarios are considered Tier 1 scenarios and are mandatory for all climate models participating in the Scenario

Model Intercomparison Project (SMIP) of CMIP6. In essence, they represent the four emission trajectories that current climate research indicates are the most probable paths for the world to take in the future. Specifically, among these scenarios, SSP5-8.5 is the sole scenario that yields a radiative forcing of 8.5 W·m^{-2} in the year 2100, indicating a high level of emissions. SSP3-7.0 combines a relatively elevated degree of social vulnerability with a forcing of 7.0 W·m^{-2}. In the context of SSP2-4.5, a moderate level of social vulnerability aligns with a moderate forcing level of 4.5 W·m^{-2}. SSP1-2.6, on the other hand, combines attributes of low vulnerability, limited mitigation challenges, and a low forcing level of 2.6 W·m^{-2}.

2.3. Population data

Under the umbrella of the four SSPs—namely, SSP1, SSP2, SSP3, and SSP5—the population dataset offers global population estimates spanning intervals of a decade from 2010 to 2100, with a spatial resolution of 0.125° (32). Each SSP corresponds to a distinct developmental trajectory: SSP1 signifies sustainable development characterized by reduced reliance on natural and fossil fuels. SSP2 embodies a business-as-usual scenario that maintains the growth patterns of recent decades, achieves growth targets, and progressively diminishes reliance on fossil fuels. SSP3 encapsulates a global landscape of regional competition, featuring pronounced disparities between regions, a significant gap between affluence and poverty, challenges in achieving developmental objectives, and escalating reliance on fossil fuels. SSP5 represents a fossil-fueled development approach, prioritizing economic expansion and addressing socioeconomic issues through self-interested actions (19). To ensure compatibility with the NEX-GDDP-CMIP6, we performed bilinear interpolation to adjust the population data to a resolution of 0.25° × 0.25°.

2.4. Study periods and regions

Consistent with previous studies (16, 33), the period from 1995 to 2014 is designated as the baseline, while the period spanning 2030 to 2100 is considered as the future timeframe. Additionally, we have segmented the future into 10 years intervals to analyze the projections for each decade: the 2030s (2030–2039), 2040s (2040–2049), 2050s (2050–2059), 2060s (2060–2069), 2070s (2070–2079), 2080s (2080–2089), and 2090s (2090–2099).

The geographic zoning of China (Figure 1A) is used to identify seven subregions: South China (SC), East China (EC), Northeast China (NE), Northwest China (NW), North China (NC), Central China (CC), and Southwest China (SW).

2.5. Calculation for heat stress index

Episodic temperature is a measurement of heat stress in humans that takes into account ambient factors such as temperature and humidity (34, 35). The HSI is a composite index that combines temperature and humidity to establish an equivalent temperature that reflects human perception (36). It is derived from Rothfusz's multiple regression analysis and is as follows.

$$\begin{aligned}\mathrm{HSI} = {} & 2.04901523 \times T - 42.379 + 10.14333127 \times \mathrm{RH} \\ & - 0.22475541 \times T \times \mathrm{RH} - 0.00683783 \times T^2 \\ & - 0.05481717 \times \mathrm{RH}^2 + 0.00122874 \times \mathrm{RH} \times T^2 \\ & + 0.00085282 \times T \times \mathrm{RH}^2 - 0.00000199 \times T^2 \times \mathrm{RH}^2 \end{aligned} \quad (1)$$

If the relative humidity drops below 13% and the temperature falls within the range of 26.7°C to 44.5°C, subtract the specified value, Adj, from the HSI, where T represents the temperature in degrees Celsius, HSI signifies the heat stress in degrees Celsius, and RH represents the relative humidity in percent.

$$\mathrm{Adj} = \frac{13 - \mathrm{RH}}{4} \times \sqrt{1 - \frac{|9T - 315|}{85}} \quad (2)$$

For relative humidity above 85% and temperatures between 26.7°C and 30.5°C, add the following Adj to the HSI:

$$\mathrm{Adj} = \frac{\mathrm{RH} - 85}{10} \times \frac{275 - 9T}{25} \quad (3)$$

In situations where temperature and relative humidity outcomes indicate that the HSI value falls below approximately 26.7°C, the applicability of the Rothfuss regression method becomes limited. In such cases, a more straightforward formula can be employed to compute values that align with the results derived from Steadman's approach (35).

$$\mathrm{HSI} = 1.98T + 24.9 + 0.047\mathrm{RH} \quad (4)$$

2.6. HSI-mortality relationship

Utilizing data from 195 sites in China, a two-stage analysis is employed to quantify the existing relationship between the HSI and mortality. In the initial stage, daily recorded data on HSI and mortality are employed to create quasi-Poisson regressions integrated with distributed lag nonlinear models (DLNM). This approach is adopted to establish the connection between HSI and mortality for each specific location, following the methodology outlined by Gasparrini et al. (37). Within the DLNM framework, cross-basis functions are introduced to model the non-linear and lagged effects of HSI on mortality. To facilitate prediction and compute the reference prediction, the "crosspred" function is employed.

$$\log\left[E\left(\mathrm{mort}_i\right)\right] = \alpha + \beta \mathrm{HSI}_{i,l} + ns\left(\mathrm{time,df}\right) + \mathrm{DOW} \quad (5)$$

where mort_i is the daily mortality on the day i. The parameter α stands for the intercept. DOW signifies the impact of the day of the week. $\mathrm{HSI}_{i,l}$ denotes the cross-base matrix of the two dimensions of the HSI and lag days. β is the coefficient vector for $\mathrm{HSI}_{i,l}$. ns is the normal three-spline function. df represents the degree of freedom. For controlling long-term trends, a natural cubic spline with 7 degrees of freedom per year is employed for a time. Our previous studies have indicated that heat has an impact

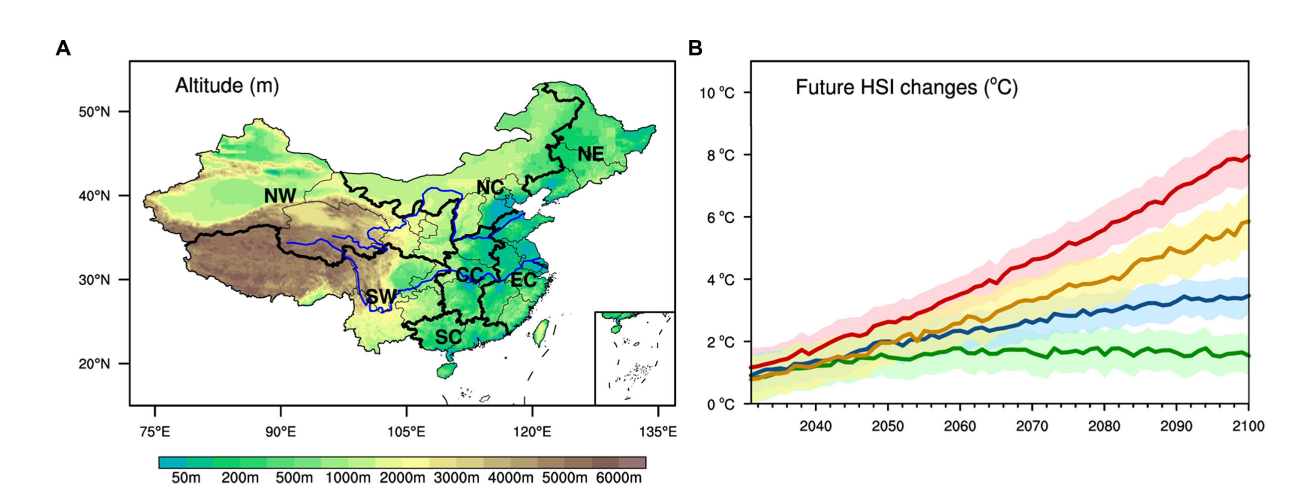

FIGURE 1
(A) Cartographic representation of China's topography (units: meters). **(B)** Changes in China's annual HSI projected for the period 2031–2100, relative to the present levels (units: °C). The delineations in green, blue, yellow, and red correspond to SSP1-2.6, SSP2-4.5, SSP3-7.0, and SSP5-8.5, respectively. The shaded area depicts the model's variations within a 95% CI.

on mortality within a period of approximately 3 weeks, taking into consideration potential influences related to harvesting (38). Therefore, a lag of 21 days is selected, which is considered adequate for capturing the hysteresis effect of temperature without excessive complexity. The association between cumulative temperature and mortality in each district or county is quantified as a relative risk. The risk for each temperature series is compared to the minimum mortality HSI, which represents the HSI with the lowest mortality risk. Additional insights can be derived from prior studies (14, 38).

Owing to variations in health impacts between urban and rural settings, it was not feasible to assess the HSI-mortality relationship within provincial capitals. However, it's noteworthy that heat-related risks exhibit similarities within the same climatic subregions (39). In the subsequent phase, a multivariate meta-analysis is conducted using the constrained maximum likelihood approach to investigate the HSI-mortality relationship. This analysis aims to reveal zonal patterns in the risk of HSI-related mortality. Subsequently, the best linear unbiased prediction (BLUP) method is employed to forecast the cumulative HSI-mortality relationship for each subregion. Detailed procedures can be found in the work by Gasparrini et al. (40). Heterogeneity is assessed through the utilization of Cochran's *Q* approach and an extension of the I^2 statistic.

The methodology described above for analyzing the relationship between HSI and mortality is similar to the widely accepted approach used for analyzing the relationship between temperature and mortality. By aggregating data points from a specific region, it is possible to construct an HSI-mortality exposure-response curve that provides an overall understanding of the impact within that region (15, 41, 42).

2.7. Estimated heat-related mortality

Following a methodology similar to the prior investigations (14, 38, 43, 44), we conduct estimations of heat-related mortality utilizing the NEX-GDDP-CMIP6 datasets. The number of daily HSI-related deaths for each grid point is first calculated. Deaths due to high temperatures are calculated by summing the subset of days with temperatures above minimum mortality HSI (relative risk of 1). Then we sum the deaths with HSI above the minimum mortality HSI to give the number of heat-related deaths for the year. Additionally, the heat-related mortality is derived by dividing the number of heat-related deaths by the relevant grid population. Importantly, it's noteworthy that regional heat-related mortality pertains to the ratio of regional heat-related deaths to the regional population. The calculation methodology is outlined as follows:

$$\mathrm{AF} = \frac{\mathrm{RR}-1}{\mathrm{RR}} \tag{6}$$

$$D_{x,d} = Mt_{x,y} \times P_{x,y} \times \mathrm{AF}_{x,d} \tag{7}$$

$$\mathrm{HD}_{x,y} = \Sigma\{D_{x,d}\}\ldots\ldots(\text{When } \mathrm{HSI}_{x,d} > \mathrm{MMHSI}) \tag{8}$$

$$\mathrm{HM}_{x,y} = \frac{\mathrm{HD}_{x,y}}{\mathrm{Pop}_{x,y}} \tag{9}$$

$$\mathrm{Reg\_HD}_y = \Sigma\{\mathrm{HD}_{x,y}\} \tag{10}$$

$$\mathrm{Reg\_HM}_y = \frac{\mathrm{Regional\_HD}_y}{\Sigma\{\mathrm{Pop}_{x,y}\}} \tag{11}$$

The attribute fraction (AF) for a specific HSI value is computed from the relative risk (RR) determined using DLNM and meta-analyses across distinct subregions. This calculation assumes a consistent exposure-response relationship throughout the study timeframe. In the provided equations, $P_{x,y}$ and $Mt_{x,y}$ are the population and baseline mortality at grid x in year y. $D_{x,d}$ and $HSI_{x,d}$ are the daily HSI-related deaths and the HSI for day d in year y. $HM_{x,y}$ (Reg_HM_y) and $HD_{x,y}$ (Reg_HD_y) symbolize the (regional) annual heat-related mortality and deaths, respectively. In this study, the minimum mortality HSI for NE, NC, NW, EC, CC, SW, and SC is about 24°C, 26°C, 25°C, 25°C, 35°C, 29°C, and 32°C, respectively (Figure 2). The above steps are performed for each model and then average the outcomes of the models to get the ensemble mean.

2.8. Uncertainty analysis

Similar to previous research (21, 45), the principal sources of uncertainty in projecting future heat-related mortality within this study are attributed to the relationship between the HSI and mortality, as well as the divergences in HSI emanating from different model simulations. To address these uncertainties, a methodology involving Monte Carlo simulation (46) is harnessed to generate 1,000 samples of adjusted BLUP coefficients. This approach operates on the assumption that the estimations adhere to a multivariate normal distribution.

Subsequently, evaluations are conducted for each selected NEX-GDDP-CMIP6 simulation (45, 47). By aggregating the outputs from NEX-GDDP-CMIP6, the ensemble mean across multiple models is adopted as a representative depiction of the overall outcomes (16). The associated level of uncertainty is conveyed using a 95% confidence interval (CI). This interval, spanning the spectrum from the 2.5th to the 97.5th percentiles of the empirical distribution across the NEX-GDDP-CMIP6 results, serves as a quantification of the extent of uncertainty.

2.9. Contributions attributed to temperature and humidity

To examine the effects of temperature and humidity variations on heat-related mortality, we employ the Gini importance metric derived from the Random Forest algorithm (48). This approach allows us to elucidate the separate contributions of these intrinsic factors. The architecture of the random forest consists of decision trees, each comprising internal nodes and leaves. These internal nodes use specific features to split the dataset into two subsets with similar outcomes. Feature selection criteria, such as Gini impurity for classification or information gain, along with variance reduction for regression, guide the choice of features at internal nodes. The reduction in impurity attributed to each feature is measured, and the feature that leads to the most significant reduction is selected as the internal node. The significance of a feature is determined by calculating the average reduction in impurity across all trees in the forest.

In this study, we evaluate the individual impacts of temperature and humidity on heat-related mortality in each subregion across different scenarios. Utilizing data from multiple models, we incorporate annual temperature, humidity, and heat-related mortality data into the Random Forest model for simulation at each inhabited grid point within the subregion. It's important to note that we exclusively consider temperature and humidity values for days when the HSI exceeds the minimum mortality HSI. The resulting Gini importance values for temperature and humidity, obtained from the Random Forest analysis, are scaled by a factor of 100% to represent their respective distinct contributions.

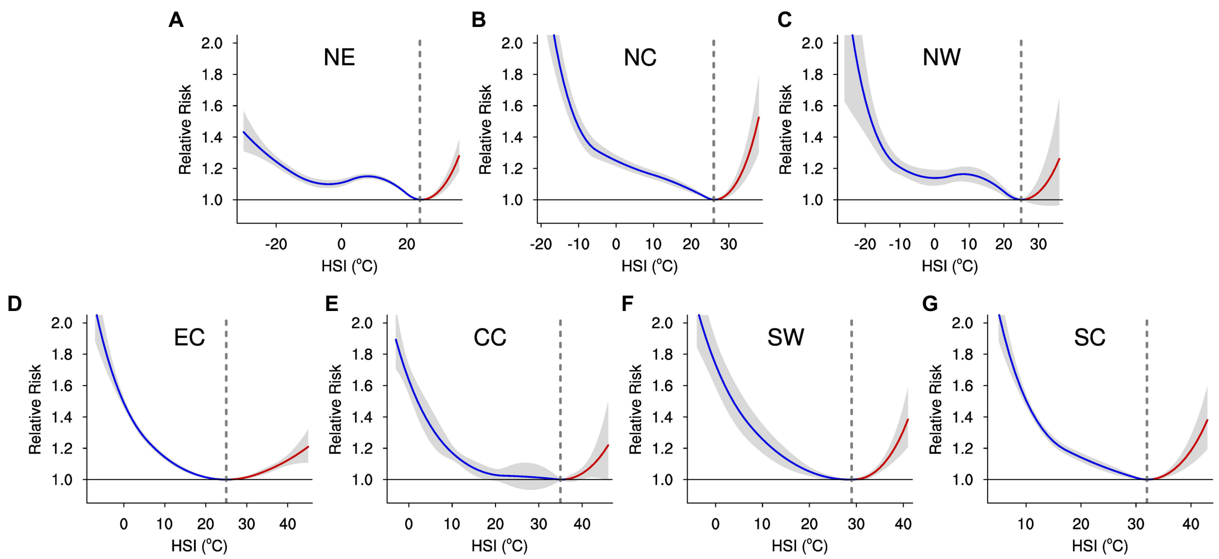

FIGURE 2
Collective cumulative non-linear associations between the HSI and daily mortality across lag days ranging from 0 to 21 are presented for each subregion within China. The curved lines illustrate the relative risk of HSI in comparison to the optimal HSI (signified by vertical gray dashed lines) associated with the lowest risk. The red and blue curved lines indicate the impact of heat and cold, respectively. The shaded regions encompass the 95% CI. **(A–G)** are for NE, NC, NW, EC, CC, SW, and SC, respectively.

3. Results

3.1. Future heat stress changes across China

The future annual HSI for China is anticipated to escalate across various scenarios, with the most substantial increase observed under SSP5-8.5 (Figure 1B). Specifically, for SSP5-8.5, the projected HSI increase in 2031 is estimated to be 1.16°C (95% CI: 0.51–1.81°C) higher than the present, and this elevation is anticipated to reach 7.96°C (95% CI: 7.02–8.90°C) by the year 2100. In contrast, under lower emission scenarios such as SSP1-2.6, the projected HSI elevations in China are forecasted to be 0.78°C (95% CI: 0.06–1.54°C) in 2031 and merely 1.54°C (95% CI: 0.92–2.16°C) by 2100. This projection under SSP1-2.6 represents approximately 20% of the increase witnessed under SSP5-8.5.

Importantly, it is noteworthy that under the SSP1-2.6 scenario, the growth of HSI will reach a plateau after 2060 and exhibit a decline in the 2090s (Figure 3A). Specifically, during the 2090s, China is projected to encounter an annual HSI increase of about 1.60°C (95% CI: 0.96–2.23°C), which is lower than the increase of 1.67–1.69°C (95% CI: 0.99–2.34°C) anticipated during the period from the 2060s to the 2080s. This disparity could be attributed to the fact that under SSP1-2.6, China's temperature escalation will plateau by the end of the century, while humidity levels are projected to decrease (Supplementary Figures S1A, S2A). In contrast, under other scenarios (SSP2-4.5, SSP3-7.0, and SSP5-8.5), despite a projected decline in humidity after the 2060s (Supplementary Figure S2A), temperatures will persistently rise (Supplementary Figure S1A), thereby perpetuating the growth of HSI through the year 2100 (Figure 1B).

Focusing on future changes in the subregions, the projections consistently indicate significant HSI changes, with the highest increases observed under the high-emission scenario (Figure 3). Among the seven subregions, SC is projected to undergo the greatest HSI growth, with an estimated increase of 10.46°C (95% CI: 9.17–11.74°C) relative to the present in the 2090s under SSP5-8.5.

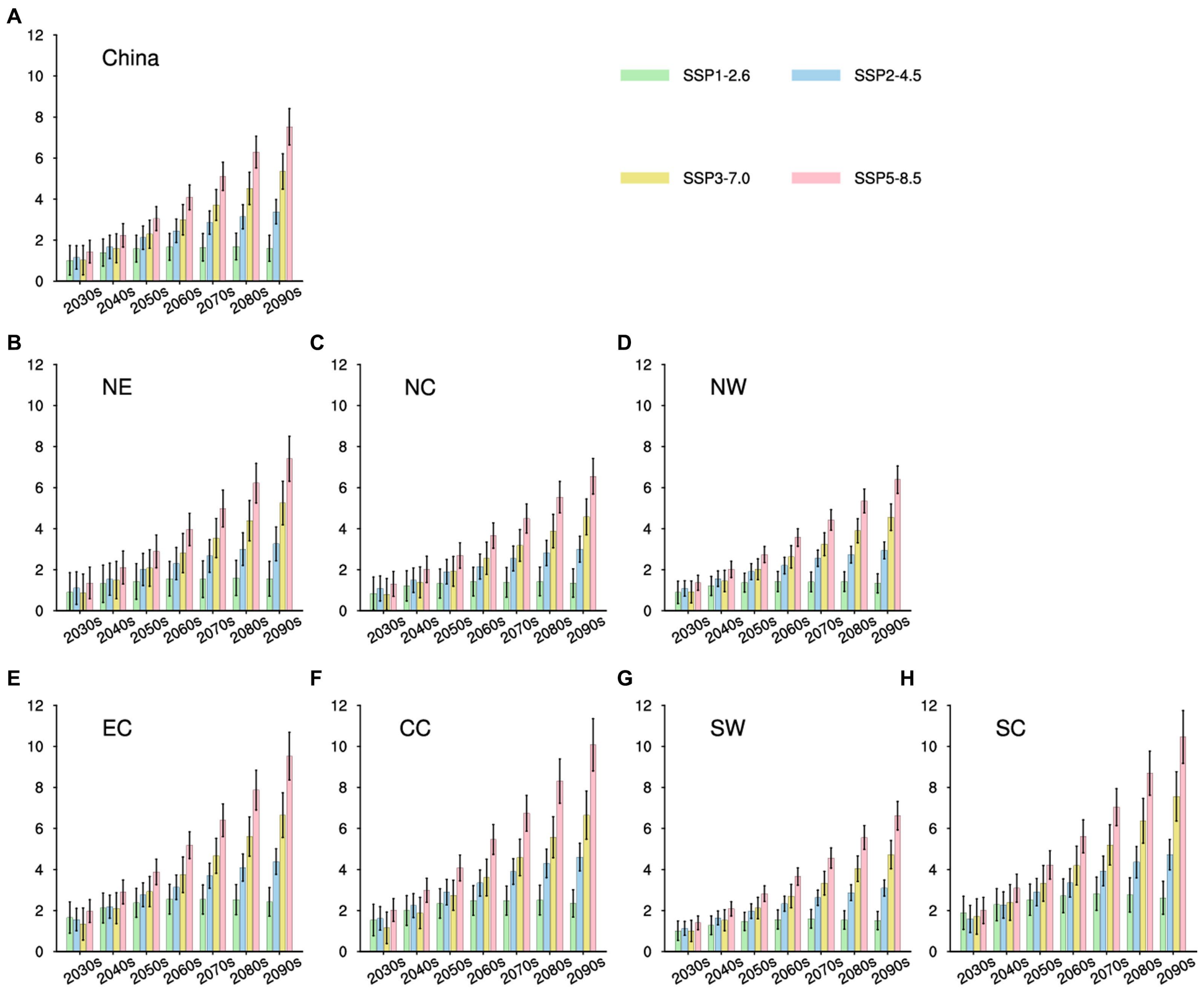

FIGURE 3
Projected alterations in HSI for China and its seven subregions are illustrated. The bars in green, blue, yellow, and red symbolize the averaged results for every 10 years under SSP1-2.6, SSP2-4.5, SSP3-7.0, and SSP5-8.5, respectively (units: °C). At the upper part of each bar, a vertical black line signifies the range of model variations within a 95% confidence interval. **(A–H)** are for China, NE, NC, NW, EC, CC, SW, and SC, respectively.

Conversely, NW is projected to have the lowest increase among the subregions, approximately 6.39°C (95% CI: 5.72–7.05°C) under SSP5-8.5 in the 2090s. Furthermore, the HSI increases in NW, NC, NE, and SW are expected to be lower than the national average. Interestingly, these regions are all characterized by high latitude and high altitude areas in China.

The projections of future temperatures align closely with the HSI trends (Supplementary Figure S1), and there are regional differences in changes in relative humidity (Supplementary Figure S2). Overall, a decrease in relative humidity is anticipated for China and most regions in the future. However, the relative humidity in NC and NW is projected to increase across all scenarios, and additionally in EC and CC by 2070 under SSP3-7.0. When considering the future changes in HSI, temperature, and humidity together, although humidity is expected to decrease in most areas, the HSI remains relatively consistent with the temperature trend. This may be attributed to small variations in humidity (no more than ±3%), resulting in a minor effect on HSI.

3.2. Projected future HSI-related mortality

Drawing upon the historical correlations between HSI and mortality, as gleaned from the two-stage analysis (Figure 2), alongside the corresponding location-specific daily HSI data, we have derived estimations for the foundational heat-related mortality rates in China and its subregions (Supplementary Table S3). At present, SC exhibits the highest heat-related mortality, in contrast to NW which displays the lowest rates. Assuming a consistent relationship between HSI and mortality from the present into the future, we can project the heat-related mortality for the period between 2031 and 2100 by amalgamating the anticipated daily HSI values from NEX-GDDP-CMIP6 with the current exposure-response correlation (Figure 4).

In the forthcoming decades of the 21st century, heat-related mortality in China and its subregions is anticipated to exceed current levels across all scenarios. As depicted in the future HSI projections (Figure 3), heat-related mortality under high-emission scenarios will outpace that under low-emission scenarios. For instance, China's annual heat-related mortality during the period 2031–2100 is projected to span from 0.09–0.12‰ (95% CI: 0.08–0.13‰), 0.09–0.17‰ (95% CI: 0.07–0.19‰), 0.09–0.23‰ (95% CI: 0.08–0.25‰), and 0.10–0.30‰ (95% CI: 0.08–0.33‰) for SSP1-2.6, SSP2-4.5, SSP3-7.0, and SSP5-8.5, respectively (Figure 4).

In contrast, scenarios that exclude SSP1-2.6 project a continued elevation in China's heat-related mortality throughout the century, culminating in the highest rate during the 2090s. However, under the SSP1-2.6 scenario, heat-related mortality is expected to peak in the 2070s at around 0.12‰ (95% CI: 0.10–0.13‰). Consistent with regional variations in HSI, SC is anticipated to experience the highest heat-related mortality among the seven subregions, ranging approximately from 0.18–0.48‰ (95% CI: 0.15–0.51‰), while NW is projected to have the lowest, ranging approximately from 0.02–0.13‰ (95% CI: 0.02–0.15‰). Additionally, NC, SW, and CC are anticipated to have higher heat-related mortality compared to the national average in the future, whereas other subregions are predicted to remain below the national average.

Considering the anticipated alterations in future ratios as compared to the present (Figure 5), it is foreseeable that China's annual heat-related mortality will undergo substantial escalation, encompassing a range of 215 to 380% overall. Notably, the most notable and minimal increments are projected under the SSP5-8.5 and SSP1-2.6 scenarios, respectively. This underscores the notion that even in the scenario where the most modest emission reduction goals established by the IPCC are realized, China's heat-related mortality is still expected to double in comparison to the current baseline.

Among the various subregions, those situated at high latitudes and altitudes (excluding NC) are anticipated to undergo a more pronounced growth rate in heat-related mortality compared to other regions. Throughout 2031–2100, SW is expected to witness the highest annual increase in heat-related mortality, ranging approximately from 254% to 554% compared to the current level, marking the highest among the seven subregions. Conversely, EC is projected to experience the lowest increase, ranging approximately from 179% to 274%.

For all scenarios except SSP1-2.6, the average heat-related mortality in subregions during the period of 2031–2100 is projected to rise to at least 200% of their current levels. Notably, under SSP5-8.5, SW and NE will experience increases exceeding 500%. Analyzing the increases per decade (Supplementary Figure S3), differences among the scenarios are relatively modest in the 2030s, with almost no subregion surpassing a 200% increase. However, these differences become more pronounced in the subsequent decades. By the 2090s, heat-related mortality in most areas under SSP5-8.5 could be 6–7 times higher than the present levels, while under SSP1-2.6, it is projected to remain under 3 times the current level. This underscores the potential benefits of emission reduction in mitigating heat-related risks. However, it's important to note that immediate success in risk reduction might not be achievable in the short term, emphasizing the necessity of strategic planning to effectively manage the impacts of climate change.

3.3. Temperature and humidity contributions to heat-related mortality

Assessing the individual impacts of temperature and humidity on heat vulnerabilities within each subregion can enhance the precision of climate change adaptation strategies (12, 42). Firstly, our analysis only considers grids with inhabited residences. Secondly, it's important to clarify that we exclusively include dates linked to heat risk, where the HSI for a given day surpasses the minimum mortality HSI threshold (i.e., corresponding to heat-related mortality above 0). Consequently, our investigation focuses on understanding the impact of temperature or humidity on heat-related mortality when a state of vulnerability to heat has already been established. In simpler terms, the discussion regarding humidity's influence on heat mortality does not suggest that humidity alone can create vulnerability to heat. Our consistent perspective is that the effect of humidity on the risk of heat-related mortality is contingent upon elevated temperature conditions.

As depicted in Figure 6, the impacts of temperature and humidity on heat-related mortality in China and its subregions are analyzed for both current and future periods. Currently (Figure 6A), the contribution of China's humidity and temperature to heat-related mortality change is about 59.4% and 40.6%, suggesting that humidity changes have a greater impact. Similar patterns are observed in NE, NC, NW, and CC, where humidity in NC contributes to 64.3% of

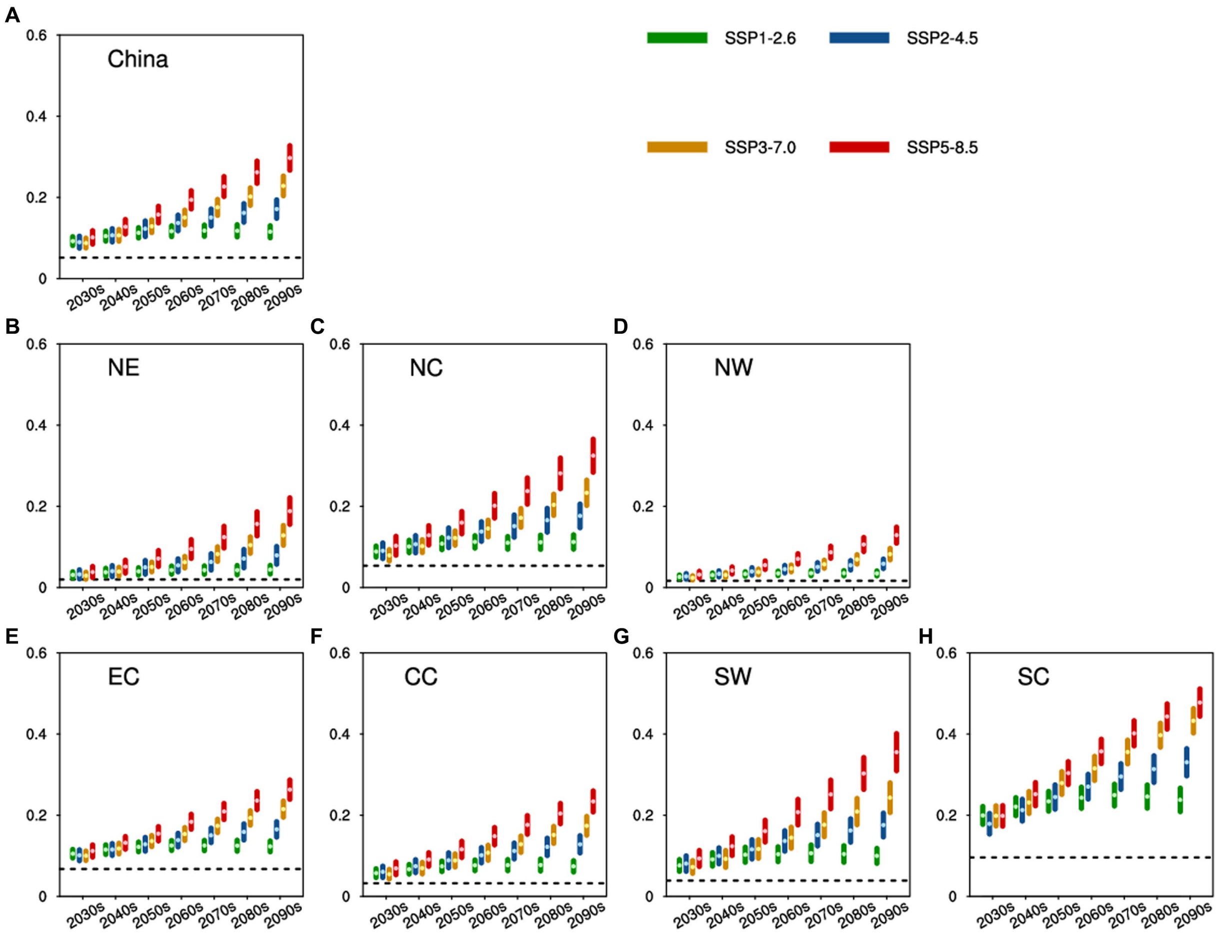

FIGURE 4
Future heat-related mortality for China and seven subregions. Green, blue, yellow, and red dots (accompanied by lines) signify the results (with model spreads shown within a 95% CI) averaged for every 10 years spanning 2031 to 2100 under SSP1-2.6, SSP2-4.5, SSP3-7.0, and SSP5-8.5, respectively (units: ‰). The black dashed lines depict the baseline heat-related mortality for each subregion. **(A–H)** are for China, NE, NC, NW, EC, CC, SW, and SC,respectively.

heat-related mortality changes. In most southern areas (EC, SW, and SC), temperature plays a more important role.

In the future (2031–2100), with rising emissions and ongoing global warming, the influence of temperature will become more prominent (Figures 6B–E). For China, temperature is projected to be the predominant factor driving changes in heat-related mortality, contributing to 59.1%, 68.1%, 73.3%, and 79.3% of heat mortality changes under SSP1-2.6, SSP2-4.5, SSP3-7.0, and SSP5-8.5, respectively. Under SSP1-2.6 (Figure 6B), the humidity will still exert a stronger influence on heat mortality changes than the temperature in the northern subregions (NC, NE, and NW). However, its impact will diminish compared to the present, with the most significant decrease occurring in NC (almost 10%). Under SSP2-4.5 and SSP3-7.0 (Figures 6C,D), only one subregion each, NC and NW respectively, will have slightly higher contributions from humidity compared to temperature. In the case of SSP5-8.5, temperature will hold a greater sway on heat-related mortality than humidity across all subregions, particularly in SC, where temperature is projected to account for 85.9% of the contributions. Overall, the future impacts of temperature on heat-related mortality will amplify as emissions-driven climate warming intensifies.

4. Discussion

Humidity emerges as a pivotal factor in shaping heat-related health vulnerabilities. This study leverages the NEX-GDDP-CMIP6 datasets to project forthcoming heat-related mortality in China, incorporating the HSI that encapsulates both temperature and humidity. The results underscore a future surge in heat-related mortality across China and its subregions due to the confluence of climate change and emissions. A noteworthy and intriguing discovery lies in the higher contribution of humidity to changes in heat mortality within the northern subregions compared to their southern counterparts. This phenomenon might be attributed to the prevalence of wet and dry heat events, often coinciding with extreme heat occurrences. In regions marked by predominantly wet and warm conditions, like the south, high humidity during heat events mitigates the impact, rendering humidity-driven changes less influential. In contrast, the northern areas witness fluctuations in humidity that can convert a dry heat event into a moist one, leading the HSI to surpass critical risk thresholds. In such scenarios, the effect of humidity is amplified, accentuating its role in shaping heat-related mortality.

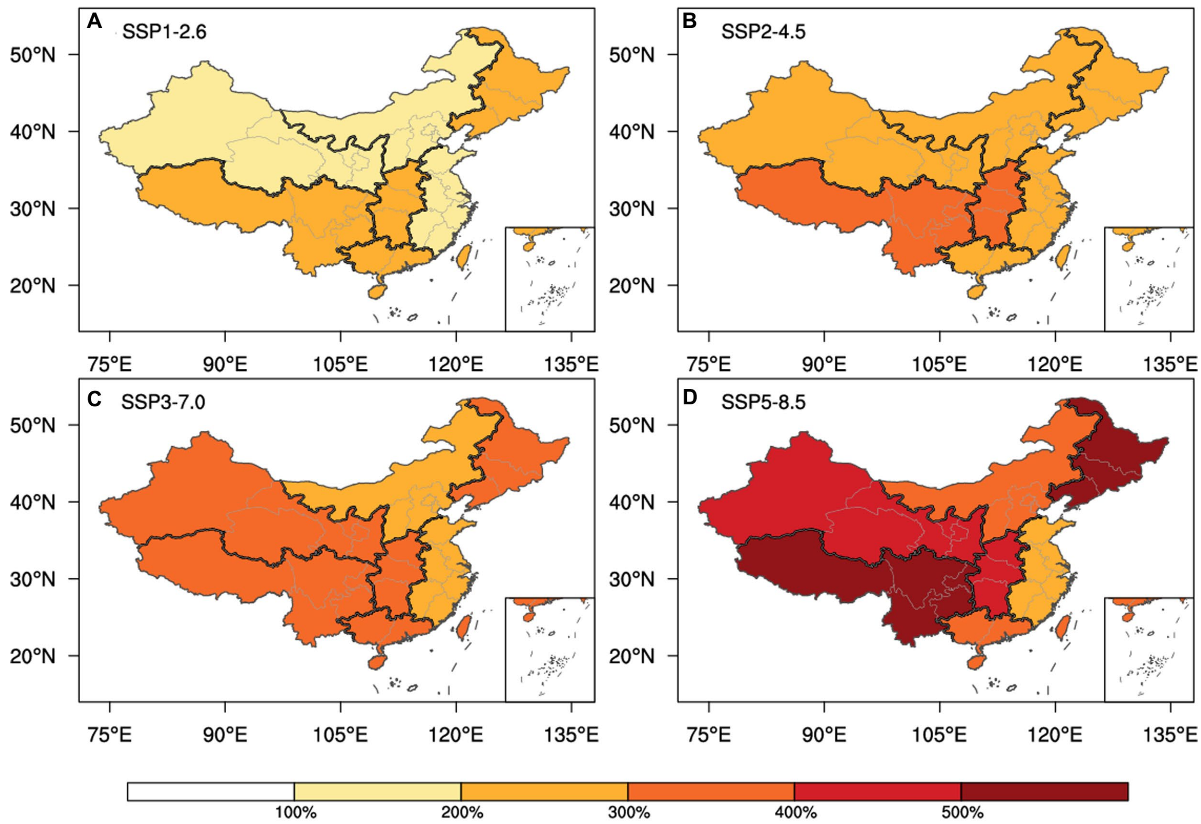

FIGURE 5
Altering proportions of upcoming heat-related mortality as compared to the present baseline, averaged across the period 2031 to 2100, across the scenarios SSP1-2.6 **(A)**, SSP2-4.5 **(B)**, SSP3-7.0 **(C)**, and SSP5-8.5 **(D)**.

Furthermore, our findings reveal a noteworthy similarity in the anticipated heat-related hazards across various emissions scenarios prior to 2040. This resemblance can be attributed to the persistent nature of greenhouse gases in the environment, suggesting that alterations in carbon emissions will not yield immediate climate effects. Consequently, the populace of China will persist in confronting noteworthy heat vulnerabilities in the forthcoming decades. It's important to emphasize that even within a trajectory of lower emissions (SSP1-2.6), the future toll of heat-related fatalities is projected to exceed current levels, thereby presenting substantial challenges for both emergency response protocols and healthcare systems. Hence, in conjunction with the endeavor to curtail emissions for the purpose of achieving carbon neutrality, it becomes imperative to formulate localized emergency strategies that adeptly manage the repercussions of extreme heat on human well-being.

Our findings exhibit both similarities and differences when compared to previous studies utilizing raw CMIP6 simulations (11, 12, 16, 33, 42, 49). Specifically, we find that future HSI with the related heat risks will increase with higher emissions across China, particularly in high latitude and high altitude areas. Additionally, we note that the humidity in NC is projected to increase in the future. This aligns with the findings of Zhang et al. (16), which indicated an increase in humidity for the Beijing-Tianjin-Hebei urban agglomeration. These consistent results support the robustness of our and previous conclusions. However, it is worth mentioning that the future increases in HSI projected in our study are slightly lower compared to previous CMIP6-based findings, particularly in northern areas. This discrepancy may be attributed to the bias correction and statistical downscaling applied by NEX-GDDP-CMIP6, which could lead to a reduction in the estimated future temperatures (24). Furthermore, our study suggests that future changes in humidity are unlikely to exceed ±3% across China, whereas a previous study indicated a reduction in humidity exceeding 4% in CC (16). The reasons behind these differences require further investigation and may also be associated with the BCSD method performed by NEX-GDDP-CMIP6.

This study presents several limitations that warrant consideration. The influence of societal progressions on human adaptation to elevated temperatures cannot be overlooked. Factors such as economic prosperity, medical advancements, and educational improvements can potentially reshape baseline mortality, consequently impacting heat-related fatalities. Within the scope of this investigation, we operate under the assumption that forthcoming populations will maintain a comparable baseline mortality rate and a similar relationship between HSI and mortality as observed presently. However, it's important to acknowledge that the HSI-mortality relationship is poised to change in response to the evolution of human tolerance to elevated temperatures. For instance, as human resilience to heat stress strengthens, the HSI value associated with the lowest mortality is likely to rise. These dynamic elements introduce intricacies and uncertainties into the risk assessment undertaken within this study. Subsequent assessments could enhance precision in forecasting

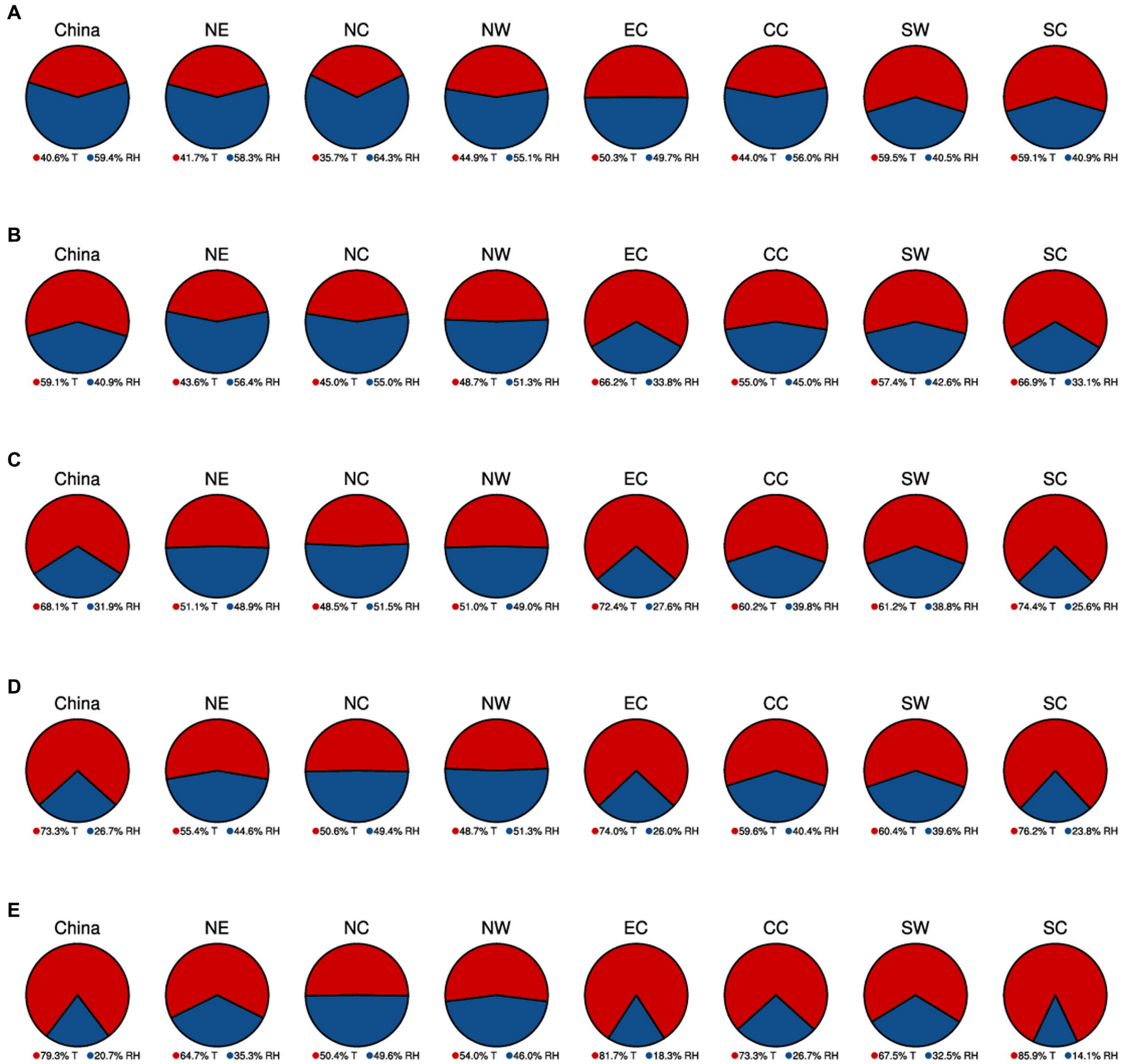

FIGURE 6
The pie charts illustrate the combined impacts of humidity (blue) and temperature changes (red) on heat-related mortality in China and its seven subregions for the period 2031 to 2100. These projections encompass scenarios from SSP1-2.6 **(A)**, SSP2-4.5 **(B)**, SSP3-7.0 **(C)**, and SSP5-8.5 **(D)**.

HSI-related fatalities by recalibrating exposure-response connections and baseline mortality figures, leveraging more advanced data. Additionally, it's worth noting that the methodology of statistical downscaling primarily hinges on statistical correlations and pattern assimilation, without direct modeling of physical mechanisms. This could potentially introduce biases between downscaled projections and actual physical processes, particularly on a global scale where future conditions deviate from the present circumstances.

5. Conclusion

In summary, this study offers projections of forthcoming alterations in heat stress and heat-associated mortality across China and its subregions within the context of diverse emission scenarios. The outcomes underscore a universal escalation in the annual heat stress index (HSI) across all envisaged pathways, with the most significant surge anticipated within the high-emission context (SSP5-8.5). By the year 2100, China's HSI will amplify by 7.96°C under SSP5-8.5. Notably, among the subregions, the most substantial HSI augmentation is expected within SC, whereas NW is poised to exhibit the slightest rise. Furthermore, the prognosis reveals a projected increase in future heat-related mortality, eclipsing current benchmarks across all scenarios. The acutest escalation in heat-related mortality emerges for SSP5-8.5. However, even within the relatively moderate emission framework of SSP1-2.6, China's heat-related mortality is poised to potentially double the present rate. Within the analysis, we also delve into the contributions of temperature and humidity to shifts in heat-related mortality. Presently, humidity exerts a more pronounced influence on these variations. Yet, with the trajectory of heightened emissions and impending global warming, temperature is anticipated to evolve into the predominant determinant. These revelations underscore the exigency for adaptive strategies to ameliorate the repercussions of heat stress and heat-related mortality across China. The imperative lies in not only emissions reduction but also in the strategic implementation of planning measures to adeptly navigate climate transformations and safeguard public well-being.

Code availability

The above analyses were performed using R (version 4.2), Python (version 3.9), and NCL (version 6.6), and the code is available on request.

Data availability statement

The raw data supporting the conclusions of this article will be made available by the authors, without undue reservation.

Author contributions

GZ: Conceptualization, Data curation, Funding acquisition, Methodology, Project administration, Writing – original draft, Writing – review & editing. LH: Data curation, Formal analysis, Methodology, Writing – review & editing. JnY: Investigation, Methodology, Project administration, Writing – review & editing. JiY: Conceptualization, Investigation, Project administration, Supervision, Validation, Visualization, Writing – review & editing, Funding acquisition, Resources. ZX: Data curation, Project administration, Supervision, Visualization, Writing – original draft. XC: Writing – review & editing. JH: Writing – review & editing. LP: Formal analysis, Investigation, Visualization, Writing – review & editing.

Funding

The author(s) declare financial support was received for the research, authorship, and/or publication of this article. Financial support for this research is provided by several sources, including the "Unveiling and Commanding" from CMA (No. CMAJBGS202207), the National Natural Science Foundation of China (Grant Nos. 42205170 and 42305200), the CMA Key Open Laboratory of Transforming Climate Resources to Economy (No. 2023009), the Public Health Service Capability Improvement Project from the National Health Commission of the People's Republic of China (No. 2100409034), the Key Innovation Team of China Meteorological Administration (No. CMA2022ZD09), and the Open Grants of the State Key Laboratory of Severe Weather (No. 2023LASW-B19), and the BMBKJ202201005 from Beijing Meteorological Service.

Acknowledgments

The authors thank the reviewers for their constructive comments.

Conflict of interest

The authors declare that the research was conducted in the absence of any commercial or financial relationships that could be construed as a potential conflict of interest.

Publisher's note

All claims expressed in this article are solely those of the authors and do not necessarily represent those of their affiliated organizations, or those of the publisher, the editors and the reviewers. Any product that may be evaluated in this article, or claim that may be made by its manufacturer, is not guaranteed or endorsed by the publisher.

Supplementary material

The Supplementary material for this article can be found online at: https://www.frontiersin.org/articles/10.3389/fpubh.2023.1282497/full#supplementary-material

References

1. IPCC. Climate change 2021 In: V Masson-Delmotte, P Zhai, A Pirani, SL Connors, C Péan and S Bergeret al, editors. *The physical science basis. Contribution of Working Group I to the sixth assessment report of the intergovernmental panel on climate change*. Cambridge: Cambridge University Press (2021).

2. IPCC. Climate change 2022: mitigation of climate change. *In:* Shukla PR, Slade R, Khourdajie AAl, Van Diemen R, Mccollum D, Pathak M, et al. *Contribution of Working Group III to the sixth assessment report of the intergovernmental panel on climate change*. Cambridge: Cambridge University Press (2022).

3. Casanueva A, Kotlarski S, Herrera S, Fischer AM, Kjellstrom T, Schwierz C. Climate projections of a multivariate heat stress index: the role of downscaling and bias correction. *Geosci Model Dev*. (2019) 12:3419–38. doi: 10.5194/gmd-12-3419-2019

4. Baldwin JW, Dessy JB, Vecchi GA, Oppenheimer M. Temporally compound heat wave events and global warming: an emerging hazard. *Earths Future*. (2019) 7:411–27. doi: 10.1029/2018EF000989

5. Dematte JE, O'Mara K, Buescher J, Whitney CG, Forsythe S, McNamee T, et al. Near-fatal heat stroke during the 1995 heat wave in Chicago. *Ann Intern Med*. (1998) 129:173–81. doi: 10.7326/0003-4819-129-3-199808010-00001

6. Robine JM, Cheung SL, Le Roy S, Van Oyen H, Griffiths C, Michel JP, et al. Death toll exceeded 70,000 in Europe during the summer of 2003. *C R Biol*. (2008) 331:171–8. doi: 10.1016/j.crvi.2007.12.001

7. Fischer EM, Knutti R. Anthropogenic contribution to global occurrence of heavy-precipitation and high-temperature extremes. *Nat Clim Chang*. (2015) 5:560–4. doi: 10.1038/nclimate2617

8. Schiermeier Q. Climate change made North America's deadly heatwave 150 times more likely. *Nature*. (2021). doi: 10.1038/d41586-021-01869-0

9. Cai W, Zhang C, Suen HP, Ai S, Bai Y, Bao J, et al. The 2020 China report of the Lancet Countdown on health and climate change. *Lancet Public Health*. (2021) 6:e64–81. doi: 10.1016/S2468-2667(20)30256-5

10. Cai W, Zhang C, Zhang S, Ai S, Bai Y, Bao J, et al. The 2021 China report of the Lancet Countdown on health and climate change: seizing the window of opportunity. *Lancet Public Health*. (2021) 6:e932–47. doi: 10.1016/S2468-2667(21)00209-7

11. Yang J-X, Zhou B-Q, Zhai P-M. Constrained high-resolution projection of hot extremes in the Beijing–Tianjin–Hebei region of China. *Adv Clim Chang Res*. (2023) 14:387–93. doi: 10.1016/j.accre.2023.04.008

12. Zhang G, Ma J, Meng C, Wang J, Xu Z, Gou P. Increasing heatwave with associated population and GDP exposure in North China. *Int J Climatol*. (2023) 43:4716–32. doi: 10.1002/joc.8113

13. Zhang GW, Zeng G, Yang XY, Iyakaremye V. Two spatial types of North China heatwaves and their possible links to Barents-Kara Sea ice changes. *Int J Climatol*. (2022) 42:6876–89. doi: 10.1002/joc.7617

14. Xing Q, Sun Z, Tao Y, Zhang X, Miao S, Zheng C, et al. Impacts of urbanization on the temperature-cardiovascular mortality relationship in Beijing, China. *Environ Res*. (2020) 191:110234. doi: 10.1016/j.envres.2020.110234

15. Yang J, Zhou M, Ren Z, Li M, Wang B, Liu L, et al. Projecting heat-related excess mortality under climate change scenarios in China. *Nat Commun*. (2021) 12:1039. doi: 10.1038/s41467-021-21305-1

16. Zhang GW, Zeng G, Liang XZ, Huang CR. Increasing heat risk in China's urban agglomerations. *Environ Res Lett*. (2021) 16:064073. doi: 10.1088/1748-9326/ac046e

17. Moss RH, Edmonds JA, Hibbard KA, Manning MR, Rose SK, Van Vuuren DP, et al. The next generation of scenarios for climate change research and assessment. *Nature*. (2010) 463:747–56. doi: 10.1038/nature08823

18. Kriegler E, O'Neill BC, Hallegatte S, Kram T, Moss RH, Lempert RJ, et al. Socio-economic scenario development for climate change analysis In: *CIRED working papers hal-00866437*. Paris, France: CIRAD. (2010).

19. O'Neill BC, Kriegler E, Ebi KL, Kemp-Benedict E, Riahi K, Rothman DS, et al. The roads ahead: narratives for shared socioeconomic pathways describing world futures in the 21st century. *Glob Environ Change*. (2017) 42:169–80. doi: 10.1016/j.gloenvcha.2015.01.004

20. Eyring V, Bony S, Meehl GA, Senior CA, Stevens B, Stouffer RJ, et al. Overview of the Coupled Model Intercomparison Project Phase 6 (CMIP6) experimental design and organization. *Geosci Model Dev*. (2016) 9:1937–58. doi: 10.5194/gmd-9-1937-2016

21. Wang J, Chen Y, Liao WL, He GH, Tett SFB, Yan ZW, et al. Anthropogenic emissions and urbanization increase risk of compound hot extremes in cities. *Nat Clim Chang*. (2021) 11:1084–9. doi: 10.1038/s41558-021-01196-2

22. Wang J, Chen Y, Tett SFB, Yan Z, Zhai P, Feng J, et al. Anthropogenically-driven increases in the risks of summertime compound hot extremes. *Nat Commun*. (2020) 11:528. doi: 10.1038/s41467-019-14233-8

23. Chai YF, Yue Y, Slater LJ, Yin JB, Borthwick AGL, Chen TX, et al. Constrained CMIP6 projections indicate less warming and a slower increase in water availability across Asia. *Nat Commun*. (2022) 13:424. doi: 10.1038/s41467-022-31782-7

24. Thrasher B, Wang W, Michaelis A, Melton F, Lee T, Nemani R. Nasa global daily downscaled projections, CMIP6. *Sci Data*. (2022) 9:262. doi: 10.1038/s41597-022-01393-4

25. Wood AW, Leung LR, Sridhar V, Lettenmaier DP. Hydrologic implications of dynamical and statistical approaches to downscaling climate model outputs. *Clim Chang*. (2004) 62:189–216. doi: 10.1023/B:CLIM.0000013685.99609.9e

26. Wood AW, Maurer EP, Kumar A, Lettenmaier DP. Long-range experimental hydrologic forecasting for the eastern United States. *J Geophys Res-Atmos*. (2002) 107:ACL 6-1–ACL 6-15. doi: 10.1029/2001JD000659

27. Chen M, Chen L, Zhou Y, Hu M, Jiang Y, Huang D, et al. Rising vulnerability of compound risk inequality to ageing and extreme heatwave exposure in global cities. *npj Urban Sustain*. (2023) 3:38. doi: 10.1038/s42949-023-00118-9

28. Wu F, Jiao D, Yang X, Cui Z, Zhang H, Wang Y. Evaluation of NEX-GDDP-CMIP6 in simulation performance and drought capture utility over China—based on DISO. *Hydrol Res*. (2023) 54:703–21. doi: 10.2166/nh.2023.140

29. Xu L, Zhang T, Yu W, Yang S. Changes in concurrent precipitation and temperature extremes over the Asian monsoon region: observation and projection. *Environ Res Lett*. (2023) 18:044021. doi: 10.1088/1748-9326/acbfd0

30. Zhang Y, You Q, Ullah S, Chen C, Shen L, Liu Z. Substantial increase in abrupt shifts between drought and flood events in China based on observations and model simulations. *Sci Total Environ*. (2023) 876:162822. doi: 10.1016/j.scitotenv.2023.162822

31. Thrasher B, Maurer EP, Mckellar C, Duffy PB. Technical note: Bias correcting climate model simulated daily temperature extremes with quantile mapping. *Hydrol Earth Syst Sci*. (2012) 16:3309–14. doi: 10.5194/hess-16-3309-2012

32. Jones B, O'Neill BC. Spatially explicit global population scenarios consistent with the shared socioeconomic pathways. *Environ Res Lett*. (2016) 11:084003. doi: 10.1088/1748-9326/11/8/084003

33. Zhang GW, Zeng G, Yang XY, Jiang ZH. Future changes in extreme high temperature over China at 1.5 degrees C-5 degrees C global warming based on CMIP6 simulations. *Adv Atmos Sci*. (2021) 38:253–67. doi: 10.1007/s00376-020-0182-8

34. Russo S, Sillmann J, Sterl A. Humid heat waves at different warming levels. *Sci Rep*. (2017) 7:7477. doi: 10.1038/s41598-017-07536-7

35. Steadman RG. The assessment of sultriness. Part I: a temperature-humidity index based on human physiology and clothing science. *J Appl Meteorol*. (1979) 18:861–73. doi: 10.1175/1520-0450(1979)018<0861:TAOSPI>2.0.CO;2

36. Buzan JR, Oleson K, Huber M. Implementation and comparison of a suite of heat stress metrics within the Community Land Model version 4.5. *Geosci Model Dev*. (2015) 8:151–70. doi: 10.5194/gmd-8-151-2015

37. Gasparrini A, Armstrong B, Kenward MG. Distributed lag non-linear models. *Stat Med*. (2010) 29:2224–34. doi: 10.1002/sim.3940

38. Xing Q, Sun Z, Tao Y, Shang J, Miao S, Xiao C, et al. Projections of future temperature-related cardiovascular mortality under climate change, urbanization and population aging in Beijing, China. *Environ Int*. (2022) 163:107231. doi: 10.1016/j.envint.2022.107231

39. Chen H, Zhao L, Dong W, Cheng L, Cai W, Yang J, et al. Spatiotemporal variation of mortality burden attributable to heatwaves in China, 1979–2020. *Sci Bull*. (2022) 67:1340–4. doi: 10.1016/j.scib.2022.05.006

40. Gasparrini A, Guo Y, Hashizume M, Lavigne E, Zanobetti A, Schwartz J, et al. Mortality risk attributable to high and low ambient temperature: a multicountry observational study. *Lancet*. (2015) 386:369–75. doi: 10.1016/S0140-6736(14)62114-0

41. Yang J, Yin P, Sun J, Wang B, Zhou M, Li M, et al. Heatwave and mortality in 31 major Chinese cities: definition, vulnerability and implications. *Sci Total Environ*. (2019) 649:695–702. doi: 10.1016/j.scitotenv.2018.08.332

42. Zhang G, Sun Z, Han L, Iyakaremye V, Xu Z, Miao S, et al. Avoidable heat-related mortality in China during the 21st century. *npj Clim Atmos Sci*. (2023) 6:81. doi: 10.1038/s41612-023-00404-4

43. Hu J, He G, Meng R, Gong W, Ren Z, Shi H, et al. Temperature-related mortality in China from specific injury. *Nat Commun*. (2023) 14:37. doi: 10.1038/s41467-022-35462-4

44. Huang C, Cheng J, Phung D, Tawatsupa B, Hu W, Xu Z. Mortality burden attributable to heatwaves in Thailand: a systematic assessment incorporating evidence-based lag structure. *Environ Int*. (2018) 121:41–50. doi: 10.1016/j.envint.2018.08.058

45. Gasparrini A, Guo Y, Sera F, Vicedo-Cabrera AM, Huber V, Tong S, et al. Projections of temperature-related excess mortality under climate change scenarios. *Lancet Planet Health*. (2017) 1:360–367. doi: 10.1016/S2542-5196(17)30156-0

46. Bonate PL. A brief introduction to Monte Carlo simulation. *Clin Pharmacokinet*. (2001) 40:15–22. doi: 10.2165/00003088-200140010-00002

47. Vicedo-Cabrera AM, Sera F, Gasparrini A. Hands-on tutorial on a modeling framework for projections of climate change impacts on health. *Epidemiology*. (2019) 30:321–9. doi: 10.1097/EDE.0000000000000982

48. Breiman L. Random forests. *Mach Learn*. (2001) 45:5–32. doi: 10.1023/A:1010933404324

49. Sun Z, Wang Q, Chen C, Yang Y, Yan M, Du H, et al. Projection of temperature-related excess mortality by integrating population adaptability under changing climate—China, 2050s and 2080s. *China CDC Wkly*. (2021) 3:697–701. doi: 10.46234/ccdcw2021.174

TYPE Original Research
PUBLISHED 03 October 2023
DOI 10.3389/fpubh.2023.1266643

OPEN ACCESS

EDITED BY
Zhaobin Sun,
Chinese Academy of Meteorological Sciences, China

REVIEWED BY
Guwei Zhang,
China Meteorological Administration, China
Bo Wang,
Hanzhong Central Hospital, China

*CORRESPONDENCE
Guiqin Fu
✉ fgq84@tom.com

RECEIVED 25 July 2023
ACCEPTED 29 August 2023
PUBLISHED 03 October 2023

CITATION
Fu GQ, Cheng HM, Lu Q, Liu HY, Zhang XH and Zhang XS (2023) The synergistic effect of high temperature and ozone on the number of deaths from circulatory system diseases in Shijiazhuang, China.
Front. Public Health 11:1266643.
doi: 10.3389/fpubh.2023.1266643

The synergistic effect of high temperature and ozone on the number of deaths from circulatory system diseases in Shijiazhuang, China

Guiqin Fu[1,2,3]*, Haimin Cheng[2,3], Qian Lu[1,2,4], Huayue Liu[1,3], Xiaohui Zhang[4] and Xingshan Zhang[5]

[1]China Meteorological Administration Xiong'an Atmospheric Boundary Layer Laboratory, Xiong'an, China, [2]Key Laboratory of Meteorology and Ecological Environment of Hebei Province, Shijiazhuang, China, [3]Hebei Meteorological Service Center, Shijiazhuang, China, [4]Chengde Meteorological Service of Hebei Province, Chengde, China, [5]Handan Meteorological Service of Hebei Province, Handan, China

Introduction: Urban ozone pollution in China is becoming increasingly serious. Climate warming, high temperatures, and ozone pollution all have significant impacts on human health. However, the synergistic effects of high temperatures and ozone pollution in summer on human health are rarely studied. China is at a critical stage of environmental pollution control. Assessing the health impact of high temperatures and ozone exposure on the number of deaths from circulatory diseases is of great significance for formulating ozone-related prevention and control policies.

Methods: This study uses daily data on deaths from circulatory system diseases in Shijiazhuang from June to August during the summer of 2013–2016, as well as concurrent meteorological data and concentration of O_3 and $PM_{2.5}$ pollution data. The generalized additive model (GAM) with Poisson distribution, smooth curve threshold effect, and saturation effect method is used to control for confounding effects.

Results: The study evaluates the impact of short-term exposure to temperature and ozone on deaths from circulatory system diseases and the synergistic effect after controlling for confounding factors. The results show that the impact of temperature and ozone on deaths from circulatory system diseases in Shijiazhuang is nonlinear, with a temperature threshold of 27.5°C and an ozone concentration threshold of 100 $\mu g/m^3$. With an increase of temperature by 1°C, the risk of deaths for total population, men and women are 6.8%, 4.6% and 9.3%, respectively. The increase in temperature and ozone concentration has a greater impact on women; in men, the increase has a lag effect of 2 to 3 days, but the lag did not affect women.

Discussion: In conclusion, high temperatures and high ozone concentration have synergistic enhancement effects on circulatory system diseases. Prevention and scientific management strategies of circulatory system diseases in high temperatures and high ozone environments should be strengthened.

KEYWORDS
high temperature and ozone concentration, circulatory diseases, the number of deaths, synergistic effect, health effect

1. Introduction

China used to suffer from serious air pollution. With the Chinese government's efforts to reduce emissions, $PM_{2.5}$ and other fine particulate matter pollution has been significantly improved. However, ozone (O_3) pollution has become increasingly serious in recent years, and has become a serious problem for China's urban environment (1–3). Especially against the background of global warming, the frequency and intensity of heat wave events has increased. The dual effects of high temperatures and ozone pollution may coexist for a long time, and will seriously threaten people's health and become a new focus of attention (4–6).

According to the Lancet Countdown China report, the number of heatwave exposure days *per capita* in China increased by 4.51 days in 2020 compared to the 1986–2005 average, resulting in an increase of about 92% in heatwave related deaths, and the impact on human health is increasing. High ozone pollution can lead to an increase in related diseases and deaths (7–9). Previous studies focused more on the impact of one atmospheric environmental condition on health, such as high temperatures or ozone. However, there are few studies on whether high temperatures and ozone exposure have synergistic effects on human health.

The Beijing-Tianjin-Hebei region is an area with serious air pollution, and the ozone concentration has been on the rise in recent years (10, 11). Shijiazhuang, the capital city of Hebei Province, is also a representative city in northern China. In this paper, ozone concentration data published on the website of the Ministry of Environmental Protection of China during 2013–2016 and circulatory system disease deaths in Shijiazhuang during the same period are used. Based on epidemiological analysis, a generalized additive model and nonparametric binary response model are used to evaluate the effects of air temperature and short-term exposure to ozone on the number of deaths from circulatory system diseases in Shijiazhuang. The objective is to further explore the impact risks of high temperatures and O_3 pollution on human health in an environment with multiple exposures, so as to strengthen the proactive prevention awareness of highly sensitive people and provide a basis for the government to formulate scientific prevention and control policies.

2. Data and methods

2.1. Data sources

This study is conducted in Shijiazhuang (114° 48'e, 38° 03'n), the capital of Hebei Province in northern China. The number of daily circulatory disease deaths in Shijiazhuang during the summer (from 1 June to 31 August) from 2013 to 2016 is obtained from the Chinese Center for Disease Control and Prevention. According to the 10th edition of the International Classification of Diseases (IDC-10, coded as I00-99), deaths from coronary heart disease, ischemic heart disease, ischemic stroke, cerebral hemorrhage, and cerebral infarction are included.

The data of daily mean temperature, relative humidity, and air pressure in Shijiazhuang during the summer (from 1 June to 31 August) from 2013 to 2016 are provided by Hebei Meteorological Information Center. Data of O_3 (O_3-8h) and $PM_{2.5}$ average daily concentration of atmospheric pollutants during the same period are obtained from the website of the Ministry of Environmental Protection of China. All of this data are quality-controlled before being released by professional organizations.

2.2. Research methods

The daily death number of circulatory system diseases is calculated according to time series, and the influence of temperature and O_3 short-term exposure on death number of circulatory system diseases is evaluated using a generalized additive model (GAM) of Poisson distribution (12, 13). Before assessing the synergistic effect of air temperature and O_3 on the daily death number of circulatory system diseases, the influences of daily mean air temperature and O_3 concentration on daily death number of circulatory system diseases are studied, respectively, to determine whether there is a curve relationship. In this model, the daily death number of circulatory system diseases is taken as the dependent variable, the air temperature (O_3) as the independent variable, and the regression spline function is used to control the confounding effects of time trend (Time), annual change (Year), Holiday effect (Holiday), relative humidity (RH), and $PM_{2.5}$ concentration. The partial autocorrelation function (PACF) is used to select the degrees of freedom for the time trend until the absolute value of the sum of PACFs reaches a minimum. The research formula is as follows:

$$\log\left[\mathrm{E}\left(Y_t|\mathrm{X}\right)\right]=\alpha+\beta\mathrm{X}+s\left(time, df=4\right)+s\left(PM_{2.5}, df=2\right)$$
$$+RH+Year+Holiday$$

In the formula, Y_t is the daily death number of circulatory diseases on day t, E ($Yt|X$) is the expected daily number of deaths from circulatory system diseases on day t, α is the intercept, β is the regression coefficient, X is the temperature T (ozone O_3), $s()$ is a nonlinear spline function, and df is the degree of freedom.

Secondly, stratified thresholds of daily mean temperature and O_3 concentration are analyzed according to threshold effect and saturation effect of smooth curves, and tested by logarithmic likelihood ratio. Third, the synergistic effect of air temperature and O_3 on the daily death number of circulatory diseases is analyzed.

All results are expressed as relative risk (RR) and 95% confidence interval (95% CI), with $p < 0.05$ as the test of statistical significance. In addition, the impact on different genders is assessed.

3. Results

3.1. Background analysis of air pollution in Shijiazhuang

According to GB 9137–88 and HJ 633–2012, the concentrations of major air pollutants O_3 and $PM_{2.5}$ in Shijiazhuang are calculated from June to August in the summers of 2013–2019, and their

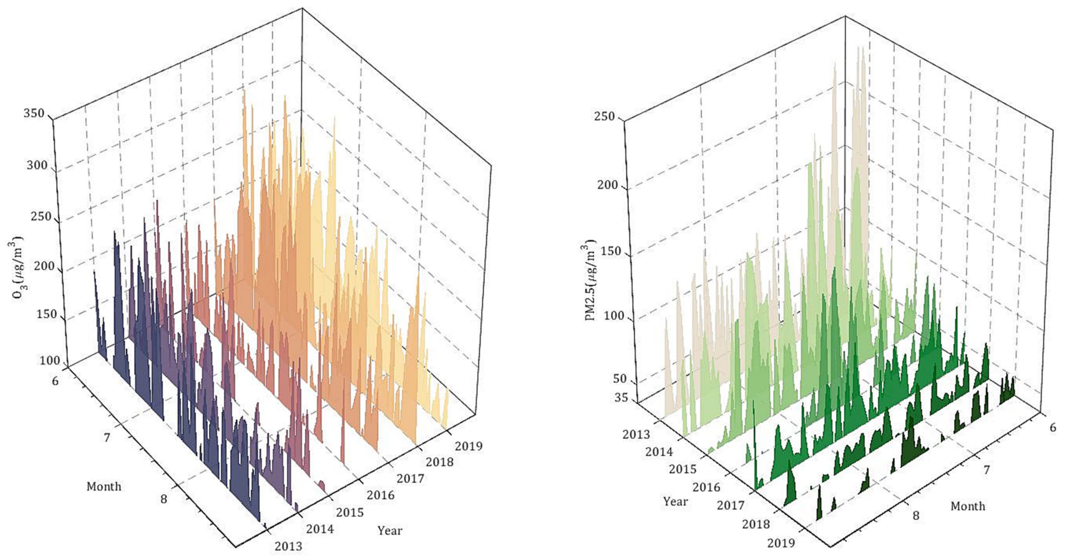

FIGURE 1
$PM_{2.5}$ and ozone concentrations in summer (June to August) from 2013 to 2019 in Shijiazhuang City.

concentrations relative to $O_3 < 100\,\mu g/m^3$ (Grade I: excellent) and the number of days exceeding the standard compared with $PM_{2.5} < 35\,\mu g/m^3$ (Grade I: excellent) to analyze the change characteristics of air pollution in Shijiazhuang. Figure 1 shows the number of days when the concentration of main air pollutants O_3 and $PM_{2.5}$ exceeded the standard in Shijiazhuang and their variation trends. Over the past 7 years, as the government has stepped up to address pollution, the $PM_{2.5}$ concentration in Shijiazhuang has dropped significantly in summer, with the number of days with $PM_{2.5}$ exceeding $35\,\mu g/m^3$ decreasing by 5.3 days per year on average. The average $PM_{2.5}$ concentration in the summer of 2013 was $94.3\,\mu g/m^3$, and by the same period in 2019 it was $34.3\,\mu g/m^3$, which means the average $PM_{2.5}$ air quality level throughout the summer is excellent. However, the O_3 concentration shows an obvious upward trend. In the summer of 2013, the average O_3 concentration was $137.3\,\mu g/m^3$, while in the summer of 2019, the average O_3 concentration was $137.3\,\mu g/m^3$. The average O_3 concentration increased by 27.6% over the past 7 years. The number of days exceeding the O_3 standard increased from 66 days in 2013 to 84 days in 2019, with an annual growth rate of 3.6. It can be seen that ozone pollution should become a new focus of attention.

3.2. Statistical characteristics of circulatory system disease deaths, pollutant concentration, and meteorological elements in Shijiazhuang

Table 1 shows the statistical characteristics of circulation system deaths and meteorological environment elements in Shijiazhuang. In the summer (1 June to 31 August) from 2013 to 2016, 4,420 people died from circulatory diseases in Shijiazhuang city, of which 54.3% were men and 45.7% were women. The average daily death number from circulatory system diseases in Shijiazhuang city was 12.0, and the maximum daily death number was 40.0. During the corresponding period, the average daily temperature was 26.8°C, the relative humidity was 64.7%, O_3 concentration was $123.6\,\mu g/m^3$, and $PM_{2.5}$ concentration was $71\,\mu g/m^3$.

3.3. Exposure-response relationship between daily mean temperature, ozone, and deaths from circulatory diseases in Shijiazhuang

Figure 2 shows the exposure-response relationship between daily mean temperature, ozone concentration, and the number of deaths from circulatory diseases in Shijiazhuang. The model controls the confounding effects of time trend, annual change, holiday effect, relative humidity, and $PM_{2.5}$ concentration. The daily mean temperature, ozone concentration, and the number of deaths from circulatory diseases show nonlinear changes. The increased risk of daily deaths from circulatory diseases is 1.6% (95%CI: 1.001, 1.032) for every 1°C increase in daily mean temperature. The increased risk of daily death from circulatory disease is 2.1% for every $10\,\mu g/m^3$ increase in O_3 concentration (95%CI: 1.007, 1.034). It can be seen that rising temperatures and increasing ozone concentration are associated with an increased risk of death from circulatory diseases.

3.4. Effects of air temperature and ozone on circulatory disease deaths under different thresholds

Based on the previous analysis, the smoothing curve threshold effect and saturation effect method are used to analyze the threshold

TABLE 1 Statistical characteristics of circulatory system disease deaths and meteorological elements and air pollutants in Shijiazhuang from June to August, 2013 to 2016.

		Average	Standard deviation	Min	P25	P50	P75	Max
Deaths from circulatory diseases	Total number	12.0	4.4	4.0	9.0	12.0	14.2	40.0
	male	6.5	2.9	0.0	4.0	6.0	8.2	21.0
	female	5.5	2.7	1.0	4.0	5.0	7.0	19.0
Daily mean of meteorological elements	T	26.8	2.6	19.7	25.1	27.0	28.6	33.1
	RH	64.7	15.8	24.0	53.0	65.0	77.0	99.0
	P	993.3	3.8	981.8	990.6	993.5	996.0	1004.7
Daily mean of air pollution	O_3-8h	123.6	48.5	24.0	86.0	118.0	159.4	251.4
	$PM_{2.5}$	71.0	44.8	3.0	36.0	62.8	95.0	241.1

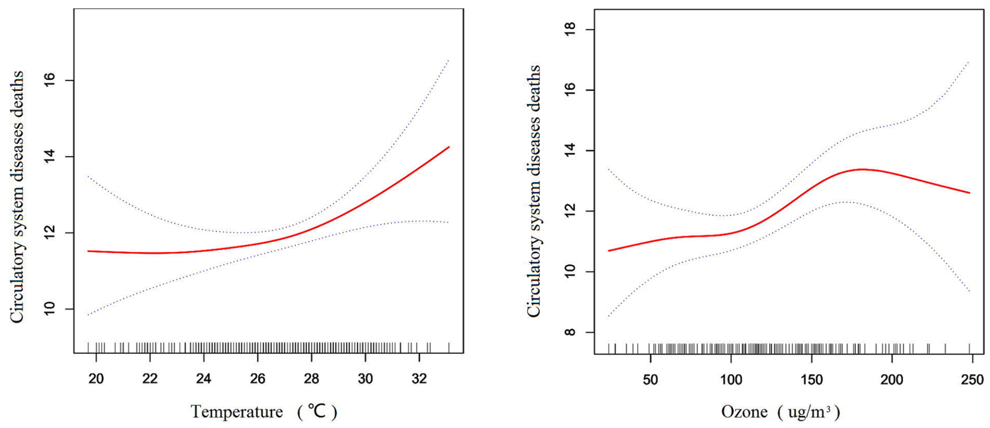

FIGURE 2
Variation curves of average temperature, O_3, and circulatory system disease deaths in Shijiazhuang from June to August, 2013 to 2016.

effect of temperature and ozone on the death number of circulatory system diseases. Table 2 shows the relative risk and 95% confidence interval (95%CI) of the influence of daily mean temperature on the number of deaths from circulatory diseases under the stratification of temperature and ozone threshold. When the daily mean temperature is higher than 27.5°C, the daily death number of circulatory diseases changes steadily with temperature. The relative risk (RR) of increased daily deaths from circulatory diseases is 0.997 (95%CI:0.976, 1.019) for every 1°C increase in mean temperature. If the RR is less than 1, no risk relationship is found. The RR of daily deaths from circulatory diseases increases by 1.049 (95%CI: 1.017, 1.083) for every 1°C increase in mean temperature above 27.5°C. RR greater than 1 is associated with an increased risk of 4.9% and is tested for significance at $p < 0.05$. The log-likelihood ratio of air temperature between the two layers is 0.023, and the threshold stratification is statistically significant.

Similarly, when the O_3 concentration is lower than 100 μg/m³, the RR for increasing the number of daily deaths from circulatory diseases is 0.994 (95%CI: 0.965, 1.025) with an increase of 10 μg/m³, and no risk relationship is found. When O_3 concentration is higher than 100 μg/m³, the RR of daily deaths from circulatory diseases increases by 1.037 (95%CI: 1.015, 1.059) and the risk increases by 3.7% for every 10 μg/m³ increase in O_3 concentration ($p < 0.0001$). The risk relationship passes the significance test.

3.5. Synergistic effects of air temperature and ozone on circulatory disease deaths

According to the stratification of ozone concentration and daily mean temperature threshold, the influence of every 1°C increase in daily mean temperature on the number of deaths from circulatory system diseases and the relationship between men and women are calculated, respectively, under different ozone concentrations and different temperature threshold intervals (Table 3). When the O_3 concentration is less than 100 μg/m³, the temperature effects of different stratifications are different. When the temperature is less than 27.5°C, no significant risk relationship is found among the total population or among men.

When the temperature is higher than 27.5°C, with an increase of temperature by 1°C, the risk of the total number of deaths from circulatory diseases is 6.8% (95% CI:0.929, 1.228), but there are only 33 samples, and $p < 0.05$ is not statistically significant. When the O_3 concentration is greater than 100 μg/m³ and the temperature is lower than 27.5°C, no significant risk is found in the total population or among

TABLE 2 Relative risk and 95% confidence interval (95%CI) for the effect of temperature and O3 on the number of circulatory system deaths in Shijiazhuang from June to August, 2013 to 2016.

Environmental element	Threshold value	RR (95%CI)	*p*
T (°C)	$T < 27.5$	0.997 (0.976, 1.019)	0.023
	$T \geq 27.5$	1.049 (1.017, 1.083)*	
O_3 (μg/m^3)	$O_3 < 100$	0.994 (0.965, 1.025)	0.063
	$O_3 \geq 100$	1.037 (1.015, 1.059)*	

*$p < 0.05$.

TABLE 3 Relative risk and 95% confidence interval (95%CI) of circulatory system deaths with every 1°C increase between different concentrations of temperature and O_3 interval.

People	O_3 (μg/m^3)	*T* (°C)	sample	Mean value	RR (95%CI)
Total number	<100	<27.5	97	11.8	0.992 (0.957, 1.027)
		≥27.5	33	13.1	1.068 (0.929, 1.228)
	≥100	<27.5	104	11.7	0.995 (0.955, 1.037)
		≥27.5	134	12.2	**1.068 (1.025, 1.114)***
Male	<100	<27.5	97	6.4	0.969 (0.924, 1.017)
		≥27.5	33	6.9	1.029 (0.848, 1.247)
	≥100	<27.5	104	6.5	0.987 (0.934, 1.042)
		≥27.5	134	6.5	**1.046 (0.988, 1.109)**
Female	<100	<27.5	97	5.4	1.020 (0.968, 1.074)
		≥27.5	33	6.1	1.005 (0.944, 1.070)
	≥100	<27.5	104	5.1	1.115 (0.909, 1.368)
		≥27.5	134	5.7	**1.093 (1.029, 1.162)***

*$p < 0.05$.

men. However, when the temperature is greater than or equal to 27.5°C, every 1°C increase in daily mean temperature has an increased risk for the total number of deaths from circulatory diseases, for men and women, of 6.8% (95%CI: 1.025, 1.114), 4.6% (95%CI: 0.988, 1.109), and 9.3% (95%CI: 1.029, 1.162). In conclusion, when the O_3 concentration is greater than 100 μg/m3 and the air temperature is greater than 27.5°C, both the total number and the number of male and female deaths show the greatest risk effect value, indicating that higher air temperature and high ozone pollution have a synergistic enhancement effect on the number of circulatory deaths, especially for women.

3.6. Lagged effects of temperature and ozone on deaths from circulatory diseases

Based on the analysis of the synergistic effect of temperature and ozone on the death number of circulatory system diseases, the lag effect is further analyzed. Table 4 shows the relative risk and 95% confidence interval (95%CI) of the total number of deaths in the circulatory system in Shijiazhuang for every 1°C increase in temperature when $O_3 \geq 100$ μg/m^3 and $T \geq 27.5$°C, with 0 to 9 days lag. It can be seen that the lag effect of the synergistic effect of temperature and ozone is more complex. The risk of 3 days lag (T.3) is 6.9% (95%CI:1.029, 1.111), and the risk of 9 days lag (T.9) increases to 7.7% (95%CI: 1.034, 1.121), $p < 0.001$, where the statistical significance is increased. For men, the risk increases to 6.4% at 2 to 3 days lag, and reaches the maximum of 7.7% at 7 days lag (95%CI: 1.021, 1.136), which passes the significance test of $p < 0.05$. While for women, it is still the same day that has the greatest impact risk and no lagged effect is found. In conclusion, the synergistic effect of air temperature and ozone has the highest risk for women and no lag effect is found, while for men there is a lag effect of 2 to 3 days and 7 days. The total number shows three high risk values on the same day, 3 days, and 9 days, respectively.

4. Discussion

It is found that the effects of daily mean temperature and ozone pollution on the number of deaths from circulatory diseases in summer are nonlinear. The threshold of daily mean temperature is 27.5°C, and the threshold of ozone pollution is 100 μg/m^3. High temperatures in summer increase the risk of death from circulatory diseases (14, 15). In terms of the temperature threshold index, the local comfortable temperature is used as a reference in many Chinese cities (16, 17) to obtain the temperature threshold that has an impact on the number of deaths from cardiovascular and cerebrovascular diseases. For example, the temperature in Chengdu, Harbin, Changsha, and Guangzhou is 22.2°C, 20.6°C, 25.1°C, and 26.5°C, respectively. In Shanghai (18), the median daily mean temperature of 18.2°C is taken as the reference, and

TABLE 4 The relative risk and 95% confidence interval (95%CI) of the effect of temperature increases of 1°C with different lag days on the total number of circulatory system deaths and gender in Shijiazhuang.

T (°C)	Total number	Men	Women
T	**1.068 (1.025, 1.114)***	1.046 (0.988, 1.109)	**1.093 (1.029, 1.162)***
T.1	1.061 (1.020, 1.103)*	1.045 (0.990, 1.102)	1.079 (1.020, 1.142)*
T.2	1.065 (1.025, 1.106)*	**1.064 (1.010, 1.121)***	1.066 (1.009, 1.127)*
T.3	**1.069 (1.029, 1.111)****	**1.064 (1.009, 1.122)***	1.075 (1.016, 1.13)*
T.4	1.065 (1.025, 1.107)*	1.061 (1.006, 1.118)*	1.071 (1.013, 1.132)*
T.5	1.067 (1.027, 1.108)**	1.066 (1.011, 1.123)*	1.068 (1.010, 1.128)*
T.6	1.066 (1.026, 1.107)**	1.072 (1.017, 1.129)*	1.059 (1.003, 1.119)*
T.7	1.071 (1.030, 1.113)**	**1.077 (1.021, 1.136)***	1.065 (1.006, 1.126)*
T.8	1.074 (1.033, 1.11)**	1.075 (1.018, 1.135)*	1.074 (1.014, 1.137)*
T.9	**1.077 (1.034, 1.121)****	1.070 (1.013, 1.131)*	1.084 (1.022, 1.149)*

*$p < 0.05$; **$p < 0.001$.

the risk effect of high temperatures of 30.1°C (95th percentile of temperature) on stroke can reach 26%. In Hong Kong (19), the 75th percentile of 27.8°C is used as the control, and the mortality risk of cardiovascular and cerebrovascular accidents is 9% (95%CI: 1.006, 1.125) when the temperature is higher than 31.5°C (99th percentile). Giang PN et al. (20) showed that when the average temperature in Vietnam is higher than 26°C, the risk of admission for cardiovascular and cerebrovascular diseases increase with the increase of temperature. In this paper, aiming at the influence of summer temperature on circulatory diseases, the threshold of 27.5°C is higher than the annual comfortable temperature, but it is equivalent to the 55th percentile for summer. The death risk of circulatory system diseases caused by high temperatures is mainly related to heat stimulation of the nervous regulation of the circulatory system, increased sweating, blood viscosity, blood vessel dilation, accelerated blood circulation, tachycardia, blood pressure changes, and internal blood insufficiency (21).

When O_3 concentration is higher than 100 μg/m^3, the risk of daily deaths from circulatory diseases in Shijiazhuang increased by 3.7% with every increase of 10 μg/m^3 in O_3 concentration, and the risk is statistically significant ($p < 0.05$). Gu et al. (22) studied the exposure-response relationship between ozone and the number of emergency patients with cardiovascular and cerebrovascular diseases in Ningbo, and showed that when ozone concentration increased by 10 μg/m^3 in the warm season, the number of emergency patients with cardiovascular and cerebrovascular diseases increased by 1.17%. Tao et al. (23) studied the acute effects of ozone pollution in the Pearl River Delta, and the total mortality rate increased by 0.81% when ozone concentration increased by 10 μg/m^3, which is consistent with the results of this study. Dong et al. (24) conducted a meta-analysis of short-term ozone exposure and mortality risk in a Chinese population, and demonstrated that the rise of atmospheric ozone concentration would lead to an increase in non-accidental total mortality, cardiovascular system disease mortality, and respiratory system disease mortality. However, Hu et al. (25) studied the relationship between atmospheric ozone concentration and residents' first aid in Shijiazhuang city from 2013 to 2015 and found that, when ozone concentration increased by 10 μg/m^3, the number of residents requiring first aid for respiratory diseases increased by 1.21%, but there was no significant change in the number of residents requiring first aid for circulatory diseases. This may be related to seasonal differences and whether to adjust the confounding effect of $PM_{2.5}$ pollutant (22, 26). This study mainly focuses on summer and adjusts the confounding effect of $PM_{2.5}$. Ozone has a strong oxidizing ability, and short-term exposure to ozone causes the increase of systemic oxidative stress, which is related to human platelet activation and blood pressure increase, thus affecting cardiovascular health (27, 28).

The synergistic effect of temperature and ozone on population health is less studied. The North China Plain is a region with high temperatures and ozone concentrations in the summer (11). It is found that, when $O_3 \geq 100$ μg/m^3 and $T \geq 27.5$°C, the risk of death in the circulatory system is the highest 6.8% (95%CI:1.025, 1.114), with it growing with every 1°C increase in temperature. When $O_3 < 100$ μg/m^3 and $T \geq 27.5$°C, the risk of circulatory death is still 6.8% (95%CI:0.929, 1.228), but is not statistically significant. When $T < 27.5$°C, no risk relationship is found whether ozone concentration is greater than 100 μg/m^3 or not. It shows that high temperatures mainly affect the death number of circulatory system diseases in summer, and high temperatures and high ozone pollution have a synergistic enhancement effect. The study by Zhang et al. (16) showed that the interaction between air temperature and pollutants had a very complex relationship on the number of deaths from diseases. When high temperatures and high ozone concentration co-existed, there was a synergistic strengthening effect on the number of deaths from respiratory and cardiovascular diseases, which was consistent with the results of this study. Zhang (29) studied the interaction effect between air temperature and $PM_{2.5}$ pollutant in Beijing and showed that when the air temperature was higher than 24°C, the risk of death from cardiovascular and cerebrovascular diseases caused by air temperature and $PM_{2.5}$ together reached 3.97%, which increased the risk of death from circulatory diseases in a high temperature and high pollution environment. Ren C (30) studied the short-term effects of air temperature and ozone on the total mortality in 60 communities in the eastern United States and pointed out that high temperatures could regulate the risk of ozone death, with certain regional differences.

In the study of the lag effect and gender difference, this study finds that under a high temperature and high ozone concentration environment, there is a 3-day lag effect on the total number of deaths on men from circulatory system diseases, but there is a lag effect on women. Zhang et al. (16) performed a single ozone lag analysis and found that the risk of death from cardiovascular and cerebrovascular diseases increased by 0.66% (95%CI: 0.42, 0.90) for every increase of ozone concentration of 10 μg/m^3 after 1 day's lag. Cao et al. (31) analyzed the impact of high temperatures and heat waves on death from cardiovascular and cerebrovascular diseases in Jinan and found that there was a lag of 1 to 2 days. Gu et al. (22) analyzed the influence of ozone concentration on cardiovascular and cerebrovascular diseases by using the reception data of emergency vehicles in Ningbo and found that when ozone concentration increased by 10 μg/m^3, the excess risk of the number of emergency patients for cardiovascular and cerebrovascular diseases was greater for men than women, and there was no lag effect. There are some similarities and differences between the above studies and the results of this study. In many studies, there is a lag analysis for high temperature, and there is also a lag analysis for the impact of pollutants, but the analysis of the synergistic lag of temperature and ozone is rare. Theoretically, there is a lag effect on circulatory disease from high temperatures, and there is also a lag effect from ozone. The high temperature and high ozone environment in summer enhances the risk of circulatory death, and the lag results obtained in this study are reliable.

In this study, Shijiazhuang, a representative city in northern China with frequent high temperatures in summer and serious ozone pollution, is selected. Disease data are circulatory system disease death data, and the selected cities and health conditions are more representative than outpatient case data. This study analyzes the single factor influence relationship, threshold index, synergistic effect, and lag effect of temperature and ozone, which is more comprehensive than previous analysis. It reflects the relationship based on the impact of temperature and ozone pollution on the number of deaths from circulatory system diseases, which is a common issue, but there may be certain limitations in individual exposure.

5. Conclusion

In this paper, daily circulatory system disease death data, meteorological data, and O_3 and $PM_{2.5}$ concentration pollution data in Shijiazhuang city from June to August in the summers of 2013 to 2016 were used to evaluate the impact of high temperatures and short-term exposure to O_3 on the number of deaths from circulatory system diseases after controlling the confounding effect. It was found that high temperatures and O_3 pollution had a synergistic effect on circulatory system diseases. It provides evidence for strengthening the prevention and scientific management of circulatory system diseases under high temperatures and in high ozone environments.

Data availability statement

The original contributions presented in the study are included in the article/supplementary material, further inquiries can be directed to the corresponding author.

Author contributions

GQF: Formal analysis, Methodology, Writing – original draft. HMC: Data curation, Writing – original draft. QL: Writing – review & editing. HYL: Validation, Writing – original draft. XHZ: Data curation, Writing – original draft. XSZ: Visualization, Writing – original draft.

Funding

The author(s) declare financial support was received for the research, authorship, and/or publication of this article. This study was co-funded by the Open Fund of the Public Service Center of China Meteorological Administration (grant No. M2022008) and the Health Meteorology Research and Development Project of Hebei Province (grant No. FW202150).

Conflict of interest

The authors declare that the research was conducted in the absence of any commercial or financial relationships that could be construed as a potential conflict of interest.

Publisher's note

All claims expressed in this article are solely those of the authors and do not necessarily represent those of their affiliated organizations, or those of the publisher, the editors and the reviewers. Any product that may be evaluated in this article, or claim that may be made by its manufacturer, is not guaranteed or endorsed by the publisher.

References

1. Cai S Y，Wang Y J，Zhao B， Wang S., Chang X., Hao J. The impact of the air pollution prevention and control action plan on $PM_{2.5}$ concentrations in Jing-Jin-Ji region during 2012–2020. *Sci Total Environ*，(2017) 580:197–209, doi: 10.1016/j.scitotenv.2016.11.188

2. Lu X，Hong J Y，Zhang L， Cooper O. R., Schultz M. G., Xu X., et al., *Environ Sci Technol Lett* (2018) 5:487–494, Severe surface ozone pollution in China: a global perspective, doi: 10.1021/acs.estlett.8b00366

3. Li K，Jacob D J，Liao H， Shen L, Zhang Q, Bates K H Anthropogenic drivers of 2013-2017 trends in summer surface ozone in China. *Proc Natl Acad Sci* (2019) 116:422–427, doi: 10.1073/pnas.1812168116

4. Sun, Q H， Ban, J， Chen, C，Li, TT. Heat wave health tisk early warning system:a review of recent studies. *J Environ Health* (2015) 32:1026–1030.

5. Zhang X，Liu Q Y. Overview of impact of heat wave on cardiovascular diseases. *Chin J Public Health* (2014) 30:242–243.

6. Anderson G B，Bell M L. Heat waves in the United States: mortality risk during heat waves and effect modification by heat wave characteristics in 43 U.S. communities. *EHP Toxicogenomics* (2011) 119:210–218, doi: 10.1289/ehp.1002313

7. Hu J X，Hou Z L, Xu Y J，，Zhou M., Zhou C., Xiao Y., et al. Life loss of cardiovascular diseases per death attributable to ambient temperature: a national time series analysis based on 364 locations in China. *Sci Total Environ*. (2020):142614, 756, doi: 10.1016/j.scitotenv.2020.142614

8. Eremenko M，Dufour G，Foret G，Keim C., Orphal J., Beekmann M. et al. Tropospheric ozone distributions over Europe during the heat wave in July 2007 observed from infrared nadir spectra recorded by IASI. *Geophys Res Lett* (2008) 35:60–74, doi: 10.1029/2008GL034803

9. Filleul L，Cassadou S，Médina S.，Fabres P., Lefranc A., Eilstein D., et al. The relation between temperature, ozone, and mortality in nine French cities during the heat wave of 2003. *Environ Health Perspect* (2006) 114:1344–1347, doi: 10.1289/ehp.8328

10. Wang, M，Zheng, YF， Liu, YJ，Li, QP, Ding, YH. Characteristics of ozone and its relationship with meteorological factors in Beijing-Tianjin-Hebei region. *China Environ Sci* (2019) 39:2689–2698.

11. Pu Q. *Analysis of elevated ozone formation mechanism and radiative effect during heat waves in Yangtze River Delta*. Nanjing University. (2017).

12. Fu G Q，Tian Y Q，Zhang C W. Synergistic effect of temperature and O_3 on the numbers of COPD hospitalizations. *China Environ Sci* (2019) 39: 5312–5318.

13. Fu G Q，Jiang Y F，Liu L P， Liu HY, Zhou J, Cui XW, Wang SG Effects of $PM_{2.5}$ exposure in different air quality grades on daily outpatient visits for childhood asthma in Shijiazhuang. China *Biomed Environ Sci* (2018) 31: 888–892, doi: 10.3967/bes2018.120

14. Cheng, Y B，Jin, YL， Li, YH，Gong, J, Yang, NN, Wang, M. Impacts of high temperature on death caused by Cerebrocardiovascular diseases in Wuhan. *J Environ Health* (2009) 26: 224–225.

15. Fu G Q，Lu Q， Zhang Y N. Analysis of the influence of high temperature, heatwave and sweltering weather on the death number of cardiovascular and cerebrovascular diseases in Shijiazhuang. *Acta Meteor Sin* (2022) 80:403–409.

16. Zhang, Y，Xin, JY，Ma, P，Feng, XY, Zhang, XL, Wang, SG. Interaction effects between ambient temperature and PM2.5 and O3 on mortality in Chengdu. China *Environ Sci* (2021)41:3887–3895.

17. Yang J，Yin P.，Zhou M G，Ou C.Q., Guo Y., Gasparrini A., et al. Cardiovascular mortality risk attributable to ambient temperature in China. *Heart* (2015) 101:1966–1972, doi: 10.1136/heartjnl-2015-308062

18. Chen, Y C， Chen, H，Qu, X B，Sun, LH, Chen, YH, and Li, XP. Impact of average daily temperature on stroke mortality in community: a time-series analysis. *Chin Gen Pract* (2022) 25: 1838–1844.

19. Yi W ，Chan AP. Effects of temperature on mortality in Hong Kong: a time series analysis. *Int J Biometeorol* (2015) 59::937, doi: 10.1007/s00484-014-0906-5

20. Giang P N，Dung DV，Giang KB，Vinhc HV, Rocklöv J The effect of temperature on cardiovascular disease hospital admissions among elderly people in Thai Nguyen Province, Vietnam, *Suppl Glob Health Action* (2014) 7::23649, doi: 10.3402/gha.v7.23649

21. Basu R. High ambient temperature and mortality: a review of epidemiologic studies from 2001 to 2008. *Environ Health*. (2009) 8:11. doi: 10.1186/1476-069X-8-40

22. Gu, S H， Lu, BB，Wang, G，He, TF, Wang, AH. Seasonal variation in the acute effect of ozone on emergency ambulance dispatches for cardiovascular diseases. *Chin J Health Stat* (2019) 36:52–56.

23. Tao Y B，Huang W，Huang X L， Zhong L, Lu SE, Li Y, Dai L, Zhang Y, Zhu T Estimated acute effects of ambient ozone and nitrogen dioxide on mortality in the pearl river delta of southern China. *Environ Health Perspect* (2011) 120:393–398, doi: 10.1289/ehp.1103715

24. Dong, JY，Liu, XR，Zhang, BZ，Wang, JY, Shang, KZ. Meta-analysis of association between short-term ozone exposure and population mortality in China. *Acta Sci Circumst* (2016) 36: 1477–1485.

25. Hu, Y，Guo, Y，Guan, MY，Chen, FG, Xu, DQ, and Song, J. Time-series analysis of association between ozone concentration and daily emergency ambulance dispatches in Shijiazhuang. *J Environ Health* (2016) 33:872–875.

26. Ma, L，Yan, H L，Xiao, X， Yang, YL. Effects of season and temperature on gastrointestinal bleeding in patients with ischemic heart disease. *Chin Gen Pract* (2022) 25:2589–2595.

27. Day D B， Xiang J，Mo J， Li F, Chung M, Gong J, et al. Association of Ozone exposure with cardiorespiratory pathophysiologic mechanismsin healthy adults. *JAMA Intern Med* (2017) 1344–E10, 177, doi: 10.1001/jamainternmed.2017.2842

28. Fakhri AA，Ilic LM，Wellenius GA， Urch B, Silverman F, Gold DR, Mittleman MA Autonomic effects of controlled fine particulate exposure in young healthy adults: effect modification by ozone. *Environ Health Perspect* (2009) 117: 1287–1292, doi: 10.1289/ehp.0900541

29. Zhang, Y，Xin, JY，Zhang, XY，Ni, CJ, Ma, P, Wang, SG. Interaction effects between ambient temperature and black carbon and PM2.5 on mortality in Beijing. *China Environ Sci* (2020) 40:3179–3187.

30. Ren C，Williams G M，Mengersen K，, Morawska L., Tong S. Does temperature modify short-term effects of ozone on total mortality in 60 large eastern US communities-an assessment using the NMMAPS data. *Environ Int* (2008) 34:451–458, doi: 10.1016/j.envint.2007.10.001

31. Cao R，Zhou L，Xu J，Cui L Associations of extremely hot weather and cardiovascular disease mortality: results from 2011 to 2017, Jinan City, China. *Cardiol Plus* (2019) 4:29–34, doi: 10.4103/cp.cp_36_18

frontiers | Frontiers in Public Health

TYPE Original Research
PUBLISHED 10 October 2023
DOI 10.3389/fpubh.2023.1278516

Check for updates

OPEN ACCESS

EDITED BY
Zhaobin Sun,
Chinese Academy of Meteorological Sciences, China

REVIEWED BY
Yike Shen,
University of Texas at Arlington, United States
Yefei Zhu,
Lakeland Regional Medical Center, United States
Mengyi Li,
University of California, Irvine, United States

*CORRESPONDENCE
Luojing Zhou
✉ 18051063088@yzu.edu.cn

†These authors have contributed equally to this work

RECEIVED 16 August 2023
ACCEPTED 26 September 2023
PUBLISHED 10 October 2023

CITATION
Guo Z, Wang Y, Li Y and Zhou L (2023) Impact of meteorological factors on the incidence of hand-foot-mouth disease in Yangzhou from 2017 to 2022: a time series study. *Front. Public Health* 11:1278516. doi: 10.3389/fpubh.2023.1278516

Impact of meteorological factors on the incidence of hand-foot-mouth disease in Yangzhou from 2017 to 2022: a time series study

Zaijin Guo[1,2†], Yin Wang[3†], Yunshui Li[1,2] and Luojing Zhou[1,2*]

[1]Clinical Medical College, Yangzhou University, Yangzhou, China, [2]Northern Jiangsu People's Hospital, Yangzhou, China, [3]Department of Acute Infectious Disease Control and Prevention, Yangzhou Centre for Disease Control and Prevention, Yangzhou, China

Background: Hand, foot, and mouth disease (HFMD) is a significant public health issue in China, and numerous studies have indicated a close association between HFMD incidence and meteorological factors. This study aims to investigate the relationship between meteorological factors and HFMD in Yangzhou City, Jiangsu Province, China.

Methods: HFMD case reports and meteorological data from Yangzhou City between 2017 and 2022 were extracted from the National Notifiable Infectious Disease Surveillance System and the Meteorological Data Sharing Service System, respectively. A generalized additive model (GAM) was employed to assess the exposure-response relationship between meteorological factors and HFMD. Subsequently, a distributed lag nonlinear model (DLNM) was used to explore the exposure-lag-effect of meteorological factors on HFMD.

Results: HFMD in Yangzhou City exhibits obvious seasonality and periodicity. There is an inverted "U" shaped relationship between average temperature and the risk of HFMD, with the maximum lag effect observed at a temperature of 25°C with lag 0 day (RR = 2.07, 95% CI: 1.74–2.47). As the duration of sunshine and relative humidity increase, the risk of HFMD continuously rises, with the maximum lag effect observed at a sunshine duration of 12.4 h with a lag of 14 days (RR = 2.10, 95% CI: 1.17–3.77), and a relative humidity of 28% with a lag of 14 days (RR = 1.21, 95% CI: 1.01–1.64). There is a "U" shaped relationship between average atmospheric pressure and the risk of HFMD, with the maximum effect observed at an atmospheric pressure of 989 hPa with no lag (RR = 1.45, 95% CI: 1.25–1.69). As precipitation increases, the risk of HFMD decreases, with the maximum effect observed at a precipitation of 151 mm with a lag of 14 days (RR = 1.45, 95% CI: 1.19–2.53).

Conclusion: Meteorological factors including average temperature, average atmospheric pressure, relative humidity, precipitation, and sunshine duration significantly influenced the risk of HFMD in Yangzhou City. Effective prevention measures for HFMD should be implemented, taking into account the local climate conditions.

KEYWORDS

hand, foot and mouth disease, meteorological factors, generalized additive model, distributed lag nonlinear model, China

Introduction

Hand, foot, and mouth disease (HFMD) is an acute infectious disease caused by enteroviruses, primarily Coxsackievirus A16 (CV A16) and Enterovirus 71 (EV71). HFMD is characterized by the development of characteristic lesions on the hands, feet, and mouth. The transmission routes of HFMD mainly include contact transmission, respiratory transmission, and fecal-oral transmission. This disease predominantly affects children under the age of 5 (1, 2). The majority of patients with HFMD present with symptoms such as fever, as well as vesicular or popular eruptions on the hands, feet, and oral mucosa. The prognosis is generally favorable, with self-resolution occurring within approximately 1 week. However, a small proportion of patients may develop severe complications, including aseptic meningitis, encephalitis, pulmonary edema, and other severe manifestations. In rare cases, HFMD can progress to a critical condition and even result in death (3, 4). In recent years, the Asia-Pacific region has experienced frequent outbreaks of HFMD, posing a significant threat to the lives and health of children and adolescents in affected countries. These outbreaks have also imposed a substantial disease burden on the social and economic aspects of these nations (5–7).

Meteorological factors play a pivotal role in the transmission and epidemiology of infectious diseases, and they have been identified as significant risk factors contributing to the spread of HFMD (8–10), being a seasonal infectious disease, exhibits distinct patterns during specific periods in various regions and countries (11). Notably, several Asian countries, including Japan, Singapore, and mainland China, have observed a seasonal occurrence pattern of HFMD (12). Researchers from diverse countries and regions have conducted investigations on the influence of climate on HFMD, encompassing factors such as temperature, sunshine duration, relative humidity, wind speed, and precipitation. However, the findings from these studies exhibit some inconsistencies (13, 14). Analyzing the impact of meteorological factors on the incidence of HFMD can yield valuable insights for future prevention and control endeavors. The conclusions derived from such analyses can effectively guide the development of appropriate intervention measures.

It has been established that meteorological factors possess the capacity to exert a significant influence on the transmission and dissemination of HFMD, primarily by modulating the behavioral patterns of the pathogens or the hosts involved (15). The distributed lag nonlinear model (DLNM) can be employed to investigate the relationship between meteorological factors and HFMD. Meteorological factors such as temperature, humidity, and rainfall may exhibit certain associations with the incidence rate of HFMD. By utilizing the DLNM model, meteorological factors can be treated as independent variables, while the incidence rate of HFMD serves as the dependent variable. This model incorporates lag terms and nonlinear functions to capture the delayed effects of HFMD incidence and the nonlinear relationship with meteorological factors. The advantages of DLNM include its ability to address non-linear and delayed associations, such as exposure-lag-response, through cross-basis functions. Additionally, DLNM can automatically handle various regression function models such as linear models (LM), generalized linear models (GLM), and generalized additive models (GAM). A study conducted in Beijing utilizing a case-crossover design and DLNM revealed a non-linear relationship between temperature and hand, foot, and mouth disease (HFMD), indicating that the risk of HFMD increases with rising temperatures, with the highest risk observed at 25°C–27°C (16). Another study conducted in Sichuan Province using DLNM identified the interactive effects of meteorological factors and air pollutants on HFMD, highlighting that the combined presence of SO_2 and high temperature and humidity exerted the strongest impact on HFMD (17). Laboratory and epidemiological research has also demonstrated the crucial role of humidity in the transmission of HFMD, with relative humidity accounting for over 84% of the impact on pediatric HFMD, and each 1% increase in relative humidity associated with a 0.34% increase in pediatric HFMD (18, 19). A study conducted in Vietnam demonstrated that an increase in average rainfall is associated with an increased risk of HFMD, an increase in 1 unit of rainfall was associated with a 0.5% increase of HFMD rate on the lag 1 and 6 days (20). A previous study indicated that diurnal temperature range altered the relationship between temperature and pediatric HFMD, with a higher diurnal temperature range associated with a greater risk of HFMD (21), another study found that climate indicators specific to certain cities, including temperature, sunshine duration, and atmospheric pressure, modified the relationship between relative humidity and HFMD, with an overall pooled humidity-HFMD relationship displaying an approximate U-shaped curve with substantial spatial heterogeneity ($I^2 = 77.8\%$), and a reference relative humidity of 70% associated with an RR value of 0.83 (22).

Since being classified as a Class C notifiable infectious disease in China in 2008 (23), HFMD has consistently ranked high in terms of reported cases and fatalities. The generalized additive model (GAM), a flexible and effective approach for parametric, non-parametric, and semi-parametric regression analysis, has been widely employed in time series studies and can be used to identify the relationships between meteorological factors and infectious diseases such as bacterial dysentery, mumps, and hemorrhagic fever with renal syndrome (24, 25).

In recent years, the incidence rate of HFMD in Yangzhou City has remained high, making it the leading notifiable infectious disease in the region (26). This study aims to describe the epidemiological trends of HFMD in Yangzhou City from 2017 to 2022. The GAM will be employed to explore the exposure-response relationship between meteorological factors and HFMD. Additionally, DLNM will be used to assess the exposure-lag-response effects of meteorological factors on HFMD.

Data and methods

Study area

Yangzhou, situated at the heart of Jiangsu Province, assumes a pivotal role in the advancement of the Yangtze River Economic Belt. Geographically, this city spans an expansive area of 6591.21 square kilometers and is demarcated into three districts, one county, and two county-level cities, as visually depicted in Figure 1. The climatic conditions in Yangzhou exhibit distinctive seasonal variations, characterized by copious precipitation, ample sunshine, and discernible shifts in wind patterns corresponding to the changing

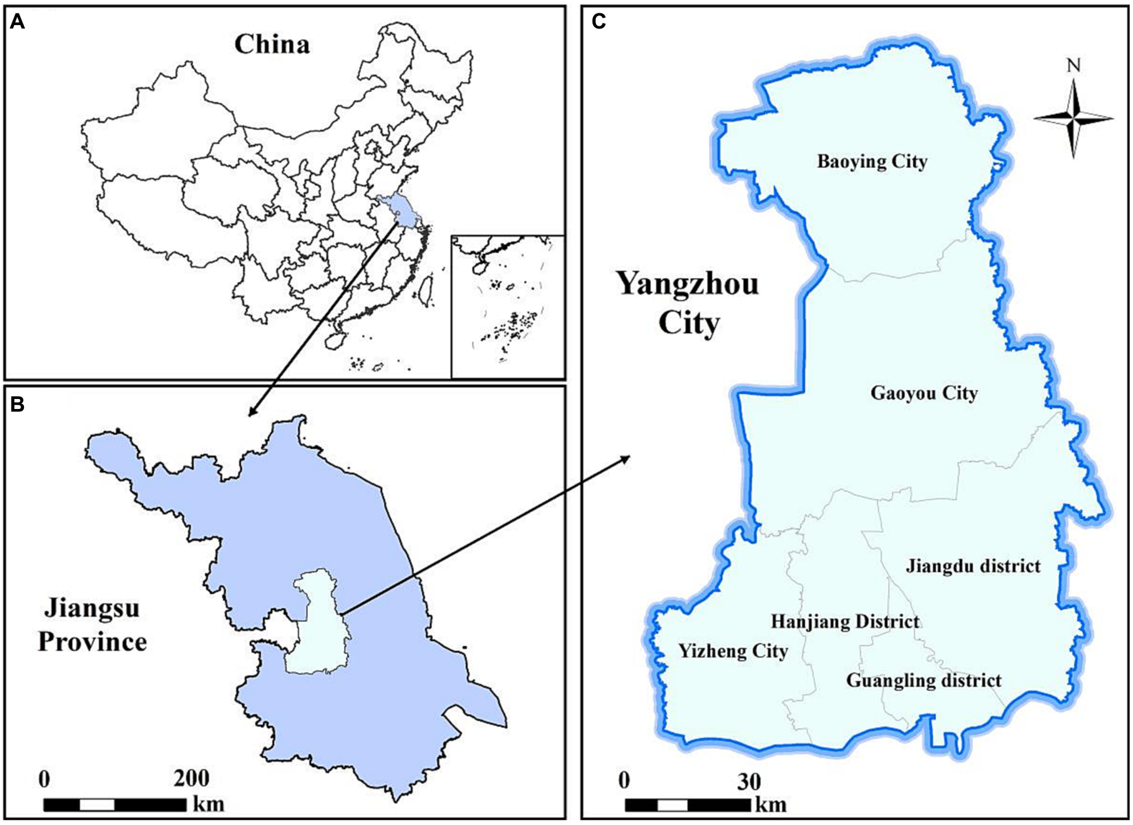

FIGURE 1
Geographical location of Yangzhou City, China. **(A)** China; **(B)** Jiangsu Province; **(C)** Yangzhou City.

seasons. Notably, no reports have been documented regarding the influence of meteorological factors on HFMD and its predictive capabilities within the confines of Yangzhou. Consequently, it becomes imperative to comprehend the precise impact of meteorological factors on HFMD within the context of Yangzhou.

HFMD and meteorological data

The daily reported data on HFMD cases in Yangzhou City from 2017 to 2022 were obtained from the National Infectious Disease Information Monitoring and Reporting Management System. HFMD is classified as a Class C notifiable infectious disease, and all cases diagnosed by qualified doctors in hospitals at all levels nationwide are required to be reported through this system within 24 h. According to the HFMD diagnostic guidelines issued by the Chinese Ministry of Health, all HFMD cases are diagnosed based on clinical symptoms and laboratory test results. The information for each reported HFMD case includes a case number, gender, age, population category, date of onset, and residential address. The meteorological data used in this study was obtained from the China Meteorological Data Sharing Service System.[1]

1 http://data.cma.gov.cn/

Statistical methods

Spearman correlation analysis

Spearman's rank correlation analysis is a non-parametric statistical method used to assess the correlation between two variables. The formula for Spearman's rank correlation coefficient, denoted as r_s, is as follows:

$$r_S = 1 - \frac{6\sum_{i=1}^{n} d_i^2}{n\left(n^2 - 1\right)}$$

where r_s represents the Spearman's rank correlation coefficient, n represents the sample size, and di represents the difference in ranks between the two sets of data. The coefficient ranges from −1 to 1, where −1 indicates a perfect negative correlation, 0 indicates no correlation, and 1 indicates a perfect positive correlation. In this study, Spearman's analysis was employed to evaluate the correlation between meteorological factors and the incidence rate of HFMD, in order to determine which meteorological factors may have an impact on the disease incidence rate.

Generalized additive model

Given the non-linear relationship between HFMD and meteorological factors, as well as the monthly periodicity of HFMD incidence, we applied a generalized additive model (GAM) to estimate the impact of meteorological parameters on monthly HFMD cases (27). GAM is helpful in determining the exposure-response relationships of various types of data, particularly when exploring non-parametric relationships (28). The dependent variable in this study is the cases of HFMD in Yangzhou city, which is a small probability event relative to the whole Yangzhou city population, and can be approximated as its obeying Poisson distribution, so the LOG function is chosen as the link function. In addition, as the spline function has strong ability to apply data and function transformation, and has certain overall smoothness, it is an ideal tool for function approximation, so the function corresponding to each independent variable in this study is set as the spline function, and the model is as follows:

$$\log\left[E\left(Y_{t}\right)\right]=\alpha+s\left(tl,df\right)+s\left(ts,df\right)+\sum_{i=1}^{k}s\left(X_{i},df\right)$$

Y_t is the number of HFMD cases in month t; $E(Y_t)$ is the expected value of HFMD cases in month t; α is the constant term of the model; $s()$ denotes the spline function; tl is used to control for long-term trends; ts is used to control for seasonal trends X_i denotes the independent variable (contemporaneous meteorological factors); df denotes the degrees of freedom on the spline function of the independent variable, obtained from generalized cross-validation.

Distributed lag non-linear model

It is used to quantitatively assess the "exposure-lag-effect" relationships between variables. The DLNM model builds upon the framework of traditional models by utilizing cross-basis functions, allowing for the simultaneous modeling of non-linear and lagged effects in exposure-response relationships. It has been widely employed in studying the associations between environmental exposures and infectious diseases (29). The model is as follows:

$$Y_{t}\sim\text{Poisson}\left(u\right)=\alpha^{*}cb\left(M,df,lag,df\right)+\sum ns\left(X_{i},df\right)+ns\left(\text{Time},df\right)+\beta\text{DOW}_{t}$$

In the model, t represents the observation date, Y_t represents the number of HFMD cases on day t, α represents the intercept, cb represents the cross-basis functions used to assess the non-linear relationship and lagged effects between meteorological factors and HFMD cases, ns represents natural cubic spline functions, M represents the study variables (various meteorological factors), X_i refers to other factors except M in the model to control the confounding effect. Time represents seasonal and long-term trends, and DOW refers to the day of the week effect. Based on the incubation period of HFMD and existing research (30, 31), set maximum lag days lag to 14.

Results

Characterization of research data

From January 1, 2017, to December 31, 2022, a total of 23,652 cases of HFMD were reported in Yangzhou City. Among these cases, there were 13,858 male and 9,794 female patients. The annual reported cases were 5,935, 9,431, 4,437, 884, 1,765, and 1,200, exhibiting a pattern of "high-low" years. During the same period, the daily average temperature, atmospheric pressure, relative humidity, precipitation, and sunshine duration in Yangzhou City were 16.81°C (range: −6.5°C to −35.7°C), 1014.94 KPa (range: 999–1041.1 hPa), 74.19% (range: 28–100%), 2.83 mm (range: 0.1–156.2 mm), and 4.7 h (range: 0–12.6 h), respectively. Table 1 and Figure 2 summarize the basic information of HFMD cases and meteorological data. Figure 3 depicts the monthly distribution of HFMD cases in Yangzhou City.

Analysis of the correlation between hand-foot-mouth disease and meteorological factors in Yangzhou

The Spearman correlation analysis matrix is presented in Table 2. In this study, temperature, relative humidity, precipitation, and sunshine duration showed positive correlations with the number of HFMD cases, while atmospheric pressure exhibited a negative correlation. Among these variables, temperature, atmospheric pressure, and precipitation were significantly correlated with HFMD cases ($p < 0.05$), while relative humidity and sunshine duration showed no statistically significant association ($p > 0.05$). Temperature had the highest correlation coefficient with HFMD cases ($r = 0.37$), followed by atmospheric pressure ($r = -0.36$).

Exposure-response relationship between meteorological factors and hand, foot and mouth disease

The results of the generalized additive model are shown in Figure 4. It can be observed that temperature exhibits a "inverted U-shaped" relationship with the incidence rate of HFMD. As temperature increases, the risk of HFMD initially rises, reaching its peak around 17°C, and then decreases. Atmospheric pressure shows a "U-shaped" relationship with the incidence rate of HFMD. With increasing atmospheric pressure, the risk of HFMD initially decreases, reaching its lowest point around 1,016 KPa, and then increases again.

TABLE 1 Descriptive study of HFMD and meteorological factors in Yangzhou City, 2017–2022.

Variables	Mean	Min	25th	50th	75th	Max
Number of cases/day	15	0	2	7	15	109
Mean temperature (°C)	16.81	−6.5	8.7	17.0	25.1	35.7
Atmospheric pressure (hPa)	1014.94	989	1007.1	1015.8	1023.0	1041.1
Relative humidity (%)	74.19	28	65	75	84	100
Precipitation (mm)	2.83	0	0	0	0.5	156.2
Sunshine hours (h)	4.70	0	0.2	4.85	8.3	12.6

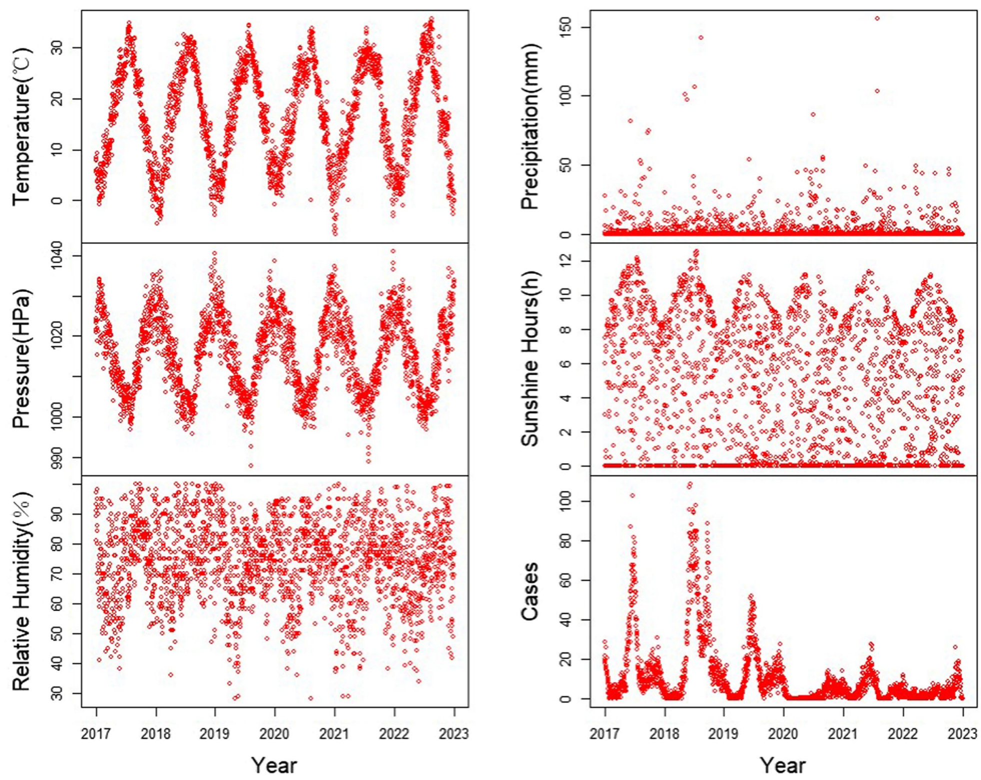

FIGURE 2
Time series of meteorological factors and number of HFMD cases in Yangzhou City, 2017–2022.

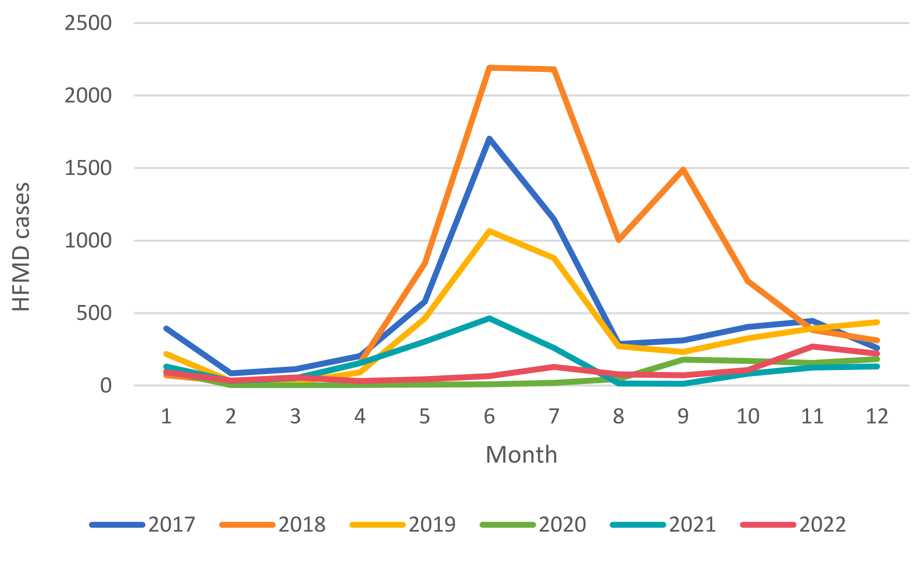

FIGURE 3
Number of cases of hand, foot and mouth disease in Yangzhou City, 2017–2022.

Relative humidity and sunshine duration have similar response on the risk of HFMD, showing a predominantly linear relationship. As relative humidity and sunshine duration increase, the risk of HFMD also increases. On the other hand, the risk of HFMD decreases with increasing precipitation, which is contrary to the effects of relative humidity and sunshine duration.

Distributed lag nonlinear model

We presented the exposure-lag-effect relationships between various meteorological factors and HFMD using a three-dimensional plot. Additionally, we depicted the cumulative effects at the maximum lag of 14 days (Figure 5).

TABLE 2 Correlation analysis of meteorological factors, hand, foot and mouth disease cases in Yangzhou City.

Variables	Case	Temperature	Pressure	Relative humidity	Precipitation	Sunshine hours
Case	1					
Temperature	0.37*	1				
Pressure	0.37*	−0.89*	1			
Relative humidity	0.027	0.072*	−0.061*	1		
Precipitation	0.043*	−0.28*	−0.20*	0.35*	1	
Sunshine hours	0.032	0.14*	−0.03	−0.61	−0.28*	1

*$p < 0.05$.

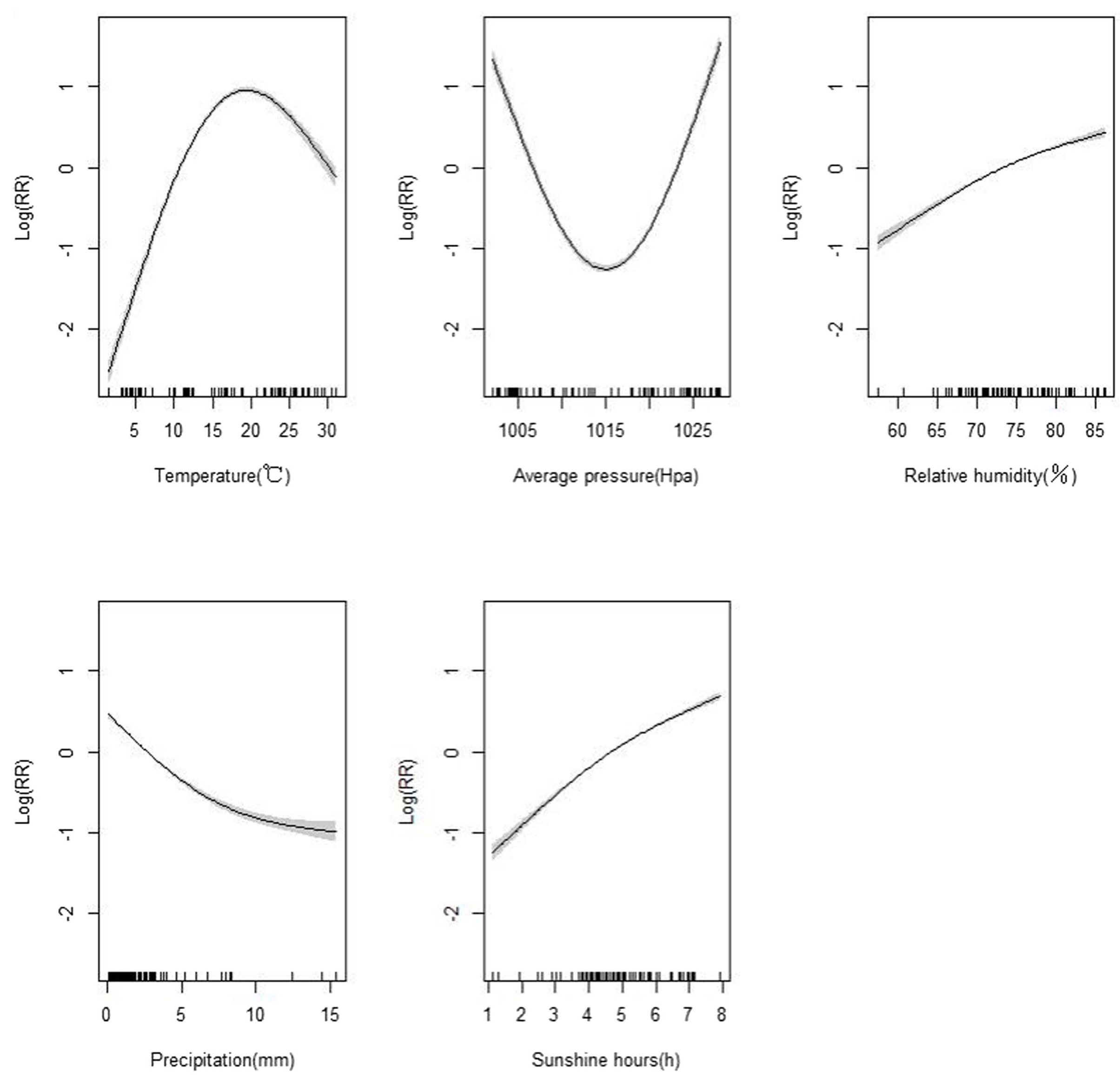

FIGURE 4
Exposure-response curve of meteorological factors and hand, foot and mouth disease.

The impact of temperature on HFMD at the maximum lag of 0 days showed that the highest relative risk (RR) value was observed at a temperature of −6°C (RR = 2.07, 95% CI: 1.74–2.47). Using the median temperature as the reference, the cumulative effect of temperature on HFMD approximately followed an inverted U-shaped curve. The maximum cumulative effect was observed at around 25°C (RR = 1.12, 95% CI: 1.05–1.23).

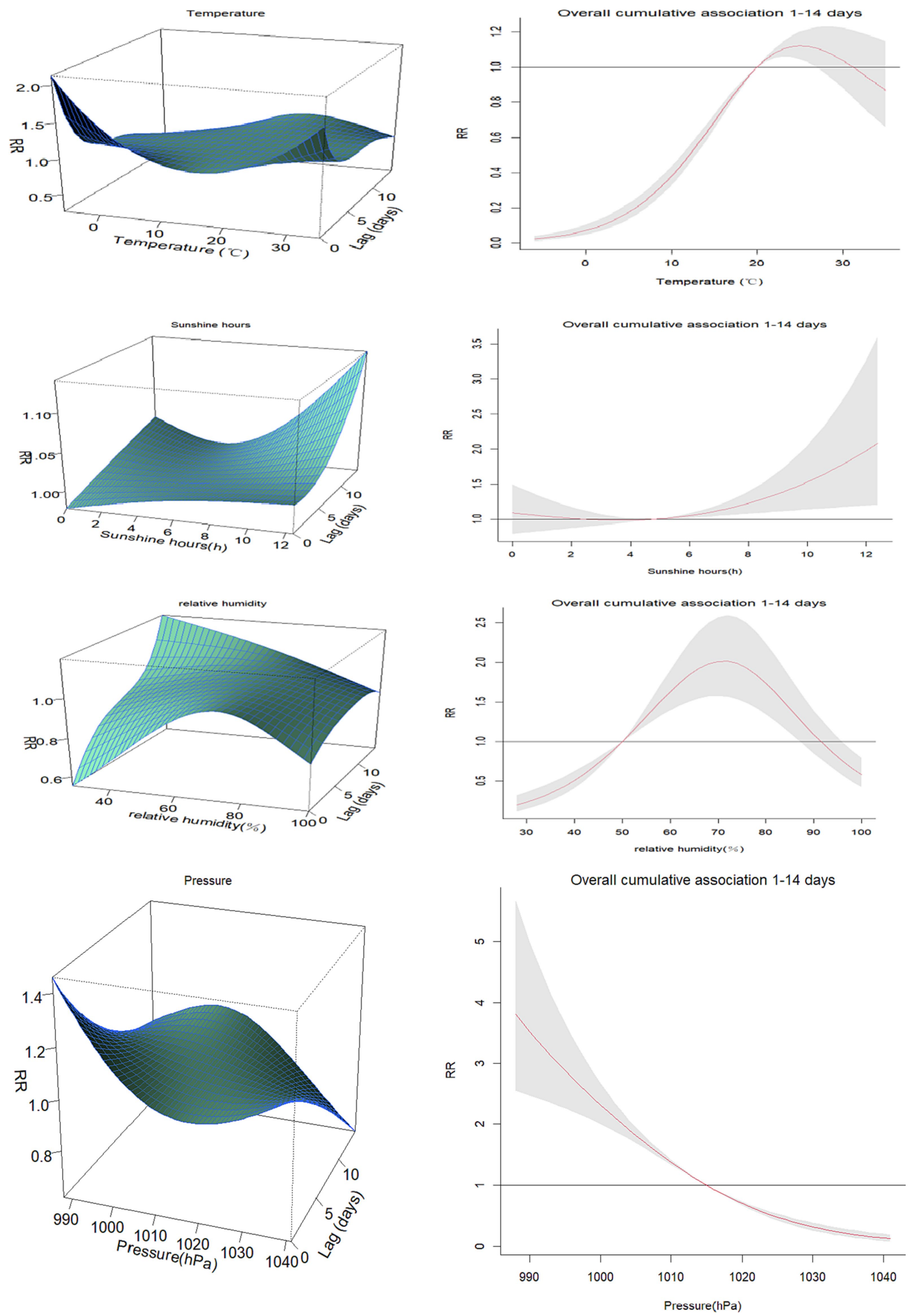

FIGURE 5 (Continued)

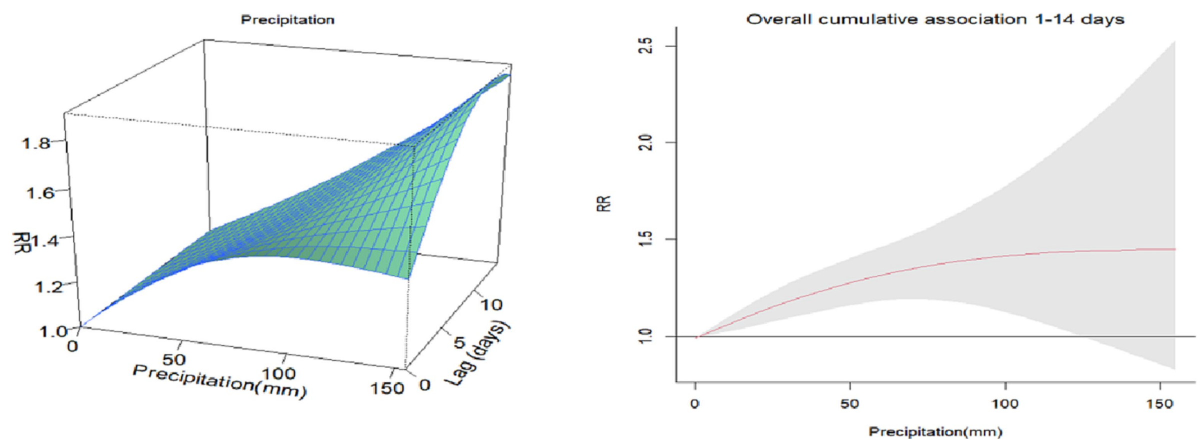

FIGURE 5
3D plots and cumulative lag effect plots of the impacts of meteorological factors on the risk of HFMD.

The impact of sunshine duration on HFMD at the maximum lag of 14 days was observed to be highest at 12.4 h (RR = 2.10, 95% CI: 1.17–3.77). Using the median sunshine duration as the reference, the cumulative effect of sunshine duration on HFMD gradually increased. The maximum cumulative effect was observed at 12.6 h of sunshine duration (RR = 2.08, 95% CI: 1.20–3.60).

The impact of relative humidity on HFMD at the maximum lag of 14 days was found to be highest at 28% (RR = 1.21, 95% CI: 1.01–1.64). Using the median relative humidity as the reference, the cumulative effect of relative humidity on HFMD exhibited an inverted U-shaped pattern. As relative humidity increased, the RR value initially increased and then decreased. The peak cumulative effect was observed at a relative humidity of 70% (RR = 2.01, 95% CI: 1.57–2.59).

The impact of atmospheric pressure on HFMD at the maximum lag of 0 days was found to be highest at 989 hPa (RR = 1.45, 95% CI: 1.25–1.69). Using the median atmospheric pressure as the reference, the cumulative effect of atmospheric pressure on HFMD gradually decreased. The maximum cumulative effect was observed at an atmospheric pressure of 990 hPa (RR = 3.79, 95% CI: 2.54–5.66).

The impact of precipitation on HFMD at the maximum lag of 14 days was found to be highest at 151 mm (RR = 1.90, 95% CI: 1.30–3.88). Using the median precipitation as the reference, the cumulative effect of precipitation on HFMD increased initially and then leveled off as precipitation … increased. The maximum cumulative effect was observed at a precipitation of 156 mm (RR = 1.45, 95% CI: 1.19–2.53).

Discussion

Since its first reported case in New Zealand in 1957, HFMD has rapidly spread to most countries and regions worldwide. In China, HFMD has become a significant public health issue since 2008. The Chinese government has implemented a series of measures to address this problem, including strengthening surveillance and reporting systems, enhancing vaccine research and promotion, and improving public education and health campaigns. Despite some achievements, HFMD remains an important challenge in China, requiring continuous attention and efforts to combat it (32). The impact of meteorological factors on human health has received extensive attention and is closely associated with the occurrence and transmission of various infectious diseases (27, 33, 34). The aim of this study is to investigate the relationship between HFMD cases and meteorological factors, examining the impact of meteorological factors on HFMD from two temporal dimensions: monthly data and daily data.

We conducted an observational analysis of HFMD cases and meteorological data in Yangzhou City from 2017 to 2022. The study revealed that HFMD in Yangzhou City exhibits clear seasonality and periodicity, with a bimodal distribution: the onset of cases begins in May, with the first peak occurring in June and a smaller peak in August. Overall, HFMD has a higher incidence during the summer and autumn seasons, while it decreases during the winter and spring seasons. In terms of epidemic years, HFMD showed a high incidence from 2017 to 2019, followed by a decline likely influenced by the COVID-19 pandemic. These findings are consistent with studies conducted in other Provinces of China (35, 36).

The impact of meteorological factors on HFMD is believed to be influenced by the intricate interplay among the pathogen, environmental factors, and the host population (22). Our research findings have revealed a non-linear relationship, characterized by an "inverted U-shaped" curve, between the average temperature and the incidence of HFMD. This implies that the risk of HFMD tends to be lower at extremely low and high temperatures, while it is higher within the temperature range that is more conducive to disease transmission. The DLNM also revealed that the cumulative effect is highest at 25°C during the 14 days lag period. It is important to note that our research outcomes may diverge from studies conducted in other regions of China, where the relationship between average temperature and HFMD may exhibit an "M-shaped" pattern (37, 38). Moreover, we have also observed a positive correlation between relative humidity and the occurrence of HFMD. On one hand, in conditions of high relative humidity, the pathogens associated with HFMD may thrive, endure for longer durations, and exhibit heightened infectivity. On the other hand, elevated relative humidity can impede sweating and disrupt the metabolic processes in children. This finding aligns with research conducted in other regions of China.

Our study has also unveiled a U-shaped correlation between average atmospheric pressure and HFMD, albeit without the ability to definitively establish a causal relationship between the two. In terms of sunshine duration, our results show that there is a positive relationship between hand-foot-mouth disease and sunshine duration.

As the duration of sunshine increases, the risk of HFMD escalates accordingly. It is worth noting that this conclusion contradicts the findings of other studies (39). Conversely, as precipitation levels rise, the risk of HFMD diminishes. This finding aligns with research conducted in other regions of China (40, 41). The reduced risk of HFMD with increased precipitation can plausibly be attributed to the unfavorable conditions for the survival of enteroviruses in high rainfall. Moreover, during periods of heavy precipitation, children may exhibit reduced inclination towards outdoor activities, thereby minimizing their exposure to the virus. Consequently, it is imperative to remain vigilant during periods characterized by high levels of sunshine duration and precipitation. The varying impact of meteorological factors on HFMD across different regions can be attributed to factors such as climate variations, disparities in viral strains, and divergent population behaviors among these regions (42).

This is the first study to explore the impact of meteorological conditions in Yangzhou City on the association with HFMD, expanding our understanding of the influence of meteorological factors on the risk of HFMD. Our research findings have practical implications in two aspects. Firstly, in the formulation of public health policies, our study results indicate that meteorological conditions affect the incidence rate of HFMD in Yangzhou City. For example, high rainfall and prolonged sunshine hours are associated with an increased incidence rate of HFMD, suggesting the need for different policies during the rainy season and dry season. Secondly, in the development of individual-level intervention measures, our research can serve as a reference. Children should develop healthy hygiene habits, such as washing hands before meals and after using the restroom. During HFMD outbreaks, parents or guardians should pay attention to reducing children's outdoor activities. Additionally, it is necessary to check weather forecasts and air quality before going out.

However, this study has certain limitations. Firstly, time series analysis is an ecological study and may be susceptible to ecological fallacy. This study only focuses on the overall population and does not stratify by gender or pathogen. Secondly, the epidemic process of HFMD is influenced by both natural and social factors (43). Despite the paramount importance of meteorological factors in the transmission dynamics of HFMD, it is imperative to acknowledge that social behavior, economic factors, population mobility, and air quality may also exert significant influences on the occurrence and dissemination of the disease. Regrettably, our study did not encompass an examination of these multifaceted factors, thereby limiting the comprehensive understanding of the complex interplay between various determinants and the epidemiology of HFMD.

Conclusion

Meteorological factors such as average temperature, average atmospheric pressure, relative humidity, precipitation, and sunshine duration have a significant impact on the risk of HFMD in Yangzhou City. The relationship between average temperature and HFMD risk follows an inverted U-shaped pattern, while the relationship between average atmospheric pressure and HFMD risk exhibits a U-shaped pattern. The risk of HFMD continuously increases with increasing relative humidity and sunshine duration, while it gradually decreases with increasing precipitation, showing a negative correlation. Our study fills a research gap regarding the impact of meteorological factors on HFMD in Yangzhou City. These findings can provide scientific evidence for relevant authorities to implement preventive measures and offer practical recommendations for establishing an early warning and prevention system for infectious diseases.

Data availability statement

The raw data supporting the conclusions of this article will be made available by the authors, without undue reservation.

Author contributions

ZG: Writing – original draft, Writing – review & editing. YW: Data curation, Methodology, Project administration, Writing – original draft. YL: Conceptualization, Investigation, Software, Writing – review & editing. LZ: Funding acquisition, Validation, Writing – original draft, Writing – review & editing.

Funding

The author (s) declare that no financial support was received for the research, authorship, and/or publication of this article.

Conflict of interest

The authors declare that the research was conducted in the absence of any commercial or financial relationships that could be construed as a potential conflict of interest.

Publisher's note

References

1. Solomon T, Lewthwaite P, Perera D, Cardosa MJ, McMinn P, Ooi MH. Virology, epidemiology, pathogenesis, and control of enterovirus 71. *Lancet Infect Dis*. (2010) 10:778–90. doi: 10.1016/s1473-3099(10)70194-8

2. Xing W, Liao Q, Viboud C, Zhang J, Sun J, Wu JT, et al. Hand, foot, and mouth disease in China, 2008–2012: an epidemiological study. *Lancet Infect Dis*. (2014) 14:308–18. doi: 10.1016/s1473-3099(13)70342-6

3. Liu B, Luo L, Yan S, Wen T, Bai W, Li H, et al. Clinical features for mild hand, foot and mouth disease in China. *PLoS One*. (2015) 10:e0135503. doi: 10.1371/journal.pone.0135503

4. Cai K, Wang Y, Guo Z, Yu H, Li H, Zhang L, et al. Clinical characteristics and managements of severe hand, foot and mouth disease caused by enterovirus A71 and coxsackievirus A16 in Shanghai. *Infect Dis*. (2019) 19:285. doi: 10.1186/s12879-019-3878-6

5. Puenpa J, Wanlapakorn N, Vongpunsawad S, Poovorawan Y. The history of enterovirus A71 outbreaks and molecular epidemiology in the Asia-Pacific region. *J Biomed Sci*. (2019) 26:75. doi: 10.1186/s12929-019-0573-2

6. Sabanathan S, Tan le V, Thwaites L, Wills B, Qui PT, Rogier van Doorn H. Enterovirus 71 related severe hand, foot and mouth disease outbreaks in South-East Asia: current situation and ongoing challenges. *J Epidemiol Community Health*. (2014) 68:500–2. doi: 10.1136/jech-2014-203836

7. Han Y, Ji H, Shen W, Duan C, Cui T, Chen L, et al. Disease burden in patients with severe hand, foot, and mouth disease in Jiangsu Province: a cross-sectional study. *Hum Vaccin Immunother*. (2022) 18:2049168. doi: 10.1080/21645515.2022.2049168

8. Grassly NC, Fraser C. Seasonal infectious disease epidemiology. *Proc Biol Sci*. (2006) 273:2541–50. doi: 10.1098/rspb.2006.3604

9. Cherrie MPC, Nichols G, Iacono GL, Sarran C, Hajat S, Fleming LE. Pathogen seasonality and links with weather in England and Wales: a big data time series analysis. *BMC Public Health*. (2018) 18:1067. doi: 10.1186/s12889-018-5931-6

10. Sumi A, Toyoda S, Kanou K, Fujimoto T, Mise K, Kohei Y, et al. Association between meteorological factors and reported cases of hand, foot, and mouth disease from 2000 to 2015 in Japan. *Epidemiol Infect*. (2017) 145:2896–911. doi: 10.1017/s0950268817001820

11. Koh WM, Bogich T, Siegel K, Jin J, Chong EY, Tan CY, et al. The epidemiology of hand, foot and mouth disease in Asia: a systematic review and analysis. *Pediatr Infect Dis J*. (2016) 35:e285–300. doi: 10.1097/inf.0000000000001242

12. Chen Y, Badaruddin H, Lee VJ, Cutter J, Cook AR. The effect of school closure on hand, foot, and mouth disease transmission in Singapore: a modeling approach. *Am J Trop Med Hyg*. (2018) 99:1625–32. doi: 10.4269/ajtmh.18-0099

13. Chen S, Liu X, Wu Y, Xu G, Zhang X, Mei S, et al. The application of meteorological data and search index data in improving the prediction of HFMD: a study of two cities in Guangdong Province, China. *Sci Total Environ*. (2019) 652:1013–21. doi: 10.1016/j.scitotenv.2018.10.304

14. Song C, He Y, Bo Y, Wang J, Ren Z, Yang H. Risk assessment and mapping of hand, foot, and mouth disease at the county level in mainland China using spatiotemporal zero-inflated Bayesian hierarchical models. *Int J Environ Res Public Health*. (2018) 15:1476. doi: 10.3390/ijerph15071476

15. Cheng Q, Bai L, Zhang Y, Zhang H, Wang S, Xie M, et al. Ambient temperature, humidity and hand, foot, and mouth disease: a systematic review and meta-analysis. *Sci Total Environ*. (2018) 625:828–36. doi: 10.1016/j.scitotenv.2018.01.006

16. Xu M, Yu W, Tong S, Jia L, Liang F, Pan X. Non-linear association between exposure to ambient temperature and Children's hand-foot-and-mouth disease in Beijing, China. *PLoS One*. (2015) 10:e0126171. doi: 10.1371/journal.pone.0126171

17. Huang J, Ma Y, Lv Q, Liu Y, Zhang T, Yin F, et al. Interactive effects of meteorological factors and air pollutants on hand, foot, and mouth disease in Chengdu. *BMJ Open*. (2022) 12:e067127. doi: 10.1136/bmjopen-2022-067127

18. Yang H, Wu J, Cheng J, Wang X, Wen L, Li K, et al. Is high relative humidity associated with childhood hand, foot, and mouth disease in rural and urban areas? *Public Health*. (2017) 142:201–7. doi: 10.1016/j.puhe.2015.03.018

19. Abad FX, Pintó RM, Bosch A. Survival of enteric viruses on environmental fomites. *Appl Environ Microbiol*. (1994) 60:3704–10. doi: 10.1128/aem.60.10.3704-3710.1994

20. Nguyen HX, Chu C, Nguyen HLT, Nguyen HT, Do CM, Rutherford S, et al. Temporal and spatial analysis of hand, foot, and mouth disease in relation to climate factors: a study in the Mekong Delta region, Vietnam. *Sci Total Environ*. (2017) 581-582:766–72. doi: 10.1016/j.scitotenv.2017.01.006

21. Hu Y, Liu F, Zhao X, Ma Y, Lan T, Yang F, et al. The modification effect of the diurnal temperature range on the exposure-response relationship between temperature and pediatric hand. *Sci Total Environ*. (2020) 722:137921. doi: 10.1016/j.scitotenv.2020.137921

22. Bo Z, Ma Y, Chang Z, Zhang T, Liu F, Zhao X, et al. The spatial heterogeneity of the associations between relative humidity and pediatric hand. *Sci Total Environ*. (2020) 707:136103. doi: 10.1016/j.scitotenv.2019.136103

23. MoHotP China. *Hand, foot and mouth disease prevention and control guide* (2009). Available at: http://www.gov.cn/gzdt/2009-06/04/content_1332078.htm

24. Hao J, Yang Z, Huang S, Yang W, Zhu Z, Tian L, et al. The association between short-term exposure to ambient air pollution and the incidence of mumps in Wuhan. *Environ Res*. (2019) 177:108660. doi: 10.1016/j.envres.2019.108660

25. Gopalkrishna V, Patil PR, Patil GP, Chitambar SD. Circulation of multiple enterovirus serotypes causing hand, foot and mouth disease in India. *J Med Microbiol*. (2012) 61:420–5. doi: 10.1099/jmm.0.036400-0

26. Liu WJ, Zhou LP, Dong YY, Xu CH, Cui LB, Wu Q. Epidemiological characterization of hand, foot and mouth disease in Yangzhou City, China, 2014–2017. *Chin J Health Inspec*. (2019) 29:2272–5. doi: 10.3760/cma.j.cn112150-20200512-00721

27. Du Z, Lawrence WR, Zhang W, Zhang D, Yu S, Hao Y. Interactions between climate factors and air pollution on daily HFMD cases: a time series study in Guangdong, China. *Sci Total Environ*. (2019) 656:1358–64. Epub 2019/01/11. doi: 10.1016/j.scitotenv.2018.11.391

28. Hastie T, Tibshirani R. Generalized additive models for medical research. *Stat Methods Med Res*. (1995) 4:187–96. doi: 10.1177/096228029500400302

29. Gasparrini A, Armstrong B, Kenward MG. Distributed lag non-linear models. *Stat Med*. (2010) 29:2224–34. doi: 10.1002/sim.3940

30. Liu Z, Meng Y, Xiang H, Lu Y, Liu S. Association of short-term exposure to meteorological factors and risk of hand, foot, and mouth disease: a systematic review and meta-analysis. *Int J Environ Res Public Health*. (2020) 17:8017. doi: 10.3390/ijerph17218017

31. Xiao X, Gasparrini A, Huang J, Liao Q, Liu F, Yin F, et al. The exposure-response relationship between temperature and childhood hand, foot and mouth disease: a multicity study from mainland China. *Environ Int*. (2017) 100:102–9. doi: 10.1016/j.envint.2016.11.021

32. Zhu L, Wang X, Guo Y, Xu J, Xue F, Liu Y. Assessment of temperature effect on childhood hand, foot and mouth disease incidence (0–5 years) and associated effect modifiers: a 17 cities study in Shandong Province, China, 2007–2012. *Sci Total Environ*. (2016) 551–552:452–9. doi: 10.1016/j.scitotenv.2016.01.173

33. Peng L, Zhao X, Tao Y, Mi S, Huang J, Zhang Q. The effects of air pollution and meteorological factors on measles cases in Lanzhou. *Environ Sci Pollut Res*. (2020) 27:13524–33. doi: 10.1007/s11356-020-07903-4

34. Yu G, Li Y, Cai J, Yu D, Tang J, Zhai W, et al. Short-term effects of meteorological factors and air pollution on childhood hand-foot-mouth disease in Guilin, China. *Sci Total Environ*. (2019) 646:460–70. doi: 10.1016/j.scitotenv.2018.07.329

35. Hu H, Ge W, Yan J. Analysis of the epidemiologic characteristics of children with hand, foot and mouth disease in China. *Iran J Public Health*. (2023) 52:773–9. doi: 10.18502/ijph.v52i4.12450

36. Wang W, Rosenberg MW, Chen H, Gong S, Yang M, Deng D. Epidemiological characteristics and spatiotemporal patterns of hand, foot, and mouth disease in Hubei, China from 2009 to 2019. *PLoS One*. (2023) 18:e0287539. doi: 10.1371/journal.pone.0287539

37. Qi H, Chen Y, Xu D, Su H, Zhan L, Xu Z, et al. Impact of meteorological factors on the incidence of childhood hand, foot, and mouth disease (HFMD) analyzed by DLNMs-based time series approach. *Infect Dis Poverty*. (2018) 7:7. doi: 10.1186/s40249-018-0388-5

38. Luan G, Liu S, Zhang W, Zhai L, Zhang Y, Sun L, et al. Estimating the influence of high temperature on hand, foot, and mouth disease incidence in China. *Environ Sci Pollut Res Int*. (2023) 30:1477–84. doi: 10.1007/s11356-022-22038-4

39. Xu J, Yang M, Zhao Z, Wang M, Guo Z, Zhu Y, et al. Meteorological factors and the transmissibility of hand, foot, and mouth disease in Xiamen City, China. *Front Med*. (2021) 7:597375. doi: 10.3389/fmed.2020.597375

40. Zhu H, Chen S, Liang R, Feng Y, Joldosh A, Xie Z, et al. Study of the influence of meteorological factors on HFMD and prediction based on the LSTM algorithm in Fuzhou. *Infect Dis*. (2023) 23:299. doi: 10.1186/s12879-023-08184-1

41. Wang Y, Feng Z, Yang Y, Self S, Gao Y, Longini IM, et al. Hand, foot, and mouth disease in China: patterns of spread and transmissibility. *Epidemiology*. (2011) 22:781–92. doi: 10.1097/EDE.0b013e318231d67a

42. Peng H, Chen Z, Cai L, Liao J, Zheng K, Li S, et al. Relationship between meteorological factors, air pollutants and hand, foot and mouth disease from 2014 to 2020. *BMC Public Health*. (2022) 22:998. doi: 10.1186/s12889-022-13365-9

43. Wang W, Song J, Wang J, Li Y, Deng H, Li M, et al. Cost-effectiveness of a national enterovirus 71 vaccination program in China. *PLoS Negl Trop Dis*. (2017) 11:e0005899. doi: 10.1371/journal.pntd.0005899

frontiers | Frontiers in Public Health

TYPE Original Research
PUBLISHED 19 October 2023
DOI 10.3389/fpubh.2023.1290303

Check for updates

OPEN ACCESS

EDITED BY
Zhaobin Sun,
Chinese Academy of Meteorological Sciences, China

REVIEWED BY
Pan Ma,
Chengdu University of Information Technology, China
Yuxin Zhao,
Chinese Academy of Meteorological Sciences, China

*CORRESPONDENCE
Shijian Liu
✉ arrow64@163.com
Dan Wang
✉ 16174684@qq.com

†These authors have contributed equally to this work

RECEIVED 07 September 2023
ACCEPTED 29 September 2023
PUBLISHED 19 October 2023

CITATION
Guan H, Yang G, Gao J, Lin X, Liu C, Ren H, Chen D, Zhou L, Hu Q, Huang Y, Zhao Y, Tong S, Lu Z, Liu S and Wang D (2023) Sanya climatic-treatment cohort profile: objectives, design, and baseline characteristics. *Front. Public Health* 11:1290303. doi: 10.3389/fpubh.2023.1290303

Sanya climatic-treatment cohort profile: objectives, design, and baseline characteristics

Haidao Guan[1†], Guiyan Yang[2†], Jiashi Gao[1], Xiaoya Lin[1], Chao Liu[1], Han Ren[2], Duyue Chen[2], Lingyao Zhou[2], Qian Hu[3], Yongzhen Huang[3], Yumei Zhao[4], Shilu Tong[5,6], Zhaohui Lu[7], Shijian Liu[1,5,8]* and Dan Wang[1]*

[1]Department of Science and Education, Hainan Branch, Shanghai Children's Medical Center, School of Medicine, Shanghai Jiao Tong University, Sanya, China, [2]Department of Hospital Management, Hainan Branch, Shanghai Children's Medical Center, School of Medicine, Shanghai Jiao Tong University, Sanya, China, [3]Department of Hospital Infection, Hainan Branch, Shanghai Children's Medical Center, School of Medicine, Shanghai Jiao Tong University, Sanya, China, [4]Department of Nursing, Hainan Branch, Shanghai Children's Medical Center, School of Medicine, Shanghai Jiao Tong University, Sanya, China, [5]Department of Clinical Epidemiology and Biostatistics, Children Health Advocacy Institute, School of Medicine, Shanghai Jiao Tong University, Shanghai, China, [6]School of Public Health and Social Work, Queensland University of Technology, Brisbane, QLD, Australia, [7]Department of Pediatric Surgery, Hainan Branch, Shanghai Children's Medical Center, School of Medicine, Shanghai Jiao Tong University, Sanya, China, [8]Department of Big Center, Hainan Branch, Shanghai Children's Medical Center, School of Medicine, Shanghai Jiao Tong University, Sanya, China

Background: The prevalence of allergic diseases has increased globally, climate and environment also have important effects on respiratory or allergic diseases. However, population-based studies investigating the impact of tropical climates and environments on migratory-bird old people (MBOP) are lacking.

Methods/Design: For this prospective cohort study, we recruited 756 participants from the community in Sanya City, Hainan Province, China. In addition to the completed baseline survey, a follow-up survey will be conducted during the periods of October–December and March–April for the next 3 years of MBEPs from northern China who spend the winter in Sanya. We will continue to record the height, weight, and blood pressure of all participants, as well as lung function for those with asthma and chronic obstructive pulmonary disease (COPD). Venous blood at baseline and urine samples will be collected during follow-up.

Results: A total of 756 volunteers were recruited. Their average age is 66.1 years; 32.1% of them have high-school educations, while 37.3% have graduated from college or done undergraduate studies. The top five diseases in this cohort are allergic rhinitis (57.9%); eczema, urticaria, or dermatitis (35.6%); bronchitis and bronchiectasis (35.6%); asthma (14.7%); and emphysema (11.7%). Compared with their symptoms while at their summer places of residence, rates of remission reported by participants while living in Sanya were 80.4% for allergic rhinitis, 82.3% for bronchitis and emphysema, 85.2% for asthma, 96.0% for COPD ($P < 0.001$).

Conclusions: The baseline survey has been completed. The preliminary findings support that a tropical climate may relieve the symptoms of allergic diseases in migratory-bird old people.

KEYWORDS

tropical climate, environmental factors, migratory people, asthma, allergic diseases

Introduction

The prevalence of allergic diseases has increased globally in recent decades (1, 2). According to the World Health Organization's (WHO) 2019 report, approximately 262 million people worldwide suffered from asthma at the time, resulting in 455,000 deaths. Allergic diseases, including allergic rhinitis and eczema, together constitute a major global public-health burden (3). China is also facing this issue: according to epidemiological surveys, the prevalence of allergic diseases (4, 5) such as asthma (6, 7), allergic rhinitis (8), and eczema are increasing in China. Influencing factors include climate change (9), air pollution (10), environmental temperature (11), meteorological factors (12), and allergens (13).

Current studies on allergic diseases mainly focus on the effects of climate and environmental factors. There are reports on the treatment and relief of asthma in alpine environments (14, 15). However, population-based research is lacking on the effect of tropical climate and environment on migratory-bird old people (MBOP). Sanya, China has a unique tropical climate, with a minimum temperature of >15°C in winter; by contrast, the minimum winter temperature in northern China is below −40°C (16). Therefore, many MBEPs relocate from northern China to Sanya for the winter. It is reported that more than 1 million people spend the winter in Sanya every year (17).

In addition to drug treatment, climate, and environment also have important effects on respiratory or allergic diseases. In Europe, cave therapy is widely used to treat chronic airway diseases. Some studies have shown that exercise in winter combined with cave therapy can improve the quality of life (QoL) and allergic symptoms of adults with allergic rhinitis and/or asthma (18, 19). A systematic review showed that high-altitude climate therapy improved the lung function of adult asthma patients (15, 20). However, there is no relevant evidence that symptoms and climate-related factors of allergic diseases improve in MBEPs who move from high latitudes to low ones. The establishment of this cohort will help us better study the effect of Sanya's tropical climate on respiratory or allergic diseases, clarify risk factors related to these diseases, and determine whether such a climate effectively mitigates these diseases in MBEPs.

Cohort description

Study design, setting, and participants

This is a prospective cohort study whose subjects were recruited from the community in Sanya City, Hainan, the southernmost province in China from 2022 to 2025. We will conduct a follow-up survey focused on allergic diseases in MBEPs from northern China who move to Sanya for the winter (Figure 1). Northern China includes three northeastern provinces (Heilongjiang, Jilin, and Liaoning), five northern provinces (Beijing, Tianjin, Hebei, Shanxi, and the Inner Mongolia Autonomous Region), and five northwestern provinces (Xinjiang Uygur Autonomous Region; Ningxia Hui Autonomous Region; and Qinghai, Gansu, and Shaanxi Provinces). The subjects of this study are MBEPs who travel from northern China to Sanya in autumn, stay for the winter, and return to northern China in spring. The sample size was estimated by forced expiratory volume in 1 s (FEV_1) (15), which was 92.8% ± 23.1 and 86.5 ± 26.2 for the trial and control groups, respectively. A type I error $\alpha = 0.05$, $\beta = 0.10$, and loss of follow-up rate of 20% for 3 years, requiring 775 participants.

For easier follow-up, we recruited participants from communities of mainly MBEPs, who own apartments in Sanya and spend the winter there for many years. Inclusion criteria were as follows: (a) age 50–80 years; (b) suffering from allergic rhinitis, asthma, eczema, urticaria, or chronic obstructive pulmonary disease (COPD); (c) previous or winter residence in northern China; (d) willingness to participate in the study and be followed up on at the designated location for the subsequent 3 years; and (e) no difficulty in communication. Exclusion criteria were (a) other respiratory diseases and (b) communication barriers or unwillingness to cooperate with the requirements of the study.

Diagnosis of allergic rhinitis, asthma, eczema, urticaria, or COPD was based on self-reported disease history in face-to-face interviews at recruitment. Allergic rhinitis was defined as an affirmative response to the question "Do you have any nasal allergies, including hay fever?" according to the Allergic Rhinitis and Its Impact on Asthma guidelines (8). Asthma was defined as a self-reported history of asthma, diagnosis by a physician, or wheezing during the preceding 12 months (6). Eczema or urticaria was defined as self-reported history and/or diagnosis by a physician (21, 22). Atopic dermatitis was diagnosed by an affirmative response to the question "Have you had an itchy rash at any time in the past 12 months?" (8). COPD was defined as post-bronchodilator FEV_1/forced vital capacity (FVC) < 0.7 according to the 2017 Global Initiative for Chronic Obstructive Lung Disease guidelines (23). Chronic bronchitis was defined as self-reported phlegm production for at least 3 months each year over 3 successive years (24).

Data collection

Demography and outcomes

A paper questionnaire was used to collect a range of basic information in march 2022. After obtaining informed consent, trained investigators collected relevant information in face-to-face interviews. The questionnaire covered demographic data, socioeconomic status, clinical disease characteristics, living habits, and past medical history (Table 1). Participants with asthma and COPD were evaluated using the Asthma Quality of Life Questionnaire (AQLQ) (25) and Saint George Respiratory Questionnaire (SGRQ) (26), respectively; SGRQ assesses the quality of life of participants with COPD. The primary outcome was the effect of Sanya's tropical climate

Abbreviations: WHO, World Health Organization; MBOP, Migratory bird's old people; FEV1, Forced expiratory volume in 1 s; COPD, Chronic obstructive pulmonary disease; FVC, Forced vital capacity; AQLQ, Asthma quality of life questionnaire; SGRQ, Saint George respiratory questionnaire.

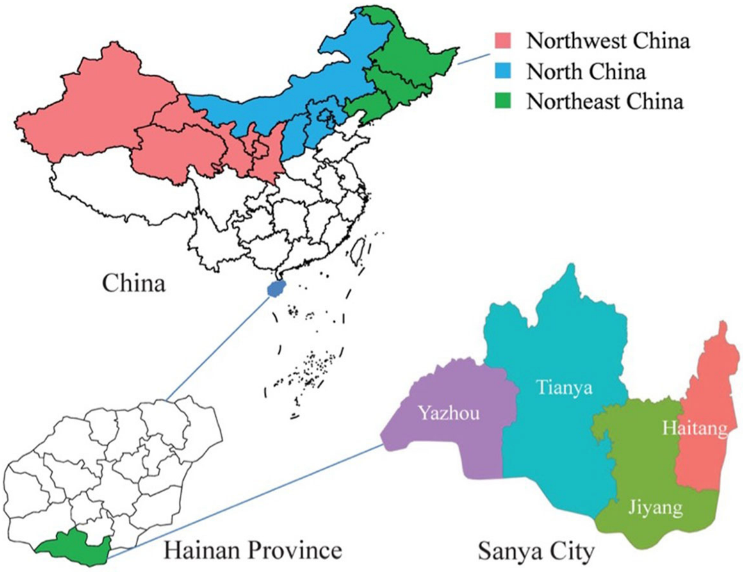

FIGURE 1
Geographical location of the Sanya migratory cohort. The shaded regions represent participants' original places of residence, red indicates the northwest China, blue represents the north China, and green signifies the northeast China.

TABLE 1 Data collected from participants in the Sanya migratory cohort.

Category	Data
Demographics/socioeconomic factors	Date of birth, ethnicity, educational level, working status, sex, previous location of residency, and location and duration of current residency
Physical examination	Height, weight, BP, and lung function
Lifestyle	Diet, smoking, exercise, sleep, work, and living environments
Medical history	Allergic history, and family history of respiratory and allergic diseases
QoL evaluation	AQLQ and SGRQ

BP, Blood pressure; QoL, quality of life; AQLQ, Asthma Quality of Life Questionnaire; and SGRQ, Saint George Respiratory Questionnaire.

on MBEPs with allergic or respiratory diseases, including symptoms evaluated by questionnaires, for example, frequency of mitigations and exacerbations. Potential confounding factors included the psychological effects of living in this famous tourist city.

Physical examination

We used a unified measuring tool for physical examination. After calibration, we measured the height, weight, and blood pressure of all participants, and in those with asthma and COPD, we also measured lung function. Participants were asked to take off their shoes and coats before their heights and weights were measured.

Collection and measurement of biological samples

Nurses from local hospitals traveled to the community, collected 5–10 mL of patients' venous blood, and then transferred the samples to the laboratory at Sanya Women and Children's Hospital (SWCH) for centrifugation and subpackaging. Whole blood was used for routine blood tests; serum was used to test for liver and kidney function, blood sugar, blood lipids, and allergen. Some samples were stored in a freezer at −80°C. Table 2 lists the types of samples and main tests using these samples.

Quality control

All investigators received unified training. Two investigators independently input the results of all questionnaires into database using EpiData 3.0 software (EpiData, Copenhagen, Demark). A Portion of the data underwent double entry, and in cases where inconsistencies arose, a third researcher reviewed and resolved them to guarantee data accuracy.

We adopted various policies to retain participants in the cohort. Health consultation was and will be provided during recruitment and follow-up, and free health examinations were and will be provided during baseline and follow-up. We are following up on participants in the spring (March–April) and autumn (October–December) every year for the next 3 years and providing them with timely reminders to take advantage of the free health examinations.

TABLE 2 Collection of biological samples from participants in the Sanya migratory cohort.

Biological samples	Clinical examinations	Specific tests
Venous blood	Routine blood	White blood cell (WBC), red blood cell (RBC), hemoglobin concentration (HGC), platelet count (PLT), neutrophil percentage (NEU%), lymphocyte percentage (LYM%), monocyte percentage (MPN%), eosinophil percentage (EOS%), and basophil percentage (BAS%)
	Liver function	Total protein (TP) level, albumin (ALB) level, globulin/white cell ratio (A/G), glutamic pyruvic transaminase (GPT), glutamic oxaloacetic transaminase (GOT), aspartate transaminase (AST)/alanine transaminase (ALT) ratio, total bilirubin (TBIL), direct bilirubin (DBIL), and indirect bilirubin (IBIL)
	Blood lipids and sugar	Glucose (Glu); total cholesterol (TC), triglyceride (TG), high-density lipoprotein cholesterol (HDL-C), low-density lipoprotein cholesterol (LDL-C), and blood glucose (BG)
	Allergens	Animal allergens (cat, horse, cow, and dog dander); house dust (household dust, dust mites, and cockroaches); food allergens (milk, eggs, soybeans, peanuts, cod, wheat, and millet); plant allergens (grass, French chrysanthemum, dandelion, plantain, *Chenopodium* [goosefoot], and a yellow flower); mycoallergens (*Penicillium punctatum*, *Aspergillus fumigatus*, *Polydendrosporium*, *Candida albicans*, *Alternaria alternata*, and *Helminthosporium longum*)
Urine	Routine urine	Environmental-pollution exposure

Statistical analysis

Baseline characteristics of participants who stayed in or withdrew from the cohort, and loss of follow-up, were described. All missing data were noted. We analyzed classification data using a χ^2 test and continuous data using Student's t test. All analyses were conducted using SPSS version 25.0 (IBM Corp., Armonk, NY, USA). $P < 0.05$ was considered to indicate a statistically significant difference.

Ethical approval

The research protocol and informed-consent form of this study were reviewed and approved by the Ethics Committee of Sanya Women and Children's Hospital (Approval No. SYFYIRB2022009). All participants signed their informed consent before participating.

TABLE 3 Baseline characteristics of the Sanya migratory cohort.

Characteristics	Recruited for cohort (*N*)	Proportion (%) or Mean
Gender		
Male	231	33.3
Female	462	66.7
Age (years)	693 (50–80)	66.1*
Height (cm)	671	162.0*
Weight (kg)	670	64.5*
BMI (kg/m^2)	670	24.1*
Educational level		
Junior high school or lower	185	26.7
High school or technical secondary school	223	32.1
Undergraduate or junior college	258	37.3
Postgraduate or higher	9	1.3
Respiratory/allergic disease		
Asthma	102	14.7
COPD	77	10.6
Allergic rhinitis/pharyngitis	401	57.9
Eczema/urticaria/dermatitis	247	35.6
Food/drug allergy	60	8.7
Bronchitis/bronchiectasis	247	35.6
Emphysema	81	11.7
Hypertension	165	23.8
Diabetes	92	13.3
Other	51	7.4
The original location of residence		
Heilongjiang province	280	40.9
Jilin province	71	10.4
Liaoning province	82	12.0
Inner Mongolia Autonomous Region	40	5.8
Xinjiang Uygur Autonomous Region	21	3.1
Gansu province	6	0.9
Shanxi province	6	0.9
Beijing	48	6.9
Hebei province	51	7.4
Tianjin	10	1.4
Shaanxi province	26	3.8
Other	28	4.0
Sanya, > 5 years	15	2.2

BMI, Body mass index; COPD, chronic obstructive pulmonary disease; * Mean.

TABLE 4 Data collected from participants in the Sanya migratory cohort.

Participants' data	Baseline and follow-up						
	2022		2023		2024		2025
	Baseline	Autumn	Spring	Autumn	Spring	Autumn	Spring
Demographics/Social							
Date of birth	√						
Ethnicity	√						
Educational level	√						
Marital status	√						
Gender	√						
The original location of residence	√						
Current location and duration of residence	√						
Physical examination							
Height	√	√	√	√	√	√	√
Weight	√	√	√	√	√	√	√
BP	√	√	√	√	√	√	√
Pulmonary function#		√	√	√	√	√	√
Biological samples							
Blood	√	√	√	√	√	√	√
Urine		√	√	√	√	√	√
Lifestyle							
Diet	√						√
Smoking/passive-smoking status	√						√
Exercise	√						√
Sleep habits	√						√
Living environment	√						√
Medical records							
Respiratory or allergic diseases	√						
Past allergic history, family history, and disease symptoms	√						
Medical history	√						
Family medical history	√						
Clinical test results	√	√	√	√	√	√	√
Assessment of respiratory and allergic diseases							
SGRQ	√		√		√		√
AQLQ	√		√		√		√

BP, blood pressure; #for participants with COPD or asthma; SGRQ, Saint George Respiratory Questionnaire; and AQLQ, Asthma Quality of Life Questionnaire.

Findings to date

Baseline characteristics

The baseline survey was completed in March 2022 among the 756 volunteers who were recruited from the community (Table 3). After performing quality control, we excluded missing and unqualified participants, ultimately including a total of 693 in the cohort. These included 231 men (33.3%) and 462 women (66.7%), with an average age of 66.1 years. In terms of educational level, 26.7% have not completed junior high school, 32.1% have completed senior high school, and 37.3% are college graduates or undergraduates. Compared with their symptoms in their original places of residence, the initial rates of remission reported by the participants in Sanya were 80.4% for allergic rhinitis, 82.3% for bronchitis and emphysema, 85.2% for asthma, 96.0% for COPD ($P < 0.001$). The top five diseases in this cohort are allergic rhinitis (57.9%); eczema, urticaria, or dermatitis (35.6%); bronchitis and bronchiectasis (35.6%); asthma (14.7%); and emphysema (11.7%). The top five original regions of residence are Heilongjiang Province (40.9%), Liaoning Province (12.0%), Jilin Province (10.4%), Hebei Province (7.4%), and Beijing (6.9%). The first follow-up, of 682 participants, was conducted by telephone from October to December 2022. The loss of follow-up does not make sure since COVID-19.

Biological-sample collection

During the baseline survey, we collected venous blood for detection of allergen, routine blood, liver function, blood lipids and sugar, which is close linked to the allergic and immune diseases during March 2022; the collection rate was 100%. We have continued to collect venous blood and urine samples from all 693 participants for detection during the ongoing follow-up (Table 4).

Strengths and limitations

Sanya is located in the southernmost region of China, which is tropical and has a warm winter. Many MBEPs migrate from northern China to Sanya for the winter. This provides a unique opportunity to observe the effect of tropical climate and environment on allergic diseases and helps follow up with the general population. To the best of our knowledge, this is the world's first study on the effects of tropical climate and environmental factors on respiratory and allergic diseases in MBEPs. The biological samples collected will provide objective evidence of such effects. In the future, we will further explore the relationship between the climatic environment and allergic diseases in children.

However, this study has several limitations. The main disadvantage is that the volunteers recruited are migratory-bird middle-aged or old people, who have relatively high educational levels and socioeconomic status and are therefore not representative of the general population. This limits the generalization of our findings. In addition, MBEPs return to their original residences in spring, and the effect on participants living in northern regions during the spring and summer will be difficult to assess. Notably, such potential confounding variables were not adjusted for statistical adjustments, such as the psychological impact of living in a famous tourist city. If possible, we will perform further research into this aspect in the future.

Collaboration

This is an ongoing prospective cohort study. Preliminary findings demonstrate the beneficial impact of tropical climate on allergic diseases in migratory-bird old people.

Data availability statement

The data supporting the conclusions of this article will be made available by reasonable request.

Ethics statement

The studies involving humans were approved by the Ethics Committee of Sanya Women and Children's Hospital (Approval No. SYFYIRB2022009). The studies were conducted in accordance with the local legislation and institutional requirements. Written informed consent for participation in this study was provided by the participants.

Author contributions

HG: Data curation, Formal analysis, Investigation, Methodology, Project administration, Writing–original draft, Writing–review and editing. GY: Investigation, Methodology, Project administration, Resources, Writing—review and editing. JG: Investigation, Project administration, Resources, Writing—review and editing. XL: Formal analysis, Investigation, Project administration, Writing–review and editing. CL: Formal analysis, Investigation, Project administration, Writing—review and editing. HR: Data curation, Investigation, Writing–review and editing. DC: Investigation, Writing–review and editing. LZ: Investigation, Writing–review and editing. QH: Formal analysis, Investigation, Writing–review and editing. YH: Formal analysis, Investigation, Writing–review and editing. YZ: Project administration, Resources, Writing–review and editing. ST: Conceptualization, Methodology, Supervision, Writing–review and editing. ZL: Funding acquisition, Project administration, Resources, Writing–review and editing. SL: Conceptualization, Data curation, Formal analysis, Funding acquisition, Investigation, Methodology, Project administration, Resources, Supervision, Writing—original draft, Writing—review and editing. DW: Conceptualization, Formal analysis, Funding acquisition, Investigation, Methodology, Project administration, Resources, Writing—review and editing.

Funding

The author(s) declare financial support was received for the research, authorship, and/or publication of this article. The study was supported by the Unveiling the Top Project of Sanya Women and Children's Hospital (No. SYFY-JBGS-202201), National Science Foundation of China (82173534 and 81872637), Special Program for Women and Children health (2020YJZX0212), Cultivation Project of Clinical Research from SCMC (LY-SCMC2020-06).

Acknowledgments

We are grateful to all participants for their cooperation.

Conflict of interest

The authors declare that the research was conducted in the absence of any commercial or financial relationships that could be construed as a potential conflict of interest.

Publisher's note

All claims expressed in this article are solely those of the authors and do not necessarily represent those of their affiliated organizations, or those of the publisher, the editors and the reviewers. Any product that may be evaluated in this article, or claim that may be made by its manufacturer, is not guaranteed or endorsed by the publisher.

References

1. Brozek G, Lawson J, Szumilas D, Zejda J. Increasing prevalence of asthma, respiratory symptoms, and allergic diseases: four repeated surveys from 1993-2014. *Respir Med.* (2015) 109:982–90. doi: 10.1016/j.rmed.2015.05.010

2. Biagioni B, Annesi-Maesano I, D'Amato G, Cecchi L. The rising of allergic respiratory diseases in a changing world: from climate change to migration. *Expert Rev Respir Med.* (2020) 14:973–86. doi: 10.1080/17476348.2020.1794829

3. WHO. *Asthma.* World Health Organization (2022). Available online at: https://www.who.int/news-room/fact-sheets/detail/asthma (accessed October 20, 2022).

4. Deng S-Z, Jalaludin BB, Antó JM, Hess JJ, Huang C-R. Climate change, air pollution, and allergic respiratory diseases: a call to action for health professionals. *Chin Med J.* (2020) 133:1552–60. doi: 10.1097/CM9.0000000000000861

5. Brusselle GG, Wai-San Ko F. Prevalence and burden of asthma in China: time to act. *Lancet.* (2019) 394:364–66. doi: 10.1016/S0140-6736(19)31349-2

6. Huang K, Yang T, Xu J, Yang L, Zhao J, Zhang X, et al. Prevalence, risk factors, and management of asthma in China: a national cross-sectional study. *Lancet.* (2019) 394:407–18. doi: 10.1016/S0140-6736(19)31147-X

7. Lin J, Wang W, Chen P, Zhou X, Wan H, Yin K, et al. Prevalence and risk factors of asthma in mainland China: the CARE study. *Respir Med.* (2018) 137:48–54. doi: 10.1016/j.rmed.2018.02.010

8. Wang XD, Zheng M, Lou HF, Wang CS, Zhang Y, Bo MY, et al. An increased prevalence of self-reported allergic rhinitis in major Chinese cities from 2005 to 2011. *Allergy.* (2016) 71:1170–80. doi: 10.1111/all.12874

9. Yan S, Wang X, Yao Z, Cheng J, Ni H, Xu Z, et al. Seasonal characteristics of temperature variability impacts on childhood asthma hospitalization in Hefei, China: Does PM2. 5 modify the association? *Environ Res.* (2022) 207:112078. doi: 10.1016/j.envres.2021.112078

10. Aslam R, Sharif F, Baqar M, Nizami A-S, Ashraf U. Role of ambient air pollution in asthma spread among various population groups of Lahore City: a case study. *Environ Sci Pollut Res Int.* (2022) 30:8682–97. doi: 10.1007/s11356-022-19086-1

11. Schinasi LH, Kenyon CC, Hubbard RA, Zhao Y, Maltenfort M, Melly SJ, et al. Associations between high ambient temperatures and asthma exacerbation among children in Philadelphia, PA: a time series analysis. *Occup Environ Med.* (2022) 79:326–32. doi: 10.1136/oemed-2021-107823

12. Li M, Chen S, Zhao H, Tang C, Lai Y, Ung COL, et al. The short-term associations of chronic obstructive pulmonary disease hospitalizations with meteorological factors and air pollutants in Southwest China: a time-series study. *Sci Rep.* (2021) 11:12914. doi: 10.1038/s41598-021-92380-z

13. Schoos AMM, Chawes BL, Bønnelykke K, Stokholm J, Rasmussen MA, Bisgaard H. Increasing severity of early-onset atopic dermatitis, but not late-onset, associates with development of aeroallergen sensitization and allergic rhinitis in childhood. *Allergy.* (2022) 77:1254–62. doi: 10.1111/all.15108

14. Fieten KB, Rijssenbeek-Nouwens LH, Hashimoto S, Bel EH, Weersink EJ. Less exacerbations and sustained asthma control 12 months after high altitude climate treatment for severe asthma. *Allergy.* (2019) 74:628–30. doi: 10.1111/all.13664

15. Rijssenbeek-Nouwens LH, Fieten KB, Bron AO, Hashimoto S, Bel EH, Weersink EJ. High-altitude treatment in atopic and nonatopic patients with severe asthma. *Eur Respir J.* (2012) 40:1374–80. doi: 10.1183/09031936.00195211

16. Wang P, Wang J, Zhang J, Ma X, Zhou L, Sun Y. Spatial-temporal changes in ecosystem services and social-ecological drivers in a typical coastal tourism city: a case study of Sanya, China. *Ecol Indic.* (2022) 145:109607. doi: 10.1016/j.ecolind.2022.109607

17. Chen J, Bao J. Chinese 'snowbirds' in tropical Sanya: retirement migration and the production of translocal families. *J Ethn Migr Stud.* (2021) 47:2760–77. doi: 10.1080/1369183X.2020.1739377

18. Freidl J, Huber D, Braunschmid H, Romodow C, Pichler C, Weisböck-Erdheim R, et al. Winter exercise and speleotherapy for allergy and asthma: a randomized controlled clinical trial. *J Clin Med.* (2020) 9:3311. doi: 10.3390/jcm9103311

19. Allahverdiyeva L, Khalilova A, Efendiyeva N, Samedi V. Role of speleotherapy in complex treatment of pediatric asthma: single centre experience. *J Allergy Clin Immunol.* (2019) 143:AB104. doi: 10.1016/j.jaci.2018.12.316

20. Vinnikov D, Khafagy A, Blanc PD, Brimkulov N, Steinmaus C. High-altitude alpine therapy and lung function in asthma: systematic review and meta-analysis. *ERJ Open Res.* (2016) 2:48. doi: 10.1183/13993003.congress-2016.PA4293

21. Leshem YA, Chalmers JR, Apfelbacher C, Katoh N, Gerbens LAA, Schmitt J, et al. Measuring atopic eczema control and itch intensity in clinical practice: a consensus statement from the harmonising outcome measures for eczema in clinical practice (HOME-CP) initiative. *JAMA Dermatol.* (2022) 158:1429–35. doi: 10.1001/jamadermatol.2022.4211

22. Ellwood P, Asher MI, Björkstén B, Burr M, Pearce N, Robertson CF. Diet and asthma, allergic rhinoconjunctivitis and atopic eczema symptom prevalence: an ecological analysis of the international study of asthma and allergies in childhood (ISAAC) data. ISAAC phase one study group. *Eur Respir J.* (2001) 17:436–43. doi: 10.1183/09031936.01.17304360

23. Vogelmeier CF, Criner GJ, Martinez FJ, Anzueto A, Barnes PJ, Bourbeau J, et al. Global strategy for the diagnosis, management, and prevention of chronic obstructive lung disease 2017 report. GOLD executive summary. *Am J Respir Crit Care Med.* (2017) 195:557–82. doi: 10.1164/rccm.201701-0218PP

24. Miele CH, Jaganath D, Miranda JJ, Bernabe-Ortiz A, Gilman RH, Johnson CM, et al. Urbanization and daily exposure to biomass fuel smoke both contribute to chronic bronchitis risk in a population with low prevalence of daily tobacco smoking. *Copd.* (2016) 13:186–95. doi: 10.3109/15412555.2015.1067765

25. Khusial RJ, Honkoop PJ, van der Meer V, Snoeck-Stroband JB, Sont JK. Validation of online asthma control questionnaire and asthma quality of life questionnaire. *ERJ Open Res.* (2020) 6:00289–2019. doi: 10.1183/23120541.00289-2019

26. Zhu B, Wang Y, Ming J, Chen W, Zhang L. Disease burden of COPD in China: a systematic review. *Int J Chron Obstruct Pulmon Dis.* (2018) 13:1353. doi: 10.2147/COPD.S161555

frontiers | Frontiers in Public Health

TYPE Original Research
PUBLISHED 07 December 2023
DOI 10.3389/fpubh.2023.1322019

Check for updates

OPEN ACCESS

EDITED BY
Shupeng Zhu,
University of California, Irvine,
United States

REVIEWED BY
Xiaoyi Hang,
Beijing University of Chinese Medicine, China
Zhaobin Sun,
Chinese Academy of Meteorological Sciences,
China

*CORRESPONDENCE
Yuxia Ma
✉ mayuxia07@lzu.edu.cn

†These authors have contributed equally to this work and share first authorship

RECEIVED 15 October 2023
ACCEPTED 22 November 2023
PUBLISHED 07 December 2023

CITATION
Wang W, Ma Y, Qin P, Liu Z, Zhao Y and Jiao H (2023) Assessment of mortality risks due to a strong cold spell in 2022 in China. *Front. Public Health* 11:1322019. doi: 10.3389/fpubh.2023.1322019

Assessment of mortality risks due to a strong cold spell in 2022 in China

Wanci Wang[1†], Yuxia Ma[1*†], Pengpeng Qin[1], Zongrui Liu[1], Yuhan Zhao[1] and Haoran Jiao[2]

[1]College of Atmospheric Sciences, Key Laboratory of Semi-Arid Climate Change, Ministry of Education, Lanzhou University, Lanzhou, China, [2]Liaoning Provincial Meteorological Bureau, Shenyang, China

Background: With the intensification of global climate warming, extreme low temperature events such as cold spells have become an increasingly significant threat to public health. Few studies have examined the relationship between cold spells and mortality in multiple Chinese provinces.

Methods: We employed health impact functions for temperature and mortality to quantify the health risks of the first winter cold spell in China on November 26th, 2022, and analyzed the reasons for the stronger development of the cold spell in terms of the circulation field.

Results: This cold spell was a result of the continuous reinforcement of the blocking high-pressure system in the Ural Mountains, leading to the deepening of the cold vortex in front of it. Temperature changes associated with the movement of cold fronts produced additional mortality risks and mortality burdens. In general, the average excess risk (ER) of death during the cold spell in China was 2.75%, with a total cumulative excess of 369,056 deaths. The health risks associated with temperatures were unevenly distributed spatially in China, with the ER values ranging from a minimum of 0.14% to a maximum of 5.72%, and temperature drops disproportionately affect southern regions of China more than northern regions. The cumulative excess deaths exibited the highest in eastern and central China, with 87,655 and 80,230 respectively, and the lowest in northwest China with 27,474 deaths. Among the provinces, excess deaths pronounced the highest in Shandong with 29,492 and the lowest in Tibet with only 196.

Conclusion: The study can provide some insight into the mortality burden of cold spells in China, while emphasising the importance of understanding the complex relationship between extreme low temperature events and human health. The outcomes could provide valuable revelations for informing pertinent public health policies.

KEYWORDS

cold spell, temperature change, mortality, excess death, health risks

1 Introduction

In the context of global warming, the frequency and intensity of extreme weather events such as cold spells and heat waves are increasing (1–3). The association between climate and public health has become a pressing issue that will likely result in more health crises in the future (4). According to the Sixth Assessment Report of IPCC (5), climate change may exacerbate the occurrence of extreme weather events, which leads to the increase in the incidence and mortality of climate sensitivity diseases in many places in the world, especially in extremely low temperature weather condition (6, 7). The occurrence of climatic events will cause relevant sensitive diseases to be more affected. Due to the aging of the population, the proportion of vulnerable groups in society is also increasing, which further the health risks of extreme weather are exacerbated (8). It's imperative to investigate the connection between climatic and environmental factors and human health.

Temperature is a crucial factor that influences human health (9, 10). Extensive studies have consistently demonstrated a non-linear relationship between temperature and health outcomes, with exposure-response curves for morbidity or mortality in populations typically having a "U," "V" or "J" shape (9, 11–13). A study encompassing 15 European cities revealed that a 1°C drop in temperature resulted in an increase of 1.35, 1.72, 3.30, and 1.25% in daily natural deaths, cardiovascular diseases, respiratory diseases, and cerebrovascular diseases, respectively (14). Intriguingly, low temperature contributes to a greater proportion of cardiovascular disease-related deaths compared to heat-related conditions. An extensive study from 15 major cities in China from 2007 to 2013 elucidated that 15.8% of cardiovascular mortality was attributable to low temperatures, whereas a mere 1.3% could be attributed to high temperatures (15).

The cold spell is a typical extreme low temperature event. In recent years, extreme cold weather events have been creeping up in many regions of the world and are becoming increasingly fierce. For instance, during the strong cold spell in February 2021, North America experienced record-breaking low temperatures that resulted in 100 deaths and left 5.5 million households suffering from power outages (16). Similarly, in December 2022, an "epic cold spell" swept through the United States, causing over 60 deaths (17). In different studies, the definition of cold spells is inconsistent, leading to differences in analysis results. Wang et al. (18) defined the period when the temperature was lower than the 5th percentile and lasted more than 2 days as a cold spell. The study found that the overall cumulative excess risk (CER) of non-accidental deaths during cold weather in China from 2006 to 2011 was 28.2% (95% CI: 21.4, 35.3%), and the impact was more severe in southern China compared to the northern region. Sun et al. (19) use the definition of a cold spell with temperature below the 5th percentile and lasting more than 7 days. Compared to non-cold spell days, the risk of non-accidental mortality, circulatory mortality, and respiratory mortality increased by 17.4% (95% CI: 15.8, 19.0%), 20.8% (95% CI: 18.8, 23.0%), and 22.7% (95% CI: 19.5, 25.9%) respectively on cold spell days.

To gain a deeper insight into the health risks associated with cold spells, in the current study, we focused on the initial cold spell event of winter in China that occurred on November 26th, 2022. This particular cold spell was characterized by rapid spread, wide-reaching impacts, complex precipitation and snow phases, and significant temperature drops across over 30 provinces. This can be considered as a typical outbreak of cold spell weather process. A correlation between the temperature reduction of the cold spell and mortality was established, and then it could provide a quantitative estimation of the health risks associated with this specific cold wave event. The findings will enhance our comprehension of the connection between extreme cold events and mortality rates in various regions, as well as aid in the development of effective adaptation strategies to mitigate the adverse effects of future extreme cold events.

2 Data and methods

2.1 China meteorological data set

Daily meteorological station data were collected from China Meteorological Data Service Centre,[1] including average temperature, atmospheric pressure, sea level pressure, relative humidity, precipitation, wind direction, and wind speed before and after the onset of the cold spell. These data are sourced from national-level surface meteorological stations managed and subject to quality control by the China Meteorological Administration. The data are primarily collected from the major cities in the country, making it representative and reliable.

The reanalysis data were obtained from ERA5, the fifth generation of ECMWF atmospheric reanalysis global climate data with high temporal and spatial resolution. It provides hourly estimates of atmospheric, terrestrial, and oceanic climate variables, including 137 layers of atmospheric data. The selected time period ranges from 26 November to 5 December 2022 and consists of 2 m temperature, 500 hPa geopotential height, temperature, and sea level pressure variables. The data have a horizontal resolution of 0.25° × 0.25° and a temporal resolution of 1 h.

2.2 Population and baseline mortality data

Highly accurate population data in 2019, precise to $1 \times 1\ km^2$, were provided by the Resource and Environment Science and Data Center.[2] These data are based on multiple population-relevant characteristics, including land-use type, night light brightness, and settlement density, ensuring accurate representation of the spatial distribution of China's population. The population distribution of China in 2022 is calculated using the annual population growth rate of China's population since 2019 (Supplementary Table S1).

The baseline mortality data for each province were gathered from the National Bureau of Statistics,[3] including various indicators such as the national economy, population, education, and health. The data is reliable, complete and accurate, and it can reflect diverse social and economic activities across the country and. However, the mortality rate data used in the study is only counted to 2021, as the latest data for 2022 has not yet been updated by the country.

2.3 Definition of a cold spell

A cold spell was defined as below by the Central Meteorological Observatory: when the temperature drops were more than 8°C within

1 https://data.cma.cn
2 https://www.resdc.cn
3 https://data.stats.gov.cn/

24 h or 10°C in 48 h or 12°C in 72 h and the minimum temperature is below 4°C.[4]

2.4 Calculation of excess deaths

Firstly, the relative risk (*RR*) of the temperature reduction of cold spell is calculated using the following equation:

$$RR_i = \exp(\beta \cdot \Delta x_i) \quad (1).$$

Where β is the exposure response relationship coefficient, which represents the additional mortality risk per 1°C decrease in temperature. The β value reference is chosen as 0.21% (20), and Δx_i is the difference between the maximum and minimum of the daily mean temperature at grid *i* during the cold spell.

$$ER_i = RR_i - 1 \quad (2)$$

ER_i is the excess risk (*ER*) of mortality related to temperature at grid *i*, it reflects the variation in the *ER* of mortality associated with every 1°C change in temperature.

We evaluated the mortality burden attributed to this cold spell in China using the following formula (21):

$$\Delta Mortality = Y_i \cdot ER_i \cdot POP_i \quad (3)$$

Where $\Delta Mortality$ indicates the excess mortality rate related to temperature, Y_i is the baseline mortality rate, and POP_i is the total population exposed to low temperature.

As the spatial resolution of the population data differs from that of the 2 m temperature, we used geographic information system (*GIS*) technology to resample the population data raster to 0.25° using bilinear interpolation. The mortality attributed to low temperature exposure in each grid in China was subsequently estimated by utilizing the combined exposure-response coefficient. After calculating the mortality in each grid separately, subdivisional statistics in each province by using the spatial analyst tool in ArcMap (version 10.8). We have also divided China into seven geographical regions based on variations in climate and population, encompassing Northeast China, including Heilongjiang, Liaoning, and Jilin; North China, consisting of Beijing, Tianjin, Hebei, Shanxi, and Inner Mongolia; Northwest China, comprising Shaanxi, Gansu, Ningxia, Xinjiang, and Qinghai; East China, encompassing Jiangsu, Zhejiang, Anhui, Shandong, and Shanghai; Central China, consisting of Henan, Hubei, Hunan, and Jiangxi; Southwest China, encompassing Sichuan, Tibet, Guizhou, Yunnan, and Chongqing; and South China, comprising Fujian, Guangdong, Guangxi, Hainan, and Taiwan. Additionally, to verify the rationality of the ERA5 reanalysis data, we employed two commonly used indexes to evaluate and compare it with observation station data. The results can be found in Supplementary Figure S1 in the Appendix.

4 http://www.cma.gov.cn

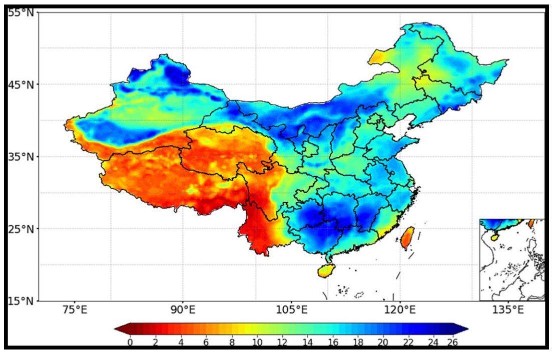

FIGURE 1
The temperature drops from November 26th to December 5th, 2022.

3 Results

3.1 Cold spell process

As illustrated in the Figure 1, the cold spell from November 26th to December 5th, 2022 had caused a significant cooling effect across most parts of China, with the maximum temperature drop between 8°C and 16°C, which was particularly pronounced in Xinjiang, Gansu, Inner Mongolia, Shanxi, Guizhou, Hunan, Jiangxi, and other provinces where temperature drops exceeded 20°C. The temperature showed the decreasing trend evidently in the northwestern, eastern as well as in southern China, where the big cities with dense population are also greatly affected and expected to pose greater health risks. The temperature drop exceeded 16°C over a national area of 2.15 million square kilometres (about 22% of the country). According to the statistics from the China Meteorological Administration, certain regions in northwest, northern, eastern China, western and southern Jiangnan, as well as north-central China experienced the earliest temperature drops in recorded history, reaching a level of extremity. In addition, we summarized the descriptive statistics for the major cities in the 14 provinces with the highest range of temperature dropping process (see Table 1). It is evident that despite the notable differences in average temperatures between the north and south, all of these regions have experienced temperature drop exceeding 15°C, as well as significant increases in sea level pressure before and after the cold spell. The Chinese meteorological authorities have assessed the overall intensity of the cold spell that swept through most of China to be the fifth strongest one on record for the same period in November.

3.2 Analysis of the causes of the cold spell

As indicated in Figure 2, at 12:00 on 25 November, a circulation pattern manifested in the 500 hPa height field, revealing the presence of two ridges and a trough. This configuration established an inverted Ω-flow pattern over East Asia. Concurrently, a deep closed cold low-pressure system developed in the northwestern vicinity of Lake Baikal. Additionally, an extensive east–west oriented cross trough was observed in the northwestern region. The persistent transport of cold advection preceding the ridge positioned behind the trough fostered the accumulation of cold air within the cross trough. The intensified

TABLE 1 Statistics of meteorological elements in major cities affected by the cold spell.

City	Temperature (°C)		Mean Maximum wind speed (m/s)	Mean relative humidity (%)	Sea level pressure (hPa)	
	The reduced temperature of the process	Mean			Min	Max
Hohhot	17.33	−8.99	4.74	35.13	1009.20	1052.90
Lüliang	19.71	−4.83	5.25	42.26	1005.90	1052.10
Nanjing	17.57	8.28	6.28	65.59	1002.40	1036.20
Nanchang	18.36	6.51	8.07	84.44	1007.70	1035.90
Hefei	17.35	7.56	4.09	70.77	1006.60	1040.40
Hangzhou	16.64	9.66	6.02	87.81	1007.80	1037.00
Nanning	18.93	17.65	7.62	88.06	1006.70	1027.80
Qingdao	19.47	5.11	11.09	61.33	1010.00	1041.10
Changsha	19.05	8.55	8.74	83.31	1005.60	1037.60
Guiyang	21.77	10.12	7.50	80.11	998.10	1034.10
Urumqi	16.27	−13.80	3.78	68.44	1012.80	1057.00
Lanzhou	15.87	−4.97	3.32	54.69	1002.80	1045.90
Yinchuan	16.78	−4.72	3.97	38.78	1003.80	1052.10
Yulin	19.61	−6.14	5.78	38.44	1007.80	1053.60

development of the blocking high located on the eastern side of the Ural Mountains, combined with the surface sea level pressure field can be seen behind a high altitude trough with negative vorticity advection behind the trough, which promoted the development of cold high pressure at the surface. By 00:00 on the 27th, the cross trough has moved to northern Xinjiang, China. Subsequently, the cold front advances towards the northern territories of Inner Mongolia and eastern Xinjiang. The cold front undergoes further intensification and propagates southeastward, thereby exerting its influence over a significant portion of northern regions within China. At 12:00 on the 28th, a notable transformation occurred as the previously established inverted Ω-flow pattern ceased to persist. This alteration was accompanied by the emergence of an outburst of cold air and a vertical reorientation of the horizontal trough. Therefore, a discernible meridional circulation pattern manifested in the wake of the trough. These atmospheric adjustments created favorable circumstances for its continued southward displacement. As the high-altitude fronts persistently advance towards the south, the cold front has extended its influence to encompass the central region of China by 00:00 on the 29th, then it reached further into southern regions of China, with particular emphasis on areas encompassing Hunan and Jiangxi provinces.

3.3 Assessment of mortality risk in the cold spell

Figure 3A presents the spatial distribution of the excess risks (ERs) for the cold spell process. The spatial distribution of ER reveals a notable discrepancy in different regions. It pronounced high ERs in the northern and southern regions, and relatively lower ERs in the central areas. Specifically, regions exhibiting higher ERs include northwestern regions of China such as northern Xinjiang, central and western Inner Mongolia, northeastern Gansu, Ningxia, Shaanxi, northern Shanxi, as well as some southern regions such as eastern Guizhou, Hunan, southern Jiangxi, and northern Guangxi. Additionally, it is noteworthy that these identified areas are concurrently characterized by significant cooling. In Figure 3B, the ERs of provincial capital cities exhibit a distinct correlation with the low temperatures. This correspondence underscores the relationship between the severity of temperature decrease and the associated health risks. Among these cities, the highest ER is recorded in Urumqi (0.0435), followed closely by Guiyang (0.0424). Among the cities counted, only three recorded temperatures below 10°C, while the southern cities experienced significant temperature declines, accompanied by high ERs. More than 90% of southern cities had ERs greater than the average value of whole country. Combined with Figures 2, 3, it can also be observed that the temperature drops aligns with the movement of cold fronts. On November 26th, a ground cold front hit northern Xinjiang. The next day, it reached the southern part of Xinjiang and moved southeast, reaching central and western Inner Mongolia, Gansu, east-central, and northern Qinghai. On November 28th, the cold front had arrived in northern China, extending to northeast regions and Huanghuai. By November 29th, it had reached Sichuan and Chongqing on the west, and extended ulteriorly its reach the coast of South China on the 30th.

Figure 4 demonstrates the spatial distribution of cumulative excess deaths by province of China. The highest number of cumulative excess deaths was identified in Shandong with 29,492 cases, exemplifying the severity of the impact seen in this particular region. Conversely, Tibet exhibited the lowest number of cumulative excess deaths, with a recorded count of 196. The cumulative excess deaths exceeding 20,000 predominantly cluster within the central-eastern regions of China. Shandong Province emerges as the most heavily impacted province, followed by Hunan, Henan, Anhui, Sichuan, Hebei, and Jiangsu provinces. The provinces showcasing cumulative excess deaths ranging from 10,000 to 20,000 are situated predominantly in the southern and northeastern parts of the country,

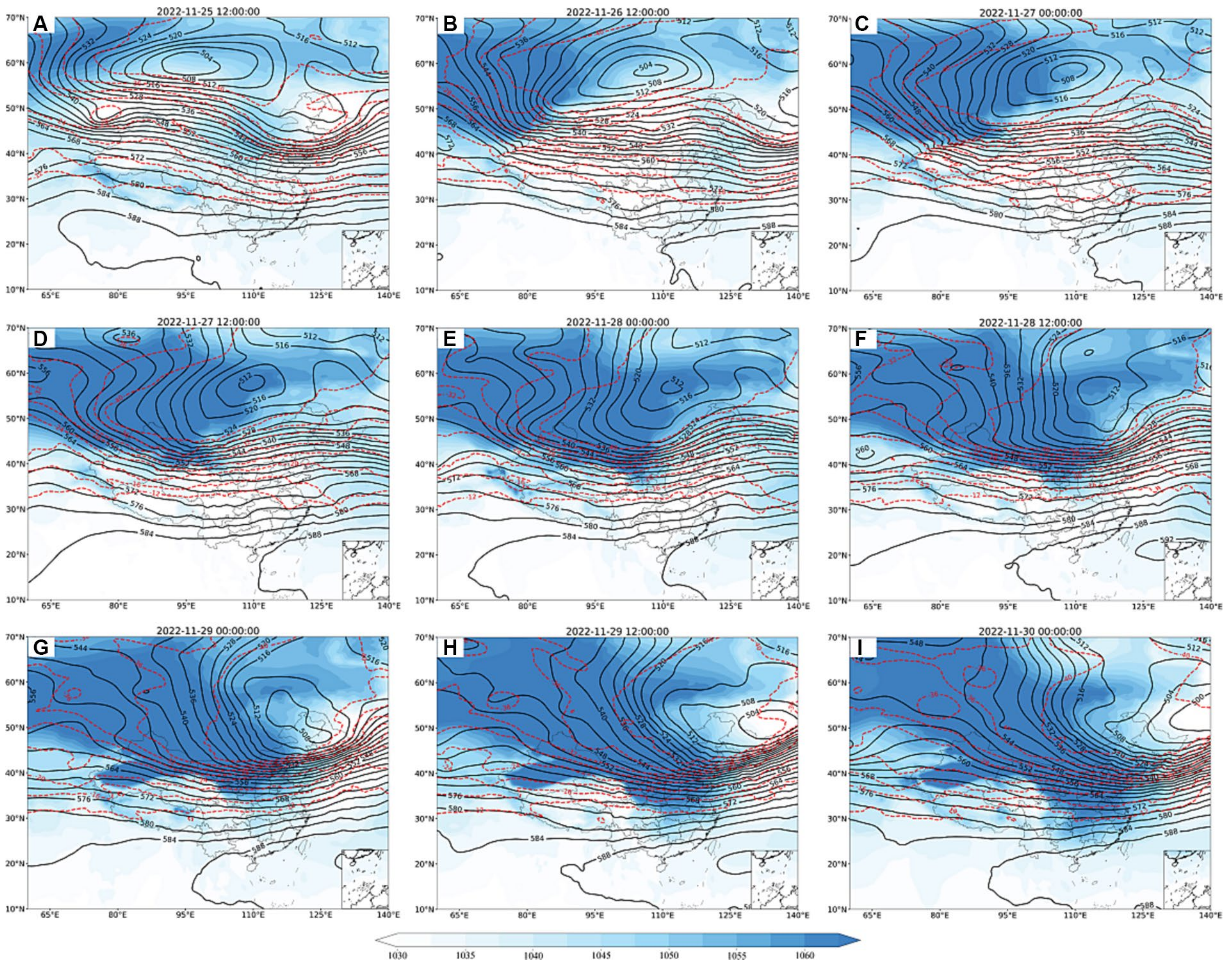

FIGURE 2
Geopotential height at 500 hPa (black solid line, unit: dagpm) and temperature field (red dashed line, unit: °C) and sea level pressure field (shaded, unit: dagpm; **A–I**) from 12:00 on 25 November to 00:00 on 30 November 2022.

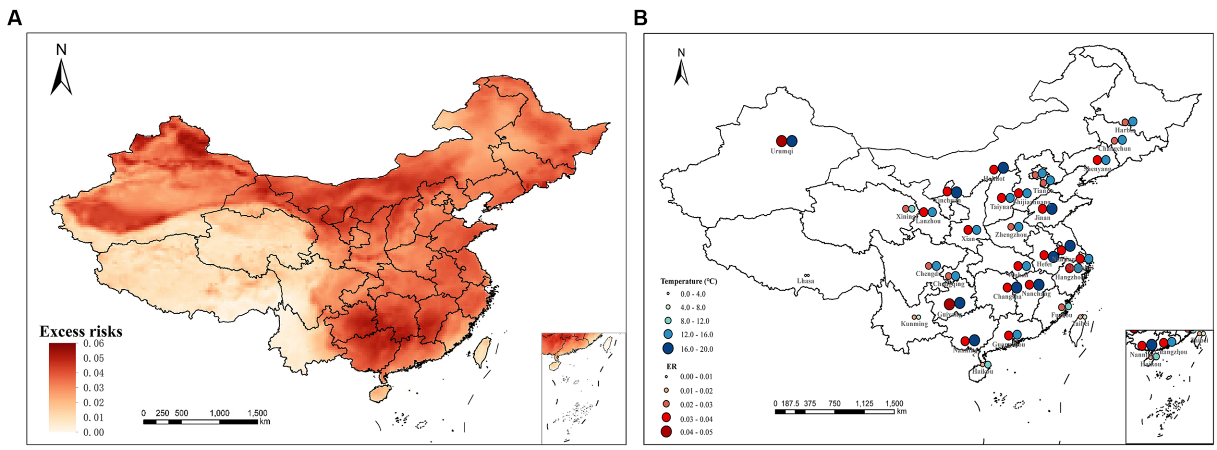

FIGURE 3
Distribution of excess risks **(A)** and the temperature drops and ERs in provincial capital cities in China **(B)**.

namely Hubei, Guangdong, Jiangxi, Guizhou, Heilongjiang, and Liaoning. In contrast, Tibet and Qinghai provinces in Tibetan Plateau have reported a comparatively lower cumulative number of excess deaths, below 1,000. Northern provinces of China, for the most part, registered cumulative excess deaths in the range of 5,000 to 10,000. Thus, regional disparities in excess mortality become evident when

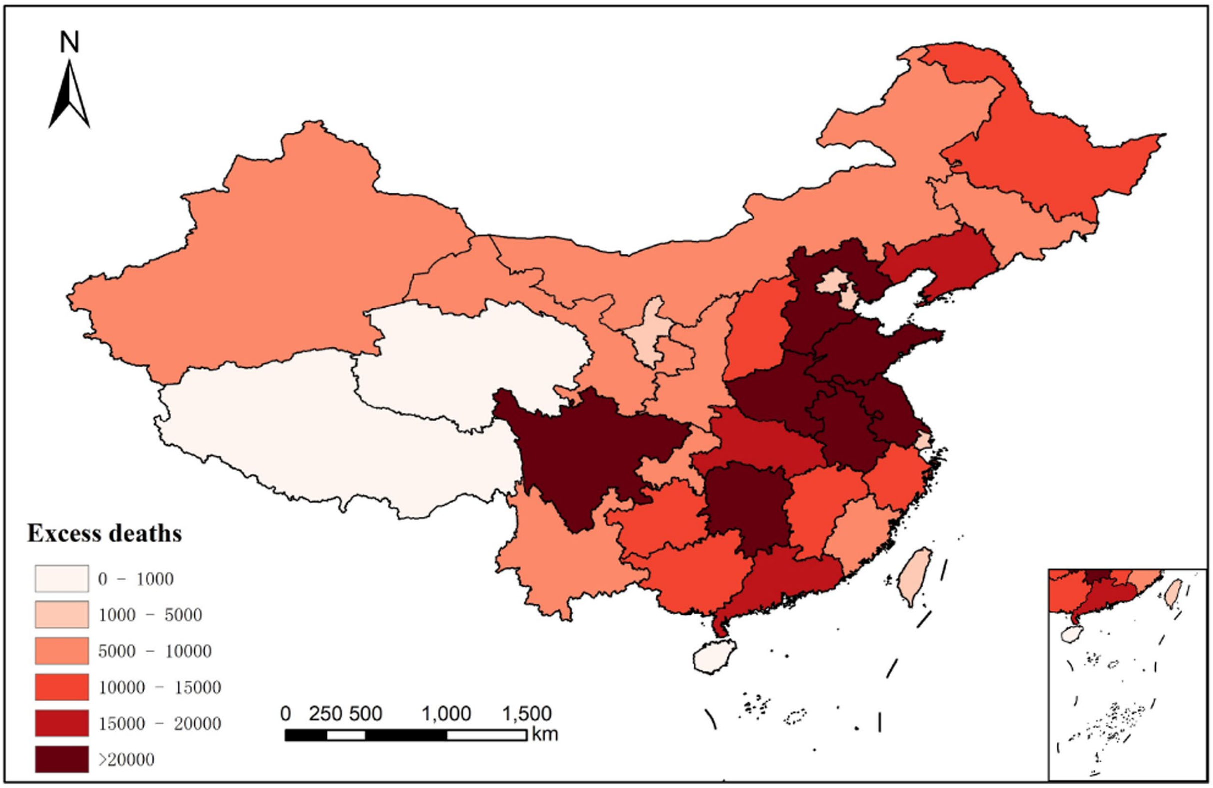

FIGURE 4
Excess deaths in China.

considering the distribution of cumulative excess deaths across various provinces in China. Despite having relatively smaller populations, the regions of Xinjiang and Inner Mongolia in China exhibit a higher risk of excess deaths and cumulative excess deaths. This can be attributed to the pronounced cooling effect prevalent in these areas.

Table 2 provided an overview of the average ERs for each individual province and whole country. The average ER for China was found to be 2.75%, indicating that for every 1°C drop in average daily temperature, the number of deaths is expected to increase by 2.75%. The excess risks of provinces unveiled both the highest and lowest values, recorded as 5.72 and 0.14%, respectively. Furthermore, a substantial 81.25% of provinces exhibit ERs surpassing the average value for whole country. Among the provinces, the top five provinces displaying the highest excess mortality risks are identified as Hunan (4.18%), Guangxi (4.17%), Guizhou (4.09%), Jiangxi (4.06%), and Ningxia (3.89%). These findings align with numerous prior studies indicating a greater influence of cold spells on southern regions of China compared to the northern areas.

Figure 5 showed the cumulative excess number of deaths recorded across the seven distinct geographical regions within China. According to the statistics of cumulative excess deaths in each region, Eastern China emerges as the region with the highest fatality count, totaling 80,000 deaths. It is closely followed by central China, which also recorded 80,000 cumulative excess deaths. In contrast, Northwest China exhibited the lowest number of fatalities among the regions, while the North, South, and Southwest regions reported figures exceeding 40,000 deaths. Additionally, we conducted an analysis of cumulative excess deaths per square kilometer across the regions (see Table 2). Notably, Shanghai, situated in the eastern region, exhibited the highest density of cumulative excess deaths, with a value of 0.5091 deaths per square kilometer. In contrast, Tibet recorded the lowest density, with a mere 0.0002 deaths per square kilometer. The top five regions with the highest rankings in terms of cumulative excess deaths per square kilometer also include Beijing (0.2376), Jiangsu (0.1976), Shandong (0.1878), and Anhui (0.1626). The region with the most substantial cumulative excess deaths per square kilometer is Eastern China, a phenomenon closely associated with its densely populated areas and heightened vulnerability to the cold spells.

4 Discussion

From a circulatory perspective, the occurrence of the cold spell is primarily associated with the establishment and subsequent collapse of middle and high latitude blocking high pressure systems. The principle is by the eastward progression of an intensifying cold high-pressure system, resulting in the influx of strong cold air. The cyclonic nature of the cold high-pressure front experiences rapid intensification, leading to the development of a horizontal trough that eventually transforms into a vertical structure. This vertical alignment facilitates the intrusion of cold air into China, ultimately triggering the outbreak of a cold spell. Extensive experience and research have enabled the classification of short-medium term cold spell weather patterns into three main types: small trough development, eastward-moving low trough, and horizontal trough turning vertical (22). It should not

TABLE 2 Average excess risks and excess deaths per kilometre in different provinces of China.

Provinces	Average ERs	Excess deaths per km^2
Tibet	1.03%	0.0002
Xinjiang	3.01%	0.0045
Inner Mongolia	3.44%	0.0078
Gansu	3.17%	0.0169
Qinhai	1.29%	0.0013
Ningxia	3.89%	0.0291
Sichuan	1.79%	0.0459
Shaanxi	3.30%	0.0462
Shanxi	3.46%	0.0771
Chongqing	3.00%	0.0896
Yunnan	1.22%	0.0167
Guizhou	4.09%	0.0592
Guangxi	4.17%	0.0611
Henan	3.06%	0.1448
Hubei	3.33%	0.0935
Hunan	4.18%	0.1230
Guangdong	3.36%	0.0962
Hebei	3.32%	0.1072
Beijing	2.88%	0.2376
Tianjin	2.89%	0.1566
Shandong	3.54%	0.1878
Anhui	3.61%	0.1626
Jiangsu	3.57%	0.1976
Zhejiang	3.47%	0.1175
Jiangxi	4.06%	0.0756
Fujian	2.79%	0.0486
Shanghai	3.03%	0.5091
Heilongjiang	3.25%	0.0280
Jilin	3.23%	0.0466
Liaoning	3.26%	0.1159
Hainan	1.69%	0.0270
Taiwan	1.15%	0.0536
Average	2.75%	0.0381

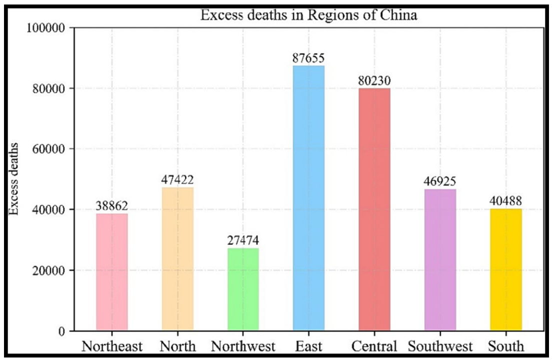

FIGURE 5
Excess deaths in seven geographical regions of China.

be disregarded that the substantial human health consequences stemming from extensive nationwide cold spells. The impacts of population vulnerability related to these cold events are anticipated to become increasingly severe under future warming scenarios (23).

Previous studies reported the possible mechanisms of influence of cold air and dramatic temperature changes during cold spells on health, especially for respiratory and circulatory diseases (18, 24–26). It is noteworthy that low temperature exerts a more pronounced impact on mortality associated with respiratory diseases (17, 27). Cold temperatures can promote the survival of bacteria and viruses in droplets, and indoor overcrowding can contribute to an increased risk of transmission among individuals (28). Abrupt temperature drops can also compromise the local defenses of the human respiratory tract, giving rise to the development of various lung ailments (29–31). Under the circumstance of sustained hypothermia and the passage of a cold front, there is an increase in blood supply and circulatory load on the human heart and brain, resulting in elevating the incidence of hypertension, and consequently raising the risk of stroke (32, 33). The activity of cold air masses and changes in meteorological factors can induce or exacerbate respiratory and circulatory diseases with a certain degree of lag (34, 35). The impacts caused by these environmental factors may not be fully recovered within a short period of time (36). Especially in vulnerable populations such as children and the older adults, their thermoregulatory systems often struggle to adapt to persistent cold temperature and drastic temperature changes (37), which may lead to the development and exacerbation of related diseases (38).

Cold fronts and cold high pressure are both weather systems controlled by cold air masses, with a cold front situated along the front of the cold high pressure. As the systems move, meteorological elements can change drastically, particularly leading to short periods of substantial cooling and rapid increases in barometric pressure (22). In the current study, we observed that such alterations in temperature and pressure caused by the movement of cold fronts often resulted in high ERs. Several studies have investigated the intricate relationship between mortality and changes in temperature and pressure, generally revealing an augmented mortality risk linked to elevated temperatures and reduced pressure (39–41). In a research conducted in the Czech Republic, changes in meteorological elements were found to be significantly correlated with mortality rates. The relationship between excess mortality and changes in temperature and pressure was more pronounced in instances of sudden fluctuations than in the passage of atmospheric fronts, and the effects were observed predominantly in populations aged 70 years and older (42). Similarly, Morabito et al. (43) identified a connection between abrupt weather changes and heightened blood pressure levels in Italy. Moreover, several other studies conducted in UK and the United States of America have also highlighted the association between sudden changes in weathers and mortality (44, 45).

Our findings indicated that the average ERs of death were greater in southern provinces of China compared to northern provinces. This discrepancy may be attributed to the differential adoption of protective measures by the public in these respective regions during cold spell events. The inhabitants of northern China exhibit a higher propensity for employing effective protective measures, including the provision of indoor heating in households and the implementation of community adaptation strategies. Individuals residing in warmer regions often face heightened vulnerability to the impacts of cold weather due to their limited physiological and behavioral adaptations (46–48). For instance, in subtropical regions, the scarcity of buildings equipped with heating systems capable of providing adequate warmth during extremely cold weather conditions contributes to an amplified risk, particularly among vulnerable groups such as the older adults (49). Conversely, northern regions exhibit greater adaptive experience with regard to lifestyle, dietary habits, clothing choices, and internal mechanisms that help regulate the body's response to cold spell exposure (50). Individuals from disadvantaged socio-economic backgrounds and with lower levels of education are often more vulnerable to the effects of cold due to their limited access to health services and poorer living conditions (18, 51). When coupled with their geographical location in the warmer southern region, these factors render them even more susceptible to the adverse effects of lower temperatures (19, 52, 53). However, Shandong has the highest cumulative excess deaths. This may be due to the calculation of cumulative excess deaths accounts for various factors, including baseline mortality rates, population, and temperature drops during cold spells. Shandong Province is a populous region in China, ranking second in terms of population according to the seventh national census, with a relatively high baseline mortality rate. Additionally, the majority of the province experienced a significant decrease in temperature during the cold spell. Other provinces such as Xinjiang and Inner Mongolia had significant cooling but sparse populations, while Guangdong and Henan had large population bases but did not experience as much overall temperature reduction as Shandong. Consequently, the comprehensive result made Shandong have the highest cumulative excess deaths.

It is significant to note the potential higher vulnerability of early winter cold events examined in this study. Previous studies have shown that the risk associated with short-term, early cold and extreme cold events is higher compared to late cold events, with longer duration of early cold events exhibiting greater vulnerability (54, 55). Nevertheless, relative risks decrease towards the latter part of winter, which may be related to people gradually adapting to the cold environment by taking appropriate warming measures. The health risks associated with the first cold spell are greater compared to previous studies. Sun et al. (19) found that 57,783 non-accidental deaths were related to the cold spell in China in 2018, while our analysis revealed a significantly higher cumulative excess mortality of 369,056. In terms of attributing the excess mortality risk associated with cold spells, the national average ER (2.75%) estimated in our study was higher than 2.10% for multiple cities in China (56) and 1.44% in South Korea and Japan (57). This implies that the first cold spell process may have a stronger harvest effect (58), which may have a greater impact on public health in the short term, particularly among individuals with underlying medical conditions. Furthermore, the cold spell in this study exhibited a protracted duration, significant intensity, and diverse spectrum of ramifications. While the intensity and duration are crucial factors influencing the cold mortality relationship, with longer and stronger cold spells being associated with a significantly increased mortality rate (59, 60). Within the context of global climate change, it has been observed that wherein cold spells are becoming less frequent but increasingly extreme in nature (61). A preceding study suggested a notable escalation in the risk and health burden associated with cold spells over the course of several decades (57). It is crucial that we should keep moving forward assessing health risks in connection with cold waves and predicting the future health impacts of climate change, and comprehend the necessity of the intricate interplay between frigid weather events and human health. Simultaneously, we also should underscore the need for proactive measures to mitigate the impacts of extreme weather events such as cold waves and reduce the burden of disease on vulnerable populations.

Several limitations should be acknowledged in this study. Firstly, our estimates are subject to the assumption that a uniform baseline mortality rate is applied to each locality within the province. This simplifying assumption may overlook potential variations in mortality rates across different sub-regions or demographic groups within each province. Secondly, the data utilized for establishing the baseline mortality rates were only updated until 2021, potentially limiting the generalizability of our findings to more recent periods. Considerable variations in mortality rates arise between urban and rural areas owing to disparities in socio-economic levels, environmental factors, and access to healthcare services (62). We have employed a single β value for China, which may lead to potential underestimation or overestimation of the health burden in certain areas. Significant demographic and epidemiological changes were driven by rapid urbanisation, new coronavirus epidemics, and ageing (63), but we were unable to acquire the exact number of deaths caused by cold wave exposure to facilitate the calculation and validation processes due to data constraints. Future studies could benefit from incorporating updated health data, which would enhance the precision and reliability of studies.

5 Conclusion

The findings indicated that temperature drops from the cold spell outbreak had placed a significant health burden on China. Southern China faced a greater health risk from the cold spell compared to the north. The economically developed and densely populated provinces and regions have a higher cumulative excess deaths. Excess deaths were the highest in Shandong province. Our research offered an evidence of the mortality risks posed by cold spells in China, and may play a crucial role in developing region-specific prediction systems, particularly vulnerable groups, from the hazards of these extreme weather events.

Data availability statement

The original contributions presented in the study are included in the article/Supplementary material, further inquiries can be directed to the corresponding author.

Author contributions

WW: Methodology, Writing – original draft. YM: Conceptualization, Methodology, Writing – review & editing. PQ: Data curation, Formal analysis, Writing – original draft. ZL: Formal Analysis, Writing – original draft. YZ: Validation, Writing – original draft. HJ: Software, Writing – original draft.

Funding

The author(s) declare financial support was received for the research, authorship, and/or publication of this article. This research was supported by the National Natural Science Foundation of China (grant nos. 41975141 and 42375177) and Natural Science Foundation of Gansu (grant no. 23JRRA1079).

Conflict of interest

The authors declare that the research was conducted in the absence of any commercial or financial relationships that could be construed as a potential conflict of interest.

Publisher's note

All claims expressed in this article are solely those of the authors and do not necessarily represent those of their affiliated organizations, or those of the publisher, the editors and the reviewers. Any product that may be evaluated in this article, or claim that may be made by its manufacturer, is not guaranteed or endorsed by the publisher.

Supplementary material

The Supplementary material for this article can be found online at: https://www.frontiersin.org/articles/10.3389/fpubh.2023.1322019/full#supplementary-material

References

1. Sun Y, Zhang XB, Zwiers FW, Song LC, Wang H, Hu T, et al. Rapid increase in the risk to extreme summer heat in eastern China. *Nat Clim Chang.* (2014) 4:1082–5. doi: 10.1038/nclimate2410

2. Liu BQ, Zhu CW, Su JZ, Ma SM, Xu K. Record-breaking northward shift of the western North Pacific subtropical high in July 2018. *J Meteor Soc Japan Ser II.* (2019) 97:913–25. doi: 10.2151/jmsj.2019-047

3. Xu K, Lu RY, Kim BJ, Park JK, Mao JY, Byon JY, et al. Large-scale circulation anomalies associated with extrem-e heat in South Korea and southern–Central Japan. *J Clim.* (2019) 32:2747–59. doi: 10.1175/JCLI-D-18-0485.1

4. Ma SM, Zhou TJ, Angélil O, Shiogama H. Increased chances of drought in southeastern periphery of the Tibetan plateau induced by anthropogenic warming. *J Clim.* (2017) 30:6543–60. doi: 10.1175/JCLI-D-16-0636.1

5. IPCC. *Climate change 2022: impacts, adaptation and vulnerability[M].* Cambridge: Cambridge University Press (2022).

6. Sun ZB, Han L, Ding AJ, Liu HN, Zhao XJ. The health impacts of aerosol-planetary boundary layer interactions on respiratory and circulatory mortality. *Atmos Environ.* (2022) 276:119050. doi: 10.1016/j.atmosenv.2022.119050

7. Han L, Sun ZB, He J, Zhang BH, Lv MY, Zhang XL, et al. Estimating the mortality burden attributable to temperature and PM2. 5 from the perspective of atmospheric flow. *Environ Res Lett.* (2020) 15:124059. doi: 10.1088/1748-9326/abc8b9

8. Li TT, Horton RM, Bader DA, Zhou MG, Liang XD, Ban J, et al. Aging will amplify the heat-related mortality risk under a changing climate: projection for the elderly in Beijing, China. *Sci Rep.* (2016) 6:28161. doi: 10.1038/srep28161

9. Wang YC, Lin YK. Temperature effects on outpatient visits of respiratory diseases, asthma, and chronic airway obstruction in Taiwan. *Int J Biometeorol.* (2015) 59:815–25. doi: 10.1007/s00484-014-0899-0

10. Gasparrini A, Guo YM, Hashizume M, Lavigne E, Zanobetti A, Schwartz J, et al. Mortality risk attributable to high and low ambient temperature: a multicountry observational study. *Lancet.* (2015) 386:369–75. doi: 10.1016/S0140-6736(14)62114-0

11. Ye XF, Wolff R, Yu WW, Vaneckova P, Pan XC, Tong SL, et al. Ambient temperature and morbidity: a review of epidemiological evidence. *Environ Health Perspect.* (2012) 120:19–28. doi: 10.1289/ehp.1003198

12. Xing Q, Sun ZB, Tao Y, Zhang XL, Miao SG, Zheng CJ, et al. Impacts of urbanization on the temperature-cardiovascular mortality relationship in Beijing, China. *Environ Res.* (2020) 191:110234. doi: 10.1016/j.envres.2020.110234

13. McMichael AJ, Wilkinson P, Kovats RS, Pattenden S, Hajat S, Armstrong B, et al. International study of temperature, heat and urban mortality: the 'ISOTHURM' project. *Int J Epidemiol.* (2008) 37:1121–31. doi: 10.1093/ije/dyn086

14. China Meteorological News Press (2022). Available at: https://www.cma.gov.cn/2011xwzx/2011xqxxw/2011xqxyw/202212/t20221229_5237243.html (Accessed December 29, 2022).

15. Yang XF, Li LF, Wang JF, Huang JX, Lu SJ. Cardiovascular mortality associated with low and high temperatures: determinants of inter-region vulnerability in China. *Int J Environ Res Public Health.* (2015) 12:5918–33. doi: 10.3390/ijerph120605918

16. United Nations News (2021). Available at: https://news.un.org/zh/story/2021/03/1079932 (Accessed March 9, 2021).

17. Analitis A, Katsouyanni K, Biggeri A, Baccini M, Forsberg B, Bisanti L, et al. Effects of cold weather on mortality: results from 15 European cities within the PHEWE project. *Am J Epidemiol.* (2008) 168:1397–408. doi: 10.1093/aje/kwn266

18. Wang LJ, Liu T, Hu MJ, Zeng WL, Zhang YH, Rutherford S, et al. The impact of cold spells on mortality and effect modification by cold spell characteristics. *Sci Rep.* (2016) 6:38380. doi: 10.1038/srep38380

19. Sun QH, Sun ZY, Chen C, Yan ML, Zhong Y, Huang ZH, et al. Health risks and economic losses from cold spells in China. *Sci Total Environ.* (2022) 821:153478. doi: 10.1016/j.scitotenv.2022.153478

20. Zeng Q, Li GX, Cui YS, Jiang G, Pan X. Estimating temperature-mortality exposure-response relationships and optimum ambient temperature at the Multi-City level of China. *Int J Environ Res Public Health.* (2016) 13:279. doi: 10.3390/ijerph13030279

21. Voorhees AS, Fann N, Fulcher C, Dolwick P, Hubbell B, Bierwagen B, et al. Climate change-related temperature impacts on warm season heat mortality: a proof-of-concept methodology using BenMAP. *Environ Sci Technol.* (2011) 45:1450–7. doi: 10.1021/es102820y

22. Zhu QG, Lin JR, Shou SW, Tang DS. *Principles and methods of synoptic science (in Chinese).* Beijing: Meteorological Press. (2000). 282–293

23. Park TW, Ho CH, Jeong SJ, Choi YS, Park SK, Song CK. Different characteristics of cold day and cold surge fre-quency over East Asia in a global warming situation. *J Geophys Res-Atmos.* (2011) 116:116(D12). doi: 10.1029/2010JD015369

24. Xu RJ, Shi CX, Wei J, Lu WF, Li YX, Liu TT, et al. Cause-specific cardiovascular disease mortality attributable to ambient temperature: a time-stratified case-crossover study in Jiangsu province, China. *Ecotoxicol Environ Saf.* (2022) 236:113498. doi: 10.1016/j.ecoenv.2022.113498

25. Phung D, Thai PK, Guo YM, Morawska L, Rutherford S, Chu C. Ambient temperature and risk of cardiovascular hospitalization: an updated systematic review and meta-analysis. *Sci Total Environ.* (2016) 550:1084–102. doi: 10.1016/j.scitotenv.2016.01.154

26. Feng FL, Ma YX, Zhang YF, Shen JH, Wang H, Cheng BW, et al. Effects of extreme temperature on respiratory diseases in Lanzhou, a temperate climate city of China. *Environ Sci Pollut Res Int.* (2021) 28:49278–88. doi: 10.1007/s11356-021-14169-x

27. Ma YX, Zhou JD, Yang SX, Yu ZA, Wang F, Zhou J. Effects of extreme temperatures on hospital emergency room visits for respiratory diseases in Beijing, China. *Environ Sci Pollut Res Int.* (2019) 26:3055–64. doi: 10.1007/s11356-018-3855-4

28. Donaldson GC, Keatinge WR. Cold exposure and winter mortality from ischaemic heart disease, cerebrovascular disease, respiratory disease, and all causes in warm and cold regions of Europe. The Eurowinter Group. *Lancet.* (1997) 349:1341–6. doi: 10.1016/S0140-6736(96)12338-2

29. Boonarkart C, Suptawiwat O, Sakorn K, Puthavathana P, Auewarakul P. Exposure to cold impairs interferon-induced antiviral defense. *Arch Virol.* (2017) 162:2231–7. doi: 10.1007/s00705-017-3334-0

30. Chmura P, Konefał M, Andrzejewski M, Kosowski J, Rokita A, Chmura J. Physical activity profile of 2014 FIFA world cup players, with regard to different ranges of air temperature and relative humidity. *Int J Biometeorol.* (2017) 61:677–84. doi: 10.1007/s00484-016-1245-5

31. Liu Y, Guo Y, Wang CB, Li WD, Lu JH, Shen SY, et al. Association between temperature change and outpatient visits for respiratory tract infections among children in Guangzhou, China. *Int J Environ Res Public Health.* (2015) 12:439–54. doi: 10.3390/ijerph120100439

32. Kyobutungi C, Grau A, Stieglbauer G, Becher H. Absolute temperature changes and stroke risk: a case-crossover study. *Eur J Epidemiol.* (2005) 20:693–8. doi: 10.1007/s10654-005-0703-x

33. Hong YC, Rha JH, Lee JT, Ha EH, Kwon HJ, Kim H. Ischemic stroke associated with decrease in temperature. *Epidemiology*. (2003) 14:473–8. doi: 10.1097/01.ede.0000078420.82023.e3

34. Basu R, Ostro BD. A multicounty analysis identifying the populations vulnerable to mortality associated with high ambient temperature in California. *Am J Epidemiol*. (2008) 168:632–7. doi: 10.1093/aje/kwn170

35. Květoň V. Weather fronts and acute myocardial infarction. *Int J Biometeorol*. (1991) 35:10–7. doi: 10.1007/BF01040957

36. Culić V, Eterović D, Mirić D. Meta-analysis of possible external triggers of acute myocardial infarction. *Int J Cardiol*. (2005) 99:1–8. doi: 10.1016/j.ijcard.2004.01.008

37. Schneider A, Schuh A, Maetzel FK, Rückerl R, Breitner S, Peters A. Weather-induced ischemia and arrhythmia in patients undergoing cardiac rehabilitation: another difference between men and women. *Int J Biometeorol*. (2008) 52:535–47. doi: 10.1007/s00484-008-0144-9

38. Lim YH, Hong YC, Kim H. Effects of diurnal temperature range on cardiovascular and respiratory hospital admissions in Korea. *Sci Total Environ*. (2012) 417-418:55–60. doi: 10.1016/j.scitotenv.2011.12.048

39. Plavcová E. Kyselý J effects of sudden air pressure changes on hospital admissions for cardiovascular diseases in Prague, 1994-2009. *Int J Biometeorol*. (2014) 58:1327–37. doi: 10.1007/s00484-013-0735-y

40. Allen MJ, Sheridan SC. High-mortality days during the winter season: comparing meteorological conditions across 5 US cities. *Int J Biometeorol*. (2014) 58:217–25. doi: 10.1007/s00484-013-0640-4

41. Plavcová E, Urban A. Intensified impacts on mortality due to compound winter extremes in the Czech Republic. *Sci Total Environ*. (2020) 746:141033. doi: 10.1016/j.scitotenv.2020.141033

42. Plavcová E, Kyselý J. Effects of sudden air temperature and pressure changes on mortality in the Czech Republic. *Epidemiol Mikrobiol Imunol*. (2009) 58:73–83.

43. Morabito M, Crisci A, Orlandini S, Maracchi G, Gensini GF, Modesti PA. A synoptic approach to weather conditions discloses a relationship with ambulatory blood pressure in hypertensives. *Am J Hypertens*. (2008) 21:748–52. doi: 10.1038/ajh.2008.177

44. Allen MJ, Lee CC. Investigating high mortality during the cold season: mapping mean weather patterns of temperature and pressure. *Theor Appl Climatol*. (2014) 118:419–28. doi: 10.1007/s00704-013-1075-x

45. Paschalidou AK, Kassomenos PA, McGregor GR. Analysis of the synoptic winter mortality climatology in five regions of England: searching for evidence of weather signals. *Sci Total Environ*. (2017) 598:432–44. doi: 10.1016/j.scitotenv.2017.03.276

46. Curriero FC, Heiner KS, Samet JM, Zeger SL, Strug L, Patz JA. Temperature and mortality in 11 cities of the eastern United States. *Am J Epidemiol*. (2002) 155:80–7. doi: 10.1093/aje/155.1.80

47. Lin YK, Wang YC, Lin PL, Li MH, Ho TJ. Relationships between cold temperature indices and all causes and cardiopulmonary morbidity and mortality in a subtropical island. *Sci Total Environ*. (2013) 461-462:627–35. doi: 10.1016/j.scitotenv.2013.05.030

48. Conlon KC, Rajkovich NB, White-Newsome JL, Larsen L, O'Neill MS. Preventing cold-related morbidity and mortality in a changing climate. *Maturitas*. (2011) 69:197–202. doi: 10.1016/j.maturitas.2011.04.004

49. Xie HY, Yao ZB, Zhang YH, Xu YJ, Xu XJ, Liu T, et al. Short-term effects of the 2008 cold spell on mortality in three subtropical cities in Guangdong Province, China. *Environ Health Perspect*. (2013) 121:210–6. doi: 10.1289/ehp.1104541

50. Stewart S, Keates AK, Redfern A, McMurray JJV. Seasonal variations in cardiovascular disease. *Nat Rev Cardiol*. (2017) 14:654–64. doi: 10.1038/nrcardio.2017.76

51. Zhou MG, Wang LJ, Liu T, Zhang YH, Lin HL, Luo Y, et al. Health impact of the 2008 cold spell on mortality in subtropical China: the climate and health impact national assessment study (CHINAs). *Environ Health*. (2014) 13:60. doi: 10.1186/1476-069X-13-60

52. Guo YM, Gasparrini A, Armstrong B, Li SS, Tawatsupa B, Tobias A, et al. Global variation in the effects of ambi-ent temperature on mortality: a systematic evaluation. *Epidemiology*. (2014) 25:781–9. doi: 10.1097/EDE.0000000000000165

53. Lee W, Choi HM, Kim D, Honda Y, Guo YL, Kim H. Temporal changes in morality attributed to heat extremes for 57 cities in Northeast Asia. *Sci Total Environ*. (2018) 616-617:703–9. doi: 10.1016/j.scitotenv.2017.10.258

54. Allen MJ, Sheridan SC. Mortality risks during extreme temperature events (ETEs) using a distributed lag non-linear model. *Int J Biometeorol*. (2018) 62:57–67. doi: 10.1007/s00484-015-1117-4

55. Deng SZ, Han AZ, Jin SY, Wang S, Zheng J, Jalaludin BB, et al. Effect of extreme temperatures on asthma hospital visits: modification by event characteristics and healthy behaviors. *Environ Res*. (2023) 226:115679. doi: 10.1016/j.envres.2023.115679

56. Lei J, Chen RJ, Yin P, Meng X, Zhang LN, Liu C, et al. Association between cold spells and mortality risk and burden: a Nationwide study in China. *Environ Health Perspect*. (2022) 130:27006. doi: 10.1289/EHP9284

57. Lee W, Choi HM, Lee JY, Kim DH, Honda Y, Kim H. Temporal changes in mortality impacts of heat wave and cold spell in Korea and Japan. *Environ Int*. (2018) 116:136–46. doi: 10.1016/j.envint.2018.04.017

58. Tsangari H, Paschalidou A, Vardoulakis S, Heaviside C, Konsoula Z, Christou S, et al. Human mortality in Cyprus: the role of temperature and particulate air pollution. *Reg Environ Chang*. (2016) 16:1905–13. doi: 10.1007/s10113-015-0793-2

59. Ma C, Yang J, Nakayama SF, Iwai-Shimada M, Jung CR, Sun XL, et al. Cold spells and cause-specific mortality in 47 Japanese prefectures: a systematic evaluation. *Environ Health Perspect*. (2021) 129:67001. doi: 10.1289/EHP7109

60. Yang ZM, Wang Q, Liu PF. Extreme temperature and mortality: evidence from China. *Int J Biometeorol*. (2019) 63:29–50. doi: 10.1007/s00484-018-1635-y

61. Wang HJ, Sun JQ, Chen HP, Zhu YL, Zhang Y, Jiang DB, et al. extreme climate in China: facts, simulation and projection. *Meteorol Z*. (2012) 21:279–304. doi: 10.1127/0941-2948/2012/0330

62. Zimmer Z, Kaneda T, Spess L. An examination of urban versus rural mortality in China using community and individual data. *J Gerontol B Psychol Sci Soc Sci*. (2007) 62:S349–57. doi: 10.1093/geronb/62.5.s349

63. Zhou MG, Liu YN, Wang LJ, Kuang XY, Xu XH, Kan HD. Particulate air pollution and mortality in a cohort of Chinese men. *Environ Pollut*. (2014) 186:1–6. doi: 10.1016/j.envpol.2013.11.010

frontiers | Frontiers in Public Health

TYPE Brief Research Report
PUBLISHED 11 December 2023
DOI 10.3389/fpubh.2023.1287821

Check for updates

OPEN ACCESS

EDITED BY
Shupeng Zhu,
University of California, Irvine, United States

REVIEWED BY
Mengyi Li,
University of California, Irvine, United States
Shijian Liu,
Shanghai Children's Medical Center, China

*CORRESPONDENCE
Zhongjie Fan
✉ Fanzhongjie@pumch.cn
Xiaofeng Jin
✉ xhjxf@aliyun.com

†These authors have contributed equally to this work and share first authorship

RECEIVED 02 September 2023
ACCEPTED 17 November 2023
PUBLISHED 11 December 2023

CITATION
Tang S, Fu J, Liu Y, Zhao Y, Chen Y, Han Y, Zhao X, Liu Y, Jin X and Fan Z (2023) Temperature fluctuation and acute myocardial infarction in Beijing: an extended analysis of temperature ranges and differences. *Front. Public Health* 11:1287821. doi: 10.3389/fpubh.2023.1287821

Temperature fluctuation and acute myocardial infarction in Beijing: an extended analysis of temperature ranges and differences

Siqi Tang[1†], Jia Fu[2†], Yanbo Liu[3], Yakun Zhao[1], Yuxiong Chen[1], Yitao Han[1], Xinlong Zhao[1], Yijie Liu[1], Xiaofeng Jin[1]* and Zhongjie Fan[1]*

[1]Department of Cardiology, Peking Union Medical College Hospital, Peking Union Medical College and Chinese Academy of Medical Sciences, Beijing, China, [2]Department of Cardiology, Fuwai Yunnan Cardiovascular Hospital, Kunming, Yunnan, China, [3]Department of International Medical Services, Peking Union Medical College Hospital, Peking Union Medical College and Chinese Academy of Medical Sciences, Beijing, China

Purpose: Few studies examined the relationship between temperature fluctuation metrics and acute myocardial infarction (AMI) hospitalizations within a single cohort. We aimed to expand knowledge on two basic measures: temperature range and difference.

Methods: We conducted a time-series analysis on the correlations between temperature range (TR), daily mean temperature differences (DTDmean), and daily mean-maximum/minimum temperature differences (TDmax/min) and AMI hospitalizations, using data between 2013 and 2016 in Beijing, China. The effects of TR_n and $DTDmean_n$ over n-day intervals were compared, respectively. Subgroup analysis by age and sex was performed.

Results: A total of 81,029 AMI hospitalizations were included. TR_1, TDmax, and TDmin were associated with AMI in J-shaped patterns. $DTDmean_1$ was related to AMI in a U-shaped pattern. These correlations weakened for TR and DTDmean with longer exposure intervals. Extremely low (1st percentile) and high (5°C) $DTDmean_1$ generated cumulative relative risk (CRR) of 2.73 (95% CI: 1.56–4.79) and 2.15 (95% CI: 1.54–3.01). Extremely high TR_1, TDmax, and TDmin (99th percentile) correlated with CRR of 2.00 (95% CI: 1.73–2.85), 1.71 (95% CI: 1.40–2.09), and 2.73 (95% CI: 2.04–3.66), respectively. Those aged 20–64 had higher risks with large TR_1, TDmax, and TDmin, while older individuals were more affected by negative $DTDmean_1$. $DTDmean_1$ was associated with a higher AMI risk in females.

Conclusion: Temperature fluctuations were linked to increased AMI hospitalizations, with low-temperature extremes having a more pronounced effect. Females and the older adult were more susceptible to daily mean temperature variations, while younger individuals were more affected by larger temperature ranges.

KEYWORDS

acute myocardial infarction, temperature range, temperature difference, age, sex

1 Introduction

Acute myocardial infarction (AMI) continues to carry a substantial health burden worldwide (1). Ambient temperature has been established to mediate an elevated risk of AMI (2–4). However, long-term cold and heat exposure generates biological and behavioral acclimatization, thus modifying the influence of absolute temperature (5, 6). For example, early studies showed a more pronounced effect of lower temperatures during warmer years (4). Prior studies linked short-term cold exposure to increased inflammation and hyper-coagulation, predisposing individuals to AMI (7). Also, temperature fluctuations disrupt autonomic function by elevating blood pressure and heart rate (8), exaggerating the myocardial oxygen demand–supply imbalance in those with preexisting coronary lesions (9).

Recent data highlighted the adverse effect of temperature fluctuation using an array of metrics (10–16). Intra-day temperature range and day-to-day temperature difference are commonly studied metrics, capturing different aspects of temperature fluctuations. In prior studies, greater neighboring day temperature differences were linked to increased cardiovascular visits and hospitalizations (17). A larger diurnal temperature range contributed to increased coronary heart disease-related death (18) and out-of-hospital cardiac arrests (19). However, few studies examined the impacts of temperature range differences within a single cohort. Also, it remains unclear whether 1-day intervals are the optimal observation periods for assessing day-to-day temperature differences and temperature ranges.

In this time-series study, we used registry data for all AMI hospitalization in Beijing, China, a heavily populated city with a humid continental climate. We performed an extended analysis on two basic measures: temperature range and daily mean temperature difference, aiming to understand their effects on AMI hospitalization and explored the optimal observation intervals. Additionally, we sought to identify susceptible age and sex subgroups for different patterns of temperature fluctuation, thus informing targeted prevention strategies.

2 Materials and methods

2.1 Data collection

We collected all cases of hospital admission for AMI between January 1st, 2013 and December 31st, 2016 in Beijing. Data were obtained from the Beijing Municipal Health Commission Information Center. Anonymous demographic and residential information was collected, including the institute of admission, date of onset, gender, age, primary diagnosis, and comorbidities. Birthplace, current residential address, and workplace address were used to exclusively include patients who resided in Beijing. Patients aged between 20–74 years old were included in the analysis. AMI hospitalization was identified by the primary diagnostic code of I21–I22, according to the International Classification of Diseases 10th revision (ICD-10). The study was approved by the Peking Union Medical College Hospital (PUMCH) Institutional Review Board.

City-level meteorological data, including daily mean temperature (Tmean), maximum temperature (Tmax), minimum temperature (Tmin), air pressure, relative humidity (RH), and wind speed (WS) were recorded by the China Meteorological Administration (CMA). The data were collected by a stationary monitoring station located near the city center (Station code: 54511). Air pollutant data were included as confounding factors, which were collected from 35 monitoring stations across Beijing. This included the hourly concentration of both the particulate ($PM_{2.5}$, PM_{10}) and gaseous air pollutants (SO_2, NO_2, O_3, CO). To address daily variations in a set of pollutants, we calculated the Air Quality Index (AQI) which combines the effects of six common air pollutants for the same period. Influenza was independently associated with an increased risk of AMI in the previous study (20). We collected data on influenza epidemic (IF), which was defined as when the positive rate of influenza isolation in any given week exceeded 20% of the maximum weekly positive rate of influenza isolation in the whole surveillance season (from the 27th week of the previous year to the 26th week of the following year) in northern China (13, 14). The influenza surveillance data were obtained from the Chinese National Influenza Center.[1]

2.2 Temperature variables

We estimated the influence of temperature range (TR_n) and daily mean temperature difference ($DTDmean_n$) on the count of AMI hospital admissions. TR_n represents the difference between maximal temperature and minimum temperature over an n-day period, ie. Tmax minus Tmin over n days. $DTDmean_n$ was derived from the mean temperature difference between the current day and n day prior. To further understand the intra-day cold and heat effects, we investigated intra-day cold and heat effects using daily maximum/ minimum and mean temperature difference (TDmax/TDmin) which represented the same-day Tmax/ Tmin minus mean temperature.

2.3 Statistical analysis

Distributed Lag Non-linear Model was established to fit the nonlinear effect and lag effect of independent variables (12–14). Long-term and seasonal trends were controlled using a natural cubic spline with 7 degrees of freedom (df) for the time. We defined the seasons based on astronomical seasons, which were spring (March 20th to March 21st), summer (June 20th to June 21st), autumn (September 22nd to September 23rd), and winter (December 20th to December 21st). Wind speed, air pressure, relative humidity, and Air Quality Index were adjusted using a natural cubic spline with 3 df. Public holiday (PH) and day of the week (DOW) were adjusted for their impacts on the behavioral patterns. The full model was as below:

$$\log\left[E\left(Y_t\right)\right] = \alpha + cb\left(Temp_t, lag, df = 4\right) + ns\left(Time, df = 7\ per\ year\right) + ns\left(WS, df = 3\right) + ns\left(AP, df = 3\right) + ns\left(RH, df = 3\right) + ns\left(AQI, df = 3\right) + \beta_1 * DOW + \beta_2 * IF + \beta_3 * PH$$

E (Yt) denotes the number of AMI hospital admissions on day *t*. *α* and *β* were the model intercept and regression coefficient, respectively. *cb* represents the cross-basis function and ns indicates the natural cubic spline function. *Tmp* refers to different temperature variables. *Time* refers to the time to control the season and long-term trends. *df* represents the degree of freedom.

1 https://ivdc.chinacdc.cn/cnic/zyzx/lgzb

3D maps depicted the overall relationship between temperature variables and AMI relative risks (RR) over 21 lag days (lag). We plotted the lag-response curves of temperature variables at 1^{st}, 5^{th}, 95^{th}, and 99^{th}, respectively. Twenty-one-day cumulative relative risk (CRR), the sum of the relative risk of each lag day within 21 days, was calculated to assess the overall effects of temperature variables and control the possible harvesting effect. The most moderate temperature difference (MMTD) was defined as the optimal temperature difference that carries the lowest risk of AMI, which served as the reference when evaluating relative risks. We performed stratification analysis by gender and age (<65 vs. ≥65 years old) and tested the reliability of the results. Statistical analyses were conducted in R software (R x64 v3.4.2) using "mgcv" and "dlnm" packages. A two-sided p value of 0.05 was considered statistically significant.

3 Results

3.1 Descriptive analysis

Between 2013 and 2016, we identified a total of 81,029 hospitalizations for AMI, with 55,669 (68.7%) being male and 36,989 (45.6%) under the age of 65. We observed a trend of increase in hospital admissions for AMI. Supplementary Table S1 shows the descriptive statistics of the study population and meteorological data in Beijing, China.

The maximum, mean, and minimum daily temperatures were 19.01°C, 12.94°C, and 7.19°C, respectively. The mean Air Quality Index, relative humidity, wind speed, and air pressure were 123.65 ± 75.17, 53.43 ± 19.86, 9.29 ± 4.75 m/s, 53.43 ± 19.86%, and 1016.555 ± 10.17 hPa, respectively. Summary statistics for meteorological and air pollution are summarized in Supplementary Table S2.

3.2 Cumulated relative risk

Compared to $DTDmean_1$, longer exposure intervals ($DTDmean_{2\text{-}4}$) attenuated the association between DTDmean and AMI hospitalization (Figure 1). Notably, $DTDmean_4$ did not increase the risk of AMI hospitalization. The exposure-response association between $DTDmean_1$ and AMI hospitalization was U-shaped. The AMI hospitalization risk reached a nadir at 1.4°C, namely MMTD for $DTDmean_1$, and marked increases in risk were observed at both low and high $DTDmean_1$. On days with $DTDmean_1$ values at the 1st percentile (−6°C) and 99^{th} percentile (5°C), the CRR reached 2.73 (95% confidence interval, CI: 1.56–4.79) and 2.15 (95% CI: 1.54–3.01), respectively (Supplementary Table S3).

The association between TR and AMI hospitalization weakened with longer exposure intervals when comparing $TR_{1\text{-}5}$ (Figure 2). No significant relationship was observed between TR_5 and the risk of AMI hospitalization. The association between TR_1 and the risk of AMI hospitalization exhibited a J-shaped pattern, where the risk increased when TR_1 exceeded 16.9°C. TR_1 at the 95th (19°C) and 99th percentile (22°C) were associated with CRRs of 1.12 (95% CI: 1.04–1.20) and 2.0 (95% CI: 1.73–2.85), respectively (Supplementary Table S4).

The overall patterns of TDmax/TDmin-AMI hospitalization association were similar to TR_1 with varying magnitude of association (Figure 3). The positive associations were observed when TDmin and TDmax exceeded 8.1°C and 8.6°C, respectively. For TDmax at the 95^{th} percentile (10°C) and 99^{th} percentile (11°C), the CRRs were 1.18 (95% CI: 1.09–1.29) and 1.71 (95% CI: 1.40–2.09), respectively (Supplementary Table S5). For TDmin at the 95th percentile (9°C) and 99^{th} percentile (11°C), the corresponding CRRs were 1.07 (95% CI: 1.00–1.15) and 2.73 (95% CI: 2.04–3.66), respectively (Supplementary Table S6).

3.3 Single-day Lag effects

Negative (temperature decline) and positive (temperature rise) $DTDmean_1$ showed different patterns of lag effects (Supplementary Figure S1). The RR of $DTDmean_1$ at −6°C (1st percentile) and −4°C (5th percentile) peaked on lag day 10 and yielded a lag effect throughout lag day 3 to 18 and lag day 3 to 21, respectively. For positive $DTDmean_1$, we observed delayed peak lag effects. The effect of $DTDmean_1$ at 5°C (99^{th} percentile) and 4°C (95^{th} percentile) both extended from lag day 1 to 21, with the RR peaked on lag day 21.

Similar lag patterns were observed among TR_1, TDmax, and TDmin at the 99^{th} percentile, which lasted for 20 days and peaked on lag day 2–3 (Supplementary Figure S2). No significant associations were found for TR_1 and TDmax at the 95th percentile. For TDmin at the 95th percentile (9°C), the lag effect was only significant on lag day 0 and 1, reaching the peak RR on lag day 0.

Supplementary Figure S3 shows the 3D mapping of the association between relative risk AMI hospitalization and $DTDmean_1$, TR_1, TDmax, and TDmin over the 21-day lag period.

3.4 Age- and sex-specific effect

Compared to their younger counterparts, individuals aged over 65 years were at higher risk of AMI hospitalization on days with negative $DTDmean_1$ (−6°C) [3.04 (95% CI: 1.48–6.22) vs. 2.40 (95% CI: 1.17–4.92)]. Negative DTD $mean_1$ was more strongly associated with the AMI hospitalization risk in females than males [3.40 (95% CI: 1.42–8.12) vs. 2.46 (95% CI: 1.29–4.67)] (Supplementary Figure S4). Comparable CRRs were observed among age and sex subgroups with positive $DTDmean_1$ (Supplementary Table S3).

In contrast, the associations between TR_1, TDmax, and TDmin were attenuated at older ages. For TR_1 at the 99^{th} (22°C) percentile, the CRR was 2.69 (95% CI: 1.07–3.68) for the younger group and 1.90 (95% CI: 1.38–2.60) for the older group. TDmax at the 99^{th} percentile (11°C) corresponded to a CRR of 2.01 (95% CI: 1.56–2.59) for the younger group and 1.49 (95% CI: 1.15–1.92) for the older group. Specifically, TDmin yielded a CRR of 3.36 (95% CI: 2.32–4.87) for the younger group and 2.29 (95% CI: 1.58–3.33) for the older group at the 99^{th} percentile (11°C) (Figure 4). Slightly increased risks were noted for females with greater TR_1, TDmax, and TDmin (Supplementary Figure S5 and Supplementary Tables S4–S6).

4 Discussion

In this study, we conducted a comprehensive analysis of the impacts of temperature range and differences on AMI hospitalization in Beijing, China. Increased temperature range and day-to-day temperature difference were both associated with higher AMI risk with the optimal 1-day observation interval. Specifically, the older adult population was

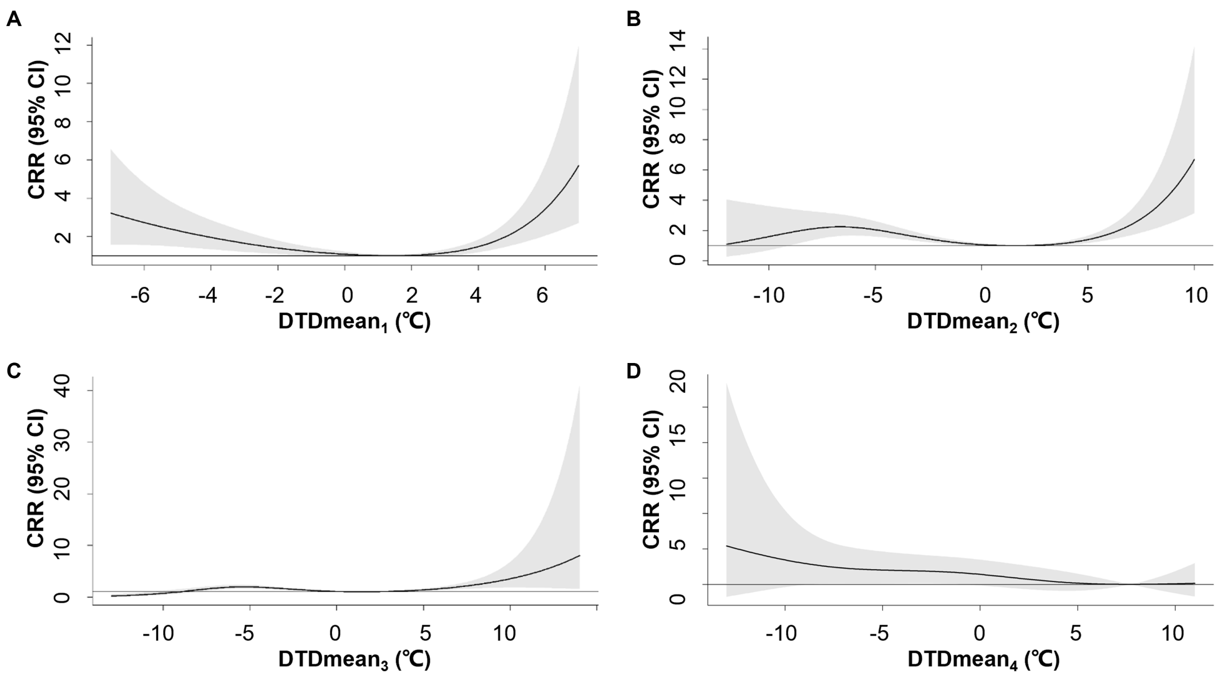

FIGURE 1
Overall exposure-response associations between neighboring-day mean temperature difference (DTDmean) over 1–4 days **(A–D)** and cumulative relative risks (CRR) for AMI hospitalization. Shaded areas represent 95% CI.

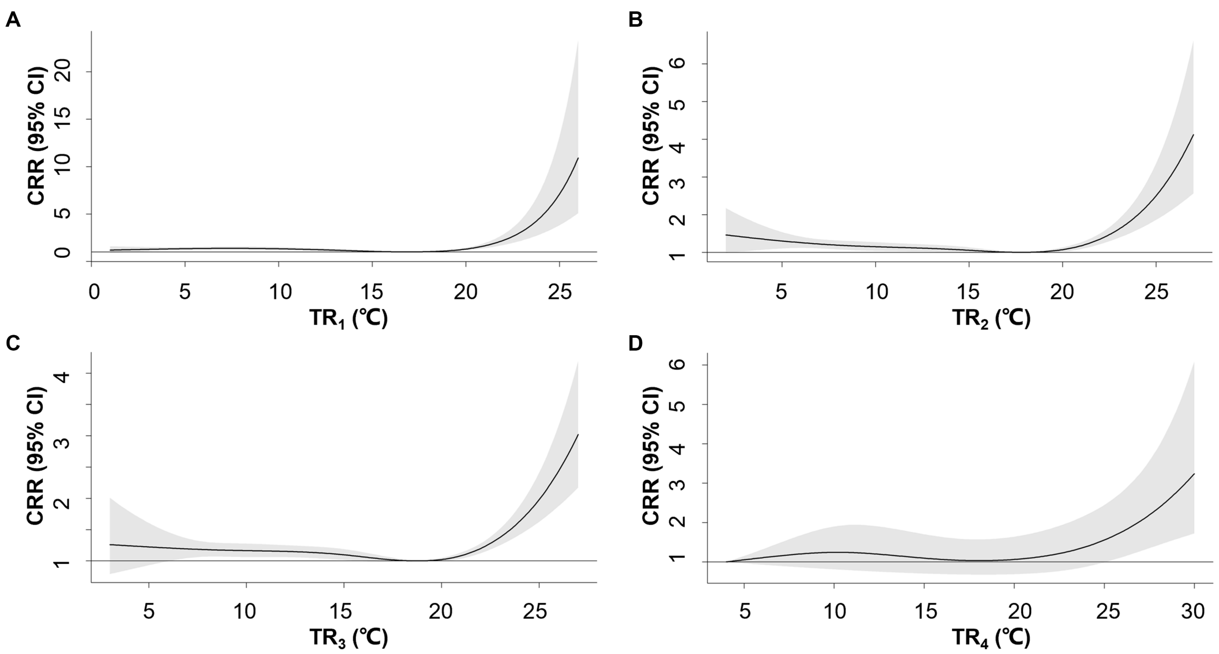

FIGURE 2
Overall exposure-response associations between temperature range (TR) over 1–4 days **(A–D)** and cumulative relative risks (CRR) for AMI hospitalization. Shaded areas represent 95% CI.

more susceptible to day-to-day temperature differences, while the younger population was subject to larger temperature ranges, represented by TR1, TDmin, and TDmax. Females were more affected by neighboring-day temperature declines.

Previous studies have linked neighboring-day temperature differences to coronary heart disease. In a study conducted in Brisbane and Los Angeles, a temperature drop and increase of more than 3°C between neighboring days were associated with a relative risk of 1.252 (95%CI: 1.131–1.386) and 1.35 (95% CI: 1.033, 1.772) for cardiovascular deaths during summer (21). Similarly, Shi et al. demonstrated a V-shaped relationship between neighboring day temperature differences and

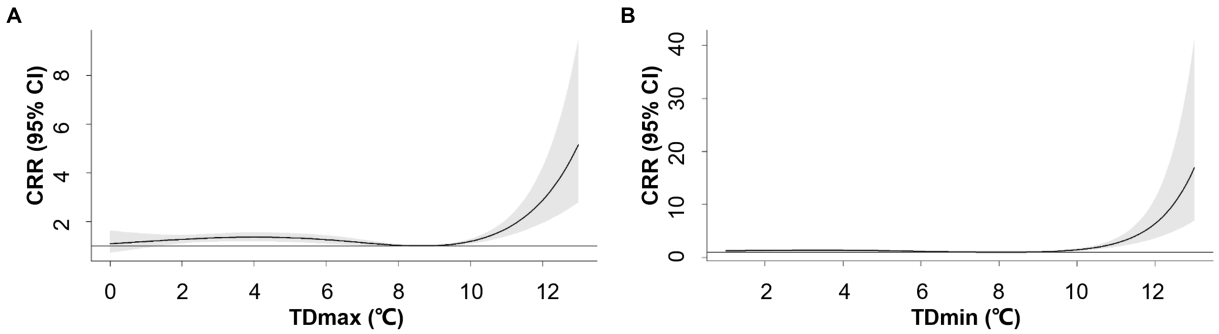

FIGURE 3
Overall exposure-response associations between maximum-mean temperature difference (TDmax, **A**), mean-minimum temperature difference (TDmin, **B**) and cumulative relative risks (CRR) for AMI hospitalization. Shaded areas represent 95% CI.

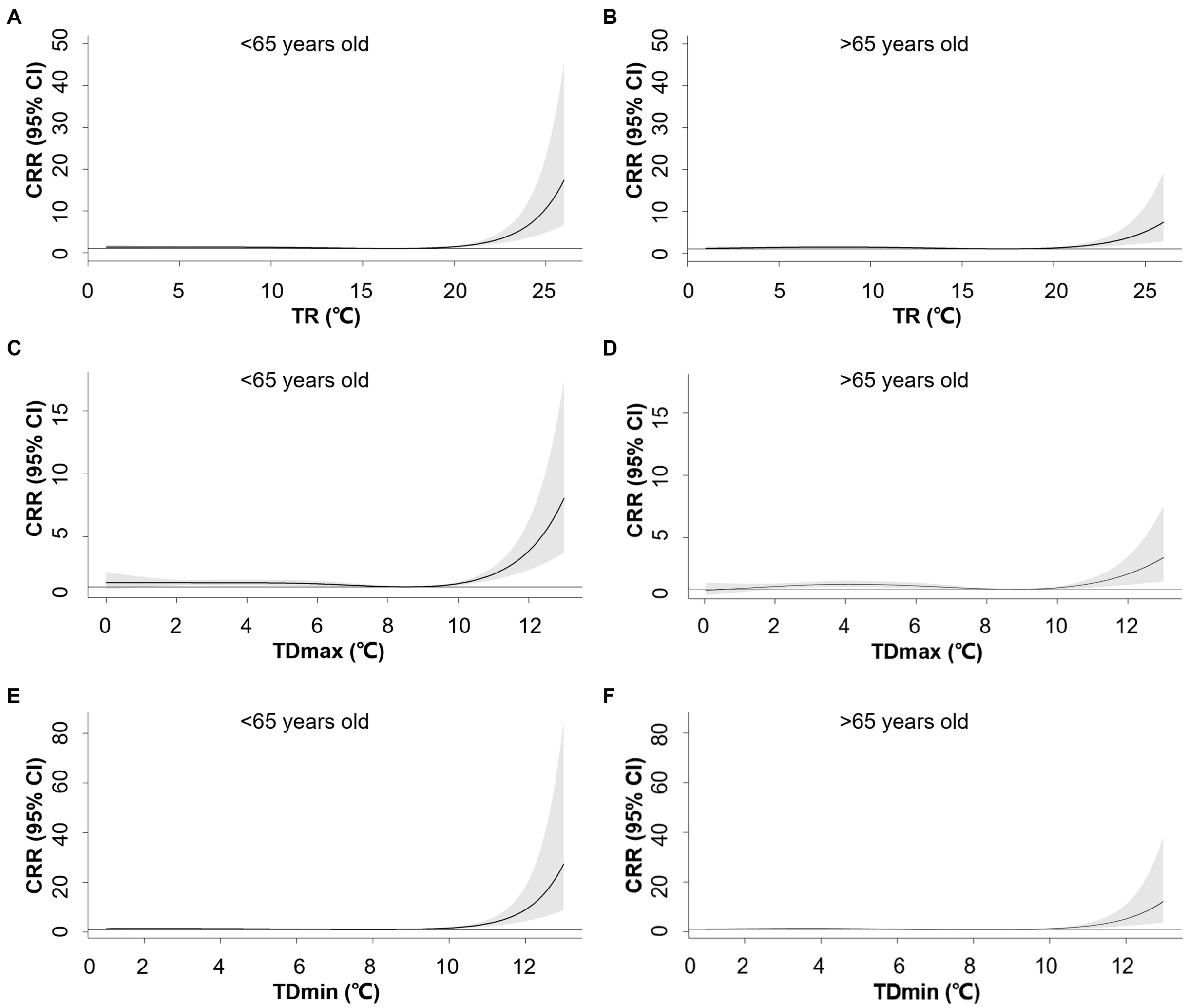

FIGURE 4
Exposure-response associations between 1-day temperature range (TR_1, **A,B**), maximum-mean temperature difference (TDmax, **C,D**), mean-minimum temperature difference (TDmin, **E,F**) and cumulative relative risks (CRR) for AMI hospitalization stratified by age. Shaded areas represent 95% CI.

cardiovascular visits and hospitalizations in northwest China (17). These findings suggest that day-to-day temperature change, regardless of the direction of the change, contributes to increased cardiovascular risks.

The diurnal temperature range (DTR), in our setting, TR_1, was also related to increased AMI risks. A study in Shanghai, China showed that a 1°C increment in the DTR yielded a 2.46% increase in coronary heart disease-related death (18). In a New York-state-based study, DTR was positively associated with AMI risk (10). In a Japanese study between 2005 and 2013, DTR was related to increased risks of out-of-hospital cardiac arrests, but less significant when compared to mean temperature (19). However, Lim et al. found an adverse effect between DTR and cardiovascular admissions, but no effect on AMI in Korea between 2003 and 2006 (22). In addition, we examined the influence of cold and heat effects by incorporating TDmin and TDmax. We found that TDmin had a more substantial impact on AMI risks, indicating a stronger association with cold temperature extremes.

Few studies examined the impacts of observation intervals, primarily focusing on 1 to 2 days of variability. A Brazilian study between 2000 and 2015 observed the most significant effect of temperature variability (measured as the standard deviation of daily minimum and maximum temperatures) on ischemic heart disease risk during 0–1 day, with the effect diminishing over 0–4 days (23). Despite the strongest estimates for 1-day exposure, we also identified a minor yet statistically significant effect of temperature fluctuation over 2 to 3 days. These results are consistent with the findings of Pearce et al., who showed that temperature trajectories in preceding days modified the associations between daily temperature and mortality in Melbourne, Australia (24).

The effect of temperature fluctuations on the risk of AMI hospitalization varied by age. In line with the previous studies, the older adult population, characterized by diminished thermoregulatory capacity, displayed greater susceptibility to day-to-day temperature variations (10, 22). Contrary to prior findings, we observed that younger participants were more prone to significant intra-day temperature ranges. In addition, low-temperature extremes, represented by TDmin may contribute to a more pronounced influence on AMI. This discrepancy might be attributed to the lower age cut-off compared to the previous studies (75 years) (22, 25), which consisted mainly of the working population. We hypothesized that daily commutes led to greater temperature fluctuation exposure, resulting in a higher risk of AMI in the younger population. Additional behavioral studies are needed to investigate these discrepancies.

Existing data demonstrated inconsistent modification effects by sex. In the WHO MONICA project between 1980 and 1995, females living in warm climates exhibited higher coronary event rates during cold periods (2). However, no gender differences in the seasonality of AMI hospitalization in the Taiwan study between 1997 and 2011 (26). An hour-to-hour study in Queensland, Australia, showed that elevated risks occurred more acutely in males following extreme cold exposure (9 h in males vs. 19 h in females) (27). Physiological studies suggest that females had weaker sweating responses, greater heat loss due to a larger surface area, and periodic thermoregulation due to menstrual cycles (28, 29). However, geographic differences may account for the divergence across the study, involving biological and habitual adaptations. For example, in the Brazilian study, males engaged in more outdoor activities, possibly making them more susceptible to ambient temperature (23).

Our study focused on observations in Beijing, a densely populated temperate city. We investigated the effects of DTDmean and TR over 1–5 days' exposure and their differential effects on age and sex. However, our study has several limitations. Firstly, as a single-city study, the findings may not apply to regions with different climate types. Secondly, the data might not represent individual-level exposure, as indoor temperature exposure was not analyzed. Lastly, using data from city-wide monitoring stations introduces potential measurement errors that cannot be fully eliminated.

5 Conclusion

Temperature fluctuations were linked to increased AMI hospitalizations, with low-temperature extremes having a more pronounced effect. Females and the older adult were more susceptible to daily mean temperature variations, while younger individuals were more affected by larger temperature ranges.

Data availability statement

The original contributions presented in the study are included in the article/Supplementary material, further inquiries can be directed to the corresponding authors.

Ethics statement

The studies involving humans were approved by Peking Union Medical College Hospital (PUMCH) Institutional Review Board. The studies were conducted in accordance with the local legislation and institutional requirements. Written informed consent for participation was not required from the participants or the participants' legal guardians/next of kin in accordance with the national legislation and institutional requirements.

Author contributions

ST: Formal analysis, Writing – original draft, Writing – review & editing. JF: Conceptualization, Data curation, Formal analysis, Writing – original draft. YL: Formal analysis, Writing – review & editing. YZ: Data curation, Writing – review & editing. YC: Methodology, Writing – original draft. YH: Software, Writing – original draft. XZ: Project administration, Writing – review & editing. YL: Software, Writing – original draft. XJ: Investigation, Project administration, Supervision, Validation, Visualization, Writing – review & editing. ZF: Funding acquisition, Project administration, Supervision, Validation, Writing – review & editing.

Funding

The author(s) declare financial support was received for the research, authorship, and/or publication of this article. This work was funded by National High Level Hospital Clinical Research Funding (2022-PUMCH-C-024, 2022-PUMCH-B-030, 2022-PUMCH-A-241), National Natural Science Foundation (12126602 and 91643208) , Chinese Academy of Medical Sciences Initiative for Innovative Medicine (2017-I2M-2-001), Yunnan Provincial Clinical Research Center for Cardiovascular Diseases (202302AA310045), and Fuwai Yunnan Cardiovascular Hospital for Cardiovascular Diseases (2019YFKT-09).

Acknowledgments

We sincerely thank Beijing Municipal Health Commission Information Center, Chinese National Influenza Center, and China Meteorological Administration for data collection.

Conflict of interest

The authors declare that the research was conducted in the absence of any commercial or financial relationships that could be construed as a potential conflict of interest.

Publisher's note

All claims expressed in this article are solely those of the authors and do not necessarily represent those of their affiliated organizations, or those of the publisher, the editors and the reviewers. Any product that may be evaluated in this article, or claim that may be made by its manufacturer, is not guaranteed or endorsed by the publisher.

Supplementary material

The Supplementary material for this article can be found online at: https://www.frontiersin.org/articles/10.3389/fpubh.2023.1287821/full#supplementary-material

References

1. Mensah GA, Roth GA, Fuster V. The global burden of cardiovascular diseases and risk factors: 2020 and beyond. *J Am Coll Cardiol*. (2019) 74:1558–3597. doi: 10.1016/j.jacc.2019.10.009

2. Barnett AG, Dobson AJ, McElduff P, Salomaa V, Kuulasmaa K, Sans S, et al. Cold periods and coronary events: an analysis of populations worldwide. *J Epidemiol Community Health*. (2005) 59:551–7. doi: 10.1136/jech.2004.028514

3. Gerber Y, Jacobsen SJ, Killian JM, Weston SA, Roger VL. Seasonality and daily weather conditions in relation to myocardial infarction and sudden cardiac death in Olmsted County, Minnesota, 1979 to 2002. *J Am Coll Cardiol*. (2006) 48:287–92. doi: 10.1016/j.jacc.2006.02.065

4. Wolf K, Schneider A, Breitner S, von Klot S, Meisinger C, Cyrys J, et al. Air temperature and the occurrence of myocardial infarction in Augsburg, Germany. *Circulation*. (2009) 120:735–42. doi: 10.1161/CIRCULATIONAHA.108.815860

5. Yurkevicius BR, Alba BK, Seeley AD, Castellani JW. Human cold habituation: physiology, timeline, and modifiers. *Temperature (Austin)*. (2022) 9:122–57. doi: 10.1080/23328940.2021.1903145

6. Young AJ, Castellani JW, O'Brien C, Shippee RL, Tikuisis P, Meyer LG, et al. Exertional fatigue, sleep loss, and negative energy balance increase susceptibility to hypothermia. *J Appl Physiol*. (1998) 85:1210–7. doi: 10.1152/jappl.1998.85.4.1210

7. Mercer JB, Østerud B, Tveita T. The effect of short-term cold exposure on risk factors for cardiovascular disease. *Thromb Res*. (1999) 95:93–104. doi: 10.1016/S0049-3848(99)00028-6

8. Tang M, He Y, Zhang X, Li H, Huang C, Wang C, et al. The acute effects of temperature variability on heart rate variability: a repeated-measure study. *Environ Res*. (2021) 194:110655. doi: 10.1016/j.envres.2020.110655

9. Hattenhaur M, Neill WA. The effect of cold air inhalation on again pectoris and myocardial oxygen supply. *Circulation*. (1975) 51:1053–8. doi: 10.1161/01.CIR.51.6.1053

10. Rowland ST, Parks RM, Boehme AK, Goldsmith J, Rush J, Just AC, et al. The association between ambient temperature variability and myocardial infarction in a New York-state-based case-crossover study: an examination of different variability metrics. *Environ Res*. (2021) 197:111207. doi: 10.1016/j.envres.2021.111207

11. Marti-Soler H, Gonseth S, Gubelmann C, Stringhini S, Bovet P, Chen PC, et al. Seasonal variation of overall and cardiovascular mortality: a study in 19 countries from different geographic locations. *PLoS One*. (2014) 9:e113500. doi: 10.1371/journal.pone.0113500

12. Zhang Y, Xiang Q, Yu C, Bao J, Ho HC, Sun S, et al. Mortality risk and burden associated with temperature variability in China, United Kingdom and United States: comparative analysis of daily and hourly exposure metrics. *Environ Res*. (2019) 179:108771. doi: 10.1016/j.envres.2019.108771

13. Chen J, Gao Y, Jiang Y, Li H, Lv M, Duan W, et al. Low ambient temperature and temperature drop between neighbouring days and acute aortic dissection: a case-crossover study. *Eur Heart J*. (2022) 43:228–35. doi: 10.1093/eurheartj/ehab803

14. Zhan Z, Zhao Y, Pang S, Zhong X, Wu C, Ding Z. Temperature change between neighboring days and mortality in United States: a nationwide study. *Sci Total Environ*. (2017) 584-585:1152–61:1152-61. doi: 10.1016/j.scitotenv.2017.01.177

15. Burkart KG, Brauer M, Aravkin AY, Godwin WW, Hay SI, He J, et al. Estimating the cause-specific relative risks of non-optimal temperature on daily mortality: a two-part modelling approach applied to the global burden of disease study. *Lancet*. (2021) 398:685–97. doi: 10.1016/S0140-6736(21)01700-1

16. Yu X, Xia L, Xiao J, Zheng J, Xu N, Feng X, et al. Association of Daily Mean Temperature and Temperature Variability with Onset Risks of acute aortic dissection. *J Am Heart Assoc*. (2021) 10:e020190. doi: 10.1161/JAHA.120.020190

17. Shi Q, Wei X, Liu Y, Meng X, Zhu W, Wang M, et al. An effect of 24-hour temperature change on outpatient and emergency and inpatient visits for cardiovascular diseases in Northwest China. *Environ Sci Pollut Res Int*. (2021) 28:45793–804. doi: 10.1007/s11356-021-13961-z

18. Cao J, Cheng Y, Zhao N, Song W, Jiang C, Chen R, et al. Diurnal temperature range is a risk factor for coronary heart disease death. *J Epidemiol*. (2009) 19:328–32. doi: 10.2188/jea.JE20080074

19. Onozuka D, Hagihara A. Associations of day-to-day temperature change and diurnal temperature range with out-of-hospital cardiac arrest. *Eur J Prev Cardiol*. (2017) 24:204–12. doi: 10.1177/2047487316674818

20. Garcia-Lledo A, Rodriguez-Martin S, Tobias A, Garcia-de-Santiago E, Ordobas-Gavin M, Ansede-Cascudo JC, et al. Relationship between influenza, temperature, and type 1 myocardial infarction: an ecological time-series study. *J Am Heart Assoc*. (2021) 10:e019608. doi: 10.1161/JAHA.120.019608

21. Guo Y, Barnett AG, Yu W, Pan X, Ye X, Huang C, et al. A large change in temperature between Neighbouring days increases the risk of mortality. *PLoS One*. (2011) 6:e16511. doi: 10.1371/journal.pone.0016511

22. Lim YH, Hong YC, Kim H. Effects of diurnal temperature range on cardiovascular and respiratory hospital admissions in Korea. *Sci Total Environ*. (2012) 417-418:55–60:55-60. doi: 10.1016/j.scitotenv.2011.12.048

23. Zhao Q, Li S, Coelho M, Saldiva PHN, Hu K, Huxley RR, et al. Temperature variability and hospitalization for ischaemic heart disease in Brazil: a nationwide case-crossover study during 2000-2015. *Sci Total Environ*. (2019) 664:707–12. doi: 10.1016/j.scitotenv.2019.02.066

24. Pearce JL, Hyer M, Hyndman RJ, Loughnan M, Dennekamp M, Nicholls N. Exploring the influence of short-term temperature patterns on temperature-related mortality: a case-study of Melbourne, Australia. *Environmental health: a global access science source*. (2016) 15:107. doi: 10.1186/s12940-016-0193-1

25. Zheng S, Wang M, Li B, Wang S, He S, Yin L, et al. Gender, age and season as modifiers of the effects of diurnal temperature range on emergency room admissions for cause-specific cardiovascular disease among the elderly in Beijing. *Int J Environ Res Public Health*. (2016) 13:447. doi: 10.3390/ijerph13050447

26. Chu ML, Shih CY, Hsieh TC, Chen HL, Lee CW, Hsieh JC. Acute myocardial infarction hospitalizations between cold and hot seasons in an island across tropical and subtropical climate zones-a population-based study. *Int J Environ Res Public Health*. (2019) 16:2769. doi: 10.3390/ijerph16152769

27. Cheng J, Su H, Xu Z, Tong S. Extreme temperature exposure and acute myocardial infarction: elevated risk within hours? *Environ Res*. (2021) 202:111691. doi: 10.1016/j.envres.2021.111691

28. Castellani JW, Young AJ. Human physiological responses to cold exposure: acute responses and acclimatization to prolonged exposure. *Auton Neurosci*. (2016) 196:63–74. doi: 10.1016/j.autneu.2016.02.009

29. Kaciuba-Uscilko H, Grucza R. Gender differences in thermoregulation. *Curr Opin Clin Nutr Metab Care*. (2001) 4:533–6. doi: 10.1097/00075197-200111000-00012

frontiers | Frontiers in Public Health

TYPE Mini Review
PUBLISHED 15 December 2023
DOI 10.3389/fpubh.2023.1335499

OPEN ACCESS

EDITED BY
Zhaobin Sun,
Chinese Academy of Meteorological Sciences, China

REVIEWED BY
文玺 阮,
Chinese Academy of Meteorological Sciences, China
Hanbin Zhang,
China Meteorological Administration, China

*CORRESPONDENCE
Lianglyu Chen
✉ chenllv214@163.com

RECEIVED 09 November 2023
ACCEPTED 04 December 2023
PUBLISHED 15 December 2023

CITATION
Chen L (2023) Application progress of ensemble forecast technology in influenza forecast based on infectious disease model. *Front. Public Health* 11:1335499.
doi: 10.3389/fpubh.2023.1335499

Application progress of ensemble forecast technology in influenza forecast based on infectious disease model

Lianglyu Chen*

Chongqing Institute of Meteorological Sciences, Chongqing, China

To comprehensively understand the application progress of ensemble forecast technology in influenza forecast based on infectious disease model, so as to provide scientific references for further research. In this study, two keywords of "influenza" and "ensemble forecast" are selected to search and select the relevant literatures, which are then outlined and summarized. It is found that: In recent years, some studies about ensemble forecast technology for influenza have been reported in the literature, and some well-performed influenza ensemble forecast systems have already been operationally implemented and provide references for scientific prevention and control. In general, ensemble forecast can well represent various uncertainties in forecasting influenza cases based on infectious disease models, and can achieve more accurate forecasts and more valuable information than single deterministic forecast. However, there are still some shortcomings in the current studies, it is suggested that scientists engaged in influenza forecast based on infectious disease models strengthen cooperation with scholars in the field of numerical weather forecast, which is expected to further improve the skills and application level of ensemble forecast for influenza.

KEYWORDS

influenza, ensemble forecast, infectious disease, numerical weather forecast, respiratory disease

1 Introduction

Influenza is a respiratory disease caused by influenza virus infection, it's highly contagious and its outbreaks have the characteristics of seasonal circulation. According to statistics, worldwide, influenza epidemics cause about 3–5 million severe cases of lower respiratory tract infection and 250,000–690,000 deaths every year (1), which poses a great threat to human public health. During the influenza epidemics, a large number of patients not only cause a serious burden on the medical resources, but also cause huge social and economic burdens.

Accurately forecasting the occurrence and development of influenza has important scientific significance for governments to formulate specific vaccination and non-drug interventions, prepare adequate medical resources in advance, and evaluate the effect of policies. Forecasting influenza cases based on infectious disease model is an important method for scientific prevention and control. Taking the widely used susceptible–infectious–recovered–susceptible (SIRS) model as an example (2), infectious disease model is usually composed of ordinary differential equations that characterize the dynamic mechanism of infectious disease transmission, and contains some sensitive parameters, such as infection rate (i.e., the probability of a patient to infect others), the probability of conversion from a latent period person to an infected person, the recovery rate of infected persons, the mortality rate and the coefficient of government interventions. After setting the relevant sensitivity parameters and the initial values of the differential equations (such as the number of cases at present, etc.) in advance, the number of influenza cases in the future can be achieved by numerical integration of the differential equations.

After decades of continuous development, the infectious disease models have shown good potentials for application. However, the initial values in infectious disease models still inevitably have certain errors, and the relevant sensitivity parameters in the models are all set according to users' experiences. Due to the high nonlinearity of infectious disease models, the error of the initial values and the relevant sensitive parameters will be amplified with the extension of forecast lead time and eventually lead to large biases of the forecast results, which limits the accuracy of the model forecast results to a certain extent. Therefore, it is worthy to quantitatively reflect the uncertainty of the initial values and sensitive parameters in infectious disease models, thus to solve the uncertainty problems in the single deterministic forecast result and improve the accuracy and application level of the infectious disease model forecasts. In view of this, learning from and applying the ensemble forecast technology developed in the field of numerical weather forecast is expected to effectively solve the above problems.

In recent years, it is noticed that the ensemble forecast technology has been applied in forecasting influenza cases based on infectious disease models, this paper will review the literature. Two keywords of "influenza" and "ensemble forecast" are selected to search and select the relevant literatures, which are then outlined and summarized. In addition, some suggestions are put forward, according to the author's experiences in research and application of ensemble forecast technology for several years.

2 Introduction of ensemble forecast technology

Ensemble forecast technology is developed in the field of numerical weather forecast. The essence of numerical weather forecast is to calculate the forecast value in the future by repeatedly integrating the differential equations representing the atmospheric motion started from the initial values, which is consistent with the essence of forecasting influenza cases based on infectious disease models. Due to the chaotic characteristics of the atmosphere, any small error in the initial values may quickly diverge the outcomes after a period of integration, and sometimes may even result in completely opposite results. In order to solve the above problems, the concept of ensemble forecast was put forward in the 1970s (3): Based on a certain mathematical method, a set of initial values with certain probability density function (PDF) distribution characteristics are firstly generated (as shown in Figure 1), each initial value may represent the real condition of the atmosphere. After this, ensemble forecast results can be achieved by numerical integration of each initial value (usually combined with different physical process parameterization schemes, planetary boundary layer conditions or even based on different models), thus to inferring

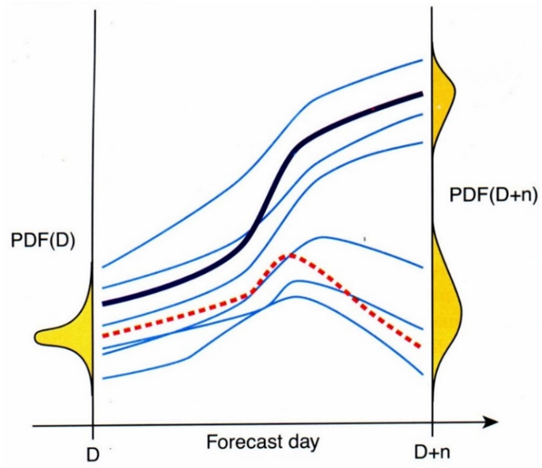

FIGURE 1
The schematic diagram of ensemble forecast (Black line: deterministic forecast; Blue line: ensemble members' forecasts; Red dotted line: observation).

the evolution of the PDF of atmospheric states over different forecast lead time.

Ensemble forecast is no longer single deterministic forecast, but a group of forecasts, each of which can be called an ensemble member, and the divergence degree of ensemble members' forecasts (i.e., the ensemble spread) can be used as a quantitative representation of the forecast uncertainty (i.e., the forecast error). Appropriate post processes for ensemble members' forecasts can achieve corresponding post-processed deterministic forecast products, and the forecast performance of these products are usually significantly better than that of the original single deterministic forecast. In addition, modern ensemble forecasts are expressed probabilistically other than deterministically, more decision mistakes could be avoided if the decisions are made based on whether the probabilities exceed some prior determined threshold for action, which is an important aspect for the application of ensemble forecast technology.

Ensemble forecast has become a relatively mature technology in the field of numerical weather forecast, and has been widely used in the operational forecasting practice (4). Meanwhile, as a scientific way to solve the uncertainty problems existing in single deterministic forecast, it has also been widely used in the fields of aviation (5), biology (6), hydrology (7), electricity (8), economy (9) and infectious disease prevention and control in recent years, providing great enlightening significance for solving the prediction problems in related fields.

3 Application progress of influenza ensemble forecast

3.1 Application progress of influenza ensemble forecast in the United States

The United States is one of the country's most seriously affected by seasonal influenza, and the Department of Environmental Health

Sciences of Columbia University has carried out several studies on influenza ensemble forecast for some megacities in the past decade.

Shaman and Karspeck (2) established an influenza ensemble forecast system based on the SIRS model and ensemble adjusted Kalman filter (EAKF) assimilation technology developed in the field of numerical weather forecast. This system uses EAKF assimilation method to assimilate the data of current influenza cases updated on relevant websites in real time, thus to generate 250 sets of initial values, the SIRS model is then used to integrate the initial values to achieve 250 sets of forecast values. On this basis, the ensemble forecast system was tested and evaluated for forecasting influenza cases in New York City from 2003 to 2008, In general, the influenza ensemble forecast system can accurately forecast the peak timing about 7 weeks in advance of the actual peak, and the spread of the ensemble members' forecasts can be used to enhance the confidence in the accuracy of forecast results.

In the influenza epidemic seasons of 2012 and 2013, the above-mentioned influenza ensemble forecast system (2) was operationally implemented in real time and provided forecast results of influenza cases in 108 cities of the United States (10), which was the first operational ensemble forecast system for influenza. According to the related evaluation results: The influenza ensemble forecast system could accurately forecast the peak timing about 9 weeks in advance of the actual peak. In general, the forecast accuracy gradually increased with the season progressed. By the 52th week, prior to peak for the majority of cities, 63% of all ensemble forecasts were accurate.

The nonlinear growth of errors is the main source of forecast errors in infectious disease models. In order to further optimize the influenza ensemble forecast system, on the basis of the previous works, Pei and Shaman (11) quantitatively estimated the nonlinear error results of the above-mentioned influenza ensemble forecast system through the error breeding analysis method and then accordingly corrected the forecast errors. After this, the ensemble forecast experiments for influenza cases in 95 cities of the United States from 2003 to 2008 were conducted, evaluation results indicate that: In general, through the nonlinear error correction process, the forecast accuracy of the peak time and peak intensity of influenza outbreak are both improved.

On the basis of the previous works, Pei et al. (12) found that the initial value error and random error in the infectious disease model have similar growth characteristics in the process of model integration through several diagnostic analysis processes, which further confirmed that the nonlinear dynamic error growth is the main source of the forecast error of infectious disease models. On this basis, the direction of the fastest growth of initial value error was found by singular vector analysis method and then accordingly used to optimize the initial value perturbation scheme. After this, the ensemble spread increases significantly so that the forecast uncertainty could be better represented, and the ensemble forecast accuracy is also further improved.

To sum up, the United States is the country with the most research on influenza ensemble forecast technology. In recent years, an influenza ensemble forecast system was built, and some ensemble forecast researches such as forecast results evaluation, error evolution characteristic diagnosis and analysis, ensemble forecasting initial value perturbation scheme optimization have been done. The newly-developed influenza ensemble forecast system has been operationally implemented and provided reference for scientific prevention and control.

3.2 Application progress of influenza ensemble forecast in subtropical regions

Influenza outbreaks in temperate regions usually present the characteristics of seasonal circulation, while that in tropical and subtropical regions presents irregular non-seasonal distribution characteristics and can breakout throughout the year. Therefore, the forecast of influenza cases in tropical and subtropical regions is more difficult.

Yang et al. (13) established an influenza ensemble forecast system with ensemble size of 500 for the Hong Kong city in subtropical region based on the SIRS model and the EAKF assimilation technology, which is similar to the ensemble forecast system constructed by Shaman and Karspeck (2). Based on this, the ensemble forecast system was tested and evaluated for influenza cases in Hong Kong from 1998 to 2013. Overall, the influenza ensemble forecast system was able to predict the peak timing and peak intensity of 44 influenza pandemics caused by single influenza strain or multiple influenza strains in the past 16 years. The overall forecast accuracy of 1–3 weeks in advance was 37%, and the forecast accuracy increased with the ensemble spread. The maximum accuracy of the peak time (intensity) of the pandemic caused by different strains is 43–93% (45–89%). In general, for non-seasonal influenza pandemics in subtropical regions, which are difficult to predict, the influenza ensemble forecast system can forecast accurately at least three weeks in advance.

The influenza ensemble forecast system for Hong Kong is generally similar to that established by the Department of Environmental Health Sciences of Columbia University, but its overall forecast accuracy is obviously worse, which may be mainly due to the lower predictability of influenza outbreaks in subtropical regions compared to temperate regions.

3.3 Application progress of super ensemble forecast technology for influenza

In addition to establishing ensemble forecast system based on a single model, the forecast results based on different models can be directly combined to form ensemble forecasts, which is called multi-model super ensemble forecast in the field of numerical weather forecast. Generally speaking, each model has its certain advantages and disadvantages. Thus, the super ensemble forecast may absorb (avoid) the advantages (disadvantages) of each single model, so as to achieve more accurate forecast results. In recent years, several studies have been fulfilled on the multi-model super ensemble forecast for influenza.

To incorporate all available data and methods to achieve a more accurate forecast of influenza cases, the Centers for Disease Control and Prevention of the United States has organized seasonal influenza forecasting challenges since the 2013 season. In the 2017 and 2018 influenza seasons, the 22 teams participating in the challenge combined the forecast results of their respective model through the machine learning method (14), and the specific weights for each model were determined by its forecast accuracy in previous seasons. It is found that the forecast results after weighted integration are obviously better than that of the 22 teams, which shows good potentials to be operationally implemented.

Yamana et al. (15) also completed a similar study on the seasonal influenza, but during the weighted integration process based on the multi-model super ensemble forecast results, the same weight was applied to each model. The results showed that the forecast results of the multi-model ensemble forecasts outperform those of each single model, and very poor forecast results were less likely to occur.

Different from the above schemes for determining weight of each single model, McAndrew and Reich (16) generated the weights of each model by its forecast accuracy updated weekly in real time and found that the forecast accuracy based on this weighting scheme are better than that of the above-mentioned two schemes (14, 15).

To sum up, scheme for determining weight should be selected according to specific needs or situations when carrying out weighted integration processes for multi-model super ensemble forecast results, since each scheme has its own advantages and disadvantages. In general, the development of super ensemble forecast and proper weighted integration process could achieve more accurate forecast results.

4 Discussion

In recent years, several influenza ensemble forecast systems were established and some related researches were conducted such as forecast results evaluation, error evolution characteristic diagnosis and analysis, ensemble forecasting initial value perturbation scheme optimization, super ensemble forecast and so on. Some well-performed influenza ensemble forecast systems have been operationally implemented and provided references for scientific prevention and control. In general, ensemble forecast can represent various uncertainties in forecasting influenza cases based on infectious disease model and achieve more accurate forecasts and more valuable information than the single deterministic forecast, showing a good prospect for application. In addition, the development of super ensemble forecast and proper weighted integration process could achieve more accurate forecast results.

However, there are still some weakness in the above-mentioned works: Firstly, some of the above-mentioned influenza ensemble forecast systems use the EAKF assimilation method to generate initial values. In fact, there are many other initial value perturbation technologies (17) in the field of numerical weather forecast that can be applied to establish influenza ensemble forecast system, which are expected to reflect the forecast uncertainty of infectious disease model more reasonably and improve the corresponding ensemble forecast skills; Secondly, at present, the post process technologies for influenza ensemble forecast products are mostly simple ensemble average or weighted average based on super ensemble forecast. It is expected to further improve the accuracy and application level of influenza ensemble forecast products by learning to and applying other mature post-process technologies (18) in the field of numerical weather forecast, such as the probability-matching ensemble mean, merged optimal ensemble quantile and Bayesian average; Thirdly, modern ensemble forecasts are expressed probabilistically other than deterministically, more decision mistakes could be avoided if the decisions are made based on whether the probabilities exceed some prior determined threshold for action, which is an important aspect for the application of ensemble forecast technology (19). However, at present, probability forecast is rarely used in the influenza ensemble forecast system, strengthening the application of ensemble probability forecast is expected to further improve the application level of influenza ensemble forecast and reduce decision-making errors.

To further improve the skills and application level of ensemble forecast for influenza, I strongly suggest that scientists engaged in influenza forecast based on infectious disease models should strengthen cooperation with scientists in the field of numerical weather forecast, which is expected to produce innovative academic ideas and achieve new breakthroughs through interdisciplinary cooperation.

Due to the limitation of words, this study only reviews the application progress of ensemble forecast technology in influenza forecast based on infectious disease model. In fact, there are many other similar studies involving other infectious diseases such as dengue (20) and COVID-19 (21), which may be reviewed in the future.

Author contributions

LC: Writing – original draft, Writing – review & editing.

Funding

The author(s) declare financial support was received for the research, authorship, and/or publication of this article. This research was supported by the Joint Research Project for Meteorological Capacity Improvement of China Meteorological Administration (22NLTSY003).

Acknowledgments

The papers outlined in this study are available at the Havard dataverse (https://doi.org/10.7910/DVN/0GBSQA).

Conflict of interest

The author declares that the research was conducted in the absence of any commercial or financial relationships that could be construed as a potential conflict of interest.

Publisher's note

References

1. Iuliano AD, Roguski KM, Chang HH, Muscatello DJ, Palekar R, Tempia S, et al. Estimates of global seasonal influenza-associated respiratory mortality: a modelling study. *Lancet*. (2018) 391:1285–00. doi: 10.1016/S0140-6736(17)33293-2

2. Shaman J, Karspeck A. Forecasting seasonal outbreaks of influenza. *Proc Natl Acad Sci USA*. (2012) 109:20425–30. doi: 10.1073/pnas.1208772109

3. Leith CE. Theoretical skill of Monte Carlo forecasts. *Mon Wea Rev*. (1974) 102:409–18. doi: 10.1175/1520-0493(1974)102<0409:TSOMCF>2.0.CO;2

4. Lewis JM. Roots of ensemble forecasting. *Mon. Wea. Rev.* (2005) 133:1865–85. doi: 10.1175/MWR2949.1

5. Storer LN, Gill PG, Williams PD. Multi-model ensemble predictions of aviation turbulence. *Meteorol Appl*. (2018) 26:416–28. doi: 10.1002/met.1772

6. Shawn MC, Solomon ZD, Alison RM. Evaluating ensemble forecasts of plant species distributions under climate change. *Ecol Model*. (2013) 266:126–30. doi: 10.1016/j.ecolmodel.2013.07.006

7. Li WT, Duan QY, Miao CY, Ye A, Gong W, di Z. A review on statistical postprocessing methods for hydrometeorological ensemble forecasting. *Wires Water*. (2017) 4:e1246. doi: 10.1002/wat2.1246

8. Thorey J, Chaussin C, Mallet V. Ensemble forecast of photovoltaic power with online CRPS learning. *Int J Forecast*. (2018) 34:762–73. doi: 10.1016/j.ijforecast.2018.05.007

9. João AB. Ensemble predictions of recovery rates. *J Financ Serv Re*. (2014) 46:177–93. doi: 10.1007/s10693-013-0165-3

10. Shaman J, Karspeck A, Yang W, Tamerius J, Lipsitch M. Real-time influenza forecasts during the 2012–2013 season. *Nat Commun*. (2013) 4:2837. doi: 10.1038/ncomms3837

11. Pei S, Shaman J. Counteracting structural errors in ensemble forecast of influenza outbreaks. *Nat Commun*. (2017) 8:925. doi: 10.1038/s41467-017-01033-1

12. Pei S, Cane MA, Shaman J. Predictability in process-based ensemble forecast of influenza. *PLoS Comput Biol*. (2019) 15:e1006783. doi: 10.1371/journal.pcbi.1006783

13. Yang W, Cowling BJ, Lau EHY, Shaman J. Forecasting influenza epidemics in Hong Kong. *PLoS Comput Biol*. (2015) 11:e1004383. doi: 10.1371/journal.pcbi.1004383

14. Reich NG, McGowan CJ, Yamana TK, Tushar A, Ray EL, Osthus D, et al. Accuracy of real-time multi-model ensemble forecasts for seasonal influenza in the U.S. *PLoS Comput Biol*. (2019) 15:e1007486. doi: 10.1371/journal.pcbi.1007486

15. Yamana TK, Kandula S, Shaman J. Individual versus superensemble forecasts of seasonal influenza outbreaks in the United States. *Public Libr Sci Comp Biol*. (2017) 13:e1005801. doi: 10.1371/journal.pcbi.1005801

16. McAndrew T, Reich NG. Adaptively stacking ensembles for influenza forecasting. *Stat Med*. (2021) 40:6931–52. doi: 10.1002/sim.9219

17. Wang X, Bishop C. A comparison of breeding and ensemble transform Kalman filter ensemble forecast schemes. *J Atmos Sci*. (2003) 60:1140–58. doi: 10.1175/1520-0469(2003)060<1140:ACOBAE>2.0.CO;2

18. Qiao X, Wang S, Schwartz CS, Liu Z, Min J. A method for probability matching based on the ensemble maximum for quantitative precipitation forecasts. *Mon. Wea. Rev.* (2020) 148:3379–96. doi: 10.1175/MWR-D-20-0003.1

19. Joslyn S, Pak K, Jones D, Pyles J, Hunt E. The effect of probabilistic information on threshold forecasts. *Weather Forecast*. (2007) 22:804–12. doi: 10.1175/WAF1020.1

20. Buczak AL, Baugher B, Moniz LJ, Bagley T, Babin SM, Guven E. Ensemble method for dengue prediction. *PLoS One*. (2018) 13:e0189988. doi: 10.1371/journal.pone.0189988

21. Cramer EY, Ray EL, Lopez VK, Bracher J, Brennen A, Castro Rivadeneira AJ, et al. Evaluation of individual and ensemble probabilistic forecasts of COVID-19 mortality in the United States. *Proc Natl Acad Sci USA*. (2022) 119:e2113561119. doi: 10.1073/pnas.2113561119

Frontiers in Public Health

TYPE Original Research
PUBLISHED 22 December 2023
DOI 10.3389/fpubh.2023.1338305

Check for updates

OPEN ACCESS

EDITED BY
Zhaobin Sun,
Chinese Academy of Meteorological Sciences, China

REVIEWED BY
Bin Luo,
Lanzhou University, China
Zhao Xiuge,
Chinese Research Academy of Environmental Sciences, China
Ling Han,
National Institute for Communicable Disease Control and Prevention (China CDC), China

*CORRESPONDENCE
Yan Tao
✉ taoyan@lzu.edu.cn

RECEIVED 14 November 2023
ACCEPTED 24 November 2023
PUBLISHED 22 December 2023

CITATION
Liao Q, Li Z, Li Y, Dai X, Kang N, Niu Y and Tao Y (2023) Specific analysis of $PM_{2.5}$-attributed disease burden in typical areas of Northwest China. *Front. Public Health* 11:1338305. doi: 10.3389/fpubh.2023.1338305

Specific analysis of $PM_{2.5}$-attributed disease burden in typical areas of Northwest China

Qin Liao[1,2], Zhenglei Li[2], Yong Li[3], Xuan Dai[2], Ning Kang[2], Yibo Niu[1,2] and Yan Tao[2]*

[1]Key Laboratory of Western China's Environmental Systems (Ministry of Education), College of Earth and Environmental Sciences, Lanzhou University, Lanzhou, China, [2]Northwest Institute of Eco-Environment and Resources, Chinese Academy of Sciences, Lanzhou, China, [3]Key Laboratory of Environmental Pollution Monitoring and Disease Control, Ministry of Education, Guizhou Medical University, Guiyang, China

Background: Frequent air pollution events in Northwest China pose a serious threat to human health. However, there is a lack of specific differences assessment in $PM_{2.5}$-related disease burden. Therefore, we aimed to estimate the $PM_{2.5}$-related premature deaths and health economic losses in this typical northwest region, taking into account disease-specific, age-specific, and region-specific factors.

Methods: We utilized the WRF-Chem model to simulate and analyze the characteristics and exposure levels of $PM_{2.5}$ pollution in Gansu Province, a typical region of Northwest China. Subsequently, we estimated the premature mortality and health economic losses associated with $PM_{2.5}$ by combining the Global Exposure Mortality Model (GEMM) and the Value of a Statistical Life (VSL).

Results: The results suggested that the $PM_{2.5}$ concentrations in Gansu Province in 2019 varied spatially, with a decrease from north to south. The number of non-accidental deaths attributable to $PM_{2.5}$ pollution was estimated to be 14,224 (95% CI: 11,716–16,689), accounting for 8.6% of the total number of deaths. The $PM_{2.5}$-related health economic loss amounted to 28.66 (95% CI: 23.61–33.63) billion yuan, equivalent to 3.3% of the regional gross domestic product (GDP) in 2019. Ischemic heart disease (IHD) and stroke were the leading causes of $PM_{2.5}$-attributed deaths, contributing to 50.6% of the total. Older adult individuals aged 60 and above accounted for over 80% of all age-related disease deaths. Lanzhou had a higher number of attributable deaths and health economic losses compared to other regions. Although the number of $PM_{2.5}$-attributed deaths was lower in the Hexi Corridor region, the per capita health economic loss was higher.

Conclusion: Gansu Province exhibits distinct regional characteristics in terms of PM2.5 pollution as well as disease- and age-specific health burdens. This highlights the significance of implementing tailored measures that are specific to local conditions to mitigate the health risks and economic ramifications associated with $PM_{2.5}$ pollution.

KEYWORDS

$PM_{2.5}$, premature mortality, specific differences, economic loss, Northwestern China

1 Introduction

Air pollution, particularly fine particulate matter ($PM_{2.5}$), is the fourth leading determinant of mortality worldwide (1). Epidemiological studies have shown that long-term exposure to ambient $PM_{2.5}$ can lead to adverse health outcomes, including increased risks of death from disease such as ischemic heart disease (IHD), stroke, chronic obstructive pulmonary disease (COPD), lower respiratory infections (LRI), and lung cancer (LC) (2–5). In the last decade, $PM_{2.5}$ has become the predominant air pollutant in China. Although there has been a significant reduction in $PM_{2.5}$ levels (6, 7), the majority (81%) of the population is still exposed to annual average $PM_{2.5}$ concentration that exceed the World Health Organization's (WHO) Air Quality Interim Target of 35 $\mu g{\cdot}m^{-3}$ (8). According to estimates from the Global Burden of Disease Study (GBD), $PM_{2.5}$ pollution resulted in ~4.14 million premature deaths worldwide in 2019, with over 1/4 of these deaths occurring in China, a notably higher number than in other countries (1). The health impacts of $PM_{2.5}$ also result in significant economic losses to society (9, 10). Guan et al. (10) estimated that the economic losses from ambient $PM_{2.5}$ pollution were 3.20–3.34 trillion yuan across China during 2015–2017. Therefore, a diligent and accurate evaluation of the disease burden caused by $PM_{2.5}$ pollution remains essential for effective policy formulation.

Many studies have utilized ground monitoring data to assess the premature mortality attributable to $PM_{2.5}$ (11–13). However, accurately understanding the characteristics of $PM_{2.5}$ pollution poses challenges due to the limited spatial coverage and uneven distribution of the $PM_{2.5}$ monitoring network (14). Methods of $PM_{2.5}$ exposure based on air quality model simulations with broader spatial coverage are considered more effective (15). For example, Wu et al. (16) and Li et al. (17) estimated $PM_{2.5}$-related premature mortality in China using $PM_{2.5}$ concentration data simulated by air quality models. Furthermore, the exposure-response function is crucial for accurately assessing premature mortality. Recent studies have recognized a non-linear relationship in the relative risk of $PM_{2.5}$ health effects (3, 4). As a result, a progression of exposure-response models have been developed, ranging from basic linear models to more advanced log-linear models (LL), integrated exposure-response model (IER), and the most recent global exposure mortality model (GEMM) (5).

Several studies have examined the national-level impact of $PM_{2.5}$ exposure on disease burden using varying $PM_{2.5}$ concentration data and exposure-response functions (6, 7, 18–20). However, there has been less focus on the disease burden of $PM_{2.5}$ in specific regions, and it is mainly done in developed regions such as the Beijing-Tianjin-Hebei region (21), the Yangtze River Delta (22), and the Pearl River Delta (23), while researches in the northwestern region of China are lacking. $PM_{2.5}$-related mortality varies significantly across regions due to disparities in air pollution levels and socio-economic status (24). Additionally, age structure plays a significant role in $PM_{2.5}$-related mortality, as different diseases and age groups contribute variably to these deaths. Xie et al. (25) found that overlooking age structure could result in an overestimation of premature deaths by 14%. Reports on the variations in $PM_{2.5}$-related mortality across different age groups are limited (7, 26). Hence, it is imperative to comprehensively estimate the specific impact of $PM_{2.5}$-related mortality on different diseases and age groups within specific regions.

Gansu Province, located in the northwest of China, is a typical underdeveloped area. It is situated at the convergence of the Loess Plateau, Qinghai-Tibet Plateau, and Inner Mongolia Plateau, making it prone to sand and dust storms (27) (Figure 1). The region is affected by both human activities and natural sources of particulate pollution. However, the extent of the disease burden caused by $PM_{2.5}$ pollution in Gansu Province is not clear. To address this knowledge gap, this study aims to assess $PM_{2.5}$-related mortality and its associated health economic losses in Gansu Province in 2019 using the WRF-Chem air quality model in combination with the optimized GEMM model. Additionally, the study quantifies the specific differences in premature deaths across different diseases, ages, and regions. The ultimate goal is to provide a scientific basis for the development of effective measures to reduce the health impacts of air pollution.

2 Methodology

2.1 Simulations of $PM_{2.5}$ concentration

The WRF-Chem air quality model was employed to estimate $PM_{2.5}$ concentrations in Gansu Province for the year 2019. The simulation domain covered the entire Gansu Province and its surrounding provinces, with a horizontal resolution of 20 × 20 km (150 × 100 grids). The meteorological initial conditions were derived from the 6-h National Centers for Environmental Prediction (NCEP) final analysis data, with a spatial resolution of 1° × 1° (28). The initial conditions for atmospheric chemistry were obtained from the Community Atmosphere Model with Chemistry (CAM-Chem) model, with a 6-h interval and a spatial resolution of 1.9° × 2.5° (29). Anthropogenic emissions data was sourced from the Multi-resolution Emission Inventory for China (MEIC) developed by Tsinghua University (30). Biomass burning emissions were derived from the Fire INventory from NCAR (FINN) (31). Biogenic emissions were based on the commonly used Model of Emissions of Gases and Aerosols from Nature (MEGAN) inventory (32). Dust emissions were implemented using the Air Force Weather Agency (AFWA) emission scheme (33). The selected physical and chemical parameterization schemes for the simulation are presented in Table 1.

The WRF-Chem model simulation results were evaluated using environmental monitoring data. The daily average $PM_{2.5}$ concentration data for Gansu Province in 2019 were sourced from the Gansu Provincial Environmental Monitoring Center Station. These data covered 33 national air quality monitoring sites across 14 cities and prefectures. Various evaluation metrics were used, including normalized mean bias (NMB), normalized mean error (NME), mean fractional bias (MFB), mean fractional error (MFE), and the correlation coefficient (R). Overall, the simulation of $PM_{2.5}$ concentrations in Gansu Province in 2019 showed good performance (34, 35). The NMB, NME, MFB, and MFE values were 0.08, 0.29, 0.04, and 0.20, respectively, and the results of R (0.56) was significant at the 1% level ($P < 0.01$).

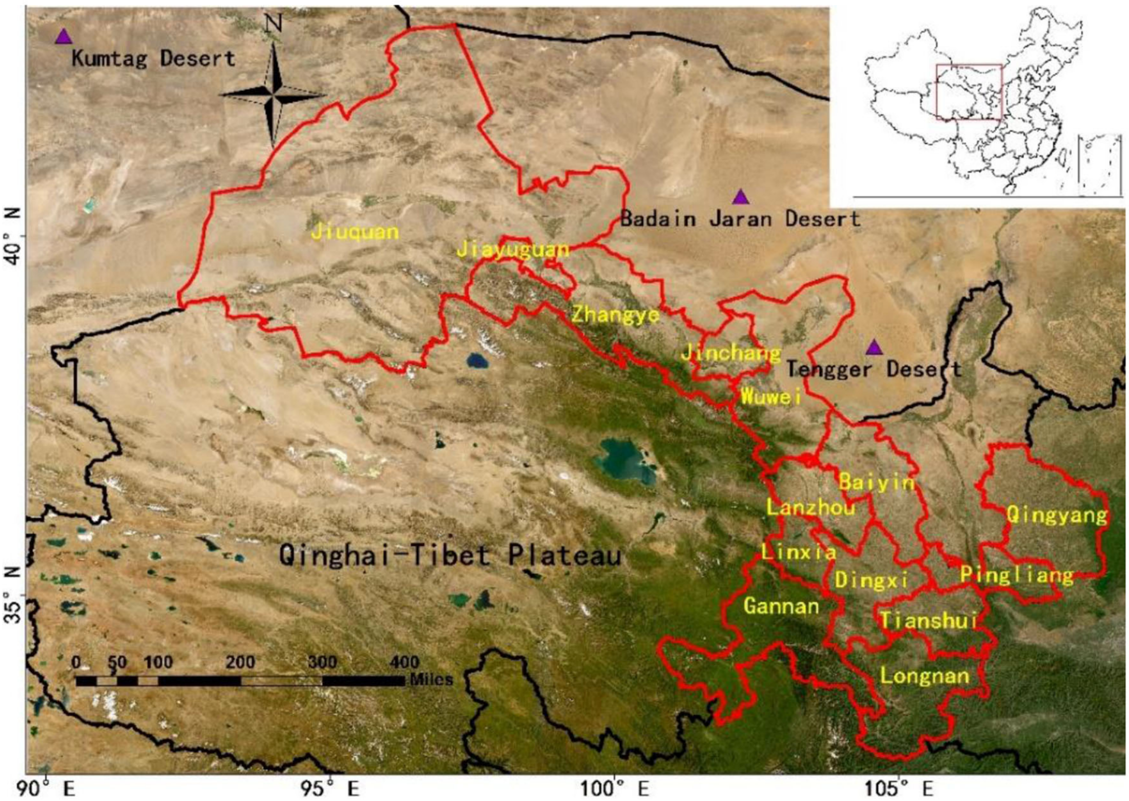

FIGURE 1
Geographical location of the study area.

TABLE 1 Main physical and chemical parameters adopted in the WRF-Chem simulation.

Type	Scheme	Parameter
Physical options	Boundary layer scheme	Mellor-Yamada Nakanishi and Niino 2.5
	Microphysics process scheme	Morrison 2-moment
	Radiation scheme	Rapid radiative transfer model for GCM
	Land surface process scheme	Noah
	Cumulus parameterization scheme	Grell-3D
Chemical options	Gas-phase chemical mechanism	Model for ozone and related tracers
	Aerosol module	Model for simulating aerosol interactions and chemistry with 4 sectional bins
	Photolysis reaction	Fast troposphere ultraviolet visible (F-TUV)

2.2 Calculation of premature mortality

The Global Exposure Mortality Model (GEMM) optimized by Burnett et al. (5) was employed to estimate premature mortality attributable to $PM_{2.5}$ pollution in adults (aged 25+). The GEMM took into account deaths from non-communicable diseases and lower respiratory infections (NCD+LRI), which are considered as non-accidental deaths. It also considers deaths from five major diseases, namely IHD, stroke, COPD, LC, and LRI, which represent deaths caused by specific diseases. The difference between non-accidental deaths and the sum of deaths from these five specific diseases represents deaths from other diseases. The computation formula used is as follows:

$$M_{i,j} = Pop \times PS_j \times B_{i,j} \times \frac{(RR_{i,j} - 1)}{RR_{i,j}} \tag{1}$$

$$RR_{i,j} = \begin{cases} \exp\left\{ \dfrac{\theta_{i,j} \log\left(\frac{C-C_0}{\alpha_{i,j}} + 1\right)}{1+exp\left(-\frac{C-C_0-\mu_{i,j}}{v_{i,j}}\right)} \right\}, & if\ C > C_{0\,i,j} \\ 1, & if\ C \leq C_{0\,i,j} \end{cases} \tag{2}$$

where the subscripts i and j represent the disease type and age structure (25–29, 30–34, 35–39, 40–44, 45–49, 50–54, 55–59, 60–64, 65–69, 70–74, 75–79 and ≥80 years old), respectively; $M_{i,j}$ is premature mortality caused by $PM_{2.5}$ exposure; Pop refers to the exposed population to $PM_{2.5}$; PS_j is the proportion of a specific age group within the exposed population; $B_{i,j}$ represents the baseline mortality rate; $RR_{i,j}$ is the relative risk; C is the annual average $PM_{2.5}$ concentration; C_0 is the counter-factual concentration below which it is assumed that there is no additional risk ($2.4\ \mu g \cdot m^{-3}$)

(1, 18); θ, α, μ, and ν are fitting parameters for the $PM_{2.5}$ exposure-response function. The values for θ, α, μ, and ν can be found in the references provided by Burnett et al. (5). Population data was sourced from the Gansu Development Yearbook 2020 (36). Age structure data and baseline mortality rates for each age group come from the China Cause-of-Death Surveillance Dataset 2019 (37), with data from the western region applied to Gansu Province.

Considering the uncertainty of RR in the model, a 95% confidence interval (CI) was calculated using the standard error in the GEMM:

$$95\%\ CI\ (RR_{i,j}) = \exp\left\{\frac{\left(\theta_{i,j} \pm 1.96 \times SE\left(\theta_{i,j}\right)\right) \times log\left(\frac{C-C_0}{\alpha_{i,j}}+1\right)}{1+exp\left(-\frac{C-C_0-\mu_{i,j}}{\nu_{i,j}}\right)}\right\} \tag{3}$$

where $SE(\theta_{i,j})$ represents the standard deviation of $\theta_{i,j}$, with its value referenced in the study by Burnett et al. (5).

2.3 Evaluation of health economic loss

The VSL was used to assess the economic losses resulting from $PM_{2.5}$-related premature deaths. VSL quantifies the monetary value individuals are willing to pay (WTP) to reduce the death risk and is commonly used in assessing health economic losses related to air pollution (13, 38). The formula is as follows:

$$EB_{g,t} = M_{i,j} \times VSL_{g,t} \tag{4}$$

where $EB_{g,t}$ represents the health economic losses in region g (i.e., Gansu Province) in year t attributed to $PM_{2.5}$. $VSL_{g,t}$ indicates the VSL in Gansu Province in year t. Since specific VSL results for Gansu Province are not available, this study adopts the VSL survey results from existing domestic regions as a reference. The benefit transfer method is employed, adjusting for differences in per capita GDP across different regions and timeframes. The formula is as follows:

$$VSL_{g,t} = VSL_b \times \left(\frac{GDP_g}{GDP_b}\right)^{\eta} \times \left(1+\Delta P_g+\Delta G_g\right)^{\eta} \tag{5}$$

where VSL_b represents the VSL of the reference region. For this study, we have selected the latest VSL survey results for Beijing in 2016 conducted by Jin et al. (39), which amount to 5.54 million yuan. GDP_g and GDP_b represent the per capita GDP of Gansu Province and Beijing in 2016, respectively. η is the income elasticity of VSL, and we have adopted the recommended value of 0.8 from the Organization for Economic Co-operation and Development (OECD) (40). ΔP_g is the percentage change in the Consumer Price Index (CPI) in year t for Gansu Province compared to 2016. ΔG_g is the percentage change in per capita GDP in year t for Gansu Province compared to 2016. The per capita GDP and CPI for Gansu Province in 2019 are sourced from the Gansu Development Yearbook 2020 (36), while the per capita GDP for Beijing in 2016 come from the China Statistical Yearbook 2017 (41).

3 Results

3.1 $PM_{2.5}$ pollution characteristics

Based on the WRF-Chem simulation data, the spatial distribution of the annual average $PM_{2.5}$ concentration in Gansu Province in 2019 is shown in Figure 2. The overall distribution exhibited higher concentrations in the north and lower concentrations in the south. The regions with higher concentrations were mainly located in the Hexi Corridor region and certain parts of the central-eastern region. Specifically, Jiuquan and Jiayuguan recorded the highest population-weighted annual mean $PM_{2.5}$ concentrations, reaching 41.48 and 40.28 $\mu g{\cdot}m^{-3}$, respectively, exceeding the Chinese Ambient Air Quality Standards (CAAQS) (35 $\mu g{\cdot}m^{-3}$ for Grade II). Qingyang, Wuwei, and Jinchang followed closely, with concentrations ranging between 32.82 and 34.86 $\mu g{\cdot}m^{-3}$. The concentrations in Lanzhou, Pingliang, Baiyin, and Zhangye all exceeded 30 $\mu g{\cdot}m^{-3}$. Gannan registered the lowest concentration at 12.22 $\mu g{\cdot}m^{-3}$. Notably, the vast majority of areas in Gansu Province had an annual average $PM_{2.5}$ concentration exceeding 15 $\mu g{\cdot}m^{-3}$ for Grade I in CAAQS.

Using the simulated $PM_{2.5}$ concentration and population data, we calculated the cumulative distribution of the population under different $PM_{2.5}$ concentrations for 2019 (Figure 2). It can be observed that in 2019, 86.6% of the population in Gansu Province lived in areas with an annual average $PM_{2.5}$ concentration below 35 $\mu g{\cdot}m^{-3}$. However, only 2.7% of the population resided in areas where the $PM_{2.5}$ concentration was smaller than 15 $\mu g{\cdot}m^{-3}$.

3.2 Cause-specific premature mortality

Using the GEMM model, we estimated the mortality burden attributable to $PM_{2.5}$ pollution in Gansu Province in 2019 (Figure 3). According to the GEMM NCD+LRI model, there were 14,224 (95% CI: 11,716–16,689) non-accidental deaths due to $PM_{2.5}$ pollution in Gansu Province in 2019, accounting for 8.6% of the total deaths. The numbers of $PM_{2.5}$-attributed deaths for IHD, stroke, LC, COPD, and LRI were 3,956 (95% CI: 3,608–4,299), 3,244 (95% CI: 1,602–4,807), 2,440 (95% CI: 1,189–3,615), 1,286 (95% CI: 780–1,764), and 853 (95% CI: 445–1,204) respectively, and represented 14.2, 8.4, 11.4, 12.8, and 24.1% of the deaths from the corresponding specific causes. It was evident that around a quarter of LRI deaths were caused by $PM_{2.5}$ pollution, followed by IHD. Meanwhile, <1/10 of stroke deaths could be attributed to $PM_{2.5}$. Although LRI deaths were more closely associated with $PM_{2.5}$ pollution, the absolute number of deaths from LRI was much lower than those from IHD and stroke due to its lower baseline mortality rate.

When examining the proportion of deaths attributable to $PM_{2.5}$ for different diseases relative to non-accidental deaths (NCD+LRI), the proportion for IHD was the highest at 27.8%, followed by stroke at 22.8%, and the combined percentage of these two diseases accounted for more than 50%. COPD, LC, and LRI constituted 17.2, 9.0, and 6.0%, respectively, while deaths from other diseases made up 17.2%. From this, it can be inferred that the majority of $PM_{2.5}$-attributed deaths come from IHD and stroke. Moreover,

10.3389/fpubh.2023.1338305

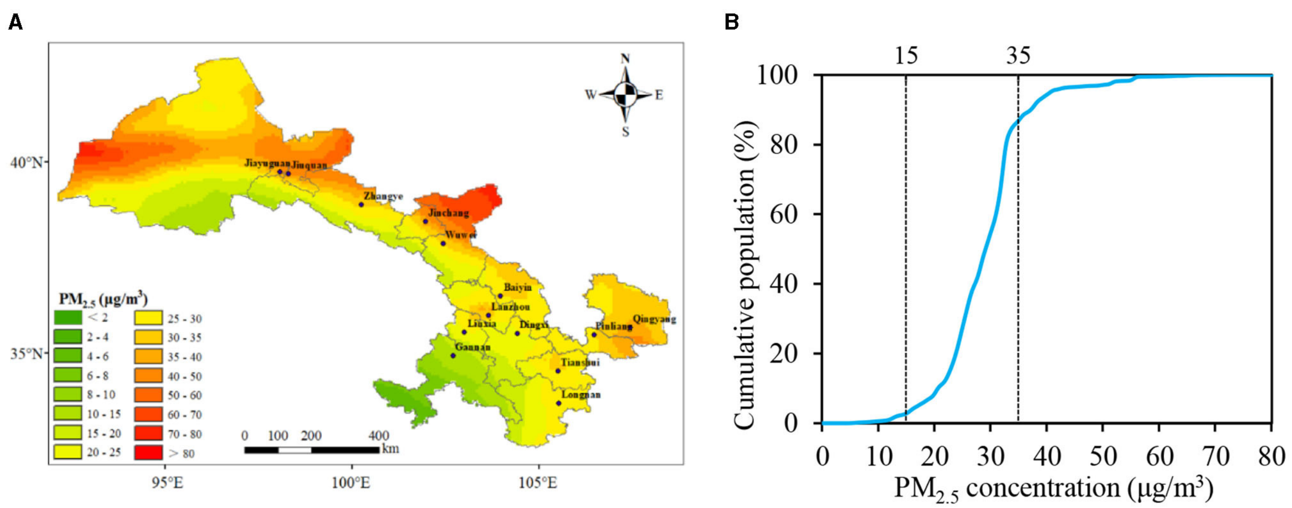

FIGURE 2
Exposure levels of $PM_{2.5}$ in Gansu Province, 2019. **(A)** Spatial distribution of $PM_{2.5}$ concentration; **(B)** cumulative distribution in various levels of $PM_{2.5}$ concentration.

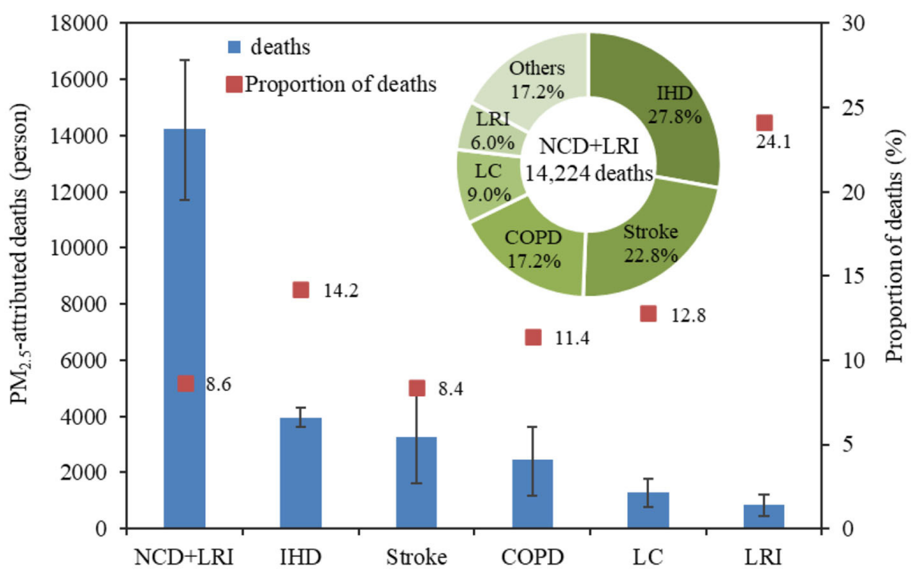

FIGURE 3
The number and proportion of $PM_{2.5}$-attributed deaths in Gansu Province, 2019.

a substantial proportion is due to causes other than these five specific diseases.

3.3 Age-specific premature mortality

Figure 4 present the number and proportion of deaths attributable to $PM_{2.5}$ pollution by age group in Gansu Province in 2019. It was obvious that there were substantial differences in the number of deaths from various diseases caused by $PM_{2.5}$ across different age groups. Generally, the number of non-accidental deaths and disease-specific deaths attributable to $PM_{2.5}$ increased with age. There were 11,615 (95% CI: 9,562–13,633) non-accidental deaths in people aged 60 and above, representing 81.7% of all non-accidental deaths, which was much higher than that of people under 60 years old. Notably, 34.0% of these deaths were reported in the age group of 80 and above.

IHD was the primary cause of death burden across all age groups. For those under the age of 80, the number of deaths from stroke exceeded that from COPD, whereas for those aged 80 and above, deaths due to COPD outnumbered those from stroke. The age distribution of IHD and stroke deaths attributable to $PM_{2.5}$ pollution mirrored the patterns seen with non-accidental deaths. Among those aged 60 and older, the numbers of IHD and stroke deaths were 3,178 (95% CI: 2,896–3,457) and 2,625 (95% CI: 1,292–3,901), respectively, accounting for 80.3 and 80.9% of the total

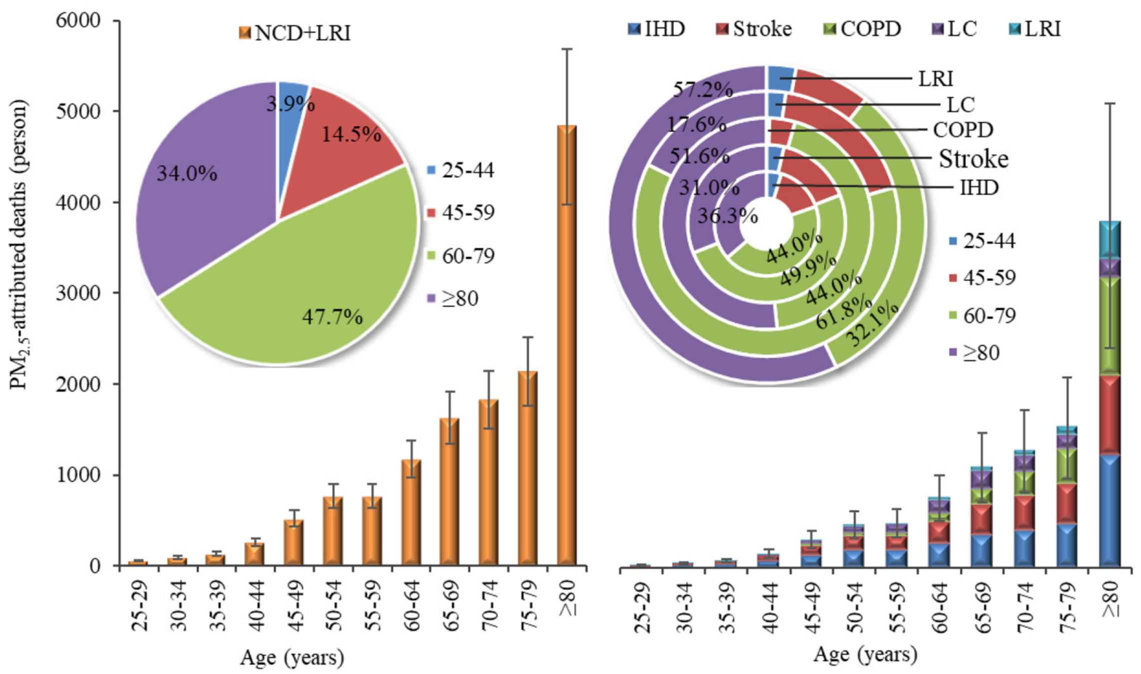

FIGURE 4
$PM_{2.5}$-attributed deaths by age group in Gansu Province, 2019.

deaths from these diseases across all age groups. For the same age bracket (aged 60+), the numbers of COPD and LRI deaths attributable to $PM_{2.5}$ were 2,334 (95% CI: 1,137–3,457) and 762 (95% CI: 398–1,075), respectively, representing a staggering 95.6 and 89.3% of the total deaths from these conditions across all ages. Within this, the contribution from those aged 80 and above alone exceeded half, at 51.6 and 57.2%, respectively. For LC deaths attributable to $PM_{2.5}$ across all age strata, the highest numbers were still among those aged 60 and above, with 1,021 (95% CI: 620–1,400) deaths, constituting 79.4% of all LC deaths. It was worth noting that, unlike other diseases, the proportion of LC deaths was highest in the 60–74 age group (17.9%) and those aged 80 and above (17.6%).

3.4 Region-specific premature mortality

The spatial distribution of non-accidental deaths attributable to $PM_{2.5}$ pollution in Gansu Province in 2019 is illustrated in Figure 5. Lanzhou, the provincial capital, recorded the highest number of $PM_{2.5}$-attributed deaths at 2,103 (95% CI: 1,733–2,467), accounting for 15.0% of the total non-accidental deaths in the province. Tianshui followed with 1,757 (95% CI: 1,447–2,062) deaths, making up 12.5% of the provincial total. The cities of Qingyang, Dingxi, Longnan, Pingliang, and Wuwei reported attributed death numbers ranging between 1,000 and 1,500. Jiayuguan, Gannan, and Jinchang, on the other hand, had lower non-accidental death counts, all under 500. It was observed that areas with higher population densities also exhibited higher numbers of non-accidental deaths attributable to $PM_{2.5}$ pollution. Although the Hexi Corridor region had relatively high $PM_{2.5}$ concentrations, the lower population density of this area, especially in Jiayuguan and Jinchang, resulted in significantly fewer $PM_{2.5}$-attributed deaths compared to other regions.

3.5 Health economic loss

Based on the assessment of deaths attributable to $PM_{2.5}$, the health economic loss associated with $PM_{2.5}$-attributed mortality in Gansu Province was estimated using the VSL method, as depicted in Figure 6. In 2019, the health economic loss caused by $PM_{2.5}$ in Gansu Province amounted to 28.66 (95% CI: 23.61–33.63) billion yuan, accounting for 3.3% of the region's GDP. The combined health economic losses for the five diseases were calculated to be 23.74 (95% CI: 15.36–31.61) billion yuan.

For the various regions (Figure 7), Lanzhou experienced the highest health economic loss, totaling 8.10 (95% CI: 6.67–9.50) billion yuan, contributing 29.0% to the overall health economic loss in Gansu Province. This was followed by Qingyang, Tianshui, and Jiuquan, whose combined contributions accounted for 27.2% of the total health economic loss in the province. Gannan reported the lowest health economic loss at 0.31 (95% CI: 0.25–0.37) billion yuan. The per capita health economic losses caused by $PM_{2.5}$ across various regions in Gansu Province ranged from 428 to 2,575 yuan. Jiayuguan recorded the highest per capita health economic loss, reaching 2,575 yuan. Jiuquan and Lanzhou followed closely with per capita losses of 2,190 and 2,135 yuan, respectively, while Jinchang also experienced a relatively high per capita loss of 1,796 yuan. Meanwhile, the ratio of per capita health economic loss to per capita GDP revealed that Jiuquan, Tianshui, Wuwei, and Baiyin had notably high proportions. Conversely, although Jiayuguan and

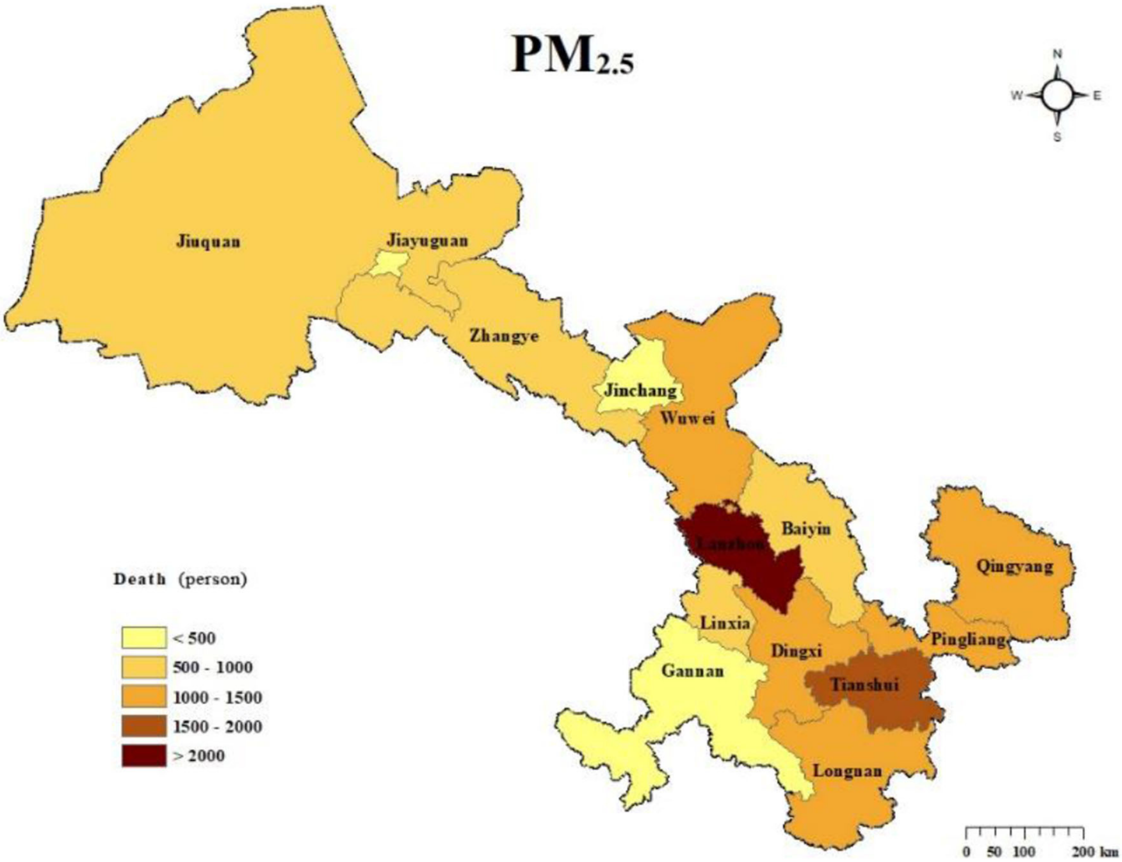

FIGURE 5
Spatial distribution of $PM_{2.5}$-attributed deaths in Gansu Province, 2019.

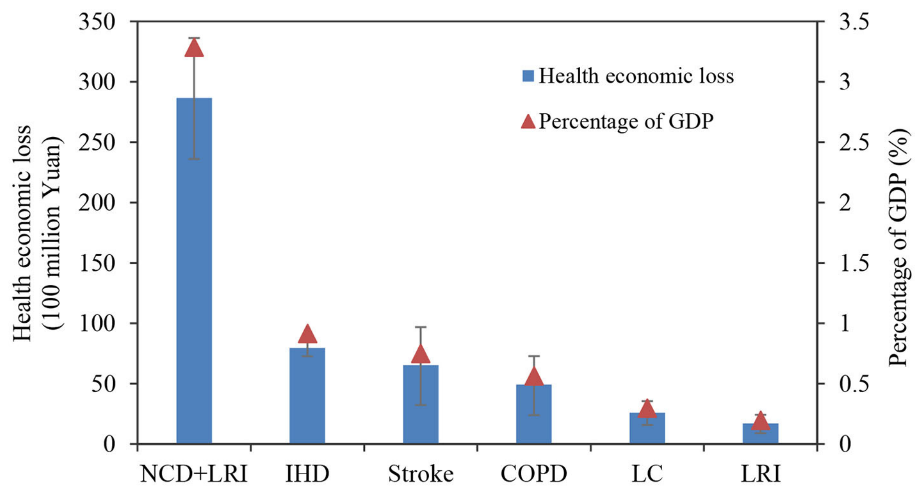

FIGURE 6
Health economic loss attributable to $PM_{2.5}$ pollution in Gansu Province in 2019.

Jinchang had elevated per capita health economic losses, their ratios in relation to per capita GDP were lower. Moreover, Gannan exhibited the lowest figures both in terms of per capita health economic loss and its proportion to per capita GDP.

4 Discussion

The spatial distribution of $PM_{2.5}$ concentrations in Gansu Province varied significantly due to the differences in sources

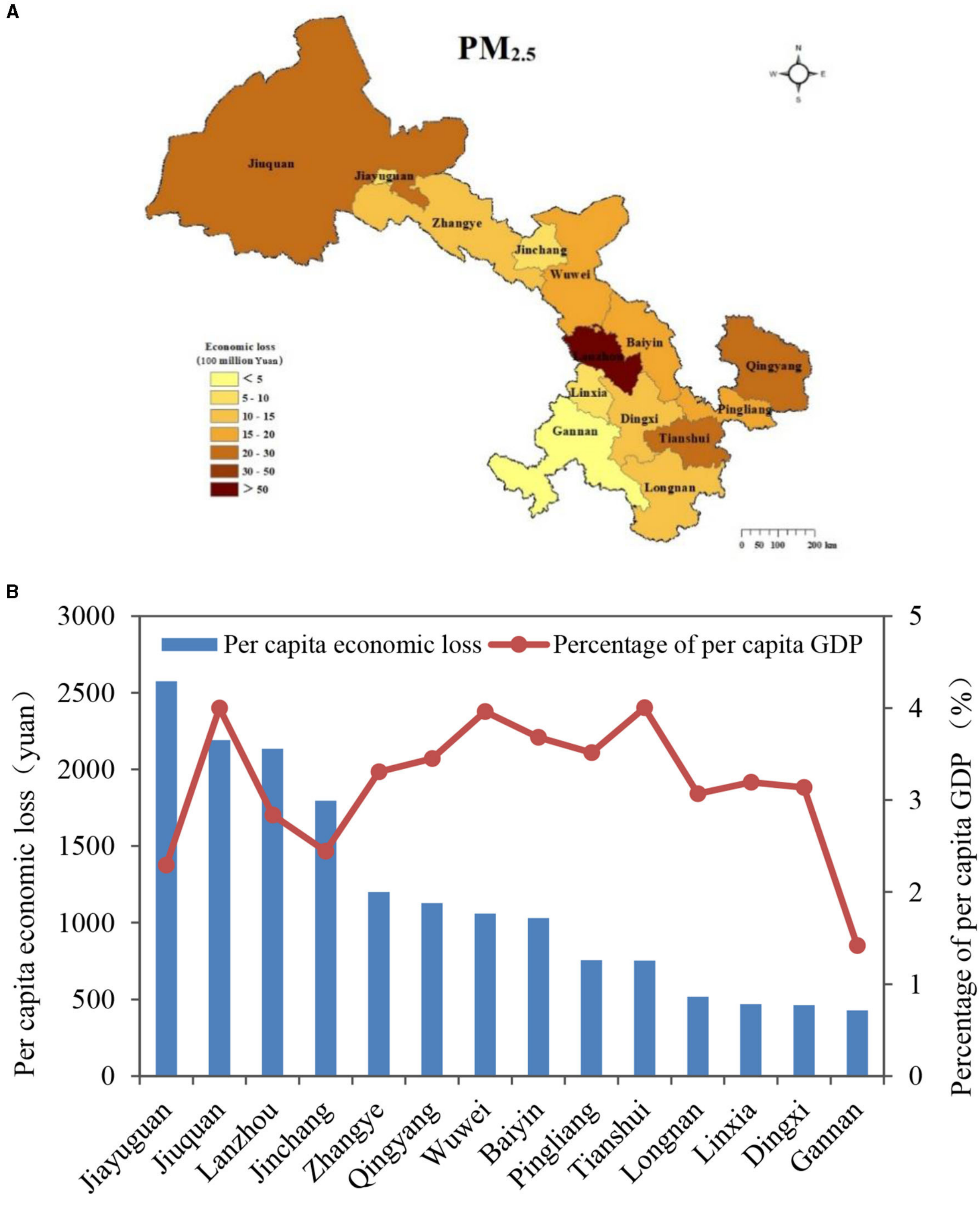

FIGURE 7
Health economic losses attributable to $PM_{2.5}$ pollution in Gansu Province in 2019. **(A)** Spatial distribution of health economic losses; **(B)** per capita health economic losses and the proportion of per capita GDP.

and emission levels of air pollutants. The Hexi region, situated in the western dust corridor of China, was severely influenced by the Tengger Desert, Badain Jaran Desert, and Kumtag Desert (42). Sandstorms had the most effect on Jiuquan and Jiayuguan, located in the westernmost part of Gansu Province (27). In the central and eastern regions of Gansu Province, cities like Lanzhou, Qingyang, Pingliang, and Baiyin had higher air pollutant emissions from anthropogenic sources such as industry and transportation. Conversely, in the southern areas, Gannan and Longnan relied more on green industries like eco-tourism and agricultural product processing, resulting in lower total air pollutant emissions (43). In conclusion, the $PM_{2.5}$ concentration in Gansu Province was influenced by both natural and anthropogenic sources. Therefore, it is crucial for Gansu Province, located in the northwest of China, to consider the multiple sources of $PM_{2.5}$ and implement region-specific measures to address $PM_{2.5}$ pollution.

The study results showed the number of cardiovascular diseases (IHD and stroke: 7,200 individuals) deaths attributable to $PM_{2.5}$ pollution in Gansu Province was higher than respiratory diseases (COPD, LC, and LRI: 4,579 individuals) deaths. This finding is consistent with previous research conducted in other regions of China (16, 26, 44). The higher number of premature cardiovascular deaths can be attributed to the generally high baseline mortality rate from cardiovascular diseases (45). In a study conducted in 2019, it was also found that IHD and stroke were the primary causes of $PM_{2.5}$-attributed mortality in China (25). However, the proportion of COPD and LRI-related deaths (15.8%) was lower compared to ours (23.2%), possibly due to higher baseline mortality rates for these diseases in western China. According to the China Cause-of-Death Surveillance Dataset 2019 (37), the baseline mortality rates for COPD and LRI in western China were notably higher than in the central and eastern regions. Some studies have also observed that while $PM_{2.5}$-attributed deaths from respiratory diseases have been decreasing, deaths from cardiovascular diseases (especially IHD) have been increasing (17). This trend is expected to continue with the rise of unhealthy lifestyles and an aging population. Therefore, in addition to reducing $PM_{2.5}$ pollution levels, it is important to focus on improving healthcare and promoting healthier lifestyles to lower the baseline mortality rate of cardiovascular diseases and reduce the number of $PM_{2.5}$-related deaths from such conditions in the future.

Considering the variations in total population among different age groups, this study further calculated the $PM_{2.5}$-attributed mortality rate to better compare the premature deaths caused by $PM_{2.5}$ pollution in different age categories (Figure 8). It was evident that the $PM_{2.5}$-attributed mortality rate showed substantial disparities among different age groups, with a noticeable increase in older age groups. The non-accidental mortality attributable to $PM_{2.5}$ reached 960 per 100,000 individuals in the population aged 80 and above. This finding is consistent with previous studies (46), indicating that older adults are more susceptible to the adverse effects of air pollution due to their elevated baseline mortality rate (16). Therefore, it is essential to consider the impacts of air pollution on different age groups and diseases and implement proactive and effective measures to shield older adults and enhance their overall health. Additionally, given the projected increase in the aging population in the future (47), it is imperative to estimate the influence of age structure on mortality attributed to air pollution in order to accurately understand the health effects on the population.

Premature deaths attributable to $PM_{2.5}$ varied significantly across different regions, with the number of deaths being mainly influenced by $PM_{2.5}$ concentration and population density when using a consistent baseline mortality rate. Lanzhou, a provincial capital, had a higher number of $PM_{2.5}$-attributed deaths compared to other regions. This can be attributed to the combination of sandstorms from the Hexi Corridor and surrounding areas, rapid economic growth, heavy industries, and transportation development in Lanzhou. As a result, Lanzhou has elevated $PM_{2.5}$ concentrations and the highest population density, leading to significant health implications. Research by Guan et al. (48) revealed that air pollution-related health impacts in regional hub cities contribute significantly to the overall health burden within the province, especially in central and western China. Although Jiayuguan, an industrially advanced city, has higher $PM_{2.5}$ concentrations, its unique population distribution with low population density results in a lower health impact. The distribution of $PM_{2.5}$-related health economic losses in different regions shows similarities, but there are still some disparities. These variations primarily stem from health economic losses being dependent on the level of attributable deaths and health costs, denoted as the value of VSL, which is influenced by the local level of economic development (13, 49). Even if the per capita health economic loss is relatively low, it can still represent a higher proportion of the per capita GDP. In other words, the economic burden caused by air pollution can be considerable.

Despite the important findings outlined above, there are still significant uncertainties and limitations in estimating the disease burden attributable to $PM_{2.5}$ pollution. First, different means of measuring $PM_{2.5}$ may affect the concentration data. Simulation results with the WRF-Chem model faced uncertainties from emission inventories and simulations of chemical-physical processes. We adopted anthropogenic emission data from MEIC, which has been widely used in air quality simulation. Meanwhile, the reliability of the WRF-Chem model simulation was evaluated using common evaluation metrics. Second, the exposure-response relationship between $PM_{2.5}$ and health outcomes was also a major source of uncertainty (44). Previous studies mainly utilized the IER model, which only incorporated cohort study data from European and American regions, potentially underestimating the health burden in areas with higher $PM_{2.5}$ concentrations. In contrast, the GEMM model considered higher air pollution levels and included the results of a cohort study in China, estimating a 120% larger mortality burden than the IER model (5). Therefore, it may be more appropriate to use exposure-response models based on specific Chinese cohort studies, although the accuracy of the GEMM model requires further scientific validation (26, 50). Third, the exposure-response model assumes that the toxicity of ambient $PM_{2.5}$ is only influenced by concentrations, but the health effects of $PM_{2.5}$ from different chemical components or different sources may vary greatly (38). This is particularly important in Gansu Province, which has complex $PM_{2.5}$ emission sources and lacks relative risk functions for specific sources. Fourth, due to more elaborate data limitations, this study used baseline mortality rates and age structure from western China for Gansu Province, and did not consider their spatial variability across the study region, which may have introduced some discrepancies in the estimated results. Fifth, the VSL played a key role but also caused uncertainties when assessing health economic losses. The VSL estimates from developed countries could not be applied to China due to differences in socio-economic characteristics and air pollution levels. There are relatively few studies on VSL conducted in China (39, 51–53). However, owing to differences in the timing of willingness-to-pay surveys and economic development levels, the values of VSL were considerable uncertainties, leading to significant variations in the estimated health economic losses. In view of the rising income level in China in recent years and the increasing public awareness of air pollution, the results of the more recent VSL survey were used in our study.

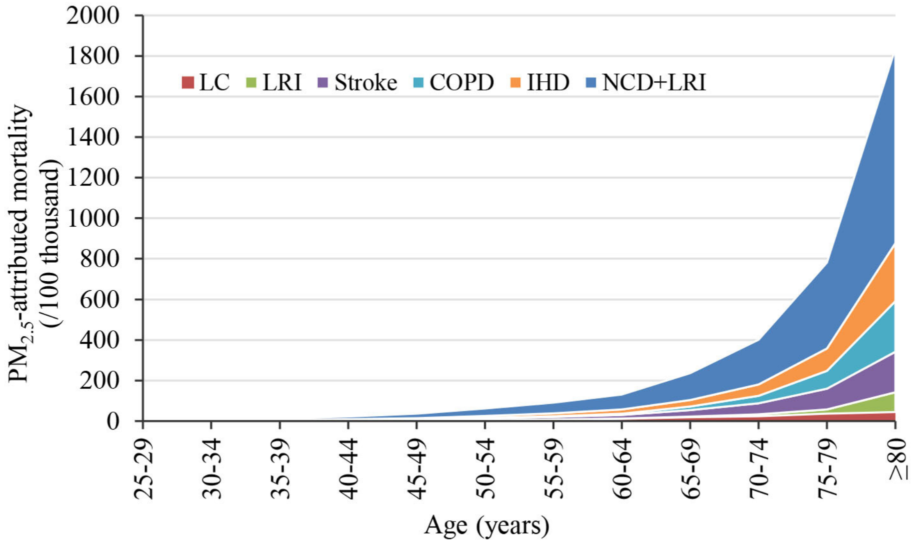

FIGURE 8
$PM_{2.5}$-attributed mortality rates for different age groups in Gansu Province, 2019.

5 Conclusion

This study utilized simulated $PM_{2.5}$ concentration data and an exposure-response model to investigate the impact of $PM_{2.5}$ pollution on premature deaths and health economic losses in Gansu Province. The results indicated that there were 14,224 non-accidental deaths attributed to $PM_{2.5}$ pollution in 2019, with the majority caused by IHD and stroke. Older adults (aged 60+) were more affected by $PM_{2.5}$ pollution than those under 60 years old. The distribution of deaths varied spatially, with high concentrations in densely populated areas like Lanzhou and Tianshui. The health economic losses due to $PM_{2.5}$ pollution accounted for 3.3% of the annual GDP, with Lanzhou contributing the most. Jiayuguan, Jiuquan, and Lanzhou had higher per capita health economic losses. In conclusion, there are significant differences in the diseases, age groups, and regional distribution of disease burden attributable to $PM_{2.5}$ in Gansu Province. It is recommended to implement region-specific measures to address $PM_{2.5}$ pollution and improve the health of older adults to prevent more deaths and economic losses.

Data availability statement

The original contributions presented in the study are included in the article/supplementary material, further inquiries can be directed to the corresponding author.

Author contributions

QL: Conceptualization, Methodology, Writing—original draft. ZL: Formal analysis, Writing—original draft. YL: Methodology, Visualization, Writing—review & editing. NK: Formal analysis, Writing—review & editing. XD: Formal analysis, Writing—review & editing. YN: Visualization, Writing—original draft. YT: Conceptualization, Writing—review & editing.

Funding

The author(s) declare financial support was received for the research, authorship, and/or publication of this article. This research was supported by the Key Research and Development Program of Gansu Province (21YF5FA109), the Youth Science and Technology Fund Program of Gansu Province (20JR5RA574), and the Youth Innovation Promotion Association, Chinese Academy of Sciences (2022434).

Conflict of interest

The authors declare that the research was conducted in the absence of any commercial or financial relationships that could be construed as a potential conflict of interest.

Publisher's note

All claims expressed in this article are solely those of the authors and do not necessarily represent those of their affiliated organizations, or those of the publisher, the editors and the reviewers. Any product that may be evaluated in this article, or claim that may be made by its manufacturer, is not guaranteed or endorsed by the publisher.

References

1. Murray CJL, Aravkin AY, Zheng P, Abbafati C, Abbas KM, Abbasi-Kangevari M, et al. Global burden of 87 risk factors in 204 countries and territories, 1990-2019: a systematic analysis for the Global Burden of Disease Study 2019. *Lancet.* (2020) 396:1223–49. doi: 10.1016/S0140-6736(20)30752-2

2. Lepeule J, Laden F, Dockery D, Schwartz J. Chronic exposure to fine particles and mortality: an extended follow-up of the Harvard Six Cities study from 1974 to 2009. *Environ Health Perspect.* (2012) 120:965–70. doi: 10.1289/ehp.1104660

3. Burnett RT, Pope III CA, Ezzati M, Olives C, Lim SS, Mehta S, et al. An integrated risk function for estimating the global burden of disease attributable to ambient fine particulate matter exposure. *Environ Health Perspect.* (2014) 122:397–403. doi: 10.1289/ehp.122-A235

4. Apte JS, Marshall JD, Cohen AJ, Brauer M. Addressing global mortality from ambient $PM_{2.5}$. *Environ Sci Technol.* (2015) 49:8057–66. doi: 10.1021/acs.est.5b01236

5. Burnett R, Chen H, Szyszkowicz M, Fann N, Hubbell B, Pope III CA, et al. Global estimates of mortality associated with long-term exposure to outdoor fine particulate matter. *Proc Nat Acad Sci.* (2018) 115:9592–7. doi: 10.1073/pnas.1803222115

6. Zhang Q, Zheng Y, Tong D, Shao M, Wang S, Zhang Y, et al. Drivers of improved $PM_{2.5}$ air quality in China from 2013 to 2017. *Proc Nat Acad Sci.* (2019) 116:24463–9. doi: 10.1073/pnas.1907956116

7. Yue H, He C, Huang Q, Yin D, Bryan BA. Stronger policy required to substantially reduce deaths from $PM_{2.5}$ pollution in China. *Nat Commun.* (2020) 11:1462. doi: 10.1038/s41467-020-15319-4

8. Yin P, Brauer M, Cohen AJ, Wang H, Li J, Burnett RT, et al. The effect of air pollution on deaths, disease burden, and life expectancy across China and its provinces, 1990-2017: an analysis for the Global Burden of Disease Study 2017. *Lancet Planet Health.* (2020) 4:e386–98. doi: 10.1016/S2542-5196(20)30161-3

9. Yin H, Brauer M, Zhang JF, Cai W, Navrud S, Burnett R, et al. Population ageing and deaths attributable to ambient $PM_{2.5}$ pollution: a global analysis of economic cost. *Lancet Planetary Health.* (2021) 5:E356–67. doi: 10.1016/S2542-5196(21)00131-5

10. Guan Y, Kang L, Wang Y, Zhang NN, Ju MT. Health loss attributed to PM2.5 pollution in China's cities: Economic impact, annual change and reduction potential. *J Clean Prod.* (2019) 217:284–94. doi: 10.1016/j.jclepro.2019.01.284

11. Song CB, He JJ, Wu L, Jin T, Chen X, Li R, et al. Health burden attributable to ambient $PM_{2.5}$ in China. *Environ Pollut.* (2017) 223:575–86. doi: 10.1016/j.envpol.2017.01.060

12. Huang J, Pan XC, Guo XB, Li G. Health impact of China's air pollution prevention and control action plan: an analysis of national air quality monitoring and mortality data. *Lancet Planet Health.* (2018) 2:e313–23. doi: 10.1016/S2542-5196(18)30141-4

13. Maji KJ, Ye WF, Arora M, Nagendra SS. $PM_{2.5}$-related health and economic loss assessment for 338 Chinese cities. *Environ Int.* (2018) 121:392–403. doi: 10.1016/j.envint.2018.09.024

14. Zheng YX, Xue T, Zhang Q, Geng G, Tong D, Li X, et al. Air quality improvements and health benefits from China's clean air action since 2013. *Environ Res Lett.* (2017) 12:114020. doi: 10.1088/1748-9326/aa8a32

15. Xue T, Liu J, Zhang Q, Geng G, Zheng Y, Tong D, et al. Rapid improvement of $PM_{2.5}$ pollution and associated health benefits in China during 2013-2017. *Sci China Earth Sci.* (2019) 62:1847–56. doi: 10.1007/s11430-018-9348-2

16. Wu WJ, Yao MH, Yang XC, Hopke PK, Choi H, Qiao X, et al. Mortality burden attributable to long-term ambient $PM_{2.5}$ exposure in China: using novel exposure-response functions with multiple exposure windows. *Atmosp Environ.* (2021) 246:118098. doi: 10.1016/j.atmosenv.2020.118098

17. Li Y, Liao Q, Zhao XG, Tao Y, Bai Y, Peng L. Premature mortality attributable to $PM_{2.5}$ pollution in China during 2008-2016: underlying causes and responses to emission reductions. *Chemosphere.* (2021) 263:127925. doi: 10.1016/j.chemosphere.2020.127925

18. Li J, Liu H, Lv ZF, Zhao R, Deng F, Wang C, et al. Estimation of $PM_{2.5}$ mortality burden in China with new exposure estimation and local concentration-response function. *Environ Pollut.* (2018) 243:1710–8. doi: 10.1016/j.envpol.2018.09.089

19. Geng G, Zheng Y, Zhang Q, Xue T, Zhao H, Tong D, et al. Drivers of $PM_{2.5}$ air pollution deaths in China 2002-2017. *Nat Geosci.* (2021) 14:645–50. doi: 10.1038/s41561-021-00792-3

20. Xu L, Chen F, Zhong X, Ye R, Cai W, Rao Q, et al. Spatial disequilibrium of fine particulate matter and corresponding health burden in China. *J Clean Prod.* (2019) 238:117840. doi: 10.1016/j.jclepro.2019.117840

21. Xu M, Qin Z, Zhang S, Xie Y. Health and economic benefits of clean air policies in China: a case study for Beijing-Tianjin-Hebei region. *Environ Pollut.* (2021) 285:117525. doi: 10.1016/j.envpol.2021.117525

22. Chen Y, Zang L, Du W, Xu D, Shen G, Zhang Q, et al. Ambient air pollution of particles and gas pollutants, and the predicted health risks from long-term exposure to $PM_{2.5}$ in Zhejiang province, China. *Environ Sci Pollut Res.* (2018) 25:23833–44. doi: 10.1007/s11356-018-2420-5

23. Lu XC, Chen Y, Huang YQ, Chen D, Shen J, Lin C, et al. Exposure and mortality apportionment of $PM_{2.5}$ between 2006 and 2015 over the Pearl River Delta region in southern China. *Atmos Environ.* (2020) 231:117512. doi: 10.1016/j.atmosenv.2020.117512

24. Han CL, Xu RB, Ye TT, Xie Y, Zhao Y, Liu H, et al. Mortality burden due to long-term exposure to ambient $PM_{2.5}$ above the new WHO air quality guideline based on 296 cities in China. *Environ Int.* (2022) 166:107331. doi: 10.1016/j.envint.2022.107331

25. Xie R, Sabel CE, Lu X, Zhu W, Kan H, Nielsen CP, et al. Long-term trend and spatial pattern of $PM_{2.5}$ induced premature mortality in China. *Environ Int.* (2016) 97:180–6. doi: 10.1016/j.envint.2016.09.003

26. Maji KJ. Substantial changes in $PM_{2.5}$ pollution and corresponding premature deaths across China during 2015-2019: a model prospective. *Sci Total Environ.* (2020) 729:138838. doi: 10.1016/j.scitotenv.2020.138838

27. Guan QY, Cai A, Wang FF, Yang L, Xu C, Liu Z. Spatio-temporal variability of particulate matter in the key part of Gansu Province, Western China. *Environ Poll.* (2017) 230:189–98. doi: 10.1016/j.envpol.2017.06.045

28. NCEP (National Center for Atmospheric Research)/National Weather Service/NOAA/US Department of Commerce. *NCEP FNL Operational Model Global Tropospheric Analyses, Continuing From July 1999.* (2000). Available online at: http://rda.ucar.edu/datasets/ds083.2 (accessed March 6, 2023).

29. Buchholz RR, Emmons LK, Tilmes S. *CESM21/CAM-chem Instantaneous Output for Boundary Conditions UCAR/NCAR - Atmospheric Chemistry Observations and Modeling Laboratory* (2019). doi: 10.5065/NMP7-EP60

30. *MEIC (Multi-resolution Emission Inventory model for Climate and Air Pollution Research).* (2021). Available online at: http://www.meicmodel.org (accessed March 10, 2023).

31. Wiedinmyer C, Akagi SK, Yokelson RJ, Emmons LK, Al-Saadi JA, Orlando JJ, et al. The Fire INventory from NCAR (FINN): a high resolution global model to estimate the emissions from open burning. *Geosci Model Dev.* (2011) 4:625–41. doi: 10.5194/gmd-4-625-2011

32. Guenther A, Karl T, Harley P, Wiedinmyer C, Palmer PI, Geron C. Estimates of global terrestrial isoprene emissions using MEGAN (Model of Emissions of Gases and Aerosols from Nature). *Atmosp Chem Phys.* (2006) 6:3181–210. doi: 10.5194/acp-6-3181-2006

33. LeGrand SL, Polashenski C, Letcher TW, Creighton GA, Peckham SE, Cetola JD. The AFWA dust emission scheme for the GOCART aerosol model in WRF-Chem v381. *Geosci Model Dev.* (2019) 12:131–66. doi: 10.5194/gmd-12-131-2019

34. Boylan JW, Russell AG. PM and light extinction model performance metrics, goals, and criteria for three-dimensional air quality models. *Atmos Environ.* (2006) 40:4946–59. doi: 10.1016/j.atmosenv.2005.09.087

35. Zhang Y, Zhang X, Wang L, Zhang Q, Duan F, He K. Application of WRF/Chem over East Asia: Part I. Model evaluation and intercomparison with MM5/CMAQ. *Atmosp Environ.* (2016) 124:285–300. doi: 10.1016/j.atmosenv.2015.07.022

36. Gansu Province Bureau of Statistics, and Survey Office of the National Bureau of Statistics in Gansu. *Gansu Development Yearbook 2020.* Beijing: China Statistics Press (2020).

37. National Center for Chronic and Noncommunicable Disease Control and Prevention, Chinese Center for Disease Control and Prevention, Center for Health Statistics and Information, National Health Commission. *National Cause-of-Death Surveillance Dataset 2019.* Beijing: China Science and Technology Press (2019).

38. Yao M, Wu G, Zhao X, Zhang J. Estimating health burden and economic loss attributable to short-term exposure to multiple air pollutants in China. *Environ Res.* (2020) 183:109184. doi: 10.1016/j.envres.2020.109184

39. Jin YN, Andersson H, Zhang SQ. Do preferences to reduce health risks related to air pollution depend on illness type? Evidence from a choice experiment in Beijing, China. *J Environ Econ Manag.* (2020) 103:102355. doi: 10.1016/j.jeem.2020.102355

40. OECD (Organization for Economic Co-operation and Development). *The Cost of Air Pollution: Health Impacts of Road Transport.* Paris: OECD Publishing (2014).

41. National Bureau of Statistics of China. *China Statistical Yearbook 2017.* Beijing: China Statistics Press (2017).

42. Yang XL, Chen L, Zhang YH, Wang S. Variation characteristic of sand-dust days and its relationship with meteorological factors in east of Hexi corridor. *Res Environ Sci.* (2018) 31:1373–81. doi: 10.13198/j.issn.1001-6929.2018.05.10

43. Zhang J, Ju T, Li B, Li C, Wang J, Xia X, et al. Spatial and temporal distribution characteristics and transport path analysis of regional particulate matter over Gansu Province. *China Environ Sci.* (2021) 41:3990–4000.

44. Zheng S, Schlink U, Ho KF, Singh RP, Pozzer A. Spatial distribution of $PM_{2.5}$-related premature mortality in China. *GeoHealth.* (2021) 5:e2021GH000532. doi: 10.1029/2021GH000532

45. Zhou MG, Wang HD, Zeng XY, Yin P, Zhu J, Chen W, et al. Mortality, morbidity, and risk factors in China and its provinces, 1990-2017: a systematic

analysis for the Global Burden of Disease Study 2017. *Lancet.* (2019) 394:1145–58. doi: 10.1016/S0140-6736(19)30427-1

46. Tang R, Zhao J, Liu Y, Huang X, Zhang Y, Zhou D, et al. Air quality and health co-benefits of China's carbon dioxide emissions peaking before 2030. *Nat Commun.* (2022) 13:1008. doi: 10.1038/s41467-022-28672-3

47. United Nations, Department of Economic and Social Affairs, Population Division. *World Population Prospects 2022*. New Yorkm NY: United Nations (2022).

48. Guan Y, Xiao Y, Wang Y, Zhang N, Chu C. Assessing the health impacts attributable to $PM_{2.5}$ and ozone pollution in 338 Chinese cities from 2015 to 2020. *Environ. Pollut.* (2021) 287:117623. doi: 10.1016/j.envpol.2021.117623

49. Li Y, Liao Q, Zhao XG, Bai Y, Tao Y. Influence of $PM_{2.5}$ pollution on health burden and economic loss in China. *Environ Sci.* (2021) 42:1688–95. doi: 10.13227/j.hjkx.202008313

50. Xue T, Zhu T, Zheng YX, Liu J, Li X, Zhang Q. Change in the number of $PM_{2.5}$-attributed deaths in China from 2000 to 2010: comparison between estimations from census-based epidemiology and pre-established exposure-response functions. *Environ Int.* (2019) 129:430–7. doi: 10.1016/j.envint.2019.05.067

51. Wang H, Mullahy J. Willingness to pay for reducing fatal risk by improving air quality: a contingent valuation study in Chongqing, China. *Sci Total Environ.* (2006) 367:50–7. doi: 10.1016/j.scitotenv.2006.02.049

52. Hoffmann S, Krupnick A, Qin P. Building a set of internationally comparable value of statistical life studies: estimates of Chinese willingness to pay to reduce mortality risk. *J Benefit Cost Anal.* (2017) 8:251–89. doi: 10.1017/bca.2017.16

53. Yang Z, Liu P, Xu X. Estimation of social value of statistical life using willingness-to-pay method in Nanjing, China. *Accid Anal Prevent.* (2016) 95:308–16. doi: 10.1016/j.aap.2016.04.026

frontiers | Frontiers in Public Health

TYPE Original Research
PUBLISHED 11 January 2024
DOI 10.3389/fpubh.2023.1322666

Check for updates

OPEN ACCESS

EDITED BY
Shupeng Zhu,
Zhejiang University, China

REVIEWED BY
Shamali De Silva,
Environmental Protection Authority (EPA), Australia
Chen Li,
Shanghai University of Engineering Sciences, China
Jinlai Wei,
Fujifilm Irvine Scientific, Inc., United States

*CORRESPONDENCE
Wenhao Xue
xuewh@mail.bnu.edu.cn

RECEIVED 16 October 2023
ACCEPTED 07 December 2023
PUBLISHED 11 January 2024

CITATION
Xu Q, Wang L, Hou H, Han Z and Xue W (2024) Does environmental regulation lessen health risks? Evidence from Chinese cities.
Front. Public Health 11:1322666.
doi: 10.3389/fpubh.2023.1322666

Does environmental regulation lessen health risks? Evidence from Chinese cities

Qingqing Xu[1], Liyun Wang[1], Hanxue Hou[1], ZhengChang Han[2] and Wenhao Xue[1]*

[1]School of Economics, Qingdao University, Qingdao, China, [2]ShanDong ZhengYuan Geophysical Information Technology Co., Ltd., Jinan, China

Introduction: Atmospheric pollution is a severe problem confronting the world today, endangering not only natural ecosystem equilibrium but also human life and health. As a result, governments have enacted environmental regulations to minimize pollutant emissions, enhance air quality and protect public health. In this setting, it is critical to explore the health implications of environmental regulation.

Methods: Based on city panel data from 2009 to 2020, the influence of environmental regulatory intensity on health risks in China is examined in this study.

Results: It is discovered that enhanced environmental regulation significantly reduces health risks in cities, with each 1-unit increase in the degree of environmental regulation lowering the total number of local premature deaths from stroke, ischemic heart disease, and lung cancer by approximately 15.4%, a finding that remains true after multiple robustness tests. Furthermore, advances in science and technology are shown to boost the health benefits from environmental regulation. We also discover that inland cities, southern cities, and non-low-carbon pilot cities benefit more from environmental regulation.

Discussion: The results of this research can serve as a theoretical and empirical foundation for comprehending the social welfare consequences of environmental regulation and for guiding environmental regulation decision-making.

KEYWORDS

environmental regulation, integrated exposure-response model, health risk, two-way fixed effects model, $PM_{2.5}$

1 Introduction

China has implemented a development strategy dominated by heavy industry since the initiation of reform and opening. This strategy has contributed to rapid economic expansion but has also been accompanied by several challenges. Particularly the large amount of pollutants emitted by industrial activities seriously harmed air quality and risked people's health and well-being (1, 2). According to the Report on the State of the Ecology and Environment in China 2020, 135 of China's 337 cities had substandard air quality in 2020, with these numbers accounting for 40% of the total number of cities. Such poor environmental conditions have caused economic losses in China ranging from 8 to 15% of GDP and have jeopardized people's health rights and interests. Residents' long-term exposure to high levels of fine particulate matter ($PM_{2.5}$) has been found to increase the incidence of stroke, ischemic heart disease, and lung cancer in epidemiological studies

(3–5). As a result, the conflict between air pollution and residents' health is becoming increasingly visible, and it has become a practical concern that cannot be disregarded in China's growth. Additionally, enhancing environmental governance to alleviate air pollution has emerged as a widely shared concern. Consequently, the Chinese government has introduced several regulations and practices to control and supervise the pollution-emitting behaviors of enterprises and individuals to alleviate the air pollution issue. For example, the Law on the Prevention and Control of Atmospheric Pollution was enacted by the Chinese government in 1987 to provide a legal basis for environmental regulation (6), followed by the Cleaner Production Promotion Law in 2003 to enhance the environmental friendliness of industrial production (7). In 2006, the Chinese government broke down the emission reduction targets for the provincial administrative regions, achieving the shift from concentration control to total pollutant amount control. As a result, environmental regulation transitioned from "soft constraints" to "hard constraints" (8), with the adoption of administrative orders or government performance assessment.

The concept of "regulation" was introduced by the American economist Kahn in his book The Economics of Regulation: Principles and Institutions (9), where he defined it as an institutional arrangement that substitutes government directives for market competition to achieve good economic performance. With the growing environmental problems resulting from the crude economic model, environmental regulation has become a significant branch of regulatory economics (10). Environmental regulation refers to the government's direct or indirect control and management of pollution sources to improve the quality of the ecological environment (11). The intensity of environmental regulation is often indirectly measured by some alternative indicators, such as industrial emissions (12), pollution control investment (13), and operating costs (14). These indicators have facilitated research on environmental regulation in the area of air pollution.

The function of environmental regulation in decreasing pollution has been well supported by evidence, and various viewpoints and levels have been adopted to examine the influence of environmental regulations and policies on pollution emissions in China. For example, Du and Li (15), Feng et al. (16), and Zhang et al. (17) analyzed the emissions of CO_2 and $PM_{2.5}$ from industrial businesses, cities, and regions, respectively, and discovered that environmental regulations can effectively lower these pollutants, especially in the eastern, central, and northeastern areas. Yu et al. (18) assessed the impact of the Air Pollution Prevention and Control Action Plan on the emissions of $PM_{2.5}$ and SO_2 from Chinese cities, and the results indicated that these policies can significantly improve air quality. Using a time-varying difference-in-difference (DID) model, Liu et al. (19) demonstrated that China's low-carbon city pilot policy effectively reduced CO_2 emissions in the pilot cities, but the effects varied across regions and administrative levels. Hu et al. (20) found that environmental protection taxes can significantly reduce air pollutants such as $PM_{2.5}$, SO_2, NOx, and CO in areas with large economic and industrial sectors with high emission intensities in the short term, as well as offering substantial co-benefits in global climate change mitigation. Meanwhile, the health benefits of environmental regulation have attracted scholarly attention as regulatory intensity has increased. The majority of the researchers argue that environmental regulation reduces health risks and mortality rates. For instance, a study conducted in China revealed that the infant mortality rates in the "two control zones" with stringent environmental regulation declined by 20% compared to other zones (21). Similarly, a study in the United States demonstrated that the shutdown of coal-fired power plants significantly decreased the percentage of low-birth-weight and preterm infants by 15 and 28 percent, respectively, in the downwind states (22). Employing the difference-in-differences (DID) model, Xu et al. (23) examined the impact of the Eleventh Five-Year Plan's environmental regulations on human health, discovering that environmental regulations reduce the risk of injury or illness among adults by 9.2 percent, with this effect being more pronounced among males, rural residents, and low-income households. Zhou et al. (24) also demonstrated that more stringent environmental regulations for businesses benefit public health. Similarly, Zhang et al. (25) examined the influence of atmospheric environmental policy on public health, demonstrating that it decreases the intensity of soot emissions and mitigates the detrimental health effects of air pollution. However, other research has implied that there is a critical value between environmental regulation and public health rather than a simple linear link: if the critical value is exceeded, environmental regulation may lead to negative economic and social consequences, such as lowering economic growth, increasing unemployment and poverty, widening the urban–rural income gap, and undermining economic efficiency, all of which have an indirect negative impact on population health (26).

Although, as mentioned earlier, studies have been conducted to examine the influence of environmental regulation on health, they are still limited and are still at the exploratory stage, with few studies probing the underlying mechanisms. Additionally, the impact of regional heterogeneity factors, such as geographic location and environmental patterns, on the health benefits of environmental regulation has tended to be overlooked in previous studies. For example, cities in different geographical locations may suffer from different levels and types of air pollution problems, necessitating different intensities and forms of environmental regulatory policies; similarly, cities with diverse environmental patterns may have varying levels of air quality and environmental governance. These characteristics of regional heterogeneity may affect the applicability and effectiveness of environmental regulation, leading to different health benefits. For this reason, by utilizing data on stroke (STK), ischemic heart disease (IHD), and lung cancer (LC) as the health endpoints for $PM_{2.5}$ health risk assessment, this study explores the effect of environmental regulation on health risk through a two-way fixed effects model. Next, the moderating role of technological innovation in the health benefits of environmental regulation is explored. Moreover, we investigate the implications of city heterogeneity characteristics on the health advantages of environmental regulation by analyzing factors based on regional location and environmental differences. The findings of this study can provide useful scientific evidence and an important frame of reference for the formulation of more strategic and sound environmental regulatory policies and for the enhancement of the health benefits stemming from environmental regulation. This study thus has both theoretical and practical relevance.

The rest of this paper is structured as follows: The study area of the research is presented in Section 2. Section 3 discusses the data sources, variable selection, and model development. Section 4 reports the results of the benchmark regression, instrumental variable model, robustness, mechanism effects, and heterogeneity analyses, as well as

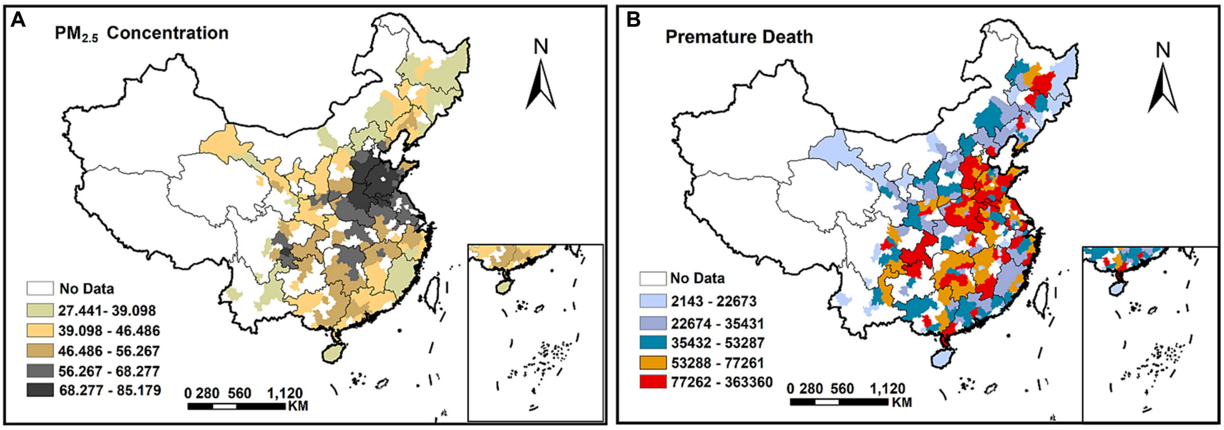

FIGURE 1
The spatial distribution in China for $PM_{2.5}$ concentrations **(A)** and the number of premature deaths (estimated by the integrated exposure-response model) from STK, IHD, and LC **(B)**.

their interpretation and analysis. Section 5 summarizes the findings, and policy recommendations are presented therein.

2 Materials and methods

2.1 Study area

There are 279 cities in mainland China included in the study area, and the study duration spans the years 2009–2020. Figure 1 depicts the study area's spatial distribution, with (a) the $PM_{2.5}$ concentration levels in each Chinese city and (b) the number of premature deaths from the three diseases of STK, IHD, and LC estimated by the integrated exposure-response model.

2.2 Data and variable selections

2.2.1 Explained variable

In this paper, three common attributable deaths from circulatory and respiratory diseases were chosen as health endpoints, e.g., stroke (STK, International Classification of Diseases Revision 10 code/ ICD-10: 160–169), ischemic heart disease (IHD, ICD-10: 120–125), and lung cancer (LC, ICD-10: C33–C34). According to Dai et al. (27) and Burnett et al. (28), the relative mortality risk of these three health endpoints due to $PM_{2.5}$ exposure was calculated using the integrated exposure-response (IER) model (Equations 1–3), and the corresponding number of premature deaths was estimated and used as the explanatory variables in this study. The specific algorithm is as follows:

Step 1: Calculation of relative mortality risk

$$RR_i(K) = \begin{cases} 1, & K \le K_0 \\ 1 + \alpha\left\{1 - \exp\left[-\gamma\left(K - K_0\right)^{\delta}\right]\right\}, & K > K_0 \end{cases} \tag{1}$$

The relative health risk of $PM_{2.5}$-producing disease i(i=1, 2, 3) at concentration K is denoted by $\mathrm{RR}_i(K)$. K_0 indicates the health effect threshold; when the $PM_{2.5}$ concentration is below K_0, there is no negative health effect and $\mathrm{RR}_i(K)=1$; however, when the concentration crosses the threshold, the relative risk increases with increasing concentration, with $RR_i(K) = 1 + \alpha\left\{1 - \exp\left[-\gamma\left(K - K_0\right)^{\delta}\right]\right\}$. The values of the parameters in Equation (1) are shown in Table 1 and are based on the research of Lee et al. (29).

Step 2: Estimation of the number of premature deaths.

$$\mathrm{ED}_i = \left(1 - 1/\mathrm{RR}_i\right) \times D_i \times P \tag{2}$$

$$\mathrm{ED} = \sum_{i=1}^{3} \mathrm{ED}_i \tag{3}$$

where ED_i denotes the premature deaths from disease i induced by outdoor $PM_{2.5}$ exposure, ED indicates the total number of premature deaths from STK, IHD, and LC, P is the number of people exposed to a given pollution concentration, and D_i refers to the baseline mortality rate for each disease for the year.

The $PM_{2.5}$ concentration data employed in this paper were obtained from the China High Air Pollutants (CHAP) database[1] (30, 31) and were collected using satellite remote sensing and machine learning technologies at high temporal and spatial resolutions of 1 day and 1 kilometer, respectively. The baseline mortality rate was derived from the National Bureau of Statistics of China data, with mortality rates for various disease categories being counted in both urban and rural areas. For this reason, the population-wide baseline mortality rates for each disease from 2009 to 2020 were calculated by employing the statistical ratios of the urban and rural populations to the total population as weights (32). The ED was logarithmized in this study to eliminate the disturbance of heteroskedasticity. The descriptive statistics for the selected variables in the model are displayed in Table 2. During the period 2009–2020, the average number of premature deaths from the three diseases that were induced by

1 https://weijing-rs.github.io/product.html

TABLE 1 Coefficients in model [Equation (1)].

	STK	IHD	LC
K_0 (μg/m³)	8.38	6.96	7.24
α	1.01	0.843	159
γ	0.0164	0.0724	0.000119
δ	1.14	0.544	0.735

TABLE 2 The results of descriptive statistics.

Variable	Unit	*N*	Mean	S. D.	Min	Max
ED	People	3,316	50,004	38,002	1,651	413,864
ER	–	3,336	0.191	0.068	0.046	0.875
RGDP	10^4CNY	3,347	1.380	0.892	0.004	14.520
PD	People/km²	3,348	444.460	344.701	4.971	3239.860
TIV	%	3,348	41.058	10.083	14.360	83.870
FSR	%	3,344	0.457	0.224	0.041	1.541
NH	–	3,329	185.441	178.006	8.000	3052.000
AR	MJ/m²	3,348	12.333	1.179	8.396	16.235
AN	–	3,069	0.499	0.136	0.059	0.780
AP	m	3,348	0.003	0.002	<0.001	0.008
AT	k	3,348	287.7	5.327	273.9	299.1

outdoor $PM_{2.5}$ exposure in China was 50,004, with a maximum value of 413,864. These numbers indicates that air pollution and related health risks are still quite serious in China.

2.2.2 Explanatory variable

Environmental regulation intensity (ER) is the explanatory variable in this research. Three indicators reflecting the level of environmental protection were chosen to capture the environmental regulation intensity of different cities (33), e.g., the comprehensive utilization rate of industrial solid waste, the centralized sewage treatment rate, and the rate of harmless treatment of domestic garbage (34). Specifically, the comprehensive utilization rate of industrial solid waste is calculated as the ratio of the comprehensively utilized industrial solid waste to the sum of the generated industrial solid waste and the comprehensively utilized storage in previous years. The rate of centralized sewage treatment is determined as the ratio of the wastewater discharged that uses centralized wastewater treatment to the total wastewater discharged. The rate of harmless treatment of domestic waste is stated as the ratio of the domestic garbage that is harmlessly disposed of to the domestic garbage created.

The entropy weighting technique, a method that can eliminate the involvement of subjective factors, was employed to identify the weights of each indicator. Then, the indicators were multiplied by their corresponding weights after normalization, and the resulting composite environmental regulatory intensity index was calculated. This composite index can reflect the degree of importance attached to environmental problems and the effectiveness of response measures in different regions. Namely, the higher the index value is, the greater the environmental regulation intensity and the importance attached to environmental protection. Data for the environmental regulation intensity are gathered from the China City Statistical Yearbook.

2.2.3 Control variable

In this research, control variables for both socioeconomic factors and natural elements are incorporated into the empirical analysis. Control variables for socioeconomic characteristics include real GDP *per capita* (*RGDP*), population density (*PD*), tertiary industry value added as a share of GDP (*TIV*), financial self-sufficiency rate (*FSR*), and number of hospitals and health centers (*NH*) (35, 36), with these variables being based on data from the China Urban Statistical Yearbook (CUSY). For natural components, the control variables include annual radiation (*AR*), annual normalized difference vegetation index (*AN*), annual precipitation (*AP*), and annual temperature (*AT*) (37, 38), with data gathered from the European Center for Medium-Range Weather Forecasts (ECMWF) ERA5 dataset (39). The variables are addressed in light of previous studies as follows: Real GDP *per capita* is calculated with deflator-adjusted GDP *per capita* (i.e., the ratio of nominal GDP to real GDP), thus eliminating the effect of the inflation factor (40). The fiscal self-sufficiency rate is expressed in terms of the proportion of local budget revenues to expenditures (41). The missing data are filled in by interpolation. Logarithmic transformation is used for processing non-ratio-type data to limit heteroskedasticity and ensure the uniformity of variables in the order of magnitude. Following the aforementioned processing, this study compiles a robust collection of fundamental data for empirical investigation.

2.2.4 Mechanism variable

The degree of science and technology is incorporated into the study framework to investigate the potential factors that influence the health advantages of environmental regulation. Specifically, the level of scientific and technological development (*TE*), expressed as the ratio of fiscal expenditure for science to fiscal revenue (42), reflects a region's capacity for scientific and technological innovation as well as the degree of scientific and technological support for environmental governance, with higher ratios suggesting higher investment in scientific and technological development and a greater contribution of science and technology to environmental governance. The information for this variable was obtained from the China Urban Statistical Yearbook.

2.3 Methodology

2.3.1 Benchmark regression model

In this research, a two-way fixed effects model is constructed to evaluate the health implications of environmental regulation, with the particular model established as follows:

$$D_{it} = \alpha + \beta ER_{it} + \gamma X_{it} + \vartheta_i + \varphi_t + \varepsilon_{it} \tag{4}$$

where D_{it} denotes the total number of STK, IHD, and LC premature deaths induced by outdoor $PM_{2.5}$ exposure in city *i* in year *t*. ER_{it} is the environmental regulation intensity index in city *i* in year *t*. X_{it} represents the set of control variables. The city-and time-fixed effects are denoted by ϑ_i and φ_t, respectively, and the random error term is denoted by ε_{it}. The coefficient β is the focus of this research, responding to the implications of environmental regulation on health risk (number of premature deaths). Additionally, the flowchart of the empirical exploration for this study is depicted in Figure 2.

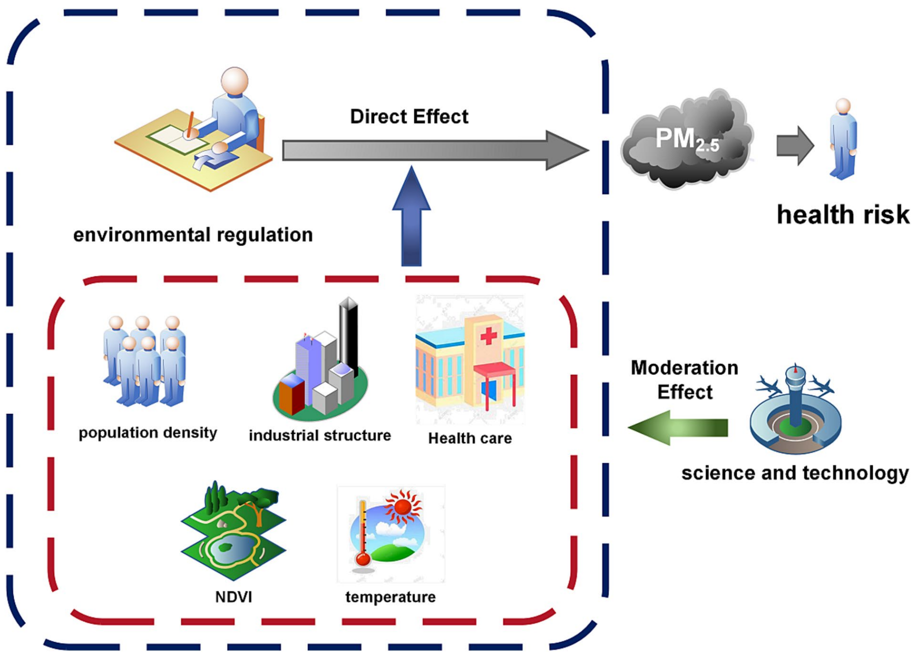

FIGURE 2
The overall process structure of the empirical model.

2.3.2 Mechanism analysis

To examine the role of science and technology as a mechanism variable, we integrated the interaction term between science and technology level (*TE*) and the environmental regulation intensity index (*ER*) in the analytical model and developed Equation (5) for regression:

$$D_{\mathrm{it}} = \alpha + \beta \mathrm{ER}_{it} + \rho \mathrm{TE}_{\mathrm{it}} \times \mathrm{ER}_{\mathrm{it}} + \gamma X_{\mathrm{it}} + \vartheta_i + \varphi_t + \varepsilon_{\mathrm{it}} \quad (5)$$

where $\mathrm{TE}_{\mathrm{it}}$ represents the mechanism variable, i.e., the level of science and technology, and the remaining variables are identical to those in Equation (4). The statistical significance of the coefficient ρ was examined to evaluate the influence of science and technology on the health outcomes of environmental regulation. As a result, the significance of *TE* as a moderating variable will be captured here.

3 Results and discussion

3.1 Results of descriptive analysis

As shown in Figure 1, areas of heavy $PM_{2.5}$ pollution and areas of high premature deaths have a high level of spatial overlap, primarily in economically developed areas such as the North China Plain and the Yangtze River Delta. Notably, the higher the $PM_{2.5}$ concentration is, the greater the number of premature deaths, with a clear positive correlation between the two.

3.2 Overall effect

Table 3 illustrates the impact of environmental regulations on health risk. Column (1) adjusts for city-and time-fixed effects. Column (2) incorporates control variables for economic and social aspects. Column (3) adds extra control variables for natural factors. It can be seen that the *ER* coefficients are negative and statistically significant ($p < 0.05$) in all models (Columns 1–3), demonstrating that increased environmental regulation intensity effectively decreases health risks. In particular, the coefficient of *ER* is-0.154 ($p < 0.05$) in the most refined model (Column 3), and there is no substantial variations in the size or significance level of the coefficient when this model is compared to the other two models, indicating that the results showing the adverse impact of environmental regulation on health risk are robust. The increased intensity of environmental regulation has raised the environmental awareness and behavior of enterprises and residents. This encourages them to adopt more energy-efficient and emission-reducing production methods as well as more environmentally friendly lifestyles, thus lowering the level of industrial pollutant emissions and pollution from anthropogenic activities (43, 44); furthermore, it has also facilitated the development and application of green technologies, such as clean energy (45), resulting in lower energy consumption. All these factors contribute to lower air pollutants such as $PM_{2.5}$, improving air quality, and reducing the risk of disease and death.

Moreover, there are some noticeable outcomes from the control variables. Population density and the number of hospitals and health centers are both positively associated with health risks, with coefficients of 0.364 ($p < 0.05$) and 0.041 ($p < 0.01$), respectively. In contrast, the value added for tertiary industry as a proportion of GDP was adversely associated with health risk, with a coefficient of −0.001 ($p < 0.05$). This is because human activities unavoidably degrade the environment as the population density of a city rises, which in turn leads to an increase in the risk of disease for residents (46). The number of hospitals and health centers in a city reflects the level of medical resources and the capacity of public health

TABLE 3 The results of the baseline regression.

	(1)	(2)	(3)
	ED	ED	ED
ER	−0.296***	−0.273***	−0.154**
	(−3.18)	(−3.41)	(−2.34)
RGDP		−0.043***	−0.005
		(−4.04)	(−0.65)
LnPD		0.707***	0.364**
		(3.44)	(1.99)
TIV		−0.003***	−0.001**
		(−3.34)	(−2.36)
FSR		−0.075**	−0.043
		(−2.11)	(−1.52)
LnNH		0.066***	0.041***
		(5.77)	(4.46)
LnAR			−0.025
			(−0.37)
LnAN			−0.722***
			(−5.07)
LnAP			2.274
			(0.69)
LnAT			4.922***
			(3.73)
_cons	10.621***	6.403***	−19.156**
	(595.00)	(5.41)	(−2.53)
City FE	Yes	Yes	Yes
Time FE	Yes	Yes	Yes
N	3,316	3,313	3,035
R^2	0.982	0.985	0.993

t statistics in parentheses; *$p < 0.10$, **$p < 0.05$, ***$p < 0.01$.

services; however, there is a positive correlation between the number of hospitals and health risks, which may indicate that there is a high demand for medical services among the population, but the distribution of urban health care resources is unbalanced, which leads to a poorer health in some areas or populations. In addition, the service-led tertiary industry is less damaging to the environment than the secondary industry, and the higher the proportion of the tertiary industry's value added in GDP, the more it indicates that the industrial structure has been optimized and industrial pollution emissions have been relatively reduced, resulting in a reduction in health risks. For natural factors, there is a promotive association between annual temperature and health risk with a coefficient of 4.922 ($p < 0.01$). Annual normalized difference vegetation index (NDVI), in contrast, was shown to be adversely connected with health risk with a coefficient of-0.722 ($p < 0.01$). The reason for this is that a higher NDVI indicates greater vegetation cover, which can capture and immobilize atmospheric particles such as $PM_{2.5}$ and PM_{10} via structures such as sticky substances and capillaries on the surface of leaves, reducing the concentration of these particles in the air and thus effectively lowering the human health risk caused by outdoor $PM_{2.5}$ pollution (47).

3.3 Robustness check

3.3.1 Endogenous treatment

The composite index of environmental regulation lagged by one period is employed as an instrumental variable for two-stage least squares (2SLS) estimation to address the potential endogeneity due to missing variables. This model has an *F* value of 385.88 in the first-stage regression, which is higher than 10 and passes the significance test at the 1% level, demonstrating that there is no issue of a weak instrumental variable (48). Additionally, the estimation results of the second stage are shown in Column (1) of Table 4. These results reveal that environmental regulation exerts a significant negative influence on health risk, and that the total number of premature deaths in STK, IHD, and LC caused by outdoor $PM_{2.5}$ pollution will be reduced by 14.7% with a 1-unit increase in the level of environmental regulation, suggesting that, after accounting for probable endogeneity, the dampening consequence of increasing the intensity of environmental regulation on health risks remains significant, which is aligned with the findings of the preceding analysis.

3.3.2 Replacement of explanatory variable measures

The entropy weight technique is employed in the baseline regression model to obtain a composite index of environmental regulation intensity. To confirm the validity of the estimates, the environmental regulation composite index (*ER1*) is also calculated using the equal-weight approach and replaces the original explanatory variables with it to conduct another regression analysis. The regression results after replacing the explanatory variable measurement method are available in Column (2) of Table 4. The coefficient of *ER1* is-0.154 ($p < 0.05$), demonstrating that the effect of the environmental regulation composite index on health risk, whether calculated by entropy or equal weighting, is negative and significant with a similar coefficient magnitude, thus confirming the robustness of the baseline regression outcomes of this study.

3.3.3 Excluding data from four municipalities

Given the large differences in administrative levels and socioeconomic development environments between the four municipalities (Beijing, Chongqing, Shanghai, and Tianjin) and other cities, these four municipalities are separated from the full sample in this study and then the regression analyses are carried out again to exclude the possible influence of these factors on the benchmark regression findings (49). Column (3) of Table 4 displays the regression results after removing the data from the four municipalities. Notably, these results are not appreciably distinct from the results of the baseline regression, with the coefficient of *ER* being-0.155 ($p < 0.05$), confirming that the core findings of the research are reliable.

3.3.4 Excluding the interference of outliers

This study winsorizes the extreme values of continuous variables to weaken the impact of outliers on the empirical analysis by replacing the values at the 1 and 99% quartiles with the corresponding truncated values, which preserves the majority of the distributional

TABLE 4 The results of the robustness test.

	(1)	(2)	(3)	(4)	(5)
	ED	ED	ED	ED	ED
*ER*1		−0.154**			
		(−2.34)			
ER	−0.147**		−0.155**	−0.208***	−0.123*
	(−2.14)		(−2.36)	(−2.78)	(−1.92)
RGDP	−0.005	−0.005	−0.005	−0.009	−0.006
	(−0.68)	(−0.65)	(−0.61)	(−1.39)	(−0.98)
LnPD	0.386**	0.364**	0.363**	0.280	0.285
	(2.12)	(1.99)	(1.99)	(1.48)	(1.54)
TIV	−0.001**	−0.001**	−0.001**	−0.001**	−0.001
	(−2.46)	(−2.36)	(−2.39)	(−2.20)	(−1.62)
FSR	−0.037	−0.043	−0.044	−0.043	−0.026
	(−1.31)	(−1.52)	(−1.54)	(−1.41)	(−0.95)
LnNH	0.039***	0.041***	0.041***	0.048***	0.033***
	(4.38)	(4.46)	(4.46)	(4.79)	(3.77)
LnAR	−0.016	−0.025	−0.029	−0.005	−0.013
	(−0.23)	(−0.37)	(−0.43)	(−0.08)	(−0.20)
LnAN	−0.664***	−0.722***	−0.713***	−0.732***	−0.491***
	(−4.81)	(−5.07)	(−4.95)	(−5.20)	(−3.54)
LnAP	3.009	2.274	2.032	3.420	8.471***
	(0.84)	(0.69)	(0.62)	(0.99)	(2.92)
LnAT	5.158***	4.922***	4.940***	3.790***	4.855***
	(4.03)	(3.73)	(3.69)	(2.87)	(3.55)
_cons	−19.736***	−19.156**	−19.260**	−12.328	−18.437**
	(−2.72)	(−2.53)	(−2.51)	(−1.63)	(−2.43)
City FE	Yes	Yes	Yes	Yes	Yes
Time FE	Yes	Yes	Yes	Yes	Yes
N	2,759	3,035	2,991	3,035	2,756
R^2	0.993	0.993	0.993	0.993	0.994

t statistics in parentheses; $*p<0.10$, $**p<0.05$, $***p<0.01$.

characteristics of the data and eliminates the interference of outliers. The findings of the second regression analysis are provided in Column (4) of Table 4. The parameter estimates and significance levels do not change substantially from the baseline regression findings, with the coefficient of *ER* on health risk being −0.208 ($p<0.01$), confirming the validity of the baseline regression results.

3.3.5 Excluding the interference of the COVID-19 pandemic

The COVID-19 pandemic has posed a global public health emergency with far-reaching economic, social, and environmental impacts for all countries. During the COVID-19 outbreak, China adopted a sequestration strategy, which led to changes in $PM_{2.5}$ concentrations. Concurrently, respiratory infection mortality increased surged. These factors influenced the health risk index we computed and confounded the results of the general analysis for the health benefits of environmental regulation. Therefore, to eliminate the potential influence of the COVID-19 pandemic on the empirical findings of this study, the observations for the years 2019–2020 were eliminated from the sample, and then a regression analysis was performed. As indicated in Column (5) of Table 4, with a coefficient of −0.123, *ER* is statistically significant at the 10% level, implying that an increase in the intensity of environmental regulation still significantly decreases health risks after controlling for potential data bias introduced by the COVID-19 pandemic.

3.4 Moderating effect of science and technology

According to the research findings, increasing the intensity of environmental regulation has a significant impact on lowering premature deaths due to the effect on $PM_{2.5}$ and minimizing health risks. Based on this, with empirical evidence and theoretical modeling, the moderating role of science and technology in the relationship between environmental regulation and health risk will be examined in this section.

The regression results of the moderated effects model are displayed in Table 5. Specifically, the coefficient of the interaction term between the level of scientific and technological development and the intensity of environmental regulation is −8.723 with a statistically significant level of 10%, indicating that scientific and technological advancement enhances the health risk reduction effect of environmental regulation. A higher proportion of fiscal expenditure on scientific activities to fiscal revenue indicates that the area values scientific and technological innovation and is more capable of offering technical assistance and solutions for environmental preservation (50). Specifically, by promoting major technological innovations and transformative applications such as ecological product design, cleaner production processes, utilization of industrial linkages, and coordinated regional waste disposal and utilization, the advancement of science and technology facilitates the reduction of pollutants at the source and supports the efficient recycling and utilization of resources at multiple levels (51). In addition, real-time monitoring and analysis of air quality, pollution sources, and emissions can be achieved using scientific and technological means such as digital techniques, remote sensing techniques, and artificial intelligence, which provide data support for the formulation of scientific and reasonable environmental standards and policies and improve the accuracy and effectiveness of environmental regulation (52, 53). Additionally, these methods contribute to the early identification and punishment of unlawful emissions, thus strengthening environmental regulation, enforcement, and supervision (54). All these factors add to the mitigating effect of environmental regulation on health risks.

3.5 Heterogeneity analysis

3.5.1 Impacts of environmental regulation by region: coastal and inland cities

There are considerable disparities between coastal and inland cities in China in terms of economic structure, resource endowment, and degree of openness. These disparities potentially lead to varied feedback and adaptation in the face of environmental pressures (55,

TABLE 5 Results of the moderating effect.

	(1)
	ED
TE×ER	−8.723*
	(−1.75)
ER	−0.025
	(−0.31)
TE	2.454**
	(2.32)
RGDP	−0.006
	(−0.83)
LnPD	0.332*
	(1.88)
TIV	−0.001**
	(−2.10)
FSR	−0.057*
	(−1.80)
LnNH	0.039***
	(4.47)
LnAR	−0.020
	(−0.31)
LnAN	−0.688***
	(−4.92)
LnAP	2.728
	(0.85)
LnAT	5.321***
	(3.99)
_cons	−21.287***
	(−2.81)
City FE	Yes
Time FE	Yes
N	3,035
R^2	0.993

t statistics in parentheses; $*p < 0.10$, $**p < 0.05$, $***p < 0.01$.

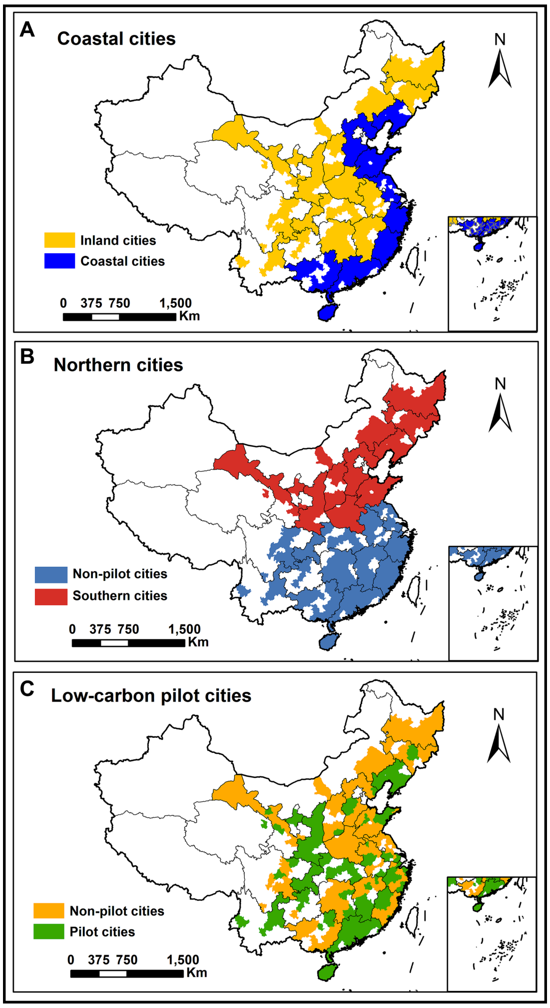

FIGURE 3
Spatial distribution by different characteristics. Northern and Southern cities **(A)**, coastal and inland cities **(B)**, low-carbon pilot and non-pilot cities **(C)**.

56). For this reason, the sample cities in this research are divided into two groups based on whether they are coastal or inland cities, with group regressions used for comparative analyses, thus revealing the disparities between coastal and inland cities in terms of environmental regulation and health risks. Figure 3A illustrates the spatial distribution features of Chinese coastal and inland cities, and it is evident that coastal cities are mostly found in the eastern and southeastern regions of China.

Columns (1) and (2) of Table 6 display the effect of environmental regulation on health risk in inland and coastal cities, respectively. In particular, environmental regulation significantly decreases health risks in inland cities with a coefficient of-0.181 ($p < 0.05$), while the effect for coastal cities is not pronounced ($p > 0.1$). This is related to the special geographical environment and economic structure of coastal cities (57). First, the industrial structure of coastal cities is more diversified, covering a variety of high-energy-consuming and high-emission industries, such as iron and steel, chemical industry, and paper manufacturing. Secondly, well-developed transportation in coastal cities has also boosted pollution sources such as vehicle exhaust and ship emissions. Thirdly, complex meteorological conditions, such as sea breeze, sea fog, typhoons, also make air management in coastal cities difficult. These factors can affect the diffusion and removal of air pollutants, thus impeding the improvement of air quality. At the same time, inland cities have higher pollutant emissions with worse fine particle contamination than coastal cities (58), making the effects of environmental regulation more pronounced in inland cities in terms of lowering pollutant emissions, including $PM_{2.5}$, and thereby mitigating health concerns.

3.5.2 Impacts of environmental regulation by region: northern and southern cities

There are nonnegligible differences in climate, environment, and lifestyle between cities in southern and northern China. Northern cities, for example, burn large amounts of coal for heating in the winter, which produces harmful gasses in the combustion

TABLE 6 Results of the heterogeneity analysis.

	(1) Inland cities	(2) Costal cities	(3) Northern cities	(4) Southern cities	(5) Non-pilot cities	(6) Pilot cities
ER	−0.181**	−0.018	−0.064	−0.209**	−0.228*	−0.075
	(−2.06)	(−0.23)	(−0.91)	(−2.23)	(−1.82)	(−1.26)
RGDP	−0.007	−0.002	0.020***	−0.026*	−0.014	−0.002
	(−0.22)	(−0.69)	(2.90)	(−1.89)	(−0.49)	(−1.10)
LnPD	0.189	0.582***	0.771***	−0.033	0.091	0.735***
	(0.72)	(4.06)	(8.13)	(−0.11)	(0.34)	(8.02)
TIV	−0.001*	0.000	−0.001	−0.000	−0.002*	−0.001
	(−1.66)	(0.00)	(−1.59)	(−0.10)	(−1.77)	(−1.59)
FSR	−0.047	0.032	0.008	−0.118**	−0.019	−0.042
	(−1.14)	(1.17)	(0.24)	(−2.44)	(−0.41)	(−1.60)
LnNH	0.047***	0.025***	0.021***	0.069***	0.051***	0.024***
	(3.77)	(3.66)	(4.27)	(3.56)	(3.81)	(3.81)
LnAR	−0.087	−0.063	0.051	−0.045	−0.150	0.079
	(−0.67)	(−0.96)	(0.60)	(−0.45)	(−1.22)	(1.03)
LnAN	−0.827***	−0.429***	−0.308**	−0.918***	−0.650***	−0.791***
	(−4.03)	(−3.12)	(−2.16)	(−4.96)	(−3.22)	(−4.70)
LnAP	−3.349	1.160	−12.341*	8.558**	−3.370	6.269*
	(−0.50)	(0.33)	(−1.95)	(2.37)	(−0.55)	(1.97)
LnAT	6.284***	0.546	8.007***	8.468***	5.541***	4.572**
	(2.91)	(0.35)	(4.72)	(2.62)	(3.09)	(2.61)
_cons	−25.688**	4.252	−39.085***	−36.931**	−20.786**	−19.600**
	(−2.15)	(0.47)	(−4.17)	(−2.09)	(−2.07)	(−1.99)
City FE	Yes	Yes	Yes	Yes	Yes	Yes
Time FE	Yes	Yes	Yes	Yes	Yes	Yes
N	1793	1,242	1,367	1,668	1718	1,317
R^2	0.992	0.997	0.997	0.990	0.991	0.997

t statistics in parentheses; *$p<0.10$, **$p<0.05$, ***$p<0.01$.

process, leading to increased air pollution and smog (59), whereas cities in the south have warmer temperatures in the winter without the need for heating but still face problems such as high humidity and poor air quality (60). In light of this, we investigated the disparities in the influence of environmental regulations on health risks in southern and northern cities. Figure 3B depicts the geographical arrangement of southern and northern cities, with the Qinling-Huaihe River serving as the dividing line.

Table 6 shows the influence of environmental regulation on health risk in southern and northern cities. Columns (3) and (4) show that the higher the intensity of environmental regulation is, the lower the health risk in southern cities, with a statistically significant coefficient of −0.209 ($p<0.05$), although this impact is not significant ($p>0.1$) in northern cities. The explanation for this discrepancy may lie in the substantial heating demand in northern cities during the winter, which leads to a multitude of dispersed pollution sources that are challenging to manage and mitigate effectively. Despite enormous expenditure, the government's environmental regulatory efforts have failed to produce the expected environmental return on winter air pollution in northern cities due to factors such as over-reliance on government and local financial resources in the treatment process (38). In contrast, southern cities predominantly witness a concentration of pollutants within sectors such as industry and transportation (61), which are subject to more stringent environmental regulations, and as a result, these regulations have greater efficacy in reducing health-related risks.

3.5.3 Impacts of environmental regulation by environmental characteristics

An arrangement for the environmental regulation of low-carbon pilot cities has been introduced in China to encourage low-carbon urban development and social reforms. This arrangement facilitates the achievement of climate goals. The implementation of the low-carbon pilot city policy has, however, led to variations in levels of pollution and environmental protection between pilot and nonpilot cities, implying that the health implications of environmental regulation may vary by city. Consequently, the sample cities in this study are separated into two categories, low-carbon pilot cities and nonpilot cities, for further examination. The spatial arrangement of low-carbon pilot and nonpilot cities is depicted in Figure 3C. As is evident from the geographical distribution, the pioneering low-carbon pilot cities have been strategically selected across several diverse provinces, encompassing both the coastal and inland areas, as well as four municipalities, covering most of the geographical area of China.

In Table 6, Columns (5) and (6) present regression results for non-low-carbon pilot cities and pilot cities, respectively. Notably, environmental regulation demonstrates a robust alleviating impact on health risk in non-low-carbon pilot cities, indicated by a coefficient of-0.228 at a significant level ($p < 0.1$). However, in the realm of low-carbon cities, the influence of environmental regulation fails to attain statistical significance. This divergence suggests that the health advantages of stringent environmental regulation are less pronounced in low-carbon pilot cities. To understand this phenomenon, one must consider the transformation of air quality. Low-carbon pilot cities have undeniably made great strides in enhancing their air quality through the proactive implementation of the low-carbon pilot program (62). As a result, the once-pervasive air pollution concerns have been noticeably mitigated, gradually fading into the now cleaner skies of these environmentally conscious cities. In contrast, non-low-carbon pilot cities still wrestle with the pressing issue of air pollution, making increased regulatory intensity more beneficial for them.

4 Discussion

Atmospheric pollution is a serious global concern, posing threats to both nature and human well-being. In response, governments have taken active measures to curb pollutant emissions and alleviate environmental damage. These measures offer more than just environmental protection, but also yield substantial health benefits, such as lower disease rates, increased life expectancy, and improved overall life quality. Consequently, appraising the health merits of environmental regulation is vital for discerning its ramifications on social welfare, enhancing cost–benefit analysis, and informing environmental policy alternatives. However, previous environmental regulation research has predominantly focused on its impacts on air pollution, greenhouse gas emissions, and energy consumption, with limited empirical studies on the implications of environmental regulation for health outcomes. Therefore, using the combined number of premature deaths from STK, IHD, and LC induced by outdoor $PM_{2.5}$ exposure as a proxy for health risk, this study delves into the effect of environmental regulations on health risk, employing panel data from 276 Chinese cities over a period spanning from 2009 to 2020 to explore effective paths that reduce health risk. The results reveal that enhancing the intensity of environmental regulation significantly reduces health risks in cities, a finding that remains valid after multiple robustness tests, which demonstrates the health advantages of environmental regulation. Atmospheric pollution is a serious environmental issue that endangers human health by allowing harmful elements to enter the body through inhalation, causing irreversible damage. Air pollution has been proven to cause greater health risks than expected. Fine particulate matter ($PM_{2.5}$), for example, with a diameter of less than 2.5 micrometers, can readily infiltrate the respiratory system and infect the lungs and bloodstream, posing a serious threat to the human body (63). Long-term exposure to high levels of $PM_{2.5}$ can weaken people's immunity and lead to chronic symptoms, such as coughing, breathlessness, migraines, and lung failure (3–5). Consequently, it is imperative to strengthen environmental regulation to reduce air pollution and protect human health. Compared with other studies that are merely theoretical, this paper quantitatively analyzes and proves the health benefits of environmental regulation by using high-precision long panel data and empirical studies, providing stronger evidence and support for proactive responses to air pollution and reducing health risks. Moreover, the policy consequences of environmental regulation are not static, but vary depending on factors such as regional location and environmental protection characteristics. This has often been overlooked in previous research on the health benefits of environmental regulation. Therefore, this paper examines not only the average impact of environmental regulation on health risks, but also the differential effect of environmental regulation on health consequences in terms of regional location and environmental protection characteristics. It also confirms the importance of scientific and technology levels in the process of environmental regulation exerting its effects, i.e., the higher the level of science and technology, the more significant the health influence of environmental regulation.

This paper investigates the impact of environmental regulations on the health risks associated with $PM_{2.5}$ exposure. Nevertheless, our analysis is subject to several limitations. Firstly, we disregard the health consequences of other air pollutants, such as O_3, which is a major contributor of respiratory and cardiovascular diseases. Therefore, future studies should examine the synergistic effects of multiple pollutants and the heterogeneity of different regions and populations in an integrated manner, to assess the implications of environmental regulation on health risks more accurately. Secondly, this paper only focuses on the health impacts of outdoor air quality, neglecting the effects of indoor air quality, which is also a crucial factor affecting residents' health (63), particularly in China during the winter, where indoor pollution from activities such as coal combustion, cooking, and smoking elevates the risk of lung cancer, chronic obstructive pulmonary disease, and other diseases. To perform more thorough and comprehensive assessments of the association between environmental pollution and health risks, future studies should incorporate more diversified and accurate data, such as indoor and outdoor air quality monitoring data, as well as data on residents' health status and behavior.

5 Conclusions and policy recommendations

This study provides evidence that an increasing intensity of environmental regulation can be associated with a reduction in health risks, with a 1-unit increase in the intensity of environmental regulation lowering the total number of local premature deaths from STK, IHD, and LC diseases by approximately 15.4%, a finding that holds up after multiple robustness tests. Additionally, the study highlights the positive synergy between scientific and technological advancements and environmental regulation in improving public health. Moreover, we also underscore the variation in health benefits across cities, with inland, southern, and non-low-carbon pilot cities experiencing more pronounced health benefits from environmental regulation. This research illuminates a promising path toward healthier and more sustainable environments.

Based on the findings of this research, three policy recommendations are proposed here. First, the social welfare effects of environmental regulation policies have been confirmed. Therefore, to enhance air quality and diminish health risks for residents, environmental regulation should be further improved by investing more in environmental protection and taking stricter measures against pollution sources. Second, the fostering of scientific and technological innovation and the promotion of clean technologies should be prioritized, along with the encouragement of enterprises to adopt eco-friendly production methods and equipment. Moreover, pollutant treatment and abatement technologies should be advanced, which will ultimately improve the health risk reduction effect of environmental policies. Third, it is crucial to tailor environmental regulatory policies by developing diverse and adaptable measures to suit the unique characteristics and needs of different cities, thereby improving the relevance and effectiveness of policies and leading to optimal health benefits for cities with varying sizes and environmental challenges.

Data availability statement

Publicly available datasets were analyzed in this study. This data can be found at: https://weijing-rs.github.io/product.html and https://www.ecmwf.int/en/forecasts/dataset/ecmwf-reanalysis-v5.

Ethics statement

Ethical approval was not required for the study involving humans in accordance with the local legislation and institutional requirements. Written informed consent to participate in this study was not required from the participants or the participants' legal guardians/next of kin in accordance with the national legislation and the institutional requirements.

Author contributions

QX: Data curation, Visualization, Writing – original draft. LW: Conceptualization, Data curation, Methodology, Writing – original draft. HH: Visualization, Writing – review & editing. ZH: Data curation, Resources, Writing – review & editing. WX: Conceptualization, Supervision, Writing – review & editing.

Funding

The author(s) declare financial support was received for the research, authorship, and/or publication of this article. This research was supported by Qingdao Philosophy and Social Science Planning Program (QDSKL2201079).

Conflict of interest

Author ZH was employed by company ShanDong ZhengYuan Geophysical Information Technology Co., Ltd.

The remaining authors declare that the research was conducted in the absence of any commercial or financial relationships that could be construed as a potential conflict of interest.

Publisher's note

References

1. Xu B, Chen J. How to achieve a low-carbon transition in the heavy industry? A nonlinear perspective. *Renew Sust Energ Rev*. (2021) 140:110708. doi: 10.1016/j.rser.2021.110708

2. Liu K, Lin B. Research on influencing factors of environmental pollution in China: a spatial econometric analysis. *J Clean Prod*. (2019) 206:356–64. doi: 10.1016/j.jclepro.2018.09.194

3. Chen Z, Liu P, Xia X, Wang L, Li X. The underlying mechanism of $PM_{2.5}$-induced ischemic stroke. *Environ Pollut*. (2022) 310:119827. doi: 10.1016/j.envpol.2022.119827

4. Raaschou-Nielsen O, Antonsen S, Agerbo E, Hvidtfeldt UA, Geels C, Frohn LM, et al. $PM_{2.5}$ air pollution components and mortality in Denmark. *Environ Int*. (2023) 171:107685. doi: 10.1016/j.envint.2022.107685

5. Hayes RB, Lim C, Zhang Y, Cromar K, Shao Y, Reynolds HR, et al. $PM_{2.5}$ air pollution and cause-specific cardiovascular disease mortality. *Int J Epidemiol*. (2020) 49:25–35. doi: 10.1093/ije/dyz114

6. Fujii H, Managi S, Kaneko S. Decomposition analysis of air pollution abatement in China: empirical study for ten industrial sectors from 1998 to 2009. *J Clean Prod*. (2013) 59:22–31. doi: 10.1016/j.jclepro.2013.06.059

7. Hicks C, Dietmar R. Improving cleaner production through the application of environmental management tools in China. *J Clean Prod*. (2007) 15:395–408. doi: 10.1016/j.jclepro.2005.11.008

8. Zhu J, Wu S, Xu J. The abatement effect of total emission control policy: evidence from China. *Energy Econ*. (2023) 126:106978. doi: 10.1016/j.eneco.2023.106978

9. Kahn AE. *The economics of regulation: Principles and institutions*. Cambridge, MA: MIT Press (1988).

10. Li B, Wu S. Effects of local and civil environmental regulation on green total factor productivity in China: a spatial Durbin econometric analysis. *J Clean Prod*. (2017) 153:342–53. doi: 10.1016/j.jclepro.2016.10.042

11. Wang Y, Shen N. Environmental regulation and environmental productivity: the case of China. *Renew Sust Energ Rev*. (2016) 62:758–66. doi: 10.1016/j.rser.2016.05.048

12. Cole MA, Elliott RJ. Determining the trade–environment composition effect: the role of capital, labor and environmental regulations. *J Environ Econ Manag*. (2003) 46:363–83. doi: 10.1016/S0095-0696(03)00021-4

13. Hou J, Teo TS, Zhou F, Lim MK, Chen H. Does industrial green transformation successfully facilitate a decrease in carbon intensity in China? An environmental regulation perspective. *J Clean Prod*. (2018) 184:1060–71. doi: 10.1016/j.jclepro.2018.02.311

14. Yuan B, Xiang Q. Environmental regulation, industrial innovation and green development of Chinese manufacturing: based on an extended CDM model. *J Clean Prod*. (2018) 176:895–908. doi: 10.1016/j.jclepro.2017.12.034

15. Du W, Li M. Assessing the impact of environmental regulation on pollution abatement and collaborative emissions reduction: Micro-evidence from Chinese industrial enterprises. *Environ Impact Assess Rev*. (2020) 82:106382. doi: 10.1016/j.eiar.2020.106382

16. Feng T, Du H, Lin Z, Zuo J. Spatial spillover effects of environmental regulations on air pollution: evidence from urban agglomerations in China. *J Environ Manag*. (2020) 272:110998. doi: 10.1016/j.jenvman.2020.110998

17. Zhang K, Xu D, Li S. The impact of environmental regulation on environmental pollution in China: an empirical study based on the synergistic effect of industrial agglomeration. *Environ Sci Pollut Res*. (2019) 26:25775–88. doi: 10.1007/s11356-019-05854-z

18. Yu Y, Dai C, Wei Y, Ren H, Zhou J. Air pollution prevention and control action plan substantially reduced $PM_{2.5}$ concentration in China. *Energy Econ*. (2022) 113:106206. doi: 10.1016/j.eneco.2022.106206

19. Liu X, Li Y, Chen X, Liu J. Evaluation of low carbon city pilot policy effect on carbon abatement in China: an empirical evidence based on time-varying DID model. *Cities*. (2022) 123:103582. doi: 10.1016/j.cities.2022.103582

20. Hu X, Sun Y, Liu J, Meng J, Wang X, Yang H, et al. The impact of environmental protection tax on sectoral and spatial distribution of air pollution emissions in China. *Environ Res Lett*. (2019) 14:054013. doi: 10.1088/1748-9326/ab1965

21. Tanaka S. Environmental regulations on air pollution in China and their impact on infant mortality. *J Health Econ*. (2015) 42:90–103. doi: 10.1016/j.jhealeco.2015.02.004

22. Yang M, Chou S-Y. The impact of environmental regulation on fetal health: evidence from the shutdown of a coal-fired power plant located upwind of New Jersey. *J Environ Econ Manag*. (2018) 90:269–93. doi: 10.1016/j.jeem.2018.05.005

23. Xu J, Wang Y, Liu W. Green to health: the impact of environmental regulation on health status. *Sustain Cities Soc*. (2023) 98:104839. doi: 10.1016/j.scs.2023.104839

24. Zhou G, Liu W, Wang T, Luo W, Zhang L. Be regulated before be innovative? How environmental regulation makes enterprises technological innovation do better for public health. *J Clean Prod*. (2021) 303:126965. doi: 10.1016/j.jclepro.2021.126965

25. Zhang Z, Zhang G, Li L. The spatial impact of atmospheric environmental policy on public health based on the mediation effect of air pollution in China. *Environ Sci Pollut Res*. (2022) 30:116584–600. doi: 10.1007/s11356-022-21501-6

26. Song Y, Wei Y, Zhu J, Liu J, Zhang M. Environmental regulation and economic growth: a new perspective based on technical level and healthy human capital. *J Clean Prod*. (2021) 318:128520. doi: 10.1016/j.jclepro.2021.128520

27. Dai J, Lv P, Ma Z, Bi J, Wen T. Environmental risk and housing price: an empirical study of Nanjing, China. *J Cleaner Prod*. (2020) 252:119828. doi: 10.1016/j.jclepro.2019.119828

28. Burnett RT, Pope CA, Ezzati M, Olives C, Lim SS, Mehta S, et al. An integrated risk function for estimating the global burden of disease attributable to ambient fine particulate matter exposure. *Environ Health Perspect*. (2014) 122:397–403. doi: 10.1289/ehp.1307049

29. Lee CJ, Martin RV, Henze DK, Brauer M, Cohen A, Donkelaar AV. Response of global particulate-matter-related mortality to changes in local precursor emissions. *Environ Sci Technol*. (2015) 49:4335–44. doi: 10.1021/acs.est.5b00873

30. Wei J. Reconstructing 1-km-resolution high-quality $PM_{2.5}$ data records from 2000 to 2018 in China: spatiotemporal variations and policy implications. *Remote Sens Environ*. (2021) 252:112136. doi: 10.1016/j.rse.2020.112136

31. Wei J, Li Z, Cribb M, Huang W, Xue W, Sun L, et al. Improved 1 km resolution $PM_{2.5}$ estimates across China using enhanced space–time extremely randomized trees. Atmos. *Chem Phys*. (2020) 20:3273–89. doi: 10.5194/acp-20-3273-2020

32. Li J, Zhu Y, Kelly JT, Jang CJ, Wang S, Hanna A, et al. Health benefit assessment of $PM_{2.5}$ reduction in Pearl River Delta region of China using a model-monitor data fusion approach. *J Environ Manag*. (2019) 233:489–98. doi: 10.1016/j.jenvman.2018.12.060

33. Du K, Cheng Y, Yao X. Environmental regulation, green technology innovation, and industrial structure upgrading: the road to the green transformation of Chinese cities. *Energy Econ*. (2021) 98:105247. doi: 10.1016/j.eneco.2021.105247

34. National Bureau of Statistics (NBS). Explanation of key statistical indicators. Available at: http://www.stats.gov.cn/zt_18555/ztsj/hjtjzl/2010/202303/t20230302_1921607.html (Accessed July 10, 2023).

35. Hao Y, Liu S, Lu Z-N, Huang J, Zhao M. The impact of environmental pollution on public health expenditure: dynamic panel analysis based on Chinese provincial data. *Environ Sci Pollut Res*. (2018) 25:18853–65. doi: 10.1007/s11356-018-2095-y

36. Gu H, Cao Y, Elahi E, Jha SK. Human health damages related to air pollution in China. *Environ Sci Pollut Res*. (2019) 26:13115–25. doi: 10.1007/s11356-019-04708-y

37. Kim MJ. Air pollution, health, and avoidance behavior: evidence from South Korea. *Environ Resour Econ*. (2021) 79:63–91. doi: 10.1007/s10640-021-00553-1

38. Fan M, He G, Zhou M. The winter choke: coal-fired heating, air pollution, and mortality in China. *J Health Econ*. (2020) 71:102316. doi: 10.1016/j.jhealeco.2020.102316

39. Di Napoli C, Barnard C, Prudhomme C, Cloke HL, Pappenberger F. ERA5-HEAT: a global gridded historical dataset of human thermal comfort indices from climate reanalysis. *Geosci Data J*. (2021) 8:2–10. doi: 10.1002/gdj3.102

40. Zhao J, Jiang Q, Dong X, Dong K, Jiang H. How does industrial structure adjustment reduce CO2 emissions? Spatial and mediation effects analysis for China. *Energy Econ*. (2022) 105:105704. doi: 10.1016/j.eneco.2021.105704

41. Zhao D, Dou Y, Tong L. Effect of fiscal decentralization and dual environmental regulation on green poverty reduction: the case of China. *Resources Policy*. (2022) 79:102990. doi: 10.1016/j.resourpol.2022.102990

42. Guo Q, Zhong J. The effect of urban innovation performance of smart city construction policies: evaluate by using a multiple period difference-in-differences model. *Technol Forecast Soc Chang*. (2022) 184:122003. doi: 10.1016/j.techfore.2022.122003

43. Zeng H, Zhang X, Zhou Q, Jin Y, Cao J. Tightening of environmental regulations and corporate environmental irresponsibility: a quasi-natural experiment. *Environ Dev Sustain*. (2022) 24:13218–59. doi: 10.1007/s10668-021-01988-8

44. Yang M, Chen H, Long R, Yang J. How does government regulation shape residents' green consumption behavior? A multi-agent simulation considering environmental values and social interaction. *J Environ Manag*. (2023) 331:117231. doi: 10.1016/j.jenvman.2023.117231

45. Fan M, Yang P, Li Q. Impact of environmental regulation on green total factor productivity: a new perspective of green technological innovation. *Environ Sci Pollut Res*. (2022) 29:53785–800. doi: 10.1007/s11356-022-19576-2

46. Rahman MM, Alam K. Clean energy, population density, urbanization and environmental pollution nexus: evidence from Bangladesh. *Renew Energy*. (2021) 172:1063–72. doi: 10.1016/j.renene.2021.03.103

47. Yitshak-Sade M, Kloog I, Novack V. Do air pollution and neighborhood greenness exposures improve the predicted cardiovascular risk? *Environ Int*. (2017) 107:147–53. doi: 10.1016/j.envint.2017.07.011

48. Stock JH, *Testing for weak instruments in linear IV regression*.

49. Xue W, Wang L, Yang Z, Xiong Z, Li X, Xu Q, et al. Can clean heating effectively alleviate air pollution: an empirical study based on the plan for cleaner winter heating in northern China. *Appl Energy*. (2023) 351:121923. doi: 10.1016/j.apenergy.2023.121923

50. Zhu Y, Liu Z, Feng S, Lu N. The role of fiscal expenditure on science and technology in carbon reduction: evidence from provincial data in China. *Environ Sci Pollut Res*. (2022) 29:82030–44. doi: 10.1007/s11356-022-21500-7

51. Sun H, Zhang Z, Liu Z. Does air pollution collaborative governance promote green technology innovation? Evidence from China. *Environ Sci Pollut Res*. (2022) 29:51609–22. doi: 10.1007/s11356-022-19535-x

52. Mishra S, Jena L, Tripathy HK, Gaber T. Prioritized and predictive intelligence of things enabled waste management model in smart and sustainable environment. *PLoS One*. (2022) 17:e0272383. doi: 10.1371/journal.pone.0272383

53. Himeur Y, Rimal B, Tiwary A, Amira A. Using artificial intelligence and data fusion for environmental monitoring: a review and future perspectives. *Inform Fusion*. (2022) 86-87:44–75. doi: 10.1016/j.inffus.2022.06.003

54. Yang X, Wu H, Ren S, Ran Q, Zhang J. Does the development of the internet contribute to air pollution control in China? Mechanism discussion and empirical test. *Struct Chang Econ Dyn*. (2021) 56:207–24. doi: 10.1016/j.strueco.2020.12.001

55. Zheng W, Chu J, Bambrick H, Wang N, Mengersen K, Guo X, et al. Impact of environmental factors on diabetes mortality: a comparison between inland and coastal areas. *Sci Total Environ*. (2023) 904:166335. doi: 10.1016/j.scitotenv.2023.166335

56. Zhu S, He C, Liu Y. Going green or going away: environmental regulation, economic geography and firms' strategies in China's pollution-intensive industries. *Geoforum*. (2014) 55:53–65. doi: 10.1016/j.geoforum.2014.05.004

57. Nie X, Mao H, Li P, Li T, Zhou J, Wu Y, et al. Total gaseous mercury in a coastal city (Qingdao, China): influence of sea-land breeze and regional transport. *Atmos Environ*. (2020) 235:117633. doi: 10.1016/j.atmosenv.2020.117633

58. Shu L, Xie M, Gao D, Wang T, Fang D, Liu Q, et al. Regional severe particle pollution and its association with synoptic weather patterns in the Yangtze River Delta region, China. *Atmos Chem Phys*. (2017) 17:12871–91. doi: 10.5194/acp-17-12871-2017

59. Zhang Z, Wang W, Cheng M, Liu S, Xu J, He Y, et al. The contribution of residential coal combustion to $PM_{2.5}$ pollution over China's Beijing-Tianjin-Hebei region in winter. *Atmos Environ*. (2017) 159:147–61. doi: 10.1016/j.atmosenv.2017.03.054

60. Li F, Zhou T. Effects of urban form on air quality in China: an analysis based on the spatial autoregressive model. *Cities*. (2019) 89:130–40. doi: 10.1016/j.cities.2019.01.025

61. Zou B-B, Huang X-F, Zhang B, Dai J, Zeng L-W, Feng N, et al. Source apportionment of $PM_{2.5}$ pollution in an industrial city in southern China. Atmospheric. *Pollut Res*. (2017) 8:1193–202. doi: 10.1016/j.apr.2017.05.001

62. Chen J, Luo W, Ren X, Liu T. The local-neighborhood effects of low-carbon city pilots program on $PM_{2.5}$ in China: a spatial difference-in-differences analysis. *Sci Total Environ*. (2023) 857:159511. doi: 10.1016/j.scitotenv.2022.159511

63. Kumar P, Singh AB, Arora T, Singh S, Singh R. Critical review on emerging health effects associated with the indoor air quality and its sustainable management. *Sci Total Environ*. (2023) 872:162163. doi: 10.1016/j.scitotenv.2023.162163

frontiers | Frontiers in Public Health

TYPE Original Research
PUBLISHED 29 January 2024
DOI 10.3389/fpubh.2024.1361911

Check for updates

OPEN ACCESS

EDITED BY
Shupeng Zhu,
Zhejiang University, China

REVIEWED BY
Chenyu Huang,
University of California, Irvine, United States
Jinlai Wei,
Fujifilm Irvine Scientific, Inc., United States

*CORRESPONDENCE
Hong Sun
✉ hongsun@jscdc.cn
Yongqing Zhang
✉ zyq6943@163.com

†These authors have contributed equally to this work and share first authorship

RECEIVED 27 December 2023
ACCEPTED 12 January 2024
PUBLISHED 29 January 2024

CITATION
Sun H, Wan Y, Pan X, You W, Shen J, Lu J, Zheng G, Li X, Xing X and Zhang Y (2024) Long-term air pollution and adverse meteorological factors might elevate the osteoporosis risk among adult Chinese. *Front. Public Health* 12:1361911. doi: 10.3389/fpubh.2024.1361911

Long-term air pollution and adverse meteorological factors might elevate the osteoporosis risk among adult Chinese

Hong Sun[1*†], Yanan Wan[1†], Xiaoqun Pan[1], Wanxi You[2], Jianxin Shen[3], Junhua Lu[4], Gangfeng Zheng[5], Xinlin Li[6], Xiaoxi Xing[7] and Yongqing Zhang[1*]

[1]Jiangsu Provincial Center for Disease Control and Prevention, Nanjing, Jiangsu, China, [2]Luhe District Center for Disease Control and Prevention, Nanjing, Jiangsu, China, [3]Wujiang District Center for Disease Control and Prevention, Suzhou, Jiangsu, China, [4]Chongchuan District Center for Disease Control and Prevention, Nantong, Jiangsu, China, [5]Jingjiang Center for Disease Control and Prevention, Taizhou, Jiangsu, China, [6]Nantong Center for Disease Control and Prevention, Nantong, Jiangsu, China, [7]Quanshan District Center for Disease Control and Prevention, Xuzhou, Jiangsu, China

Objective: This study aims to investigate the relationship between exposure to air pollution and adverse meteorological factors, and the risk of osteoporosis.

Methods: We diagnosed osteoporosis by assessing bone mineral density through Dual-Energy X-ray absorptiometry in 2,361 participants from Jiangsu, China. Additionally, we conducted physical examinations, blood tests, and questionnaires. We evaluated pollution exposure levels using grid data, considering various lag periods (ranging from one to five years) based on participants' addresses. We utilized logistic regression analysis, adjusted for temperature, humidity, and individual factors, to examine the connections between osteoporosis and seven air pollutants: PM_1, $PM_{2.5}$, PM_{10}, SO_2, NO_2, CO, and O_3. We assessed the robustness of our study through two-pollutant models and distributed lag non-linear models (DLNM) and explored susceptibility using stratified analyses.

Results: In Jiangsu, China, the prevalence of osteoporosis among individuals aged 40 and above was found to be 15.1%. A consistent association was observed between osteoporosis and the five-year average exposure to most pollutants, including $PM_{2.5}$, PM_{10}, CO, and O_3. The effects of PM_{10} and CO remained stable even after adjusting for the presence of a second pollutant. However, the levels of PM_1 and $PM_{2.5}$ were significantly influenced by O_3 levels. Individuals aged 60 and above, those with a BMI of 25 or higher, and males were found to be more susceptible to the effects of air pollution. Interestingly, males showed a significantly higher susceptibility to PM_1 and $PM_{2.5}$ compared to females. This study provides valuable insights into the long-term effects of air pollution on osteoporosis risk among the adult population in China.

Conclusion: This study indicates a potential association between air pollutants and osteoporosis, particularly with long-term exposure. The risk of osteoporosis induced by air pollution is found to be higher in individuals aged 60 and above, those with a BMI greater than 25, and males. These findings underscore the need for further research and public health interventions to mitigate the impact of air pollution on bone health.

KEYWORDS

bone mineral density, osteoporosis prevalence, particulate matter, lag times, susceptibility

1 Introduction

Osteoporosis is a systemic skeletal disorder characterized by reduced bone mass and microscopic structural deterioration of bone tissue, leading to increased fragility of bones and a higher risk of fractures (1). In older adult individuals, particularly among women, bone pain and fractures are common symptoms of osteoporosis, which can potentially lead to disability or even death. This disease imposes a significant burden on healthcare systems, and with the increasing old population, this burden continues to grow (2). Taking China as an example, there were 411,000 cases of hip fractures in 2015, and it is projected to increase to one million by 2050 (3). Based on an osteoporosis epidemiological study conducted in China, which surveyed 20,416 individuals, the prevalence of osteoporosis among adults aged 40 and above was 5.0% for men and 20.6% for women (4). When combining this data with the sixth Chinese national census (55,191,915 men aged 40 and above and 53,935,201 women aged 40 and above), we estimated that there are 13.87 million osteoporosis patients among the Chinese population aged 40 and above. Therefore, the implementation of comprehensive early prevention and treatment measures for osteoporosis has become extremely urgent and necessary.

Air pollution is recognized a global health challenge (5). As early as 1985, researchers suggested a potential link between air pollution and osteoporosis (6). The Oslo Health Study (7) initially identified a weak but significant negative correlation between a 10-year average of air pollution indicators and whole-body bone density. Recent evidence from the analysis of 9.2 million U.S. health insurance records (8) and data from over 40,000 individuals in South Korea's health insurance database (9) indicates a close association between increased $PM_{2.5}$ concentrations and higher rates of hospitalization due to fractures in the older adults, suggesting a connection between air pollution and osteoporosis. An analysis of data from 341,000 participants in the UK Biobank also suggests that exposure to higher levels of air pollution is associated with lower bone mineral density and an increased risk of osteoporosis (10). However, despite over four decades of research, the existing evidence regarding the relationship between outdoor air pollution exposure and osteoporosis-related outcomes remains scattered and inconclusive (11). Meta-analyses of limited studies indicate heterogeneous results regarding the association between air pollution exposure and osteoporosis (11), and the observed inconsistencies between studies may be attributed to heterogeneity in participant characteristics, study designs, and statistical issues (12). Furthermore, recent studies have adopted diverse lag periods for long-term exposure, while a considerable number have omitted adjustments for meteorological variables, which may constitute significant contributors to the disparate research findings.

Therefore, we conducted a retrospective cohort study in Jiangsu, China, and assessed the 5-year daily exposure of the survey participants to air pollutants and meteorological factors. Our study aimed to assess the impact of various air pollutants and adverse meteorological factors, including three kinds of Particulate Matter with different aerodynamic diameters (PM_1, $PM_{2.5}$, PM_{10}), Nitrogen Dioxide (NO_2), Sulfur Dioxide (SO_2), Carbon Monoxide (CO), and ozone (O_3), as well as high humidity and solar irradiation, on the risk of osteoporosis. This research is crucial in understanding the environmental factors contributing to osteoporosis and informing public health interventions.

2 Materials and methods

2.1 Study population

The study population for this cohort research constitutes a subset of the China National Epidemiological Survey on Osteoporosis, conducted in 2017 (4). This national study aimed to investigate the prevalence of osteoporosis and its associated risk factors. Our study was conducted in Jiangsu Province, located in the eastern part of China, from March to July 2018. Jiangsu Province is characterized by predominantly flat terrain and is considered an economically developed region in China. The survey encompassed six cities within Jiangsu Province, each representing various urban environments (Supplementary Figure S1). We employed a multi-stage, stratified cluster random sampling approach for our sampling method. In each surveyed area, we used a Probability Proportional to Size (PPS) sampling method to randomly select four townships or streets, each providing two administrative villages or communities. Afterward, we randomly selected one resident group from each administrative village or community, with each group comprising a minimum of 50 participants aged 40 years and older who met the eligibility criteria on bone mineral density measurements. Exclusion criteria included individuals diagnosed with metabolic bone diseases such as hyperthyroidism, hyperparathyroidism, renal failure, malabsorption syndrome, alcoholism, chronic colitis, multiple myeloma, leukemia, or chronic arthritis, as well as pregnant individuals.

2.2 Osteoporosis assessment

We conducted bone mineral density (BMD) measurements, including lumbar spine (L1 to L4), femoral neck, and total hip, using Hologic scanners (Hologic Inc) or GE-Lunar scanners (GE Healthcare) via dual-energy X-ray absorptiometry (DXA). Quality control procedures were rigorously implemented, encompassing the scanning of a standardized European Spine Phantom (ESP) ten times to calibrate each DXA scanner utilized during participant examinations. This meticulous calibration process was pivotal in guaranteeing the uniformity and accuracy of Bone Mineral Density (BMD) measurements, an essential factor in the scoring and analysis for this study. It underscored our commitment to maintaining consistency in data collection and analysis, thereby fortifying the reliability of our findings. Osteoporosis diagnosis adhered to the criteria set by the World Health Organization, calculated as T-score = (BMD – gender-specific peak BMD) / (SD of gender-specific peak BMD). Individuals with T-scores of −2.5 or lower at any site (L1 to L4, femoral neck, or total hip) were classified as having osteoporosis (13). The data calculation methods in this study align with those utilized in the previous study (4).

2.3 Exposure assessment

Daily ambient air pollution data, which included PM_1, $PM_{2.5}$, PM_{10}, SO_2, NO_2, CO, and O_3, were obtained from the ChinaHighAirPollutants dataset, accessible at https://weijing-rs.github.io/product.html. This dataset was generated through a combination of artificial intelligence models, ground measurements, satellite remote sensing products, and atmospheric reanalysis. It offered comprehensive spatiotemporal coverage across China during the study period, with a spatial resolution of 1 × 1 km for PM and O_3, and 10 × 10 km for SO_2, NO_2, and CO. The reliability of the exposure assessment has been validated in our previous studies (14, 15).

We collected daily pollution and meteorological exposure data for participants' residential locations from 2013 to 2018. Based on each participant's survey date, we computed annual average exposure levels for the year preceding the survey (lag0) up to 5 years before the survey (lag4). Additionally, we calculated exposure averages from 2 years before the survey (lag01) to 5 years before the survey (lag04). Note that data for PM_1 in 2013 were missing, resulting in a one-year shorter exposure period, with a maximum of 4 years.

2.4 Covariates

Meteorological data, which included air temperature (°C) and relative humidity (%), were sourced from the China Meteorological Administration Land Data Assimilation System (CLDAS version 2.0) at a spatial resolution of 0.0625° × 0.0625° (16, 17). Additionally, we retrieved data on Erythemal Daily Dose (EDD) from the Dutch-Finnish Ozone Monitoring Instrument (OMI) Level 2 UV irradiance products (OMUVB V003) at a resolution of 13 km × 24 km (18). EDD represents the cumulative UV radiation exposure individuals receive in a day, with the potential to cause skin erythema (sunburn) (19). It is measured in J/m^2 and is commonly used to assess the risk of skin damage due to UV radiation. The OMI spectrometer, hosted by the NASA Aura satellite, observes nadir views and records ultraviolet wavelengths ranging from 270 to 380 nm. We calculated daily mean EDD levels for specific locations by averaging EDD values from corresponding OMI pixels within those areas. The methodology used for assessing exposure to meteorological factors aligned with the approach employed for air pollutants. Individual covariates, such as gender, age, and body mass index (BMI), were collected through questionnaires and physical examinations.

2.5 Statistical analysis

We conducted Spearman's correlation tests to explore the relationships between air pollutant exposures and meteorological factors. Subsequently, logistic regression models were employed to assess the exposure-response associations for PM_1, $PM_{2.5}$, PM_{10}, SO_2, NO_2, CO, and O_3 exposures concerning osteoporosis incidents. Using a stepwise selection approach, individual factors such as BMI (body mass index), age, and gender were incorporated into the model. Unit-Based Root Expected Logarithmic Prediction (UBRE) is used to assess the goodness of fit of a model. These logistic regression models allowed us to estimate the percentage changes in the odds of osteoporosis incidents, expressed as ([odds ratio – 1] * 100%), across various exposure levels. Alongside these estimates, we calculated corresponding 95% confidence intervals (CIs) and determined the percentage change in the odds of osteoporosis for a unit increase in exposure. In constructing these models, we utilized natural cubic spline functions (with 3 degrees of freedom [df]) to portray the exposure to each specific pollutant, thus forming exposure-response curves. To ensure robustness, all models were adjusted for annual air temperature and relative humidity (RH), which were included as natural cubic spline functions (df = 3). Additionally, in two-pollutant models and stratified analyses, adjustments were made for additional variables, including EDD.

Furthermore, we performed a comprehensive stratified analysis based on age (<60, ≥60 years), gender (male, female), and BMI (<25, ≥25). Effect modifications were rigorously examined using two-sample z-tests, leveraging the stratification-specific point estimates (β = ln odds ratio) and their corresponding standard errors (SEs) (20):

$$z = \frac{\beta_1 - \beta_2}{\sqrt{SE_1^2 + SE_2^2}}$$

To ensure robustness, we conducted sensitivity analyses, including two-pollutant models for each of the seven air pollutants. These models integrated an additional set of pollutants for assessment, and we specifically utilized the likelihood ratio test to compare nested single-pollutant and two-pollutant models, aiming to discern differences between the models. We also considered the potential non-linear lag effects of pollutant exposure over different years. To do so, we used the Distributed Lag Non-Linear Model (DLNM) approach to assess the associations between osteoporosis occurrence and the seven pollutants, along with EDD, over various lag years.

All data analyses were performed using R version 4.3.1, with two-sided p-values, and statistical significance was set at $p < 0.05$.

3 Results

3.1 Study population and characteristics

A total of 2,399 individuals aged 40 and above participated in comprehensive health assessments and completed questionnaires, with 38 participants being excluded due to incomplete X-ray examinations. As shown in Table 1, a total of 2,361 individuals were included in this study, among whom 356 were diagnosed with osteoporosis, accounting for 15.1% of the total. A slightly higher proportion of participants were female, accounting for 57.8% of the sample. Nevertheless, the prevalence of osteoporosis among females was considerably higher, reaching 23.4%, which was 6.5 times greater than that among males (23.4/3.6). The mean age of the participants was 57.9 ± 9.7 years, with the osteoporosis group being older than the control group. Approximately 46.2% of the participants were aged 60 and above, with an osteoporosis prevalence of 24.7%, significantly higher than the prevalence in the age < 60 group (6.9%, 3.6 times higher). Regarding Body Mass Index (BMI), the participants had an average of 25.1 ± 3.4, with the BMI in the osteoporosis group being significantly lower than that in the control group. Among the surveyed individuals, 52.2% had a BMI below 25, and this group exhibited an osteoporosis prevalence of 19.2%, significantly higher than the prevalence among individuals with a BMI of 25 or greater (10.5%).

3.2 Exposure to air pollution and meteorological factors

In Table 2, we compiled data on the exposure of study participants to seven air pollutants (PM_1, $PM_{2.5}$, PM_{10}, SO_2, NO_2, CO, O_3) and meteorological factors (temperature in °C, humidity in %, and Erythemal Daily Dose – EDD in J/m^2) for various lag periods: the year before the survey (lag0), the average over the 2 years before the survey (lag01), and the average over the 5 years before the survey (lag04). Our findings indicate that between 2013 and 2018, the average concentrations of particulate matter in the surveyed areas gradually decreased. For instance, PM_{10} decreased from 99.7 μg/m^3 at lag04 (2013–2018) to 88.6 μg/m^3 at lag0 (2017–2018). Similarly, the concentration of SO_2 during this period decreased from 25.7 to 16.5 μg/m^3. In contrast, O_3 levels increased from 102.1 to 107.9 μg/m^3. NO_2, CO, and meteorological factors remained relatively stable. Figure 1 illustrates the correlations among these factors in lag04 exposure, with PM_{10}, $PM_{2.5}$, and CO exhibiting correlation coefficients exceeding 90%.

3.3 Lag and cumulative effects of pollutants on osteoporosis

We identified humidity as a significant risk factor for osteoporosis (Supplementary Figure S2) and thus deemed it necessary to adjust for its impact on our results. Figure 2 illustrates the effects of exposure

TABLE 1 Characteristics of the study population.

Characteristic	Total	Osteoporosis		p
		Yes	No	
Number	2,361	356 (15.1%)	2005 (84.9%)	
Gender				<0.01[a]
Male	996 (42.2%)	36 (3.6%)	960 (96.4%)	
Female	1,365 (57.8%)	320 (23.4%)	1,045 (76.6%)	
Age	57.9 ± 9.7	64.4 ± 7.8	56.7 ± 9.6	<0.01[a]
<60	1,270 (53.8%)	87 (6.9%)	1,183 (93.1%)	
≥60	1,091 (46.2%)	269 (24.7%)	822 (75.3%)	
BMI	25.1 ± 3.4	24.0 ± 3.6	25.3 ± 3.4	<0.01[a]
<25	1,232 (52.2%)	237 (19.2%)	995 (80.8%)	
≥25	1,129 (47.8%)	119 (10.5%)	1,010 (89.5%)	

Values are n, n (%) or means ± SD. [a]The comparison is being made regarding the distribution differences of cases and non-cases across different gender, age, or BMI groups.

TABLE 2 Distribution of exposure to ambient air pollutants and meteorological conditions of study.

	[a]Lag0 year	[a]Lag01 year	Lag02 year	Lag03year	Lag04 year
	Mean (Range)	Mean (Range)	Mean (Range)	Mean (Range)	Mean (Range)
PM_1 (μg/m^3)	33.0 (26.8 to 43.2)	33.4 (28.8 to 41.3)	34.9 (30.5 to 41.6)	36.4 (32.5 to 41.5)	37.3 (32.4 to 43.2)
$PM_{2.5}$ (μg/m^3)	51.6 (39.9 to 70.3)	51.4 (40.6 to 66.6)	54.4 (45.3 to 66.7)	57.0 (48.4 to 67.9)	60.6 (52.2 to 71.6)
PM_{10} (μg/m^3)	88.6 (66.3 to 118.4)	86.9 (65.8 to 116.1)	90.8 (71.6 to 118.9)	94.8 (77.1 to 121.7)	99.7 (83.4 to 125.3)
SO_2 (μg/m^3)	16.5 (13.1 to 20.8)	18.7 (14.0 to 25.7)	21.2 (15.8 to 30.6)	23.3 (17.2 to 34.3)	25.7 (18.7 to 38.4)
NO_2 (μg/m^3)	41.4 (36.8 to 48.7)	40.4 (35.1 to 46.9)	40.1 (33.1 to 46.2)	40.1 (31.7 to 46.2)	40.5 (32.1 to 46.0)
CO (mg/m^3)	0.9 (0.7 to 0.9)	0.9 (0.7 to 1.0)	0.9 (0.7 to 1.1)	1.0 (0.7 to 1.2)	1.0 (0.7 to 1.2)
O_3 (μg/m^3)	107.9 (100.2 to 119.8)	106.0 (97.5 to 118.8)	104.4 (96.4 to 117.5)	103.2 (95.5 to 116.0)	102.1 (94.7 to 115.0)
Erythemal Daily Dose[b] (J/m^2)	2,395 (2,181 to 2,593)	2,333 (2,138 to 2,496)	2,318 (2,131 to 2,469)	2,294 (2,117 to 2,449)	2,322 (2,139 to 2,505)
Temperature (°C)	16.9 (15.7 to 18.2)	16.9 (15.8 to 18.2)	16.7 (15.7 to 17.9)	16.6 (15.6 to 17.8)	16.6 (15.7 to 17.8)
Humidity (%)	72.9 (66.9 to 75.8)	74.2 (69.1 to 77.2)	73.9 (68.4 to 76.9)	73.5 (68.0 to 76.3)	72.8 (67.7 to 75.5)

[a]Lag0 year: The average exposure in the year immediately before the survey day; Lag01 (~04) year: The average exposure over the 2 years (~5 years) preceding the survey day. [b]Erythemal Daily Dose (J/m^2): This refers to the total amount of ultraviolet (UV) radiation exposure that the Earth's surface receives in a day, which may cause erythema (skin redness or sunburn). It represents the cumulative UV radiation dose within a day.

to 1 μg/m^3 of PM_1, $PM_{2.5}$, PM_{10}, SO_2, NO_2, and O_3, as well as 10 μg/m^3 of CO, and 10 J/m^2 of EDD on the odds percentage change of osteoporosis, after adjusting for individual gender, age, BMI, as well as temperature and humidity.

The results depict the impact of each pollutant on osteoporosis occurrence for both single-year exposure (lag0-lag4) and average exposure over the past 5 years (lag01-lag04). Notably, for most pollutants (PM_1, $PM_{2.5}$, PM_{10}, CO, and ozone), the five-year average exposure demonstrates a relatively substantial and consistent risk (or protective) effect on osteoporosis. Conversely, the results for single-year exposure appear less stable. In all lag periods, neither SO_2 nor NO_2 exhibited significant associations with osteoporosis. Interestingly, for particulate matter (PM_1, $PM_{2.5}$, and PM_{10}), the risk of osteoporosis gradually increased with increasing pollutant concentration from Lag02 to Lag04, suggesting a cumulative effect of long-term exposure. Figure 2 also indicates that long-term exposure to O_3, and EDD, as related to UV radiation, appear to be protective factors against osteoporosis. Consequently, in our subsequent multivariate analysis, we incorporate EDD as a fixed adjustment factor.

As shown in Supplementary Figure S3, the coefficients in the graph represent the effects resulting from a unit increase in pollutant concentration. Specifically, PM_1, $PM_{2.5}$, PM_{10}, SO_2, NO_2, and O_3 units were 1 μg/m^3, CO was 0.01 mg/m^3, and EDD was 10 J/m^2. Adjustments were made for gender, age, BMI, temperature, and humidity. Regarding PM_1, $PM_{2.5}$, and PM_{10}, cumulative effects resulting from 4 or 5 years of exposure demonstrated a significant association with the occurrence of osteoporosis, consistent with the observed trend in Figure 2. Notably, neither NO_2 nor SO_2 exhibited discernible cumulative effects. CO exhibited the strongest effect with a 4-year cumulative exposure. It's important to emphasize that O_3 demonstrates significant cumulative effects only within a 5-year accumulation period.

3.4 Dose–response relationships between pollutants and osteoporosis

In Figure 3, we present a clear depiction of the exposure-response relationship between six pollutants and the risk of osteoporosis. These relationships are adjusted for individual gender, age, BMI, as well as temperature, humidity, and EDD, considering a five-year average exposure (four-year average for PM). The concentrations of PM_1, $PM_{2.5}$, PM_{10}, and CO exhibit a significant, nearly linear positive correlation with the risk of osteoporosis as they increase. In contrast, NO_2 demonstrates a nonlinear relationship with osteoporosis. Additionally, O_3 shows a significant negative correlation with osteoporosis occurrence.

3.5 Two-pollutant models

Figure 4 presents the results of two-pollutant models for 10 μg/m^3 of PM_1 (lag03), $PM_{2.5}$ (lag04), PM_{10} (lag04), and O_3 (lag04) in conjunction with 100 μg/m^3 of CO (lag04). These models build upon the single-pollutant models by sequentially accounting for the influence of other pollutants. After adjusting for the second pollutant, the effects of PM_{10} and CO remained relatively stable, while PM_1 and $PM_{2.5}$ were notably influenced by O_3. However, when compared to single-pollutant models, all two-pollutant models exhibited no

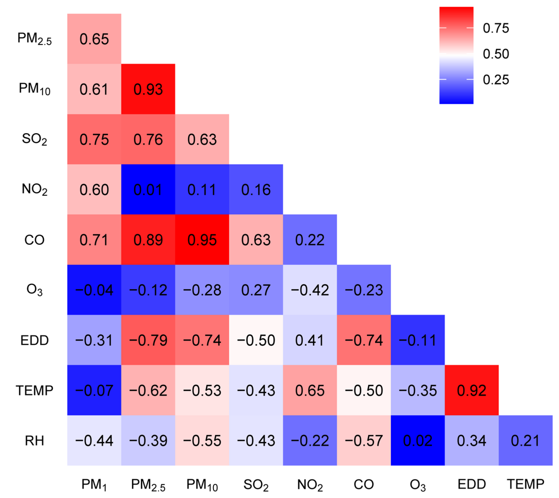

FIGURE 1
Correlation coefficients between seven air pollutants, solar radiation (EDD), temperature, and humidity.

statistically significant differences in estimating the risk of osteoporosis occurrence (P for heterogeneity). Notably, O_3 was influenced to a greater extent by PM_{10} and CO, with a change in effect direction after adjustment.

3.6 Stratified analysis

In Table 3, we present the adjusted percent change (95% CIs) for osteoporosis associated with a 1 μg/m^3 increase in exposure to PM_1, $PM_{2.5}$, PM_{10}, O_3, and a 10 μg/m^3 increase in CO, stratified by age, gender, and BMI. PM_1 and $PM_{2.5}$ showed associations with osteoporosis occurrence only among male participants ($p < 0.05$). Furthermore, their impact on osteoporosis risk in males was significantly higher than in females ($p = 0.02$). Among participants aged 60 and above, all four pollutants exhibited associations with osteoporosis, with effect sizes greater in absolute value compared to those below 60. However, these associations did not reach statistical significance. Similarly, no significant differences were observed in the associations between long-term pollutant exposure and osteoporosis across different BMI groups ($p = 0.02$). Nevertheless, it is worth noting that particle pollutants showed significant associations with osteoporosis only in individuals with a BMI greater than or equal to 25.

4 Discussion

This study presents the first evidence of a delayed effect of long-term exposure to air pollution on the occurrence of osteoporosis, with a more stable association observed at 4 to 5 years of exposure lag (lag03, lag04). The emergence of PM_{10} as a robust indicator for assessing the relationship between particulate matter and osteoporosis is particularly noteworthy. Furthermore, our research identified individuals aged 60 and above, as well as those with a BMI of ≥25, as vulnerable populations to air pollutant-related osteoporosis. These significant findings offer valuable insights for further research and

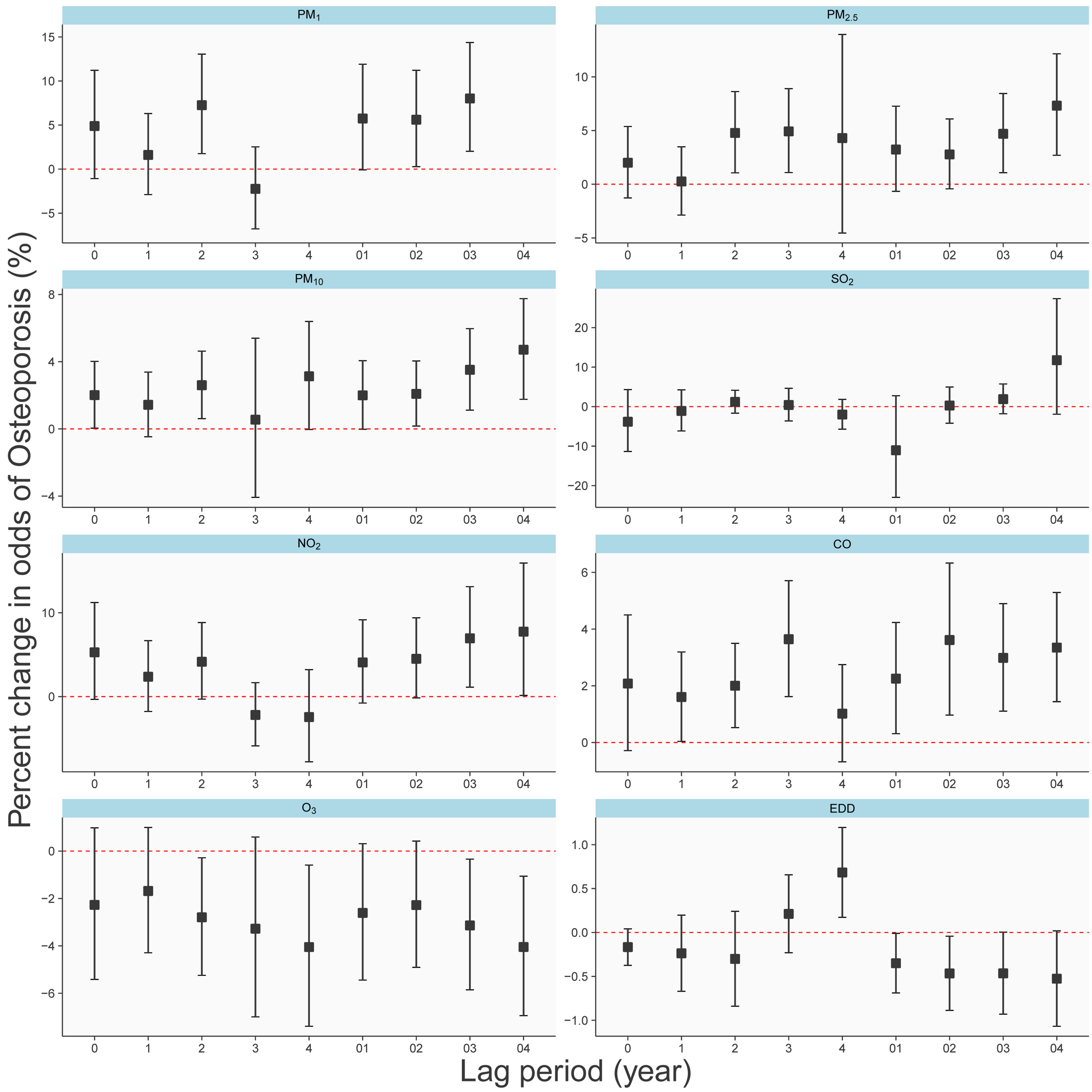

FIGURE 2
Different effects of air pollutants and EDD on the osteoporosis in single-year lag model and average lag model.

intervention strategies, contributing to the enhancement of public health and the formulation of environmental policies.

Our study revealed a dose–response relationship between long-term exposure to PM_1, $PM_{2.5}$, and PM_{10} and the risk of osteoporosis, with the odds ratios (ORs) increasing with prolonged exposure (Figure 2). More specifically, at a 5-year lag (lag04), an average increase of 1 μg/m³ in $PM_{2.5}$ and PM_{10} was associated with a 9.5 and 5.4% increased risk of osteoporosis, respectively (Figure 4). Notably, the effectiveness of $PM_{2.5}$ was slightly higher than that found in a previous study in Hubei Province, China, which reported a 5% increased risk for every 1 μg/m³ increase in $PM_{2.5}$ using a 2-year average exposure (lag01) without adjusting for temperature and humidity [OR: 1.05 (1.00, 1.11)] (21). However, they did not find a statistically significant association with osteoporosis for 1-year [OR: 1.040 (0.994, 1.088)] and 3-year [OR: 1.037 (0.990, 1.086)] average exposures, highlighting the necessity of correcting for meteorological factors and presenting lag effects comprehensively. Our results corroborated the findings of an analysis from the UK Biobank (10), which found a 9% increased risk of osteoporosis associated with a 1 interquartile range (IQR) increase (1.3 μg/m³) in $PM_{2.5}$ during the follow-up period [HR: 1.09 (1.06, 1.12)]. Another report using UK Biobank data supported our results (22), showing a 94% increased risk of osteoporosis for a 10 μg/m³ increase in PM_{10} [HR: 1.94 (1.52, 2.48)], with their $PM_{2.5}$ exposure levels ranging from 8.2 to 21.3 μg/m³, averaging 9.9 μg/m³. This highlighted the linear relationship between $PM_{2.5}$ and osteoporosis risk observed in our study (Figure 3), even at lower concentration levels. Regarding PM_{10}, the UK Biobank results demonstrated a 4% increased risk of osteoporosis associated with a 2.4 μg/m³ increase

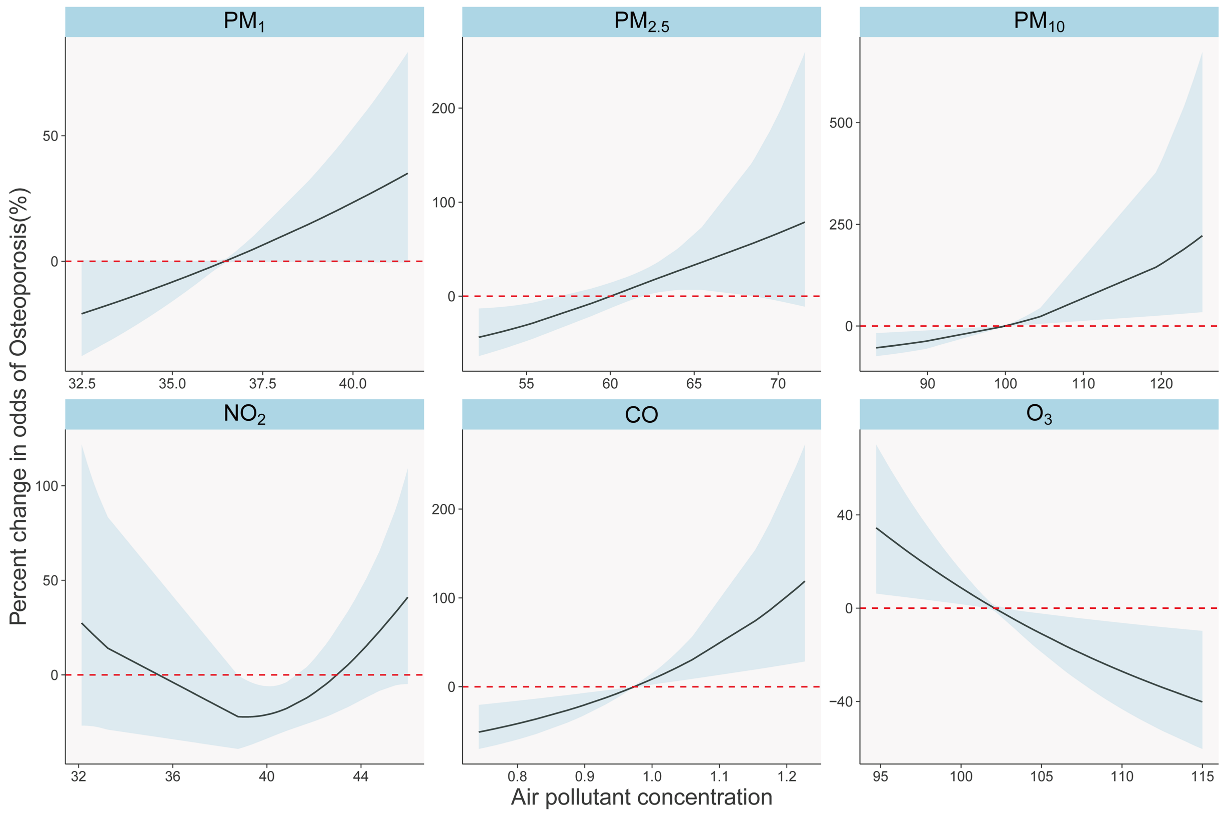

FIGURE 3
Exposure-response relationships between long-term air pollutants exposure and osteoporosis in single pollutants models. The solid black lines with shade show percent changes and 95% CI of osteoporosis odds. The dotted red lines show the referent position of 0.

[HR: 1.04 (1.01, 1.07)] (10), consistent with our findings using lag0 (Figure 3). Therefore, our Figure 2 served as a valuable reference for explaining differences in similar studies. Additionally, studies from South Korea (23) and Italy (24) reported associations between PM_{10} exposure and increased osteoporosis risk, but they employed different categorization methods for PM_{10} and did not report specific dose–response relationships. Furthermore, the Korean study (23) did not find an association between $PM_{2.5}$ and osteoporosis.

While research on PM_1 was relatively limited (11, 12), our study revealed that after adjusting for EDD (Erythemal Daily Dose), the impact of PM_1 on osteoporosis lacked statistical significance (Figure 4). In contrast, when not adjusting for EDD, PM_1 remained a risk factor (Figure 2), and the effect of PM_1 per unit dose was even more pronounced. Furthermore, it's worth noting that a study employed a 3-year average PM_1 concentration and found a correlation with a −5.38 unit decrease in quantitative ultrasound index (95% CI: −6.17, −4.60) (21), this harm had already been reflected in $PM_{2.5}$ and PM_{10}. Research on rural populations in Henan, China, also discovered that a 1 μg/m^3 increase in the three-year average of PM_1, $PM_{2.5}$, and PM_{10} resulted in a 14.9, 14.6, and 7.3% higher risk of osteoporosis, respectively (25). It's important to highlight that the efficacy of these pollutants in their study surpassed our findings, possibly due to their use of quantitative ultrasound bone density measurements to assess osteoporosis (25).

The association between PM and osteoporosis was attributed to their ability to penetrate the lower respiratory tract, exerting both direct and indirect harmful effects on various organs and tissues. These harmful effects stemmed from PM components' capability to traverse respiratory membranes, gaining access to the bloodstream. The direct effects resulted from PM components' ability to traverse respiratory membranes and enter the bloodstream, whereas the indirect effects encompassed systemic consequences of localized airway reactions, which involved four potential mechanisms reported in the literature: inflammation, vitamin D, oxidative damage, and some environmental endocrine disruptors (26).

In gaseous pollutants, we observed a relatively stable association between CO and osteoporosis (Figure 4). Previous research has reported a negative correlation between CO exposure and BMD T-scores in a study from Taiwan (27). Furthermore, a prior study based on healthcare data from Taiwan, China, found that an increase in CO exposure was associated with an increase in osteoporosis incidence from 13.58 per 1,000 person-years to 22.25 per 1,000 person-years (28). The binding affinity of CO to hemoglobin is much higher than that of oxygen (O_2) (29), which thus leads to hypoxia by reducing oxygen-carrying capacity and decreasing O_2 release to tissues (30). This hypoxia has been confirmed to reduce the growth of osteoblasts, resulting in bone thinning and osteoporosis (31).

Our study also unveiled a protective effect of O_3 against osteoporosis. This protective effect persisted even after adjusting for EDD (Erythemal Daily Dose), suggesting that O_3 may have independent effects apart from UV radiation (Figure 4). In line with our findings, a study by Lin et al. in 2022 in Taiwan (27) found a positive correlation between annual average O_3 exposure levels and

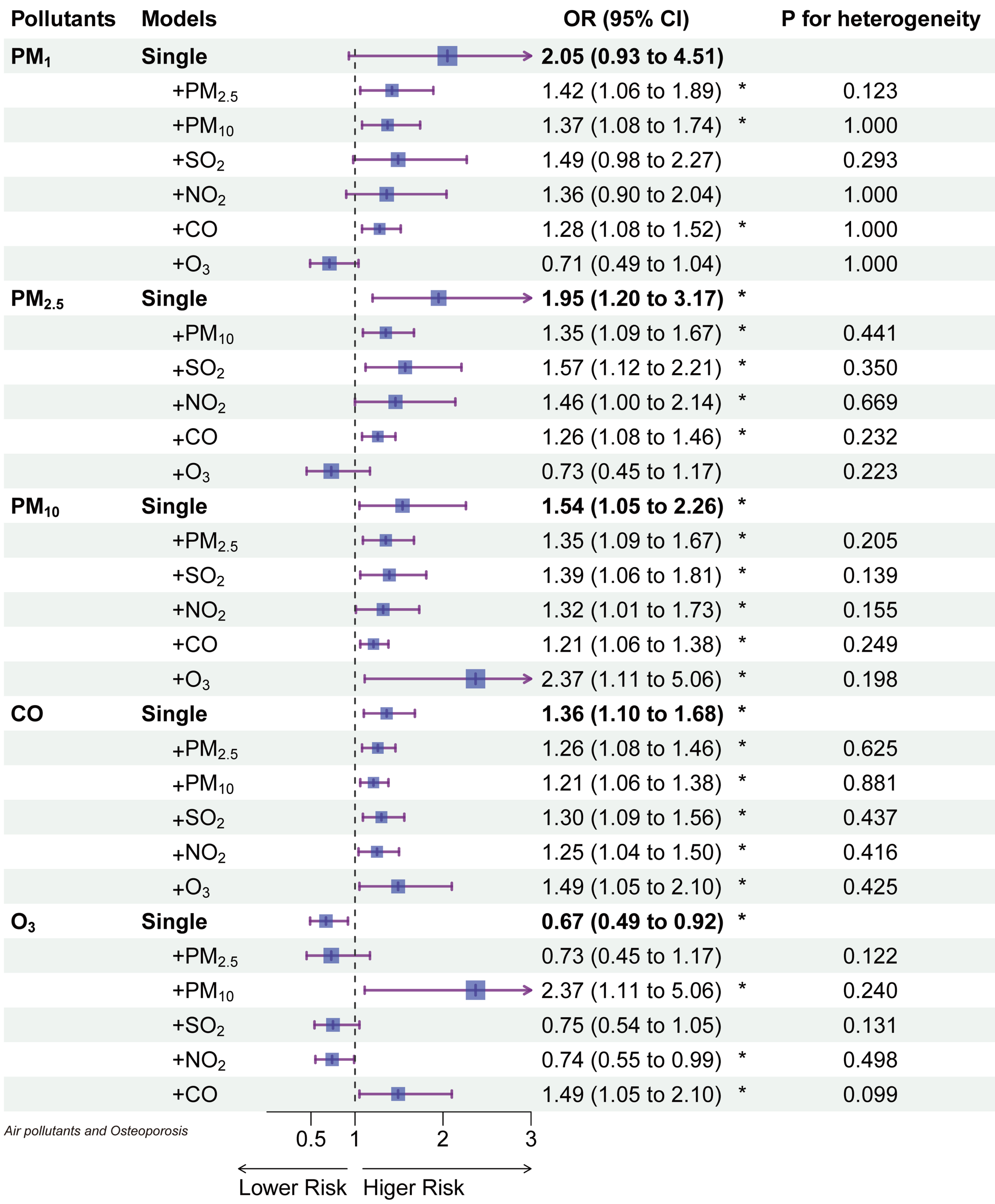

FIGURE 4
The odds ratios of osteoporosis associated with a 10 μg/m³ increase of each air pollutant (100 μg/m³ for CO) in single and 2-pollutant models.

BMD T-scores. Furthermore, literature searches have indicated an increasing clinical use of O_3 therapy for conditions such as disc herniation, jawbone necrosis, and pain management (32, 33). O_3 therapy has been demonstrated to promote complete healing of bisphosphonate-related jawbone necrosis by restoring normal function (32). Additionally, two separate studies involving rats have shown that O_3 has a positive impact on bone formation. One study involved cranial bone defects in rats (34), while another study with 48 rats demonstrated that O_3 therapy increased the number of osteoclasts and osteoblasts and stimulated bone regeneration (35). These combined findings suggest a physiological basis for the protective effect of O_3 against osteoporosis.

In our study, both SO_2 and NO_2 did not independently affect osteoporosis, which is consistent with research conducted in Hubei, China (21). Furthermore, we discovered a U-shaped relationship between NO_2 and osteoporosis, indicating a non-linear association that might have limited our ability to identify a clear link between them. Furthermore, a meta-analysis indicated that SO_2 exposure was

TABLE 3 Adjusted percent change (95% CIs) for osteoporosis associated with 1 μg/m³ increase of exposures to PM_1, $PM_{2.5}$, PM_{10}, and 10 μg/m³ CO stratified by age, gender, and BMI.

	Adjusted percent change (95% CIs)				O_3
	PM_1	$PM_{2.5}$	PM_{10}	CO	
Age					
<60	2.92 (−13.75,22.79)	0.47 (−9.88,12)	−0.37 (−7.19,6.96)	0.5 (−3.73,4.91)	−1.41 (−8.18,5.86)
≥60	**10.38 (2.93,18.37)***	**10.53 (4.37,17.05)***	**6.84 (2.48,11.39)***	**4.18 (1.61,6.82)***	**−4.90 (−8.62,-1.04)***
p value[a]	0.47	0.13	0.1	0.16	0.39
Gender					
Male	**22.24 (6.52,40.29)***	**24.1 (8.98,41.31)***	7.2 (−2.02,17.3)	4.67 (−1.02,10.68)	−6.28 (−15.06,3.4)
Female	2.46 (−3.54,8.83)	4.99 (−0.83,11.15)	3.78 (−0.06,7.76)	**2.64 (0.31,5.03)***	−2.75 (−6.11,0.74)
p value	0.02*	0.02*	0.51	0.53	0.49
BMI					
<25	5.97 (−3.98,16.96)	6.19 (−0.87,13.75)	4.06 (−0.59,8.93)	**2.95 (0.12,5.85)***	**−3.95 (−7.67,-0.08)***
≥25	**10.97 (0.51,22.53)***	**9.53 (1.61,18.07)***	**6.17 (0.47,12.2)***	**4.14 (0.70,7.70)***	−4.18 (−9.38,1.33)
p value	0.52	0.55	0.58	0.61	0.95

PM_1, $PM_{2.5}$, PM_{10} particulate matter with an aerodynamic diameter ≤ 1, 2.5,10 μm; CO, carbon monoxide; CI, confidence interval; BMI, body mass index. [a]The value of p in a z-test assesses the significance of coefficient differences between two model groups. *$p < 0.05$. The bold value were statistical significant data.

associated with a non-significant increase in bone mineral density (BMD) (11).

Subgroup analysis indicated that individuals aged 60 and above were the most susceptible to air pollution-induced osteoporosis, potentially due to age-related immunosuppression, rendering them more vulnerable to environmental pollution. We also observed that males were more sensitive to the effects of $PM_{2.5}$ and PM_1, which was consistent with previous reports that found that the non-standardized coefficient β (95% CI) between BMD T-score and each 1 μg/m³ increase in $PM_{2.5}$ was higher in males than females [−0.005 (−0.011, 0.000) for males vs. −0.001 (−0.007, 0.005) for females] (27). Notably, individuals with a BMI ≥25 were more susceptible to the impact of air pollution, despite the protective effect of higher BMI against osteoporosis (Table 1). This susceptibility among lower-risk individuals could be explained by the fact that air pollution can trigger systemic inflammation and oxidative stress. Overweight or obese individuals often exhibited a chronic inflammatory state due to the presence of inflammatory cells and mediators in adipose tissue (36). This chronic inflammation may have heightened their sensitivity to the detrimental effects of air pollutants, as inflammation can increase cellular susceptibility to the harmful effects of gasses and particulate matter.

This study is the first to correct for the influences of both humidity and solar radiation in quantitatively assessing the correlation between air pollutants and osteoporosis. Our study also has several strengths. Firstly, we employed DXA, the gold standard for diagnosing osteoporosis, to assess bone density at six sites. This was executed meticulously through a rigorous process of stratified random sampling and the use of standardized equipment. Furthermore, we diligently standardized the equipment across all hospitals involved in the project, a crucial step that ensured the uniformity and reliability of our test results. Secondly, we also considered temperature, humidity, and ultraviolet radiation in our comprehensive analysis of air pollution and osteoporosis. Finally, for the first time, we showed how osteoporosis risk varies with different pollutants and lag times. Our study strongly indicates that as exposure duration to pollutants increases, the osteoporosis risk per unit dose of pollutants fluctuates.

Our study still has some limitations, primarily the relatively small sample size. Conducting active monitoring using DXA measurement, while ensuring result reliability, constrained our sample size. The present research cohort size has already enabled us to identify a statistically significant correlation between exposure to air pollutants and osteoporosis. While a larger sample size may bolster the observed correlation between short-term exposure and osteoporosis, it is unlikely to alter our established conclusion that the association is notably stronger with long-term exposure. However, extending the conclusion to a broader scope might necessitate a wider range of exposure to pollutants, thereby gaining further insights into the health effects at higher or lower concentrations. In the future, we plan to obtain national data from all participants in our project for further analysis. Second, due to limited air pollution data availability, we could only access data from 2013 onwards, limiting our analysis of longer exposure lags on osteoporosis. Finally, despite our best efforts to adjust for confounding factors, we cannot eliminate residual confounding, especially since factors influencing osteoporosis and bone mineral density are not yet fully understood.

Conclusively, this study reveals a potential link between air pollutants and osteoporosis, particularly emphasized with prolonged exposure. The susceptibility to air pollution-induced osteoporosis seems heightened in individuals aged 60 and above, those with a BMI exceeding 25, and among males. These findings identify specific demographics requiring targeted public health interventions to mitigate the adverse effects of air pollution on their bone health.

Data availability statement

The original contributions presented in the study are included in the article/Supplementary material, further inquiries can be directed to the corresponding authors.

Author contributions

HS: Conceptualization, Formal analysis, Funding acquisition, Supervision, Writing – original draft, Writing – review & editing. YW: Conceptualization, Data curation, Methodology, Writing – original draft, Writing – review & editing. XP: Investigation, Writing – review & editing, Supervision. WY: Investigation, Writing – review & editing. JS: Investigation, Resources, Writing – review & editing. JL: Investigation, Writing – review & editing. GZ: Investigation, Writing – review & editing. XL: Investigation, Writing – review & editing. XX: Investigation, Resources, Writing – review & editing. YZ: Conceptualization, Data curation, Investigation, Resources, Writing – original draft, Writing – review & editing.

Funding

The author(s) declare financial support was received for the research, authorship, and/or publication of this article. This research received support from the Key Project of Medical Science Research of Jiangsu Provincial Health Commission (K2023045). The funding offers the publication fee.

Acknowledgments

We extend our gratitude to Haidong Kan from Fudan University for conducting the EDD exposure assessment and to Yuewei Liu from Sun Yat-sen University for their valuable contributions in assessing air pollution and meteorological factors exposure.

Conflict of interest

The authors declare that the research was conducted in the absence of any commercial or financial relationships that could be construed as a potential conflict of interest.

Publisher's note

All claims expressed in this article are solely those of the authors and do not necessarily represent those of their affiliated organizations, or those of the publisher, the editors and the reviewers. Any product that may be evaluated in this article, or claim that may be made by its manufacturer, is not guaranteed or endorsed by the publisher.

Supplementary material

The Supplementary material for this article can be found online at: https://www.frontiersin.org/articles/10.3389/fpubh.2024.1361911/full#supplementary-material

References

1. Clynes MA, Harvey NC, Curtis EM, Fuggle NR, Dennison EM, Cooper C. The epidemiology of osteoporosis. *Br Med Bull*. (2020) 133:105–17. doi: 10.1093/bmb/ldaa005

2. GBD. Global, regional, and national age-sex-specific mortality for 282 causes of death in 195 countries and territories, 1980-2017: a systematic analysis for the global burden of disease study 2017. *Lancet*. (2018) 392:1736–88. doi: 10.1016/S0140-6736(18)32203-7

3. Si L, Winzenberg TM, Jiang Q, Chen M, Palmer AJ. Projection of osteoporosis-related fractures and costs in China: 2010-2050. *Osteoporos Int*. (2015) 26:1929–37. doi: 10.1007/s00198-015-3093-2

4. Wang L, Yu W, Yin X, Cui L, Tang S, Jiang N, et al. Prevalence of osteoporosis and fracture in China: the China osteoporosis prevalence study. *JAMA Netw Open*. (2021) 4:e2121106. doi: 10.1001/jamanetworkopen.2021.21106

5. Chen B, Kan H. Air pollution and population health: a global challenge. *Environ Health Prev Med*. (2008) 13:94–101. doi: 10.1007/s12199-007-0018-5

6. Falch JA, Ilebekk A, Slungaard U. Epidemiology of hip fractures in Norway. *Acta Orthop Scand*. (1985) 56:12–6. doi: 10.3109/17453678508992970

7. Alvaer K, Meyer HE, Falch JA, Nafstad P, Sogaard AJ. Outdoor air pollution and bone mineral density in elderly men – the Oslo health study. *Osteoporos Int*. (2007) 18:1669–74. doi: 10.1007/s00198-007-0424-y

8. Prada D, Zhong J, Colicino E, Zanobetti A, Schwartz J, Dagincourt N, et al. Association of air particulate pollution with bone loss over time and bone fracture risk: analysis of data from two independent studies. *Lancet Planet Health*. (2017) 1:e337–47. doi: 10.1016/S2542-5196(17)30136-5

9. Sung JH, Kim K, Cho Y, Choi S, Chang J, Kim SM, et al. Association of air pollution with osteoporotic fracture risk among women over 50 years of age. *J Bone Miner Metab*. (2020) 38:839–47. doi: 10.1007/s00774-020-01117-x

10. Yang Y, Li R, Cai M, Wang X, Li H, Wu Y, et al. Ambient air pollution, bone mineral density and osteoporosis: results from a national population-based cohort study. *Chemosphere*. (2023) 310:136871. doi: 10.1016/j.chemosphere.2022.136871

11. Mousavibaygei SR, Bisadi A, ZareSakhvidi F. Outdoor air pollution exposure, bone mineral density, osteoporosis, and osteoporotic fractures: a systematic review and meta-analysis. *Sci Total Environ*. (2023) 865:161117. doi: 10.1016/j.scitotenv.2022.161117

12. Pang KL, Ekeuku SO, Chin KY. Particulate air pollution and osteoporosis: a systematic review. *Risk Manag Healthc Policy*. (2021) 14:2715–32. doi: 10.2147/RMHP.S316429

13. Kanis JA, Melton LJ 3rd, Christiansen C, Johnston CC, Khaltaev N. The diagnosis of osteoporosis. *J Bone Miner Res*. (1994) 9:1137–41. doi: 10.1002/jbmr.5650090802

14. Xu R, Wei J, Liu T, Li Y, Yang C, Shi C, et al. Association of short-term exposure to ambient PM1 with total and cause-specific cardiovascular disease mortality. *Environ Int*. (2022) 169:107519. doi: 10.1016/j.envint.2022.107519

15. Xu R, Huang S, Shi C, Wang R, Liu T, Li Y, et al. Extreme temperature events, fine particulate matter, and myocardial infarction mortality. *Circulation*. (2023) 148:312–23. doi: 10.1161/CIRCULATIONAHA.122.063504

16. Liu J, Shi C, Sun S, Liang J, Yang Z-L. Improving land surface hydrological simulations in China using CLDAS meteorological forcing data. *J Meteorol Res*. (2020) 33:1194–206. doi: 10.1007/s13351-019-9067-0

17. Tie R, Shi C, Wan G, Xingjie H, Kang L, Ge L. CLDASSD: reconstructing fine textures of the temperature field using super-resolution technology. *Adv Atmos Sci*. (2022) 39:117–30. doi: 10.1007/s00376-021-0438-y

18. Pan J, Yao Y, Liu Z, Meng X, Ji JS, Qiu Y, et al. Warmer weather unlikely to reduce the COVID-19 transmission: an ecological study in 202 locations in 8 countries. *Sci Total Environ*. (2021) 753:142272. doi: 10.1016/j.scitotenv.2020.142272

19. Zhou Y, Meng X, Belle JH, Zhang H, Kennedy C, Al-Hamdan MZ, et al. Compilation and spatio-temporal analysis of publicly available total solar and UV irradiance data in the contiguous United States. *Environ Pollut*. (2019) 253:130–40. doi: 10.1016/j.envpol.2019.06.074

20. Di Q, Dai L, Wang Y, Zanobetti A, Choirat C, Schwartz JD, et al. Association of Short-term Exposure to air pollution with mortality in older adults. *JAMA*. (2017) 318:2446–56. doi: 10.1001/jama.2017.17923

21. Zhang F, Zhou F, Liu H, Zhang X, Zhu S, Zhang X, et al. Long-term exposure to air pollution might decrease bone mineral density T-score and increase the prevalence of osteoporosis in Hubei province: evidence from China osteoporosis prevalence study. *Osteoporos Int*. (2022) 33:2357–68. doi: 10.1007/s00198-022-06488-7

22. Xu C, Weng Z, Liu Q, Xu J, Liang J, Li W, et al. Association of air pollutants and osteoporosis risk: the modifying effect of genetic predisposition. *Environ Int*. (2022) 170:107562. doi: 10.1016/j.envint.2022.107562

23. Shin J, Kweon HJ, Kwon KJ, Han SH. Incidence of osteoporosis and ambient air pollution in South Korea: a population-based retrospective cohort study. *BMC Public Health*. (2021) 21:1794. doi: 10.1186/s12889-021-11866-7

24. Adami G, Cattani G, Rossini M, Viapiana O, Olivi P, Orsolini G, et al. Association between exposure to fine particulate matter and osteoporosis: a population-based cohort study. *Osteoporos Int*. (2022) 33:169–76. doi: 10.1007/s00198-021-06060-9

25. Qiao D, Pan J, Chen G, Xiang H, Tu R, Zhang X, et al. Long-term exposure to air pollution might increase prevalence of osteoporosis in Chinese rural population. *Environ Res*. (2020) 183:109264. doi: 10.1016/j.envres.2020.109264

26. Prada D, Lopez G, Solleiro-Villavicencio H, Garcia-Cuellar C, Baccarelli AA. Molecular and cellular mechanisms linking air pollution and bone damage. *Environ Res*. (2020) 185:109465. doi: 10.1016/j.envres.2020.109465

27. Lin YH, Wang CF, Chiu H, Lai BC, Tu HP, Wu PY, et al. Air pollutants interaction and gender difference on bone mineral density T-score in Taiwanese adults. *Int J Environ Res Public Health*. (2020) 17:9165. doi: 10.3390/ijerph17249165

28. Chang KH, Chang MY, Muo CH, Wu TN, Hwang BF, Chen CY, et al. Exposure to air pollution increases the risk of osteoporosis: a nationwide longitudinal study. *Medicine (Baltimore)*. (2015) 94:e733. doi: 10.1097/MD.0000000000000733

29. Von Burg R. Toxicology update. *J Appl Toxicol*. (1999) 19:379–86. doi: 10.1002/(sici)1099-1263(199909/10)19:5<379::Aid-jat563>3.0.Co;2-8

30. Rose JJ, Wang L, Xu Q, McTiernan CF, Shiva S, Tejero J, et al. Carbon monoxide poisoning: pathogenesis, management, and future directions of therapy. *Am J Respir Crit Care Med*. (2017) 195:596–606. doi: 10.1164/rccm.201606-1275CI

31. Chen YL, Weng SF, Shen YC, Chou CW, Yang CY, Wang JJ, et al. Obstructive sleep apnea and risk of osteoporosis: a population-based cohort study in Taiwan. *J Clin Endocrinol Metab*. (2014) 99:2441–7. doi: 10.1210/jc.2014-1718

32. Agrillo A, Ungari C, Filiaci F, Priore P, Iannetti G. Ozone therapy in the treatment of avascular bisphosphonate-related jaw osteonecrosis. *J Craniofac Surg*. (2007) 18:1071–5. doi: 10.1097/scs.0b013e31857261f

33. Ripamonti CI, Maniezzo M, Boldini S, Pessi MA, Mariani L, Cislaghi E. Efficacy and tolerability of medical ozone gas insufflations in patients with osteonecrosis of the jaw treated with bisphosphonates-preliminary data: medical ozone gas insufflation in treating ONJ lesions. *J Bone Oncol*. (2012) 1:81–7. doi: 10.1016/j.jbo.2012.08.001

34. Kazancioglu HO, Ezirganli S, Aydin MS. Effects of laser and ozone therapies on bone healing in the calvarial defects. *J Craniofac Surg*. (2013) 24:2141–6. doi: 10.1097/SCS.0b013e3182a244ae

35. Buyuk SK, Ramoglu SI, Sonmez MF. The effect of different concentrations of topical ozone administration on bone formation in orthopedically expanded suture in rats. *Eur J Orthod*. (2016) 38:281–5. doi: 10.1093/ejo/cjv045

36. Ellulu MS, Patimah I, Khaza'ai H, Rahmat A, Abed Y. Obesity and inflammation: the linking mechanism and the complications. *Arch Med Sci*. (2017) 4:851–63. doi: 10.5114/aoms.2016.58928

frontiers | Frontiers in Public Health

TYPE Original Research
PUBLISHED 07 February 2024
DOI 10.3389/fpubh.2024.1338319

OPEN ACCESS

EDITED BY
Shupeng Zhu,
Zhejiang University, China

REVIEWED BY
Jinlai Wei,
Fujifilm Irvine Scientific, Inc., United States
Mengyi Li,
University of California, Irvine, United States

*CORRESPONDENCE
Ruiyu Wang
✉ 610383472@qq.com

†These authors share first authorship

RECEIVED 14 November 2023
ACCEPTED 26 January 2024
PUBLISHED 07 February 2024

CITATION
Liu Y, Liu N, Xiong W and Wang R (2024) Association between blood ethylene oxide levels and periodontitis risk: a population-based study.
Front. Public Health 12:1338319.
doi: 10.3389/fpubh.2024.1338319

Association between blood ethylene oxide levels and periodontitis risk: a population-based study

Yixuan Liu[1†], Nuozhou Liu[2,3,4†], Wei Xiong[2,3] and Ruiyu Wang[2,3*]

[1]State Key Laboratory of Oral Diseases, National Clinical Research Center for Oral Diseases, West China Hospital of Stomatology, Sichuan University, Chengdu, China, [2]Department of Obstetrics and Gynecology, West China Second University Hospital, Sichuan University, Chengdu, China, [3]Key Laboratory of Birth Defects and Related Diseases of Women and Children, Sichuan University, Ministry of Education, Chengdu, China, [4]West China Hospital, West China School of Medicine, Sichuan University, Chengdu, China

Background: The etiopathogenesis of periodontitis is closely associated with environmental conditions. However, the relationship between ethylene oxide exposure and periodontitis risk remains unclear.

Methods: We selected qualified participants from National Health and Nutrition Examination Survey (NHANES) 2013–2014. Periodontitis was identified according to the criteria of the Community Periodontal Index (CPI), Centers for Disease Control and Prevention (CDC)/American Academy of Periodontology (AAP) definition. Ethylene oxide exposure was quantified by hemoglobin adducts of ethylene oxide (HbEO) levels. Log2-transformation was used to normalize HbEO levels. We designed three logistic regression models to explore potential relationship between HbEO and periodontitis. Restricted cubic spline (RCS) and subgroup analysis were also conducted with all covariates adjusted. We performed multivariable linear regression to appraise the association between the risk of periodontitis and different indicators of inflammation, including white blood cells, neutrophils, lymphocytes, and monocytes. Mediation analysis was subsequently performed to examine whether ethylene oxide exposure contributed to periodontitis development through systemic body inflammation.

Results: A total of 1,065 participants aged more than 30 were incorporated in this study. We identified that participants with higher HbEO levels showed increased risk of periodontitis after adjusting for all covariates (OR = 1.49, 95% CI: 1.14, 1.95, $p = 0.0014$). The results of subgroup analysis remained stable. The restricted cubic spline (RCS) curve also revealed a non-linear correlation between log2-transformed HbEO levels with the risk of periodontitis (p for nonlinear < 0.001). Mediation analysis indicated that HbEO level was significantly associated with four inflammatory mediators, with the mediated proportions of 14.44% ($p < 0.001$) for white blood cell, 9.62% ($p < 0.001$) for neutrophil, 6.17% ($p = 0.006$) for lymphocyte, and 6.72% ($p < 0.001$) for monocyte.

Conclusion: Participants with higher ethylene oxide exposure showed higher risk of periodontitis, which was partially mediated by systemic body inflammation. More well-designed longitudinal studies should be carried out to validate this relationship.

KEYWORDS

periodontitis, ethylene oxide, NHANES, epidemiology, etiology

1 Introduction

Periodontitis is a chronic inflammatory disease characterized by impaired integrity of tooth-supporting tissue, which eventually leads to tooth looseness and the loss of teeth if not properly treated. The high prevalence of periodontitis severely affects patients' life quality and causes enormous socioeconomic burden (1, 2). The etiology of periodontitis is very complex, including but not restricted to environment, life style, diet, and genetic susceptibility (3). Multiple environmental risk factors were associated periodontitis, particularly smoking and particulate matter exposure. These risk factors were considered to have significant pro-inflammatory effects, which may lead to systemic inflammatory reaction and might contribute to periodontitis development (4, 5). Unlike genetic risk factor for periodontitis, environmental risk factors are considered modifiable, and identifying potential environment-related risk is critical to periodontitis management (6).

Ethylene oxide is a common environmental organic compound derived from the metabolism of ethylene. Hemoglobin adducts of ethylene oxide (HbEO) is a significantly sensitive biomarker for ethylene oxide assessment because of its longer half-life *in vivo*. Ethylene oxide has been widely applied as intermediates for various compounds, including ethylene glycols, glycol ethers, and other ethoxylated products (7). In addition, ethylene oxide is an important sterilizing agent for oral medical devices with excellent bactericidal, sporicidal, and virucidal activity (8). Since individuals can be exposed to ethylene oxide through inhalation, it is also recognized as an environmental pollutant derived from tobacco smoke and industrial process. Previous studies indicated that, as a highly reactive volatile organic compound, people exposed to excessive ethylene oxide were more likely to have a higher risk of cardiovascular diseases, respiratory diseases, and cancer (9–11).

However, the relevance of ethylene oxide exposure with periodontitis development remained unclear. Increasing evidence showed that ethylene oxide exposure could intensify systemic body inflammation that affected the development of periodontitis (12, 13). On the one hand, the inflammatory response is a kind of defense mechanism against the invasion of external pathogens. On the other hand, an improperly controlled inflammatory response can cause irreversible damage to periodontal tissues with typical signs of periodontitis such as deep periodontal pockets, attachment loss, and even tooth loss (14). Uncontrolled systemic inflammation not only contributes to the development of periodontitis but also its comorbidities, like cardiovascular and respiratory diseases (3, 15). Since periodontitis is also a chronic systemic inflammatory disease, we hypothesized that a correlation exists between ethylene oxide exposure and risk of periodontitis possibly mediated by systemic body inflammation.

Here, our study aimed to explore the hypothesis that ethylene oxide exposure might contribute to periodontitis, which partially mediated by systemic inflammation, using statistics from the National Health and Nutrition Examination Survey (NHANES) 2013–2014.

2 Materials and methods

2.1 Study design and population

The datasets utilized in our study were based on the National Health and Nutrition Examination Survey (NHANES) 2013–2014, a cross-sectional survey conducted by the National Center for Health Statistics (NCHS). NHANES was used to investigate the health and nutritional status of noninstitutionalized US individuals with a stratified multistage representative sample. All the participants' data collection can be publicly obtained at www.cdc.gov/nchs/nhanes.htm. The original NHANES 2013–2014 dataset was carried out in US populations with approvement from the Centers for Disease Control (CDC) and Prevention National Increase for Health Statistics Research (NCHS) Ethics Review Board. All the participants included have provided written informed consent, which can be accessed from https://www.cdc.gov/nchs/nhanes/irba98.htm. This paper followed the Strengthening the Reporting of Observational Studies in Epidemiology (STROBE) guideline (16).

A total of 19,577 participants were included from 2013 to 2014 cycles in NHANES. Incomplete data of household interviews and physical examinations were excluded ($n = 18{,}512$). As a result, 1,065 participants aged 30 or older were enrolled for the data analysis (Figure 1).

2.2 Assessment of periodontitis

Participants aged ≥ 30 were included for a full-mouth periodontal probing examinations conducted by calibrated examiners.[1] All periodontitis cases reached the criteria of the Community Periodontal Index (CPI), Centers for Disease Control and Prevention (CDC)/American Academy of Periodontology (AAP) definition. The grade of periodontal status was diagnosed according to the CDC/AAP definitions (17). The severity of periodontitis can be categorized as three levels (Supplementary Table 1). Participants were defined as periodontitis cases if they met the criteria of either mild, moderate, or severe periodontitis, while the rest of them were defined as non-periodontitis.

2.3 Assessment of blood ethylene oxide

We exploited a series of standard control strategies to find valid IVs that satisfied three, the reaction product of ethylene oxide with hemoglobin, was utilized to quantify cumulative ethylene oxide exposure for the past 4 months (18, 19). Hemoglobin adducts of ethylene oxide has been testified as a significantly sensitive mark for ethylene oxide exposure because of its longer half-life *in vivo*. Washed-packed blood samples supplied by participants in the morning were processed and stored under −30°C conditions until shipped to the National Center for Environmental Health for evaluation. The modified Edman reaction by high-performance liquid chromatography coupled with tandem mass spectrometry (HPLC-MS/MS) was utilized to assess HbEO in human whole blood or erythrocytes, using the reaction products with the N-terminal valine residue of the hemoglobin protein chains (N-[2-carbamoyl ethyl] valine and N-[2-hydroxycarbamoyl-ethyl] valine ethylene oxide adducts) measured. The results of measurements were exhibited as pmol/g Hb. The accuracy of the test results conformed the quality

1 https://doi.org/10.1111/jphd.12056

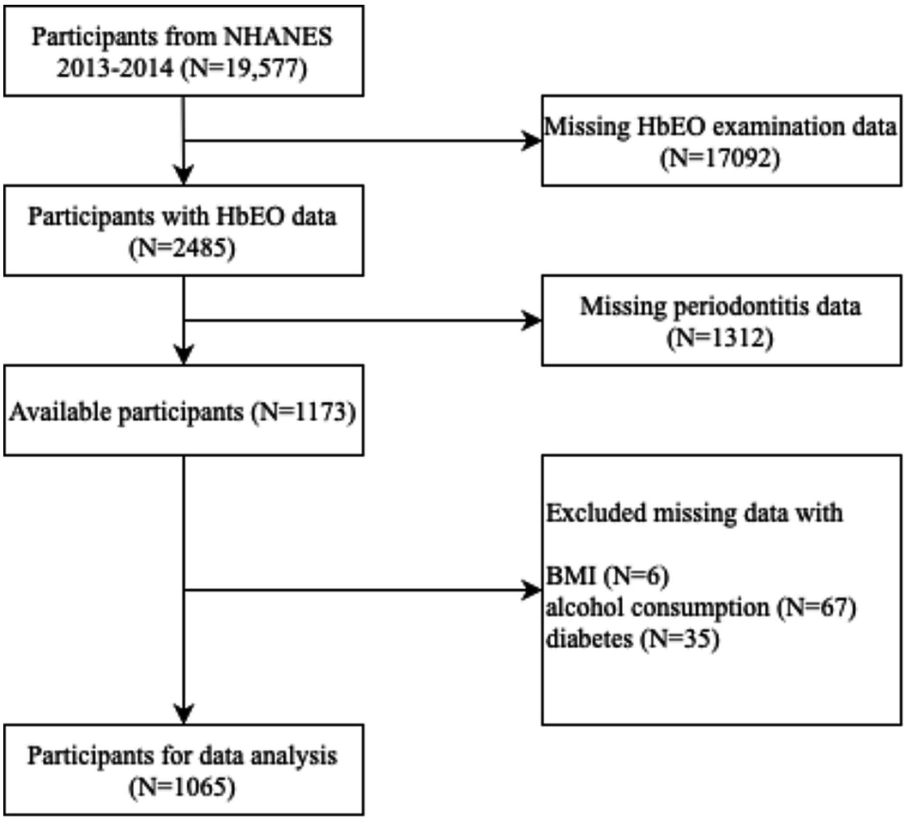

FIGURE 1
Flow chart of process for selection and inclusion of participants. NHANES, National Health and Nutrition Examination Survey; HbEO, hemoglobin adducts of ethylene.

control and quality assurance performance standards of the NCEH Laboratory Sciences Division. More details of the measurement are available at the NHANES Laboratory/Medical Technologist Procedures Manual.[2]

2.4 Covariates

Additional covariates related to periodontitis were comprehensively incorporated in our study, including: (1) demographic characteristics: age (<50, 50~70, and ≥70), gender (male and female), ethnicity (Mexican American, other Hispanic, non-Hispanic white, non-Hispanic black, and other race including multi-racial), alcohol consumption (<12 alcohol drinks/year and ≥12 alcohol drinks/year), smoking (<100 cigarettes in life and ≥100 cigarettes in life). (2) physical examinations parameters: BMI (<25 kg/m^2 and ≥25 kg/m^2). (3) medical conditions: diabetes (yes and no). These 7 cofounding factors have all been identified as risk factors of periodontitis (20–23).

Alcohol users were defined as participants who consumed at least 12 alcohol drinks in a single calendar year. Smokers were defined as individuals who had lifetime use of ≥100 cigarettes. BMI was calculated by dividing the weight (kg) by the square of height in meters (m^2). The diabetes status was identified according to previous self-reported. Individuals who answered "yes" to the question "Have you ever been told by a doctor or other health professional that you had diabetes?" were confirmed the presence of diabetes.

2.5 Statistical analysis

Given to the elaborate sampling design of NHANES, we implemented sample weighting, clustering, and stratification during statistical analysis process. R package "survey" with command "svydesign" was utilized to consider stratified multistage representative sample settings of NHANES (24). Kolmogorov–Smirnov statistical test was conducted in advance to detect the normal distribution of continuous variables. Categorical variables were analyzed by chi-square tests and presented as proportions (%). Continuous variables were presented as the mean ± standard deviation (SD) with normal distribution or medians (IQRs) with non-normal distribution. For normally distributed continuous variables, student t-test was applied to examine the difference, while Mann–Whitney U-test for non-normally distributed variables. Log2-transformed HbEO levels were divided into four intervals in accordance with quartiles and multiple logistic regression models were performed to estimate odds ratios (OR) and 95% confidence intervals (95% CI). In addition, we designed

2 https://wwwn.cdc.gov/Nchs/Nhanes/2013-2014/ETHOX_H.htm

three logistic regression models to assess potential relationship between HbEO and periodontitis. Model 1 was a crude model with no covariates adjusted. Model 2 was adjusted for age, gender and ethnicity. Model 3 was adjusted for all covariates, including age, gender, ethnicity, alcohol consumption, smoking, BMI, and diabetes. Base on this extended model, we carried out restricted cubic spline (RCS) with three knots for dose–response analysis. Subgroup analysis was conducted according to age, gender, ethnicity, alcohol consumption, smoking, BMI and diabetes, as the same way in Model 3. Moreover, we performed multivariable linear regression to appraise the association between the risk of periodontitis and different indicators of inflammation, including white blood cells, neutrophils, Lymphocytes, and monocytes. Mediation analysis was subsequently performed to examine whether ethylene oxide exposure contributed to periodontitis development through systemic body inflammation. All data analysis was operated in R (version 4.1.3) and Python. Two-side $p < 0.05$ was regarded as statistically significant.

3 Results

3.1 Baseline characteristics

We enrolled 1,065 appropriate participants from NHANES 2013–2014 cycle for data analysis. As demonstrated in Figure 2, periodontitis group has a significantly higher log2-transformed HbEO levels than non-periodontitis group ($p < 0.001$).

More details about baseline characteristics are presented in Table 1. Overall, 502 (47.1%) participants were diagnosed as periodontitis. Participants with periodontitis were more likely to be older, male (59.96%), non-Hispanic black (40.24%), and smokers (55.58%). While no significant difference was observed in alcohol consumption ($p = 0.1691$), BMI ($p = 0.5946$), or diabetes ($p = 0.1221$).

3.2 Association between HbEO and periodontitis

The association between HbEO and periodontitis is presented in Table 2. We carried out univariate logistic regression analysis to investigate overall association between continuous log2-transformed HbEO and the prevalence of periodontitis, with a notable difference detected in crude model 1(OR = 1.49, 95% CI = 1.28–1.73, $p < 0.001$). This association remained stable after adjusting for covariates in both model 2 (OR = 1.57, 95% CI = 1.28–1.92, $p < 0.001$) and model 3 (OR = 1.49, 95% CI = 1.14–1.95, $p = 0.014$) by multivariate logistic regression analysis.

Compared with Q1 group for reference, Q4 group indicated a higher risk of periodontitis in all three models: model 1 (OR = 4.18, 95% CI = 1.83–9.58, $p = 0.003$, P for trend < 0.001), model 2 (OR = 5.18, 95% CI = 1.65–16.22, $p = 0.012$, P for trend = 0.030), and model 3 (OR = 4.30, 95% CI = 0.50–36.89, $p = 0.010$, P for trend = 0.014).

The restricted cubic spline (RCS) curve also revealed a positive nonlinear correlation of log2-transformed HbEO levels with the risk of periodontitis in both adjusted and unadjusted model (Figure 3; p for non-linearity < 0.001). Briefly, higher HbEO levels were associated with an increased risk of periodontitis.

3.3 Subgroup analysis

As shown in Table 3, no significant interaction was identified (all p for interaction > 0.05) in all subgroups. The influence of HbEO on periodontitis was generally consistent among different age, gender, alcohol consumption, smoking, BMI, and diabetes subgroups. Notably, the association between ethylene oxide and periodontitis was non-significant among participants aged ≥70 (OR = 1.75, 95% CI = 0.53–5.75) or smoked ≥ 100 cigarettes in life (OR = 1.09, 95% CI = 0.65–1.82).

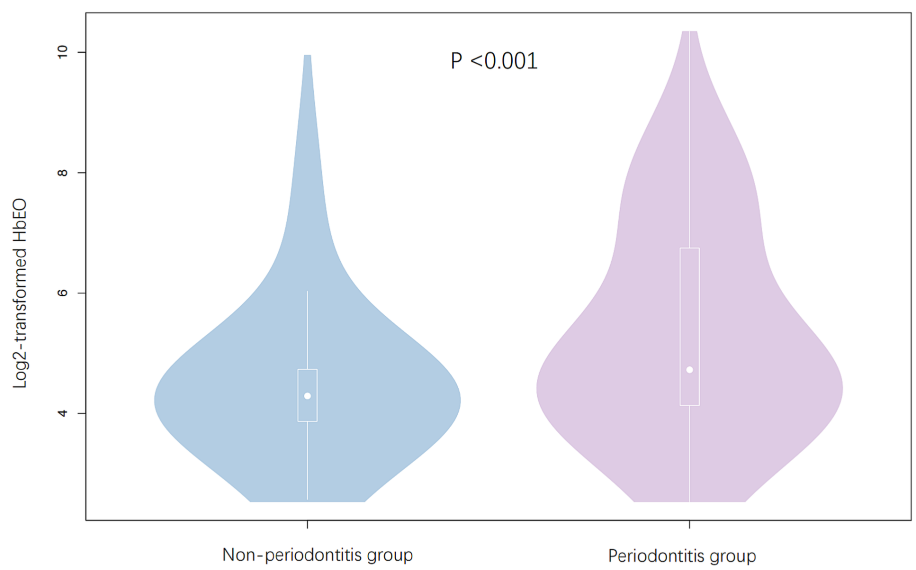

FIGURE 2
Log2-transformed HbEO levels in non-periodontitis group and periodontitis group.

TABLE 1 Characteristics of participants based on PD status.

Variables	Non-PD group (*N* = 563)	PD group (*N* = 502)	Value of *p*
Age (years)			<0.0001
(median [IQR])	47.000 [38.000, 59.000]	55.000 [43.000, 65.000]	
Gender, *n* (%)			<0.0001
Male	230 (40.85)	301 (59.96)	
Female	333 (59.15)	201 (40.04)	
Ethnicity, *n* (%)			0.0255
Mexican American	73 (12.97)	82 (16.33)	
Other Hispanic	48 (8.53)	42 (8.37)	
Non-Hispanic white	261 (46.36)	202 (40.24)	
Non-Hispanic black	94 (16.70)	114 (22.71)	
Other race including multi-racial	87 (15.45)	62 (12.35)	
Alcohol consumption, *n* (%)			0.1691
<12 alcohol drinks/year	160 (28.42)	123 (24.50)	
≥12 alcohol drinks/year	403 (71.58)	379 (75.50)	
Smoking, *n* (%)			<0.0001
<100 cigarettes in life	364 (64.65)	223 (44.42)	
≥100 cigarettes in life	199 (35.35)	279 (55.58)	
BMI (kg/m^2)			0.5946
<25.0	155 (27.53)	130 (25.90)	
≥25.0	408 (72.47)	372 (74.10)	
Diabetes, *n* (%)			0.1221
Yes	65 (11.55)	75 (14.94)	
No	498 (88.45)	427 (85.06)	

BMI, body mass index.

TABLE 2 Multivariate logistic regression analysis of log2-transformed HbEO for risk of PD.

	Model 1		Model 2		Model 3	
	Crude OR (95%CI)	*p*-value	Adjusted OR (95%CI)	*p*-value	Adjusted OR (95%CI)	*p*-value
Continuous log2-HbEO	1.49 (1.28–1.73)	<0.001	1.57 (1.28–1.92)	<0.001	1.49 (1.14–1.95)	0.014
Q1 group	Reference		Reference		Reference	
Q2 group	1.97 (1.05–3.69)	0.037	1.85(0.87–3.96)	0.095	1.72 (0.42–7.11)	0.241
Q3 group	5.43 (2.76–10.72)	<0.001	7.71 (3.21–18.51)	0.001	6.32 (1.29–30.94)	0.038
Q4 group	4.18(1.83–9.58)	0.003	5.18 (1.65–16.22)	0.012	4.30 (0.50–36.89)	0.010
P for trend	<0.001		0.030		0.014	

Model 1 was a crude model with no covariates adjusted. Model 2 was adjusted for age, gender, and ethnicity. Model 3 was adjusted for all covariates. HbEO, hemoglobin adducts of ethylene oxide; OR, odd ratio; CI, confidence interval.

3.4 Mediation analysis

Multiple linear regression analysis demonstrated that there were significant correlations between log2-transformed HbEO and white blood cells ($\beta = 0.34$, 95% CI = 0.25–0.43, $p < 0.001$, SE = 0.05), neutrophils ($\beta = 0.22$, 95% CI = 0.15–0.30, $p < 0.001$, SE = 0.04), lymphocyte ($\beta = 0.09$, 95% CI = 0.06–0.12, $p < 0.001$, SE = 0.02), and monocyte ($\beta = 0.02$, 95% CI = 0.008–0.025, $p < 0.001$, SE = 0.004; Table 4).

In addition, mediation analysis identified a mediation proportion of 14.44% ($p < 0.001$) for white blood cells (Supplementary Figure S1), 9.62% ($p < 0.001$) for neutrophils (Supplementary Figure S2), 6.17% ($p = 0.006$) for lymphocyte (Supplementary Figure S3), and 6.72% ($p < 0.001$) for monocyte (Supplementary Figure S4).

4 Discussion

To our knowledge, this is the first large-scale cross-sectional study investigating the association between environmental ethylene oxide exposure and periodontitis risk among adults in the United States and

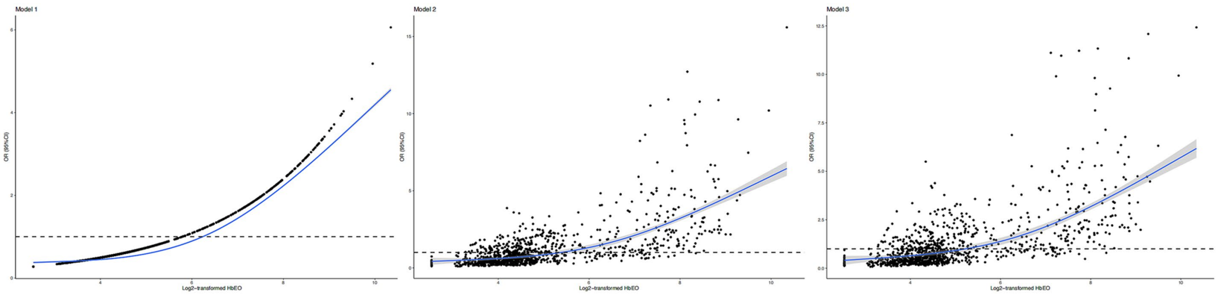

FIGURE 3
Restricted cubic spline (RCS) plots of the association of HbEO levels with periodontitis. **(A)** Model 1: no covariates adjusted; **(B)** Model 2: adjusted for age, gender, and ethnicity. **(C)** Model 3: adjusted for all covariates. OR, odd ratio; (CI), confidence interval; HbEO, hemoglobin adducts of ethylene oxide.

TABLE 3 Subgroup analysis of the association of HbEO levels with PD.

Variables	OR	95% CI	*p* for interaction
Age			0.6611
30–49 years	1.49	1.01–2.18	
50–69 years	1.35	1.01–1.82	
≥70 years	1.75	0.53–5.75	
Gender			0.6859
Male	1.55	1.02–2.35	
Female	1.47	1.16–1.86	
Alcohol consumption			0.6569
<12 alcohol drinks/year	1.87	1.14–3.08	
≥12 alcohol drinks/year	1.46	1.12–1.91	
Smoking			0.2691
<100 cigarettes in life	1.57	1.17–2.10	
≥100 cigarettes in life	1.09	0.65–1.82	
BMI			0.9291
<25.0	1.46	1.18–1.82	
≥25.0	1.52	1.11–2.09	
Diabetes			0.6021
Yes	1.42	1.10–1.83	
No	1.64	1.03–2.61	

HbEO, hemoglobin adducts of ethylene oxide; OR, odds ratio; CI, confidence interval; BMI, body mass index.

the mediation effects of systemic inflammation (including white blood cell count, neutrophil count, lymphocyte count, and monocyte count). We identified that participants with higher HbEO showed higher risk of periodontitis, which was partially mediated by systemic inflammation (Table 5).

It is well-established that periodontitis is a systemic inflammatory disease with complex etiologies at multiple levels, including environmental pollutant exposure, genetics, dysbiotic microbe infection and life styles (3, 25, 26). The prevalence rate of periodontitis in this study was 47.1%, which was generally in line with epidemiological trend report in US but lower than the pool estimate rate of 62% reported by a recent meta-analysis (27, 28). The prevalence rate difference might derive from different population settings and diagnostic criteria and cofounded by the age of participants. Notably, the application of full-mouth periodontal examination combined with details on demographic information and medical conditions among

TABLE 4 Multiple linear regression of log2-transformed HbEO with inflammatory indicators.

Mediators	β	95% CI	*p*-value	SE
White blood cell count	0.34	0.25–0.43	<0.001	0.05
Neutrophil count	0.22	0.15–0.30	<0.001	0.04
Lymphocyte count	0.09	0.06–0.12	<0.001	0.02
Monocyte count	0.02	0.008–0.025	<0.001	0.004

This model was adjusted for age, gender, ethnicity, alcohol consumption, smoking, BMI, and diabetes. HbEO, hemoglobin adducts of ethylene oxide; CI, confidence interval; SE, standard error.

TABLE 5 The mediation effects of inflammatory indicators on the association between log2-transformed HbEO and PD.

Mediators	Total effects	Indirect effects	Direct effects	Mediated proportion (%)	*p*-value
	β (95% CI)	*β* (95% CI)	*β* (95% CI)		
White blood cell count	0.05 (0.04,0.050)	0.01 (0.003,0.01)	0.04 (0.03–0.05)	14.44	<0.001
Neutrophil count	0.05 (0.04,0.05)	0.005 (0.002,0.01)	0.04 (0.04,0.05)	9.62	<0.001
Lymphocyte count	0.05 (0.04,0.05)	0.003 (0.001,0.01)	0.04 (0.04,0.05)	6.17	0.006
Monocyte count	0.05 (0.04,0.05)	0.003 (0.001,0.01)	0.04 (0.04,0.05)	6.72	<0.001

This model was adjusted for age, gender, ethnicity, alcohol consumption, smoking, BMI, and diabetes. HbEO, hemoglobin adducts of ethylene oxide; CI, confidence interval.

NHANES participants aged more than 30 provided a relatively more precise estimate for periodontitis prevalence (27). Since environmental risk factor like cigarette smoking is considered as one of the most important modifiable risk factors for periodontitis prevention and treatment, identifying potential environmental risk factors is critical to periodontitis management (29). Previous studies have shown that exposure to ethylene oxide have mutagenic and genotoxic effects and can produce numerous unfavorable health impacts (30–32). Given the potential mutagenic and genotoxic effects of ethylene oxide, it has been long hypothesized that ethylene oxide exposure from both skin and respiratory tract can increase the risk of malignancies (33–35). A recent cohort study based on the US Environmental Protection Agency's Toxics Release Inventory found that participants locating within 10 km from EtO-emitting sites showed increased risk of *in situ* breast cancer but not invasive breast cancer or non-Hodgkin lymphoma (10). And occupational exposure to ethylene oxide might increase mortality risk from lymphatic and hematopoietic malignancies (36). However, the relationship between ethylene oxide exposure and risk of malignancies remains controversial. A recent systematic review assessing the potential carcinogenicity of ethylene oxide exposure from respiratory tract suggested that there was no association between ethylene oxide exposure and breast cancer, stomach cancer, and lymphohematopoietic malignancies (31). Mundt et al. stated that there was only limited evidence supporting a causal association between ethylene oxide exposure and risk of malignancies (37). As for non-malignant diseases, He et al. reported that people with higher HbEO showed an increased risk of chronic obstructive pulmonary disease (COperiodontitis) partially mediated by inflammation (11). The prevalence rates of hypertension and high diastolic blood pressure were also significantly higher among people with higher HbEO level (38). Elevated level of HbEO was also associated with higher HbA1c, lower high-density lipoprotein cholesterol, and higher risk of diabetes mellitus (39). Peng et al. also reported a dose-dependent risk of kidney stones among people exposed to ethylene oxide (40). A significantly increased risk of spontaneous abortion and pregnancy loss was associated with ethylene oxide exposure during pregnancy. However, there is no existing study concentrating on the relationship between ethylene oxide exposure and periodontitis among general population. The current study found that people with higher HbEO level had significantly increased risk of periodontitis.

The underlying mechanism linking ethylene oxide exposure to incident periodontitis are still unclear. Our results firstly demonstrated that systemic inflammation could contribute to periodontitis development when people exposing to ethylene oxide based on epidemiological analysis, which was generally in line with previous researches. Inflammation was considered as a core part of periodontitis pathogenesis for a long period of time (41–43). Periodontitis patients always showed an obvious systemic inflammatory condition with increased level of white blood cells, segmented neutrophils, and inflammatory cytokines (44, 45). Both innate and adaptive immune response are involved in host–pathogen interactions and produce systemic pro-inflammatory milieu with elevated levels of interleukins, interferon-γ, tumor necrosis factor, and antibodies against microbial biofilm in dental plate (25). Furthermore, this host-pathogen interaction could impair periodontal epithelium leading to systemic periodontal pathogen invasion and produce harmful consequences (25, 46). Mendes et al. reported that diet-induced inflammation was associated with higher risk of periodontitis, which was partially mediated by systemic body inflammation (47). Previous studies have also indicated a significant association between ethylene oxide exposure and inflammation. Lynch et al. firstly discovered that long-period ethylene oxide exposure through respiratory tract cause inflammatory lesions in F344 rats (11, 13). Short-term repeated inhalation of ethylene oxide produced inflammatory response in rats and caused moderate to severe alveolitis after 5-day exposure (48). Sterilization procedures using ethylene oxide has also been suspected for producing post-operative inflammatory for many years (49–51). Li et al. found that ethylene oxide exposure was closely linked with unfavorable serum lipid profiles, with systemic inflammation as a key mediator (18). ethylene oxide exposure might increase the risk of asthma in general population similarly mediating by systemic inflammation (52).

This study possesses multiple strengths. Firstly, this is the first large-scale cross-sectional study assessing the association between HbEO and periodontitis risk among United States residents from NHANES. A subsequent mediation analysis was also conducted. Important cofounders for periodontitis like smoking, alcohol consumption and diabetes were adjusted. Sample weights for NHANES were carefully considered, and the STROBE guideline was followed when reporting our results. Lastly, ethylene oxide has become the mostly preferred sterilization method for medical devices because of its effective bactericidal, sporicidal, and virucidal activity (8). And the sharp increases in the demand for personal protective equipment (PPE) during COVID-19 pandemic may also increase the chance of ethylene oxide exposure. Unlike individual genetic susceptibility for periodontitis, environmental risk factors are considered comparatively modifiable, thus residue control of ethylene oxide is required and practical for periodontitis management.

However, this study still had some limitations. Firstly, the cross-sectional study design hindered us to make causal inference between HbEO and risk of periodontitis. Although NHANES analytical protocol recommended combine different cycles to recruit more participants and improve the stability of data estimates, we only select

NHANES 2013–2014 because only this cycle documented full information on both HbEO and periodontitis (53). Although the association between ethylene oxide exposure and periodontitis could be affected by other environmental pollutant exposure, such as heavy metals and multiple polyaromatic hydrocarbons (54, 55), we could not consider these above due to limited participant number. And we did not classify the severity of periodontitis in our statistical analysis due to limited number of participants. To be noted, since only ethylene oxide levels for those age ≥ 30 was documented in NHANES, we could not incorporate age groups ≤ 30 into statistical analysis. The definition of smoking and alcohol consumption was solely based on personal interview, where recall bias was inevitable. Although HbEO was considered as a cumulative indicator for ethylene oxide exposure for at least 4 months, it would be better if ethylene oxide exposure was measured dynamically (18, 19). Lastly, we could not avoid residual confounding because of the complex etiopathogenesis of periodontitis.

5 Conclusion

Participants with higher ethylene oxide exposure showed higher risk of periodontitis, which was partially mediated by systemic body inflammation. More well-designed longitudinal studies should be carried out to validate this relationship.

Resource identification initiative

1. NHANES, RRID:SCR_013201.
2. R Project for Statistical Computing, RRID:SCR_001905.

Data availability statement

The datasets presented in this study can be found in online repositories. The names of the repository/repositories and accession number(s) can be found in the article/Supplementary material.

Ethics statement

The studies involving humans were approved by the Centers for Disease Control (CDC) and Prevention National Increase for Health Statistics Research (NCHS) Ethics Review Board. The studies were conducted in accordance with the local legislation and institutional requirements. The participants provided their written informed consent to participate in this study.

Author contributions

YL: Conceptualization, Data curation, Formal analysis, Investigation, Methodology, Resources, Software, Validation, Visualization, Writing – original draft. NL: Conceptualization, Data curation, Formal analysis, Investigation, Methodology, Resources, Software, Validation, Visualization, Writing – original draft. WX: Formal analysis, Investigation, Resources, Validation, Writing – original draft. RW: Funding acquisition, Supervision, Writing – review & editing.

Funding

The author(s) declare that no financial support was received for the research, authorship, and/or publication of this article.

Conflict of interest

The authors declare that the research was conducted in the absence of any commercial or financial relationships that could be construed as a potential conflict of interest.

Publisher's note

Supplementary material

The Supplementary material for this article can be found online at: https://www.frontiersin.org/articles/10.3389/fpubh.2024.1338319/full#supplementary-material

References

1. Peres MA, Macpherson LMD, Weyant RJ, Daly B, Venturelli R, Mathur MR, et al. Oral diseases: a global public health challenge. *Lancet.* (2019) 394:249–60. doi: 10.1016/s0140-6736(19)31146-8

2. Kassebaum NJ, Bernabé E, Dahiya M, Bhandari B, Murray CJ, Marcenes W. Global burden of severe periodontitis in 1990-2010: a systematic review and meta-regression. *J Dent Res.* (2014) 93:1045–53. doi: 10.1177/0022034514552491

3. Slots J. Periodontitis: facts, fallacies and the future. *Periodontol.* (2017) 75:7–23. doi: 10.1111/prd.12221

4. Kwon T, Lamster IB, Levin L. Current concepts in the Management of Periodontitis. *Int Dent J.* (2021) 71:462–76. doi: 10.1111/idj.12630

5. Yang T-H, Masumi S-I, Weng S-P, Chen H-W, Chuang H-C, Chuang K-J. Personal exposure to particulate matter and inflammation among patients with periodontal disease. *Sci Total Environ.* (2015) 502:585–9. doi: 10.1016/j.scitotenv.2014.09.081

6. Reynolds MA. Modifiable risk factors in periodontitis: at the intersection of aging and disease. *Periodontol.* (2014) 64:7–19. doi: 10.1111/prd.12047

7. Kolman A, Chovanec M, Osterman-Golkar S. Genotoxic effects of ethylene oxide, propylene oxide and epichlorohydrin in humans: update review (1990-2001). *Mutat Res.* (2002) 512:173–94. doi: 10.1016/s1383-5742(02)00067-4

8. Mendes GC, Brandão TR, Silva CL. Ethylene oxide sterilization of medical devices: a review. *Am J Infect Control.* (2007) 35:574–81. doi: 10.1016/j.ajic.2006.10.014

9. Xie R, Liu L, Liu C, Xie S, Huang X, Zhang Y. Associations of ethylene oxide exposure and "Life's essential 8". *Environ Sci Pollut Res Int*. (2023) 30:121150–60. doi: 10.1007/s11356-023-30741-z

10. Jones RR, Fisher JA, Medgyesi DN, Buller ID, Liao LM, Gierach G, et al. Ethylene oxide emissions and incident breast cancer and non-Hodgkin lymphoma in a US cohort. *J Natl Cancer Inst*. (2023) 115:405–12. doi: 10.1093/jnci/djad004

11. Huang Q, Li S, Wan J, Nan W, He B. Association between ethylene oxide exposure and prevalence of COPD: evidence from NHANES 2013-2016. *Sci Total Environ*. (2023) 885:163871. doi: 10.1016/j.scitotenv.2023.163871

12. Weinreb BD, Shockman GD, Beachey EH, Swift AJ, Winkelstein JA. The ability to sensitize host cells for destruction by autologous complement is a general property of lipoteichoic acid. *Infect Immun*. (1986) 54:494–9. doi: 10.1128/iai.54.2.494-499.1986

13. Lynch DW, Lewis TR, Moorman WJ, Burg JR, Groth DH, Khan A, et al. Carcinogenic and toxicologic effects of inhaled ethylene oxide and propylene oxide in F344 rats. *Toxicol Appl Pharmacol*. (1984) 76:69–84. doi: 10.1016/0041-008x(84)90030-9

14. Cecoro G, Annunziata M, Iuorio MT, Nastri L, Guida L. Periodontitis, low-grade inflammation and systemic health: a scoping review. *Medicina*. (2020) 56:272. doi: 10.3390/medicina56060272

15. Teles F, Collman RG, Mominkhan D, Wang Y. Viruses, periodontitis, and comorbidities. *Periodontol*. (2022) 89:190–206. doi: 10.1111/prd.12435

16. von Elm E, Altman DG, Egger M, Pocock SJ, Gøtzsche PC, Vandenbroucke JP. The strengthening the reporting of observational studies in epidemiology (STROBE) statement: guidelines for reporting observational studies. *PLoS Med*. (2007) 4:e296. doi: 10.1371/journal.pmed.0040296

17. Eke PI, Page RC, Wei L, Thornton-Evans G, Genco RJ. Update of the case definitions for population-based surveillance of periodontitis. *J Periodontol*. (2012) 83:1449–54. doi: 10.1902/jop.2012.110664

18. Zhu X, Kong X, Chen M, Shi S, Cheang I, Zhu Q, et al. Blood ethylene oxide, systemic inflammation, and serum lipid profiles: results from NHANES 2013-2016. *Chemosphere*. (2022) 299:134336. doi: 10.1016/j.chemosphere.2022.134336

19. Törnqvist M, Fred C, Haglund J, Helleberg H, Paulsson B, Rydberg P. Protein adducts: quantitative and qualitative aspects of their formation, analysis and applications. *J Chromatogr B Analyt Technol Biomed Life Sci*. (2002) 778:279–308. doi: 10.1016/s1570-0232(02)00172-1

20. ALHarthi SSY, Natto ZS, Midle JB, Gyurko R, O'Neill R, Steffensen B. Association between time since quitting smoking and periodontitis in former smokers in the National Health and nutrition examination surveys (NHANES) 2009 to 2012. *J Periodontol*. (2019) 90:16–25. doi: 10.1002/jper.18-0183

21. Gay IC, Tran DT, Paquette DW. Alcohol intake and periodontitis in adults aged ≥30 years: NHANES 2009-2012. *J Periodontol*. (2018) 89:625–34. doi: 10.1002/jper.17-0276

22. Borgnakke WS, Genco RJ, Eke PI, Taylor GW. Oral health and diabetes In: CC Cowie, SS Casagrande, A Menke, MA Cissell, MS Eberhardt and JB Meigset al, editors. Diabetes in America is in the public domain of the United States. *Bethesda (MD) of interest.: National Institute of Diabetes and Digestive and Kidney Diseases (US)* (2018)

23. Ghassib IH, Batarseh FA, Wang HL, Borgnakke WS. Clustering by periodontitis-associated factors: a novel application to NHANES data. *J Periodontol*. (2021) 92:1136–50. doi: 10.1002/jper.20-0489

24. Lumley T. Analysis of complex survey samples. *J Stat Softw*. (2004) 9:1–19. doi: 10.18637/jss.v009.i08

25. Kinane DF, Stathopoulou PG, Papapanou PN. Periodontal diseases. *Nat Rev Dis Prim*. (2017) 3:17038. doi: 10.1038/nrdp.2017.38

26. Darby I. Risk factors for periodontitis & peri-implantitis. *Periodontol*. (2022) 90:9–12. doi: 10.1111/prd.12447

27. Eke PI, Borgnakke WS, Genco RJ. Recent epidemiologic trends in periodontitis in the USA. *Periodontol*. (2020) 82:257–67. doi: 10.1111/prd.12323

28. Trindade D, Carvalho R, Machado V, Chambrone L, Mendes JJ, Botelho J. Prevalence of periodontitis in dentate people between 2011 and 2020: a systematic review and meta-analysis of epidemiological studies. *J Clin Periodontol*. (2023) 50:604–26. doi: 10.1111/jcpe.13769

29. Nociti FH Jr, Casati MZ, Duarte PM. Current perspective of the impact of smoking on the progression and treatment of periodontitis. *Periodontol*. (2015) 67:187–210. doi: 10.1111/prd.12063

30. Kirman CR, Li AA, Sheehan PJ, Bus JS, Lewis RC, Hays SM. Ethylene oxide review: characterization of total exposure via endogenous and exogenous pathways and their implications to risk assessment and risk management. *J Toxicol Environ Health B Crit Rev*. (2021) 24:1–29. doi: 10.1080/10937404.2020.1852988

31. Lynch HN, Kozal JS, Russell AJ, Thompson WJ, Divis HR, Freid RD, et al. Systematic review of the scientific evidence on ethylene oxide as a human carcinogen. *Chem Biol Interact*. (2022) 364:110031. doi: 10.1016/j.cbi.2022.110031

32. Sheikh K. Adverse health effects of ethylene oxide and occupational exposure limits. *Am J Ind Med*. (1984) 6:117–27. doi: 10.1002/ajim.4700060206

33. Kolman A, Näslund M, Calleman CJ. Genotoxic effects of ethylene oxide and their relevance to human cancer. *Carcinogenesis*. (1986) 7:1245–50. doi: 10.1093/carcin/7.8.1245

34. Ethylene oxide--a human carcinogen? *Lancet*. (1986) 2:201–2.

35. Jinot J, Fritz JM, Vulimiri SV, Keshava N. Carcinogenicity of ethylene oxide: key findings and scientific issues. *Toxicol Mech Methods*. (2018) 28:386–96. doi: 10.1080/15376516.2017.1414343

36. Stayner L, Steenland K, Greife A, Hornung R, Hayes RB, Nowlin S, et al. Exposure-response analysis of cancer mortality in a cohort of workers exposed to ethylene oxide. *Am J Epidemiol*. (1993) 138:787–98. doi: 10.1093/oxfordjournals.aje.a116782

37. Vincent MJ, Kozal JS, Thompson WJ, Maier A, Dotson GS, Best EA, et al. Ethylene oxide: Cancer evidence integration and dose-response implications. *Dose-Response*. (2019) 17:1559325819888317. doi: 10.1177/1559325819888317

38. Wu N, Cao W, Wang Y, Liu X. Association between blood ethylene oxide levels and the prevalence of hypertension. *Environ Sci Pollut Res Int*. (2022) 29:76937–43. doi: 10.1007/s11356-022-21130-z

39. Guo J, Wan Z, Cui G, Pan A, Liu G. Association of exposure to ethylene oxide with risk of diabetes mellitus: results from NHANES 2013-2016. *Environ Sci Pollut Res Int*. (2021) 28:68551–9. doi: 10.1007/s11356-021-15444-7

40. Song W, Hu H, Ni J, Zhang H, Zhang H, Yang G, et al. The relationship between ethylene oxide levels in hemoglobin and the prevalence of kidney stones in US adults: an exposure-response analysis from NHANES 2013-2016. *Environ Sci Pollut Res Int*. (2023) 30:26357–66. doi: 10.1007/s11356-022-24086-2

41. Hajishengallis G. Immunomicrobial pathogenesis of periodontitis: keystones, pathobionts, and host response. *Trends Immunol*. (2014) 35:3–11. doi: 10.1016/j.it.2013.09.001

42. Listgarten MA. Pathogenesis of periodontitis. *J Clin Periodontol*. (1986) 13:418–25. doi: 10.1111/j.1600-051x.1986.tb01485.x

43. Bosshardt DD. The periodontal pocket: pathogenesis, histopathology and consequences. *Periodontol*. (2018) 76:43–50. doi: 10.1111/prd.12153

44. Craig RG, Yip JK, So MK, Boylan RJ, Socransky SS, Haffajee AD. Relationship of destructive periodontal disease to the acute-phase response. *J Periodontol*. (2003) 74:1007–16. doi: 10.1902/jop.2003.74.7.1007

45. Graves D. Cytokines that promote periodontal tissue destruction. *J Periodontol*. (2008) 79:1585–91. doi: 10.1902/jop.2008.080183

46. Hajishengallis G. Periodontitis: from microbial immune subversion to systemic inflammation. *Nat Rev Immunol*. (2015) 15:30–44. doi: 10.1038/nri3785

47. Machado V, Botelho J, Viana J, Pereira P, Lopes LB, Proença L, et al. Association between dietary inflammatory index and periodontitis: a cross-sectional and mediation analysis. *Nutrients*. (2021) 13:1194. doi: 10.3390/nu13041194

48. Ulrich CE, Geil RG, Tyler TR, Kennedy GL Jr, Birnbaum HA. Two-week aerosol inhalation study in rats of ethylene oxide/propylene oxide copolymers. *Drug Chem Toxicol*. (1992) 15:15–31. doi: 10.3109/01480549209035170

49. Stark WJ, Rosenblum P, Maumenee AE, Cowan CL. Postoperative inflammatory reactions to intraocular lense sterilized with ethylene-oxide. *Ophthalmology*. (1980) 87:385–9. doi: 10.1016/s0161-6420(80)35220-2

50. Zhang YZ, Bjursten LM, Freij-Larsson C, Kober M, Wesslén B. Tissue response to commercial silicone and polyurethane elastomers after different sterilization procedures. *Biomaterials*. (1996) 17:2265–72. doi: 10.1016/0142-9612(96)00055-5

51. Lomas RJ, Gillan HL, Matthews JB, Ingham E, Kearney JN. An evaluation of the capacity of differently prepared demineralised bone matrices (DBM) and toxic residuals of ethylene oxide (EtOx) to provoke an inflammatory response in vitro. *Biomaterials*. (2001) 22:913–21. doi: 10.1016/s0142-9612(00)00255-6

52. Li Z, Shi P, Chen Z, Zhang W, Lin S, Zheng T, et al. The association between ethylene oxide exposure and asthma risk: a population-based study. *Environ Sci Pollut Res Int*. (2023) 30:24154–67. doi: 10.1007/s11356-022-23782-3

53. Liu N, Zhang C, Hua W. Dietary inflammatory potential and psoriasis: a cross-sectional study. *J Dermatol*. (2023) 50:692–9. doi: 10.1111/1346-8138.16731

54. Du M, Deng K, Cai Q, Hu S, Chen Y, Xu S, et al. Mediating role of systemic inflammation in the association between heavy metals exposure and periodontitis risk. *J Periodontol*. (2023). doi: 10.1002/jper.23-0079

55. Lin F, Wang H, Wang X, Fang Y. Association between exposure to multiple polyaromatic hydrocarbons and periodontitis: findings from a cross-sectional study. *Environ Sci Pollut Res Int*. (2023) 30:112611–24. doi: 10.1007/s11356-023-29421-9